Lecture Notes
in Geoinformation and Cartography

LNG&C

Raffaela Cefalo
Janusz B. Zieliński
Maurizio Barbarella *Editors*

New Advanced GNSS and 3D Spatial Techniques

Applications to Civil and Environmental Engineering, Geophysics, Architecture, Archeology and Cultural Heritage

Springer

Lecture Notes in Geoinformation and Cartography

The Lecture Notes in Geoinformation and Cartography series provides a contemporary view of current research and development in Geoinformation and Cartography, including GIS and Geographic Information Science. Publications with associated electronic media examine areas of development and current technology. Editors from multiple continents, in association with national and international organizations and societies bring together the most comprehensive forum for Geoinformation and Cartography.

The scope of Lecture Notes in Geoinformation and Cartography spans the range of interdisciplinary topics in a variety of research and application fields. The type of material published traditionally includes:

- proceedings that are peer-reviewed and published in association with a conference;
- post-proceedings consisting of thoroughly revised final papers; and
- research monographs that may be based on individual research projects.

The Lecture Notes in Geoinformation and Cartography series also includes various other publications, including:

- tutorials or collections of lectures for advanced courses;
- contemporary surveys that offer an objective summary of a current topic of interest; and
- emerging areas of research directed at a broad community of practitioners.

More information about this series at http://www.springer.com/series/7418

Raffaela Cefalo · Janusz B. Zieliński
Maurizio Barbarella
Editors

New Advanced GNSS and 3D Spatial Techniques

Applications to Civil and Environmental Engineering, Geophysics, Architecture, Archeology and Cultural Heritage

Springer

Editors
Raffaela Cefalo
Department of Engineering and Architecture, GeoSNav Lab
University of Trieste
Trieste
Italy

Maurizio Barbarella
Department of Civil, Chemical, Environmental and Material Engineering
University of Bologna
Bologna
Italy

Janusz B. Zieliński
Department of Aviation
Air Force Academy
Dęblin, Lubelskie
Poland

ISSN 1863-2246 ISSN 1863-2351 (electronic)
Lecture Notes in Geoinformation and Cartography
ISBN 978-3-319-56217-9 ISBN 978-3-319-56218-6 (eBook)
DOI 10.1007/978-3-319-56218-6

Library of Congress Control Number: 2017935565

Printed on acid-free paper

This Springer imprint is published by Springer Nature
The registered company is Springer International Publishing AG
The registered company address is: Gewerbestrasse 11, 6330 Cham, Switzerland

1st International Conference

NEW ADVANCED GNSS AND 3D SPATIAL TECHNIQUES
APPLICATIONS to CIVIL and ENVIRONMENTAL ENGINEERING, GEOPHYSICS, ARCHITECTURE, ARCHEOLOGY and CULTURAL HERITAGE

In memory of Professor Giorgio Manzoni

Trieste, 18 – 20 February 2016

Main Conference Room - H3 Building
University of Trieste
Piazzale Europa, 1 - 34127 TRIESTE (Italy)

Giorgio Manzoni, Professor of Surveying and Mapping, at the Department of Engineering and Architecture, University of Trieste and Coordinator of the Centre of Excellence in TeleGeomatics, fostered in more than 40 years of academic activities, international cooperation and multidisciplinary Researches and Applications of GNSS and Geomatics techniques to many fields:

Archaeology, Architecture, Ecology, Civil and Environmental Engineering, Cultural Heritage, Geography, Geology, Geophysics, Health, High precision measurements, ICT, Metrology, Telematics' Networks and Humanistic Studies.

This Workshop, organized by GeoSNaV Laboratory and University of Trieste in cooperation with Ordine degli Ingegneri di Trieste, aims at gathering scientists of different fields and countries and keeping alive his spirit, creativity and great enthusiasm.

Contents

Introduction

This book contains the best papers presented at the 1st International Workshop:

"**New Advanced GNSS and 3D Spatial Techniques—Applications to Civil and Environmental Engineering, Geophysics, Architecture, Archeology and Cultural Heritage",** held at Department of Engineering and Architecture, University of Trieste, 18–20 February 2016.

The Workshop was organized by GeoSNav Lab (Geodesy and Satellite Navigation Laboratory), University of Trieste **in memory of Prof. Giorgio Manzoni**, Professor of Surveying and Mapping, at the Department of Engineering and Architecture, University of Trieste and Coordinator of the Centre of Excellence for the Research in Tele-Geomatics.

Professor Giorgio Manzoni fostered, in more than 48 years of academic activities, international cooperation and multidisciplinary researches and applications of GNSS (Global Navigation Satellite Systems) and geomatics techniques to many fields:

Archaeology, architecture, ecology, civil and environmental engineering, cultural heritage, geography, geology, geophysics, health, high-precision measurements, ICT, metrology, telematics networks and humanistic studies.

The Workshop aimed at gathering scientists of different fields and countries and keeping alive his spirit, creativity and great enthusiasm.

At the Workshop Website www.dia.units.it/gnss, readers can see and download:

- the Workshop Programme,
- the PDF presentation of all the papers,
- the videos of the opening ceremony and the presentations and
- the Workshop photogallery.

The book is divided into 3 parts:

Part I: New Advanced GNSS and 3D Spatial Techniques—Applications to Geodetic Networks, Mapping, Static and Kinematic Positioning and Timing contains 9 papers presenting new advanced GNSS techniques applied to geodetic reference networks, novel static and kinematic GNSS applications and particular mapping and timing applications.

Part II: New Advanced GNSS and 3D Spatial Techniques Applications to Photogrammetry and Remote Sensing reports 4 papers relating to advanced topics in photogrammetry and remote sensing.

Part III: New Advanced GNSS and 3D Spatial Techniques Application to GIS, Web-GIS, UAVs, Disaster Management and Cultural Heritage contains 6 papers proposing some interesting utilization of the most recent and advanced tools in digital cartography and field survey.

Raffaela Cefalo
Janusz B. Zieliński
Maurizio Barbarella

Part I
New Advanced GNSS and 3D Spatial Techniques—Applications to Geodetic Networks, Mapping, Static and Kinematic Positioning and Timing

Abstract

Part I presents new advanced GNSS techniques applied to geodetic reference networks, novel static and kinematic GNSS applications and particular mapping and timing applications.

Chapter "High Precision GNSS—Prospects for Science and Applications", by Janusz B. Zielinski[1], Agata Wielgosz[2], [1]Air Force Academy, Institute of Aeronavigation; [2]Polish Academy of Sciences, Space Research Centre, Poland, discusses the possible improvements in GNSS orbital positioning and timing accuracies and their impact on research and practical applications.

Chapter "Space, Time and Maps", by T. Bellone[1] and L. Mussio[2], [1]Polytechnic University of Turin and [2]Polytechnic University of Milan, Italy, presents the evolution in space and time concepts and their impact on surveying and mapping in Geodesy and Geomatics.

Estimating Crustal Deformations by GNSS Time Series Data Analysis by R. Barzaghi and B. Betti, DICA, Polytechnic of Milan, Italy, present a method for filtering time series data from GNSS permanent stations allowing the estimation of the crustal deformation at different scales both in time and space.

"The Actual Perspectives of GNSS Multi-Constellation Services and Receivers for Kinematic Applications" by Raffaela Cefalo[1], Mauro Calderan[1], Francesco Filippi[2], Cristoforo Montefusco[3], Andrea Piemonte[4] and Tatiana Sluga[1], [1]GeoSNav Lab, University of Trieste, Italy; [2]Department of Engineering and Architecture, University of Trieste; [3]Enav SpA, Rome, Italy; [4]Department of Civil and Industrial Engineering, University of Pisa, present the potentials on multi-constellation services and solutions for mobile applications especially in the terrestrial and special aerial sectors. The current trends and benefits of multi-constellation services and receivers as well as innovative kinematic research applications, carried out by the authors using multi-constellation receivers, are reported.

"Monitoring of the Italian GNSS Geodetic Reference Frame" by Maurizio Barbarella, Stefano Gandolfi and Luca Tavasci, DICAM, University of Bologna, Italy, reports the results of the Italian RDN GNSS network data processing relative

to all the 99 sites. The principal aim was to estimate sites displacements and velocities, using a PPP approach and applying the GIPSY-OASIS II software package. Results highlighted the residual velocities with respect to ETRS89, which can reach 5 mm/year in some areas.

The report "Interoperability of the GNSS's for Positioning and Timing" by Alessandro Caporali, Luca Nicolini, University of Padua, Italy, presents the results of a dense European multi-GNSS network formed by 31 sites equipped with different receivers and various combinations of antennas and firmware. Single point positioning (SPP) (ionofree combination of pseudoranges, broadcast ephemeris), and precise point positioning (PPP) modes (ionofree combination of carrier phases, SP3 precise ephemeris) are applied using a specific multi-GNSS software developed by the team.

In the presentation "Improvements in Geodetic Surveying Using GNSS Radio Occultation Observations" by Elisa Rosciano[1], Francesco Vespe[1], Giuseppe Vizziello[2], [1]Italian Space Agency, [2](Consorzio INNOVA, Italy), the authors propose to apply a new mapping function for the determination of the zenith GNSS total delay (ZTD). This MTMF (MT mapping function) could be defined using data from space missions such as COSMIC-FORMOSAT, METOP, CHAMP, GRACE and others. The improvement achieved with the implementation of this new mapping function is of the order of 30–35% with respect to the same solutions given by the NMF (Niell mapping function) and demonstrated to increase the positioning accuracies by 30–40%.

The contribution "Single-Frequency Receivers as Master Permanent Stations in GNSS Networks: Precision and Accuracy of the Positioning in Mixed Networks" by Paolo Dabove, Alberto Cina, Ambrogio Maria Manzino, DIATI, Politecnico of Turin, Italy, focuses the attention on the usefulness of single-frequency permanent stations for the densification of the existing CORS (Continuous Operating Reference Station) networks for monitoring purposes. Some innovative GNSS networks composed of geodetic and mass-market L1 receivers have been developed and tested, analysing the real-time performance of kinematic positioning in terms of quality, accuracy and reliability.

Chapter "Internet Platform for Improving the EGNOS Ionospheric Corrections" by Anna Swiatek, Leszek Jaworski and Lukasz Tomasik, Space Research Centre P. A.S., Warsaw, Poland, reports the results of the EEI (EGNOS EUPOS Integration) PECS (Plan for European Cooperating States) ESA Project, aimed at improving the EGNOS corrections, in particular the ionospheric ones, by using the GPS observations from Polish ASG-EUPOS stations. Kinematic experiments carried out by the authors at Biala Podlaska Airport, Poland, are presented and discussed.

Chapter "FReDNet: Evolution of a Permanent GNSS Receiver System" by David Zuliani, Paolo Fabris, Giuliana Rossi, OGS, Trieste, Italy, concerns the technical implementation of FReDNet (Friuli Regional Deformation Network) in the last years with new stations, new features and upgraded services.

The main objective of the network is the detection of tectonic plate movements in Friuli Venezia Giulia and a part of Veneto collision area: such movements can give some guidance to quantify the seismic hazard.

Joint Use of Image-based and GNSS Techniques for Urban Navigation by D. Pagliari, N.E. Cazzaniga, L. Pinto, M. Reguzzoni, L. Rossi, DICA–Department of Civil and Environmental Engineering, Polytechnic of Milan, Italy, presents two different assisted photogrammetric techniques using a combination of image-based and GNSS solutions, constrained by using ground control points extracted from urban maps.

High Precision GNSS—Prospects for Science and Applications

Janusz B. Zieliński and Agata Wielgosz

Abstract During last and coming years we are witnessing the immense qualitative and quantitative progress in the GNSS (Global Navigation Satellite Systems) domain. Two new technologies are under development offering considerable improvement of the accuracy of orbits: the on-board accelerometers and the inter satellite links. Because non-gravitational forces cannot be modeled with the desired precision, the direct on board measurements of those forces may improve the solutions for orbits, positions and timing. The range and range-rate measurements between satellites open the way to the elimination of the errors caused by the ionosphere and station uncertainties. The improvements in the on-board equipment like clocks and signal generators will provide enhanced radio signals while in the user segment the receivers of the new generation will be able to digest up to 50 signals. Combined with the MEMS (MicroElectroMechanical Systems) type inertial devices the user platforms will be able to provide the high accuracy positioning and timing even in the very unfavorable conditions, including the high dynamic motion or covered environment. The question of the usefulness of the High Precision PNT (Positioning, Navigation, Timinig) for scientific research is discussed in this paper. Here the following issues are taken into consideration: very accurate airborne gravimetry, millimeter accuracy low-altitude satellite orbit determination using GNSS observables and relativistic effects.

Keywords GNSS · Accelerometry · Precise satellite orbits

J.B. Zieliński (✉)
Institute of Navigation, Air Force Academy, Dęblin, Poland
e-mail: jbz@cbk.waw.pl

A. Wielgosz
Space Research Centre, Polish Academy of Sciences, Warsaw, Poland
e-mail: awielgosz@cbk.waw.pl

R. Cefalo et al. (eds.), *New Advanced GNSS and 3D Spatial Techniques*,
Lecture Notes in Geoinformation and Cartography,
DOI 10.1007/978-3-319-56218-6_1

1 Introduction

At the beginning of the XXI century we are witnessing an impressing expansion of the global satellite navigation systems. The GPS is still the leader—in terms of services provided, as well as in the technical progress and continuous improvement. GLONASS is operational, its constellation is complete and is striving for modernization. The Chinese Bei-Dou is almost completed and the European Galileo is on the way to be fully operational in 2020. All these systems are aiming for the best technological solutions for higher accuracy and availability. Actually, the responsibility for the precise orbit determination of this large fleet of space objects is willingly assumed by the International GNSS Service (IGS), but some other organizations are trying to undertake this task as well. However, all the systems are developing, introducing new technologies, improving the robustness, reliability and of course accuracy.

2 GNSS Systems Development

The quality of the GNSS orbit has been widely discussed since the occurrence of the GPS. The IGS (International GNSS Service) provides the best orbit solution using a rich data base of tracking data from over 400 worldwide reference stations as well as sophisticated processing procedures. The solutions are provided by different AC (Analysis Centres) which are using different software, algorithm and models. According to the IGS the mean accuracy of the GPS satellites orbit is about 2.5 cm and about 3 cm for Glonass (IGS website 2016). This is a measure of the internal consistency rather than absolute error. It is computed basing on e.g. differences between solutions delivered from different ACs or misclosures on the ends of arcs (Griffiths and Ray 2009). The only external validation of the GNSS orbit so far is the comparison to SLR measurements. In the extensive growth of the navigation satellite systems there is a problem of determining orbit for other GNSS as Beidou or Galileo. Some studies were done in the frame of MGEX project (Steigenberger et al. 2014), which gives an assessment of actual POD (Precise Orbit Determination) accuracy for five GNSS systems delivered by six AC. The differences in processing procedures concern mainly the differences in SRP (Solar Radiation Pressure) modeling, what cause differences in orbital solutions with the order of 10–20 cm. It seems that this is the range of accuracy that could be attributed to the actual level of the GNSS technology, considering all satellite systems. Apart from the difficulties in SRP modelling, there are many different error sources affecting the accuracy of the orbital solution. It seems that the most significant problems are the following:

1. Perturbation of satellites motion caused by the non-gravitational forces is not modelled perfectly;
2. Distribution of the monitoring stations and hence the coverage of the trajectory by observation is not homogenous;
3. The measurement of the pseudo-ranges by means of the L band radio signals is burdened with the influence of the ionosphere.

Here we would like to have closer look on the influence of the non-gravitational perturbations on the accuracy of the orbit determination, hence the accuracy of the position of the satellites in space. It has been analysed by a number of authors through decades (Milani et al. 1987; Springer et al. 1999; Fliegel et al. 1992; Sibthorpe et al. 2011; Rodriguez-Solano et al. 2012; Montenbruck et al. 2014). However, there is still a lot of room for development as this subject is very complex. The modelling of the NGP perturbations is very compound, it depends not only on the physical environment but also on many other parameters of the spacecraft and its motion. The most important effect is the direct solar radiation pressure, which depends on solar activity. The shape, mass, attitude, on-board activity etc. play a significant role but are very difficult to model. In addition there are some regions when the spacecraft passes through the shadow (penumbra and umbra traverse) where the NGP change significantly and the standard models are not appropriate. Among other effects we can mention the Earth radiation and changing albedo, the thermal radiation of the satellite, the antenna thrust effect, residual atmospheric drag or the technical activity in the spacecraft. Taking all above into account it become evident that the optimal solution would be the direct measurement of all resulting non-gravitational acceleration. Preliminary simulations indicate that to reach the desired accuracy of the orbital position on millimetre level the accelerometer sensitivity should be close to $10^{-11}\mathrm{m/s}^2$.

Therefore the need for the new techniques, which will allow to reach the desired level of precision for the next generation GNSS systems is obvious. The original proposal of some improvements has been done in the work of (Ash 2002) Equipping GPS Satellites with Accelerometers, where the on-board three dimensional accelerometers, satellite-to-satellite range and range-rate measurement system (ISL—Inter Satellite Links) and gyroscopes were discussed as the techniques which will allow to reach a millimetre level of accuracy. Such a high level of precision will be useful for many scientific applications including geodynamics and relativity tests. The same idea is pursued by the Galileo designers. Under the umbrella of the European Commission the expert group MEAG (Mission Evolution Advisory Group) published the report EGMER (European GNSS Mission Evolution Roadmap) (European Commission 2013), in which the future development of GNSS is discussed. In parallel ESA has established the Galileo Science Advisory Committee (GSAC) with the task to investigate more closely technical progress and the scientific benefits to be derived from the second generation Galileo system. As a result of these deliberations by both expert bodies the idea of the furnishing the next space crafts with accelerometers has been envisaged and supported.

Accelerometry is helpful for the elimination of the influence of the non-gravitational forces. Accelerometers have been successfully applied for the number of space missions, in particular for the gravimetric missions such as CHAMP, GRACE and GOCE. The interplanetary mission Bepi Colombo to the planet Mercury will also be equipped with an accelerometer (Iafolla et al. 2010). We can therefore assume that the technology is mature, although it was not applied to GNSS satellites till now. It is assumed that desirable precision of the accelerometer measurements should be of the order of 10^{-11}g. The implementation of the accelerometry technique into the POD procedure should hopefully improve the orbit accuracy in the near future.

Another innovative idea which can improve the geometric construction of the GNSS constellation as well as strengthen the orbital solution is the introduction of the Inter Satellite Links–the measurements of the range and range-rate between the spacecrafts visible one from another. In earlier literature this technique has been known as the satellite—to—satellite tracking in the low—low mode or high—low mode. There are various options under consideration and they are investigated by different expert groups (e.g. (Wolf 2000; Fernandez 2010)).

There are different technical proposals too, it seems that the most promising is the system following the one applied for the GRACE mission. The experiences from previous space missions permit us to estimate the measurements precision of the selected system to be of the order ±2–4 mm (attitude motions), antenna phase center definition, internal s/c motion etc., taken into account). Very detailed analysis of the application of the ISL technique to the orbit and position determination is presented by Wolf (2000). His simulations indicate that the orbital solution with ISL data is much stronger than with ground based data only. Accuracy of the orbital position can be improved significantly reaching the level of ISL measurement noise.

By successfully applying both techniques discussed above we will be able to model the simple gravitational motion (cleaned from the non-gravitational perturbations) of the mass particle in space with accuracy better than ±1 cm over a long time. When discussing the accuracy of position, we cannot forget about the accuracy of timing. The relevant accuracy of timing should be assumed about ±50 ps. For the following numerical modeling we shall assume σ_x = 5 mm, σ_t = 100 ps, what is well in the limits of the modern space technology.

3 Applications of the High Precision GNSS

The implementation of the new technologies and then the very precise orbit determination will open immense possibilities of the use of GNSS orbits for scientific applications. First, let us to mention the classic problems of geosciences which are supported now by space data, such as:

1. More accurate, robust, and global ground site coordinate determination;
2. Real-time determination of neutral atmosphere water vapor content for input to weather prediction models;

3. Length-of-day and earth wobble monitoring at finer detail;
4. Very accurate airborne gravimetry;
5. Millimeter accuracy low-altitude satellite orbit determination using GNSS observables.

While the first three items are discussed in the literature, let us to bring the attention to the last two.

4 Airborne Gravimetry

The airborne gravimetry is the very useful technique applied for large unsurveyed areas like deserts, arctic areas or ocean surface. The principle consists in the measurement of the acceleration occurring on the board of an aircraft. The measurement can be done with the adapted gravimeter or more sophisticated inertial measurement unit. The measured acceleration will be always the sum of the gravitational acceleration exerted by the Earth's mass and the kinematical acceleration coming from the motion of the aircraft (Fig. 1).

$$\boldsymbol{P} = \boldsymbol{g} + \boldsymbol{S} \tag{1}$$

where $\boldsymbol{P}$—total acceleration
$\boldsymbol{g}$—gravitational acceleration
$\boldsymbol{S}$—kinematic acceleration.

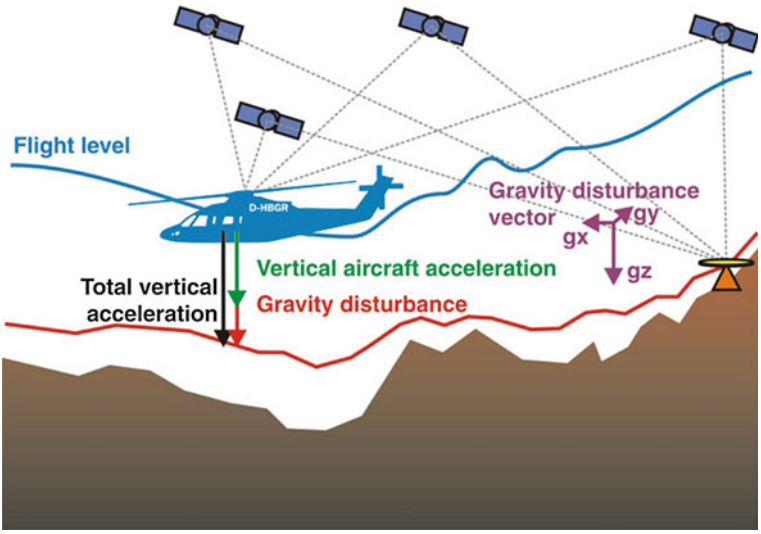

Fig. 1 Airborne gravimetry principle (*Source*: *BGR)*

The separation between these two kinds of accelerations is the most critical point of this technique (Hein 1995). However, the possibility of using the high accuracy GNSS signals for the monitoring of the airplane motion offers an interesting solution of the problem. If we assume the required accuracy of the determination of the gravity anomaly $\Delta g = \pm 0.1$ mGal, with the spatial resolution 300 m, we get the following constraints:

$$\text{Accuracy in vertical acceleration} : \pm 10^{-6}\text{m/s}^2$$
$$\text{Accuracy in vertical position} : \pm 10\,\text{cm}.$$

With the centimeter level accuracy of the position of the satellite in space and multi-system receivers the above indicated uncertainties in the monitoring of the aircraft motion are within the range of the GNSS positioning technology.

5 Low Satellites Orbital Tracking

Another interesting application of the high accuracy GNSS satellites might be the tracking and orbit control of the near Earth's satellites. Nowadays more and more satellites missions with orbits up to few thousands kilometres high are controlled from the top then with the ground based tracking system. Most satellites do not require very high position accuracy but some missions do. We could mention here the gravimetric missions GRACE and GOCE were the PNT precision was essential. E.g. the post-mission estimation of the precision of the determination of the GOCE orbit and the position in space is circa ±2 cm. But the higher orbital accuracy the better determination of other forces like the gravity field. Therefore the improvement of the orbital precision of the GOCE type satellites would be very advisable. There is a scientific and practical interest in the continuous monitoring of the Earth's gravity field and its temporal changes. The high—low satellite to satellite tracking method applying GNSS satellites is the only method to solve the problem and then the high accuracy of the GNSS orbits can be transferred to the low satellite orbits.

6 Relativistic Effects

But the possibility to monitor the pure gravitational motion of the mass particle in space connected with the high precision time measurement opens also new opportunities for research in the theory of gravitation (Ciufolini and Wheeler 1995; Ashby 2003). Let us mention here the effects related to the rotation of the Earth. The so called Lense-Thirring frame drag has been theoretically predicted by Lense

and Thirring in 20th century, soon after Einstein published his theory of General Relativity. To investigate and test the Lense-Thirring effect the very difficult and costly space mission has been performed—Gravity Probe-B. More successful experiments has been done using the laser ranging data to satellites Lageos 1 and Lageos 2 (Ciufolini and Pavlis 2004; Lucchesi and Peron 2014; Lucchesi and Peron 2010). Satellites Lageos are very well suited for this kind of experiment, because they are very heavy compact objects, playing well the role of the point test masses. Both Lageos are orbiting on the altitude about 6300 km. For the determination of the change of the right ascension of the orbital node (nodal precession) the expression is used and applied for Lageos:

$$\dot{\Omega}^{LT} = \frac{2GJ_{@}}{c^2 a^3 (1 - e^2)^{3/2}} = 31\, mas/y \tag{2}$$

where:

G—gravitational constant,

C—speed of light,

$J_{@} = 5.9 \times 10^{40}$g cm^2/s—Earth angular momentum

a, e—semi-major axis and exccentricity of the orbit.

In the case of the navigational satellites, the orbital altitude is between 20,000 and 23,000 km, therefore the effect is smaller, and orbits are almost circular, therefore only the nodal precession can be used. According to Combrinck (2013) for GPS the value

$$\dot{\Omega}^{LT} = 8,8\,\mu\text{as/d} = 3,2\,\text{mas/y}.$$

It is equivalent to orbital position differences 1,2 mm/d or cà 12 mm during the 10 days time interval. This is well within the reach of the proposed accuracy of the system.

Another closely related interesting effect is the torsion of the Earth gravitational field resulting from the finite speed of the gravity propagation. In the local inertial coordinate system the field is rotating following the rotation of the Earth. In the Newtonian interpretation the field is rotating stiffly with the Earth. However, in the post Newtonian interpretation the distant gravity field with its equipotential surfaces is not able to rotate with the same phase as the Earth. When the gravitational signal from the ground reaches the height H, the earth will rotate by the angle α

$$\alpha = \Delta t \cdot \omega = \frac{H}{c_g}\omega \tag{3}$$

where: ω—angular velocity of rotation, c_g—velocity of the gravitational signal (see Fig. 2).

The question of the detection and measurement of this last effect has been discussed in detail in (Zieliński et al. 2007; Zieliński 2013). It seems that with

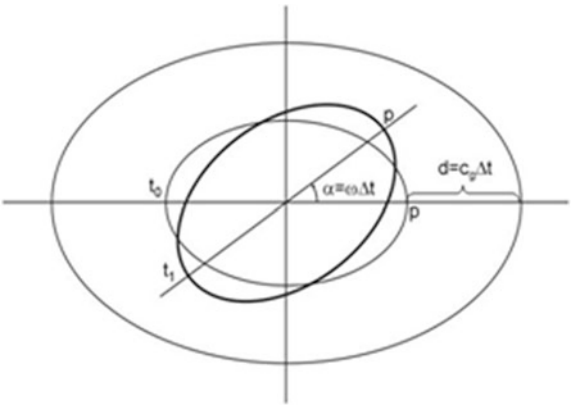

Fig. 2 Angular phase shift caused by the time of gravitational signal propagation

application of the high precision GNSS satellites and gradiometers this phenomenon could be investigated.

7 Conclusion

We can conclude that the efforts to enhance the accuracy of the determination of the orbital motion of the navigation satellites and elimination of the influence of the non-gravitational forces can bring new advances in the research and applications. With the desired accuracy of few mm level for the point position in space linked with sub-nanosecond accuracy for timing, the next generation of the GNSS will be a powerful tool for the research of gravitation with far reaching consequences for the fundamental physics as well as the Earth sciences.

References

Ash ME (2002) Equipping GPS Satellites with accelerometers and satellite-to-satellite observables. In: Proceeding of the 2002 ION National Technical Meeting, San Diego, CA, 28–30 Jan 2002

Ashby N (2003) Relativity in the global positioning system. Living Rev Relativity 6(2003):1

Ciufolini I, Pavlis E (2004) A confirmation of the general relativistic prediction of the lense-thirring effect. Nature 431:958–960

Ciufolini I, Wheeler JA (1995) Gravitation and inertia. Princeton Univ. Press,

Combric L (2013) General relativity and space geodesy. In: Xu G (ed) Sciences of geodesy, Springer, pp 53–95

European Commission (2013) Enterprise and industry directorate-general. European GNSS Mission Evolution Roadmap (EGMER) E. C. Document, Feb 2013

Fernandez FA (2010) Inter-satellite ranging and inter-satellite communication links for enhancing GNSS satellite broadcast navigation data. Adv Space Res 47:786–801

Fliegel HF, Gallini TE, Swift ER (1992) Global positioning system radiation force model for geodetic applications. J Geophys Res 97(B1):559–568

Griffiths J, Ray J (2009) On the precision and accuracy of IGS orbits. J Geod 83:277–287

Hein G (1995) Progress in airborne gravimetry. In: Proceeding of the IAG symposium on airborne gravity field. Spec. Rept. No. 60010 Department of Geomatics Engineering, University of Calgary, pp 3–11

Iafolla V, Fiorenza E, Lefevre C, Morbidini A, Nozzoli S, Peron R, Persichini M, Reale A, Santoli F (2010) Italian Spring Accelerometer (ISA): a fundamental support to BepiColombo radio science experiments. Plan. Space Sci. 58:300

IGS website, http://www.igs.org, 2016

Lucchesi DM, Peron R (2010) Accurate measurement in the field of the Earth of the general relativistic precession of the Lageos 2 pericenter and new constraints on non-newtonian gravity. Phys Rev Lett 105:231103

Lucchesi DM, Peron R (2014) LAGEOS II pericenter general relativistic precession (1993–2005): Error budget and constraints in gravitational physics. Phys Reviewed 89:082002

Milani A, Nobili AM, Farinella P (1987) Non-gravitational perturbations and satellite geodesy. Adam Hilger, Bristol

Montenbruck O, Steigenberger P, Hugentobler U (2014) Enhanced solar-radiation pressure modeling for Galileo satellites. J Geod. 89(3):283–297

Rodriguez-Solano CJ, Hugentobler U, Steigenberger P (2012) Adjustable box-wing model for solar radiation pressure impacting GPS satellites. Adv Space Res 49:1113–1128

Sibthorpe A, Bertiger W, Shailen DD, Haines B, Harvey N, Weiss JP (2011) An evaluation of solar radiation pressure strategies for the GPS constellation. J Geod. 85(8):505–517

Springer TA, Beutler G, Rothacher M (1999) A new solar radiation pressure model for GPS. Adv Space Res 23(4):673–676

Steigenberger P, Hugentobler U, Loyer S, Perosanz F, Prange L, Dach R, Uhlemann M, Gendt G, Montenbruck O (2014) Galileo orbit and clock quality of the IGS Multi-GNSS Experiment gives an assessment of the actual POD accuracy, ASR 2014

Wolf R (2000) Satellite orbit and ephemeris determination using inter satellite links. Fakultät für Bauingenieur- und Vermessungswesen der Universität der Bundeswehr München Dissertation, 2000

Zieliński JB (2013) Torsion of the Earth's anomalous gravitational field resulting from the finite speed of the gravitational interaction. In: Jantzen RT, Rosquist K, Ruffini R (eds) Proceeding of the 13th Marcel Grossmann meeting on general relativity. Stockholm, 2012, World Scientific, 2013 pp 2363–2368

Zieliński JB, Gałązka RR, Peron R (2007) On possible determination of the speed of the gravity signal in space with help of gradiometry. Artif Satellites 42:120–140

Space Time and Maps

Tamara Bellone and Luigi Mussio

Abstract Concepts of space and time were important for man, at various levels, for philosophy, science and religion. Astronomy, Philosophy, Mathematics, Physics, Geography and Cartography were most involved topics. Actually, shape and history of Universe, and specially of Earth, are related to their representation: so, ideas about space and time have largely coped with survey and mapping, from Geodesy to Geomatics.

Keywords Space · Time · Maps · History of science

1 Introduction

Concepts of space and time have always been important to man, at different levels, for everyday life, for philosophy, science and religion. The perspective here relates more closely to European science, while acknowledging the independent development of science in Middle, South and Far East. Partition of time and space is somewhat different in different ages and cultures (Chinese, Indian, Arabic/Persian, etc.). As for space, for instance, Darwin (Odifreddi 2010) used a certain number of particular homogeneous areas:

- Asia, Europe, Mediterranean Africa and North America;
- Latin America, which ends with the desert highlands of present United States;
- Sub-Saharan Africa;
- Madagascar;
- Australia, New Guinea and New Zealand.

T. Bellone
Politecnico Di Torino—DIATI, Corso Duca Degli Abruzzi 24, 10129 Turin, Italy
e-mail: tamara.bellone@polito.it

L. Mussio (✉)
Politecnico Di Milano—DICA, Piazza L. da Vinci 32, 20133 Milan, Italy
e-mail: luigi.mussio@polimi.it

R. Cefalo et al. (eds.), *New Advanced GNSS and 3D Spatial Techniques*,
Lecture Notes in Geoinformation and Cartography,
DOI 10.1007/978-3-319-56218-6_2

Indeed all cultures define time and space around them, by a imposition of a specific order (physical, mental and cultural). The following is a short history of the evolution of the concepts of space and time in Western culture, from the myths to the scientific concepts. A sense-based conception of space and time defines, that space recognizes the physical extension and it's the main object of measurement, calculation and analysis of surveying and mapping disciplines; however the notion, that time flows in one direction is merely a property of human consciousness.

Astronomy, Philosophy, Mathematics, Physics, Geography and Cartography are the subjects most involved. Indeed the shape and history of the Universe, and especially of the Earth, relate to how these have been represented. Thus ideas about space and time largely dealt with survey and mapping, from Geodesy to Geomatics. Understanding space involves two human operations, different but closely related, vision and handling. They let classify spaces and objects:

- objects, that may stay in hands;
- objects, that may be seen just moving the head;
- objects, that may be seen just walking around them;
- object, contained in a space, which may be visited by a simple walk;
- the same as above, to be recognized by more trips;
- Earth space;
- Universe space.

The first object of this classification has specific Cartesian orthogonal characteristics. Exactly by extension, the same Cartesian characteristics are attributed also to the second and third objects. On the contrary, starting from the fourth object, an important feature is the spherical form, relative to the observer's vision, which separates into a flat projection of the image and in a measure of the spherical distance. Thus according to Husserl, due to axis rotation, where distance becomes altitude and, due to curvature inversion, where a concave form becomes a convex one, recognizing the spherical form of the Earth.

Plant and animal behaviours are referred to space and time (and also number), e.g. vertical direction, season sensitivity, etc. Human behaviours extend, but not contradict their original physical nature. Animals have a kind of intuitive sense-based knowledge of physics, registered in the brain as a result of natural selection. Some animals are able to estimate quantities and to count to four. Thus shaping a branch to get a stick, in order to measure the depth of a river, is in any case an example of an elementary Geomatics procedure. The ability to represent themselves by the mind, in the past and in the futures, is a mental time travel. Cognitive scientists haven't yet determined whether this capacity belongs to animals. Anyway, there are neurons in the brain of some animals selectively sensitive to the number of objects, regardless of their size, shape or location (generally only until four).

However only the human being, through language, is able to apply grammar and syntax to the phrases and consequently to the numbers by the so-called recursively rules. For these reasons, the Kantian a priori form intuition includes the number and the capability to measure. Therefore according to Chomsky (Chomsky et al. 2002),

two a priori forms: broad and narrow, are the unique human component of the linguistic faculty:

- the Linguistic Faculty: broad, includes a sensory motor system, a conceptual intentional system and the computational mechanisms for recursion;
- the Linguistic Faculty: narrow, based on the computational mechanisms for recursion, provides the capacity to generate an infinite range of expressions from a finite set of elements (Figs. 1 and 2).

Darwin conducted experiments on plants and animals, which still today affect the research:

- plants are aware of gravity and they can distinguish up from down;
- plants to survive must know the direction of the surrounding light;
- plants don't measure the length of the day, but that of the continuous period of darkness;
- a common structure for time, space and number exists in the brain of animals and humans;

Fig. 1 Chimpanzee preparing a stick (from it.dreamstime.com)

Fig. 2 Orangutan measuring the depth of a ford (from ViralSpell.com)

- an animal evaluates how many trips it is necessary to make to obtain a finite supply of food.

2 The Thought of the Ancient Greeks

Many ancient cultures believed that the Universe was developed from the centre of the Earth, which holds together the Universe. The axis of the world establishes an order in the cosmos, but the problem, is that really the axes are two: the first axis, materialized by the feeling of gravity, connects the zenith, the location on the Earth and the nadir: this axis divides the space into three parts: Earth, Heaven and Underworld, and it's symbolized by the human being himself and by a sword; the second axis is the polar axis: this axis is indicated by a whirlpool, a mill or a round walk of an animal.

Many ancient rites provided for the alignment of the axis of gravity with the polar axis, and the ancients feared, that would return chaos, if the centre of the Earth had collapsed. For these reasons, from the beginning human beings have felt the need of a reference system (De Santillana et al. 2011).

The Greeks travelled in the Mediterranean Sea (e.g., Argonauts, Ulysses and circumnavigation of Africa by Phoenicians), approaching new concepts of space and time. Therefore geographical data, represented in maps, are acquired according to celestial and terrestrial measurements; nevertheless numbers, weights and measurements became much more important since Middle age, thanks to contributions of Indian, Persian and Arabs.

Going deeply at the origin of Western scientific thought, Cartography from the beginning has two aspects: it's the representation of the entire world, in the broadest sense, but it's often a representation of a certain territory, for immediate purposes. Indeed, Greek Geography is related to Cosmology rather than to practical purposes. Anaximander (Rovelli 2014) believed, that everything derives from a primordial substance, in which everything dissolves later (the contemporary philosopher Popper believes, that Anaximander was at the origin of scientific thought).

According to Anaximander and his Greek followers, time is derived by a cyclical conception and space is homogeneous, so that the Earth is floating in space, without falling, without the need to lean on something. There aren't absolute directions, so things don't fall to an absolute low (a direction that is the same everywhere in the universe). However the things fall to Earth and the very meaning of high and low becomes ambiguous.

Successively the concepts of space and time develop largely in the thought of ancient Greeks (Abbagnano 1982a, Vol.1). The Greeks, in particular the Pythagoreans and Aristotle, founded it difficult to conceive of the nothing and the non-being. Thus space is occupied by the objects, which it contains; however in Indian thought the idea of zero, the possibility of nothingness and the empty space are present from early times. As said above, time is mostly cyclical; indeed the Earth's rotation around its axis determines the alternation of days and nights, and its rotation, around the sun in the ecliptic, determines the changing of the seasons.

Plato and Aristotle believed the cosmos to be a finite amount of spherical form, because only the sphere is perfect. In Aristotelian cosmology, in turn, also accepted by Ptolemy, the idea of space itself doesn't change, because only individual substances exists, of which space is the premise. On the other hand, the classical Greek thought wasn't so uniform as one may think; indeed among Pythagoras' pupils, for example, there were different opinions about the possible finiteness of the Cosmos. Also the exclusion of the void wasn't so general; indeed for Democritus and Epicurus atoms move in an empty space.

Furthermore Democritus realized, that the matter can't be a continuum. Indeed if an object is continuously divided, in the end, points without extension are obtained, but putting together these un-extended points, it would be impossible to remake the object. The alternative is to assume, that any piece of matter is made up of a finite number of discrete indivisible particles, called atoms. According to Democritus, the space became the container of the world, whose constituent elements are the same for all beings. It's an immense space, undifferentiated and absolute, the space which

will be found again in the physics of Newton. Therefore Greek geometry doesn't directly affect the space, but the shape of things that fill it. These forms are considered independently of the objects, which can be assigned.

Moreover since any object of the world perceived by the senses can have the perfect forms of geometry, these can only exist as ideas. Plato's ideas are original essences, the prototype of all the sensible things. These are generated by a demiurge in the image and likeness of those ideals, which are perfect, eternal and immutable.

After Alexander's death, his empire was divided and his general Ptolemy I chose Alexandria as the capital, where he began the construction of the legendary library. Just in Alexandria, the mathematician and philosopher Eratosthenes calculated the radius of the Earth and founded the mathematical geography, where Hipparchus invented America, due to different tides in two oceans and Ptolemy drew the map of the known Earth.

For Aristotle the spheres, made of ether, rotate materially, with the planets fixed on them, but Ptolemy had an abstract perspective, as a mathematician, so that the spheres aren't real nor material. Aristotle and Ptolemy said, that a state of rest is the most favourable and the Earth doesn't move; in contrast, in modern times, both Galilei and Newton were interested to the motion of bodies. Going against the geocentric favoured configuration Aristarchus of Samos and Archimedes proposed an innovative heliocentric configuration, as Persian astronomers in the Middle Ages and Copernicus in the Renaissance would do (Figs. 3 and 4).

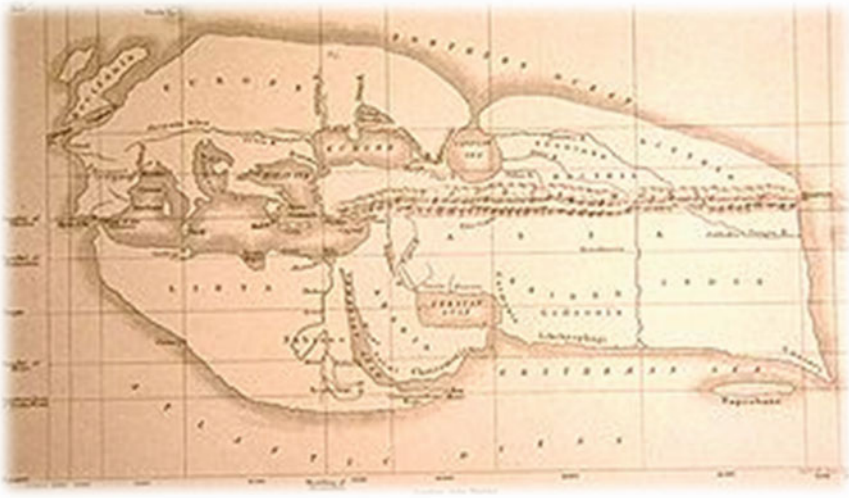

Fig. 3 Eratosthenes' map (from Wikipedia)

Fig. 4 Ptolemy's map (from Ancientcoinsforeducation.org)

3 From Middle Age to the Renaissance

As for time, Greeks saw it as cyclical and absolute; in contrast, in modern times, it will be linear and absolute (according to Newton), or linear and relative (according to Einstein). Quite the opposite was Augustine of Hippo's view, who stated, that time is related to physical perception, as it's in Leibnitz, Herbart, Gestalt theory and Psychoanalysis. Indeed in the Middle Age, time was created by God with the universe, but its nature remained deeply mysterious.

Augustine criticized Aristotle's conception of time as a measure of motion of stars and stated, that time was a stretching of the soul (distentio animi), so that time lost its absolute meaning, becoming interior time. The subject, while living only in the present, is aware of the past thanks to the memory and of the future by virtue of waiting.

From Augustine on, Christian thinking conceived the time as linear-progressive and not cyclical-circular as in the ancient world.

Travels, from Renaissance to XVIII century and over, stimulated production of maps and related instruments, finding that correct geographical coordinates are essential at sea. While fixing latitude was comparatively easy, the problem of longitude required a good timepiece; availability of accurate watches and good lenses depended on the alliance of science and technology, founding the Nova Scientia of the modern times (it's perhaps no coincidence, that Spinoza himself was a lens-maker). Renaissance went over certain limits of the Middle age:

- a copy of Lucretius' De Rerum Natura was found;
- the Elements of Euclid and the Geography of Ptolemy were translated into Latin from Greek, becoming accessible to European scholars;
- Erasmus of Rotterdam published the Encomium Moriae and Thomas More his Utopia;
- the claim of Reform favoured an increment of the economic development in Netherlands and England, and promoted the production of new maps.

For these reasons, the concept of space as an entity in itself derives from the Renaissance. It would be a symbolic form, in the sense given by the neo-Kantian Cassirer. The T-O maps expressed a Christian imago mundi (Fig. 5), but were not a realistic description of the world. (Brotton 2013). Nevertheless, it was medieval minds which invented perspective (Fig. 6), dispensing with religious reference. Just

Fig. 5 An example of TO map (from Pinterest.com)

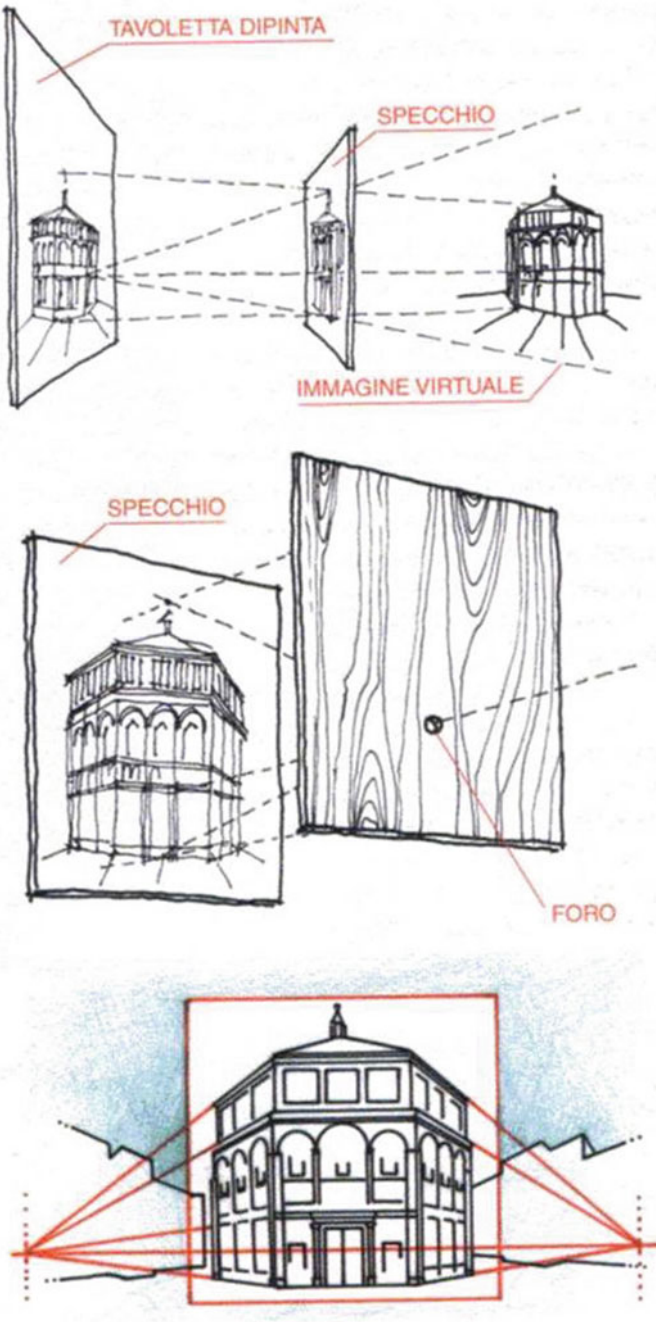

Fig. 6 Perspective view of the Baptistery of Florence (Brunelleschi) (from istitutomaserati.it)

in the Middle age, numbers, weights and measurements became much more important, thanks to contributions of Indian, Persian and Arab scientists and people.

4 The Modern Age

In the middle of XVI century, a group of cartographers and cosmographers was formed in the Netherlands, including Mercator, who reformed the Cartography. As a consequence, a map results from a plane design of Earth's surface, taking into account the Cartesian reference system, as well as Euclidean geometry and Galilean physics. The mathematician and cosmographer Mercator, that studied at the Catholic University of Leuven (the same at which Erasmus had been a student), is also known for a treatise on triangulation.

According to Descartes: the extension in length, breadth and depth, which constitutes the space occupied by a body, is exactly the same as that which constitutes the body; consequently there can't exist a space separate from body; space, time and motion are just relations among bodies and not separately existing entities or attributes, which are in any way independent of material bodies; also motion only exists as a relative difference among bodies.

According to Spinoza: number is used to determine the discrete amount and measurements determine continuous quantity; man, as mind and body, is a simple determination of two dimensions of the essence of God: thought and extension. Time, in contrast, explains duration, being relative and not an absolute entity; since it is not a divine property.

Indeed if a man observes a phenomenon knowing all its causes and all its premises, he will arrive at a statement devoid of any reference to time, and always true. However a man can't know all causes and consequences of things, and that's why he sees things arise and perish only. During the globalization of the modern era the early development was accomplished by practicability of seas, largely enhanced by availability of better maps. Also Columbus stated, that all points on Earth surface are equivalent as they may be described by merely two coordinates.

Willem Blaeu, a pupil of the astronomer Tycho Brahe, returned to the Netherlands, drew high-quality maps of various States, also forming important Atlases, and became cartographer for the Dutch East India company. Matteo Ricci, with the Chinese mathematician Xu Guangqi, translated the first books of Euclid's Elements in Chinese; he also drew a world atlas for Chinese, personally taking care of the translation of European names in the local language, and introduced in Europe many aspects of Chinese civilization.

In the same period, the Modern Physics was born. Newton assumed, that space is absolute in nature, some sort of void container of objects and facts, based on Euclidean geometry. Quite the opposite was Leibnitz's view, where space derives from relationships between objects, as in Gestalt theory and Psychoanalysis.

The philosophical insights of Cusa, Copernicus, Giordano Bruno, etc. gradually changed the conception of the Cosmos and the idea of a well-ordered world, finite and finalized. Gassend presented the atomistic conception with energy, saying that space and time were pre-conditions for the existence of the substance, not its attributes, and with his statements, he risked charges of heresy. His geometrical and mechanistic conception, which supports the origin of modern physics is the product of Plato's mathematics, evolved into a strange alliance between Plato and Democritus.

Newton founded his mechanics on the idea, that space was distinct from bodies and time would pass uniformly. His universe is an infinite space, in which the bodies move in a straight line unless they are deviated by another body exerting a force. Leibnitz, the great rival of Newton, believed that space is the order, which makes the bodies to be placed and, since they exist together, they have a relative position to each other, and the time also is a similar order, in relation to their next position.

The laws of mechanics are the same for all inertial reference systems, whatever is the velocity, is the well-known discovery of Galileo. Newton worried it, because of his belief in an absolute God. However Newton was criticized for his irrational conception, particularly by Berkeley, who believed, that all material objects, space and time were illusions

The relativity of space was implied in Bruno, who stated, that there are infinite heavenly bodies and endless motions of the universe, all of which can be used to define the time. Galileo saved only relativity of motion, Leibnitz instead followed the idea of Bruno about general relativity of motion, time and space. The phenomenological conception of Leibnitz is a necessary step to understand the next revolution done by Kant.

Locke analysed human intellect, to identify the possibilities and limits. Space and time aren't absolute realities, because space is born from simple ideas, that come from the sight and touch, and time is born by the interior experience of a continuous flow of ideas, which come one after the other (Abbagnano 1982b, Vol. 2). Hume didn't accept any external reality, but only impressions and ideas, of which people have immediate consciousness: people don't perceive a pure and absolute space, but only coloured dots, arranged in a certain order. The idea of space rises from aggregating them in a general name and the same is applied to the time. The geometry is an empirical science, because only arithmetic and algebra are rationally demonstrable. The modern philosopher Russell stated, that Hume's philosophy overcomes also Kantian critical synthesis (Figs. 7 and 8).

Fig. 7 Map of Africa by Mercator (1595) (from Wikipedia)

Fig. 8 Map of the World by Blaeu (1635) (from Wikipedia)

5 The Enlightenment

The Enlightenment and Kant are strictly linked. Indeed according to Kant's philosophical legitimation of Euclidean geometry and Newtonian physics, space and time are inner conditions of mankind, which allow the perceptions and will later be ordered by logical categories, refusing religious assumptions, as generally not done before.

Kant believed, that space and time aren't objective realities, but subjective constraints, which allow sensory-cognitive capacity of the human mind to represent objects, e.g. a priori forms of sensitive intuition. Appearances are phenomena, things in themselves noumena, while space and time, a priori forms of intuition, are transcendental and universal, i.e., they belong to human beings, endowed with reason, thorough logical categories.

The efforts to demonstrate the fifth postulate of Euclid, by Saccheri and Legendre, resulted in the emergence of new non-Euclidean geometries. Thus hyperbolic geometry was due to Gauss, Bolyai and Lobačevskij, and later, Riemann founded spherical and elliptical geometry. Riemann questioned also the uniqueness of Euclidean geometry, which was before considered the ideal abstraction of actual physical space.

At that time, the principal question was if the Earth was a spheroid flattened at the poles or at the equator. Newton preferred the second hypothesis, on the basis of physical considerations, Descartes and Cassini, according Descartes, the first one, on the basis of philosophical considerations.

Kant (Kant 1999) taught at Koenigsberg University physical geography and wrote in lecture notes for his students, that two journeys were organized to measure the degree of meridians: La Condamine, Godin, Bouguer left for Quito, a town then belonging to Peru in South America, and in the following year, Maupertuis, Clairaut, Camus and Monnier went to the Finnish town of in Tornea, to measure the meridian, which crosses the Arctic Circle. After that, the Peruvian expedition, returned in France, confirmed the hypothesis of Newton. Nevertheless the prestige of Cassini wasn't obscured; indeed their methods were used throughout the world, nor were affected by their beliefs. Cassinis and his entire family created a crystalline symbolism, typical of the views of the Enlightenment, the esprit de géometrie, without ornaments or frills, which became the rule for all the maps, since then (Figs. 9 and 10).

Fig. 9 A map of Paris by the Cassini family, (1750-1818) (from Wikipedia)

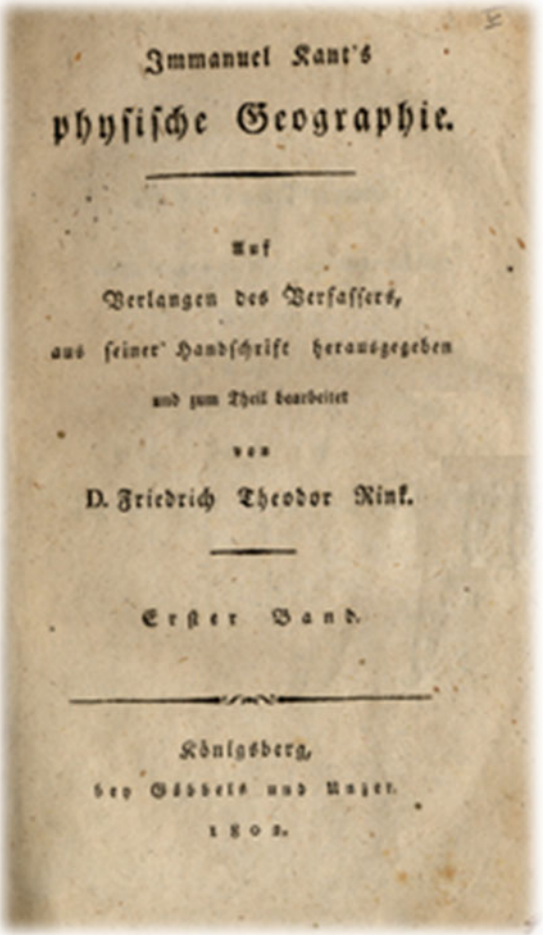
Immanuel Kant's
physische Geographie.
Auf
Verlangen des Verfassers,
aus seiner Handschrift herausgegeben
und zum Theil bearbeitet
von
D. Friedrich Theodor Rink.
Erster Band.
Königsberg,
bey Gebrüder Bornträger.
1802.

Fig. 10 Kant's lessons on Physical geography (from www.spaziofilosofico.it)

6 The Crisis of Science

Initially the crisis of science (Husserl 2008) opened the discussion questioning even Kant's philosophical perspective, whether sensations were organized according to the a priori space and time. Enriques and the Gestalt theory examined the relationship among physical, psycho-physiological and geometrical spaces. Projective Geometry and Topology are closely related to Photogrammetry and Image Analysis, where the last one gives new interest to Projective Geometry.

Poincaré said there isn't an absolute space and only relative motions are conceived, there isn't even an absolute time and the equality of two durations of time depends on conventions, the intuition of the simultaneity of events occurring in different places doesn't exist. Geometric space is different from the one perceived

by proper senses: continuous, infinite, three-dimensional, homogeneous and isotropic.

Relativity's Theory and Quantum Mechanics were the most important developments of the Physics, in the last century. Restricted and General Relativity Theories are related to Space Geodesy, while Quantum Theory relates to Nuclear medicine and Spectral Analysis of materials (whose needs may involve Survey and Mapping disciplines).

Heisenberg (Heisenberg 1994), summarizing the achievements of Quantum Mechanics, said that at the heart of the question is always the antinomy of Kant, so it's very difficult to imagine, that the matter can be divided indefinitely, on the other hand, it's equally hard to imagine, that this division has at one point an abrupt end. He put some questions: what is the proton? … the electron can be divided or not? … the quantum of light is simple or compound? … and stated, that all these questions are ill-formed, because the terms split or consist of have largely lost their meaning. Problems, language and thoughts, i.e., natural philosophy, should be adapted to this new situation created by the experiments, but this is unfortunately very difficult. The word "split" loses its meaning. If one wants to compare the knowledge of the current particle physics to some previous philosophy, this may just be the Platonic philosophy. In fact, the particles of modern physics, as taught by the quantum theory, are representations of symmetry groups and thus are comparable to symmetric bodies of the Platonic doctrine. Aristotle wondered: if between a substance and another there is nothing, how can coexist space and void? … The philosophical question was overwhelmed by the success of Newtonian physics, which allows great practical results, but remained in the background.

Einstein, with his Theory of Relativity, placed geometry within physics, where space and time aren't separate, but they are a complex structure, able to account for the limit of light speed and the effects of gravity, with the curvature of space-time. He was initially influenced by Mach, reflecting on the problem of being and non-being and answering, that the gravitational field was thus not within the space, but it was the space itself. As a consequence, space isn't a rigid container, but bends, twists, is flexible, so that the Sun bends space around and Earth then moves straight into a space, which tilts. Moreover not only the space sags, but also the time; indeed time flows more quickly rather at the top than at the bottom, near the Earth. The concepts of space and time were no more absolute, but relative, i.e., dependent on the reference system, in which is the observer. Space and time vary in function of the speed, with which the observer moves with respect to another at rest, so that the higher the speed, where the light speed in the void is the limit, the more extreme effects will be measured (the time dilatation and the contraction of the lengths). Gravity is due to geometric deformation of space-time, due to the presence of masses.

If philosophy, according to Kant, has always to be referred to a scientific fact, historically variable, what about the a priori system, shaped on the Euclidean-Newtonian geometric-scientific paradigm, that seems to be surpassed by Relativity Theory as and Quantum Mechanics. However, Cassirer (Cassirer 2015) incorporated Riemann's geometry and the Relativity Theory into neo-Kantian critical

philosophy, and showed how the Kantian philosophy enters in the development of modern science from Galileo up to Einstein and Gödel. In contrast, Reichenbach believed, that the Kantian method wasn't else than an analysis of Newtonian mechanics and the original Kantian conception of the a priori must be adjusted by the historic awareness of relativity and its new formal apparatus. The ontology should make place to the analytic intellect, studying the conditions in advance, also historical and transcendental, which govern the formation of the object of investigation in the different sciences. Terms like energy, air, atom, space and time, don't designate realities, but they are only symbols for the description of the context of possible relationships.

It's known, that the two theories are contradictory, so a new challenge of contemporary science is to find a theory, which includes the gravity into Quantum Mechanics. Anyway describing the physical laws without reference to geometry is similar to describing thoughts without words and the foundations of geometry had deep physical meaning in this problem. Both Einstein and Gödel believed, that the world was independent of the minds, yet rationally organized and open to human understanding. Both believed, that the progress of knowledge was due to a contamination of science and philosophy and, why not, symbolic moments.

Logics increased in complexity, growing from De Morgan, Boole, Frege, Peano and Russell, in the 19th century, to Tarsky, Quine, Gödel, Reichenbach, Schlick, Carnap and Popper, in the 20th century, recognizing its limits and the conflictual balance between experimentation and demonstration. As a consequence, neo-positivism philosophy is no more knowledge and becomes a mere fact of linguistic clarification. This results in a change of ontological status for Survey and Mapping disciplines, with conjectures and confutations replacing experience and, for Data Processing, Bayesian probabilities rather than frequentist inferences.

In the Knowledge of the External World, Russell had even positioned logics as the locus of scientific method in philosophy. Thus the philosopher can't do more than analyse the only meaningful discourse and, in particular, the scientific one (Abbagnano 1982c, Vol. 3). The propositions of metaphysics aren't simply false, but meaningless, because its aim is to study entities about which nothing can be said, according to the first Wittgenstein, in the Tractatus Logicus-philosophicus. Then for the second Wittgenstein, in the Philosophical Research, philosophy is something whose place is above or below the natural sciences and the human histories, not beside them.

The Vienna Circle was organized by Schlick, who was murdered on the steps of the university by a Nazi. Logical positivism (or neo-positivism, or logical empiricism) spread to the rest of Europe and in English-speaking countries. Many of the logical empiricists could see in some version of verifiability the tool, by which to carry on their anti-metaphysical program. Only empirical propositions are meaningful: they are verified by repeated experiments (as scientific theories, according Carnap and Reichenbach), or by analytic statements, which are true by definition (as mathematical propositions) and become false only by contra-examples (Popper 1970).

The goal was the Kantian theory of a priori synthetic judgments. To the logical empiricist, all statements can be divided into two classes: analytic a priori and synthetic a posteriori, where there aren't synthetic a priori statements. An important aspect of Carnap's and Quine's analysis were their attempt to give precise definition to the distinction between analytic and synthetic statements, by the Logical Syntax of Language.

A path, starting from Herbart, passing through Mach, Helmholtz and Boltzmann and leading to the mathematics of Hilbert and the philosophy of Husserl, accompanied the grow of science and technology after Kant until the modern time. Therefore the crisis of science flew along different paths.

Mach shook the faith in the mechanics, also considering, that scientific theories are only easier ways to describe large amounts of data coming from the existent. The physiological space is for Mach perspective, where all spatial sensations have the function to drive in properly movements, in order to take due care for human beings. The geometric space instead is accurate and free from any finality, where the distinction between the two spaces is based on their function.

In opposition to Mach, Boltzmann claimed, that every physical-mathematical formulation idealizes an event and must necessarily be beyond the experience, but right through the succession of hypotheses science tends to give a representation of the world more and more appropriate. Therefore science doesn't necessarily develop in a gradual way, but may progress through conflict, crisis and reconstruction, in a dialectical way. The universe is a system globally in equilibrium, where the equations of mechanics don't distinguish between what is above and below, and also the distinction between past, present and future is meaningless, because the arrow of time flows only for the people.

In this context, at the end of a long path concerning algebra and mathematical analysis, principally due to Euler and Lagrange in the 18th century, and in parallel, Kronecker, Dedekind and Cantor (for theory of numbers), Cauchy and Weierstrass (for the functional analysis), Jordan and Klein (for the topology) in the 19th century, Hilbert founded the axiomatic mathematics, incorporating geometry into algebra and mathematical analysis, and fixing common principles for arithmetic and logics. For these reasons, Mathematical analysis has a direct impact on theoretical Geodesy (and sometimes the last one promoted the grow of Mathematical analysis), while Topology has an impact on Cartography and GIS.

At the same time, Husserl founded Phenomenology, observing that the act of reflection is a process in time, so that human consciousness has an immediate experience of space and time. Empty space hasn't an independent meaning, because it's based on the concept of absence.

In the last two centuries, a similar path, concerning Linguistic analysis, was drawn by the contributions, among many others, of comparative grammar by von Humboldt, structural grammar by De Saussure and transformational-generative grammar by Chomsky, also reaching principles, sources and applications of surveying and mapping disciplines. The very immaterial nature of current Survey and Mapping disciplines may require a grammatical, syntactical and semantic analysis of their language.

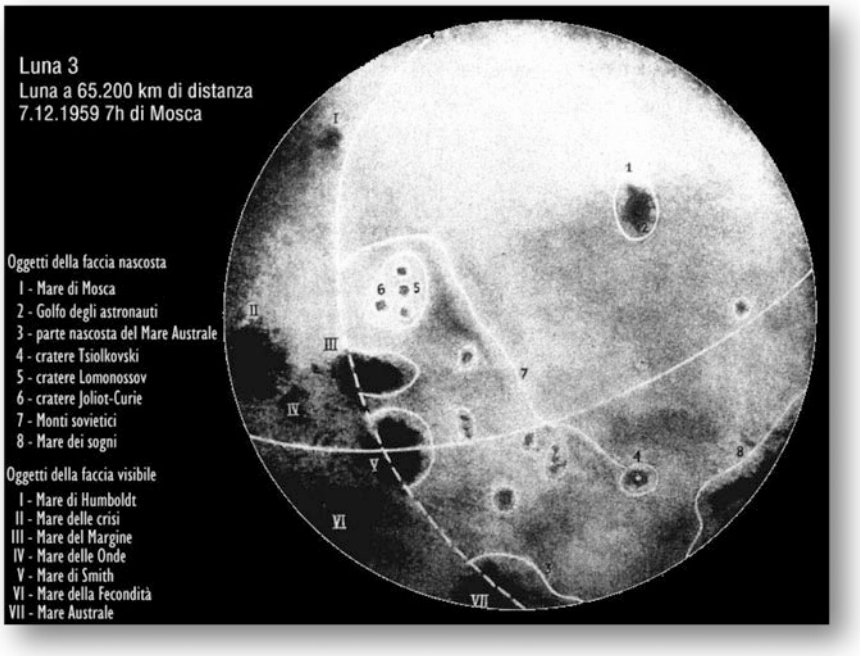

Fig. 11 The dark side of the Moon (from planet.racine.ra.it)

7 Conclusion

After Wittgenstein, philosophy appeared to focus mainly to linguistic analysis; however developments in science and technology reopened some concepts, like space and time versus a new philosophical thought (Hawking 2006), again both had to do with Geodesy and Geomatics. Indeed sometimes, it happens, that different disciplines find their close interaction, when searching for high accuracy measurement. This is the case of the relationship between the geodetic measurements of the heights and the metrology of time and frequency, leading towards a realistic scenario of relativistic geodesy. Therefore the geographical universe isn't just the information supplied by maps, the spatial isn't just the visible, the temporal isn't an independent domain and not all users see the world through the same eyes. Geography is no more than History in space, as well as History is Geography in time.

Geomatics, e.g. space geodesy, image analysis and GIS, deals with the concepts of space and time: for example, space-time integration, mapping starting from different cultural viewpoints about space and time, different scenario investigation, etc. Ideas remain ideas and have no claim to absolute truth, so that truth can only be sought step by step, but convergence isn't granted (Fig. 11).

References

Abbagnano N (1982a) Storia della filosofia, vol 1. UTET, Torino
Abbagnano N (1982b) Storia della filosofia, vol 2. UTET, Torino
Abbagnano N (1982c) Storia della filosofia, vol 3. UTET, Torino
Brotton J (2013) A history of the World in twelve maps. Penguin Books, London
Cassirer E (2015) I problem filosofici della Teoria della Relatività. Mimesis
Chomsky N, Hauser M, Fitch T (2002) The faculty of language. Science, Vol 298
De Santillana G, Von Dechend H (2011) Il mulino di Amleto. Adelphi Edizioni, Milano
Hawking S (2006) La grande storia del tempo. Feltrinelli, Milano
Heisenberg W (1994) Fisica e filosofia. IL Saggiatore, Milano
Husserl E (2008) La crisi delle scienze europee e la fenomenologia trascendentale. il Saggiatore. Milano
Kant I (1999) Géographie. Aubier, Paris
Odifreddi P (2010) C'è spazio per tutti. Mondadori, Milano
Popper K (1970) Logica della scoperta scientifica. Einaudi, Torino
Rovelli C (2014) Che cos'è la scienza. La Rivoluzione di Anassimandro. Mondadori, Milano

Estimating Crustal Deformations by GNSS Time Series Data Analysis

Riccardo Barzaghi, Barbara Betti and Carlo Iapige De Gaetani

Abstract Crustal deformation analysis in seismogenic areas is one of the most important applications of GNSS. In the last twenty years, the GNSS technology has opened new perspectives in this field allowing the estimation of the crustal deformation at different scales both in time and in space. Tectonic deformations can be reliably estimated either at regional and fault scale. This allows the analysis of the different phases of the seismic cycle. Particularly, co-seismic and post-seismic deformations can be properly evaluated. Also, recent studies aim at studying the inter-seismic phase giving important insights in the dynamic of the crust in seismic prone areas. These studies are commonly based on the analysis of time series from GNSS permanent stations. In this paper, a method for filtering these data is presented and a case study based on the FReDNet data is illustrated.

Keywords GNSS permanent stations · Crustal deformations · Seismic areas

1 Introduction

The analysis of crustal deformations plays an important role in studies related to the whole seismic cycle. Co-seismic, post-seismic and inter-seismic crustal deformations can be reliably estimated using daily coordinates time series from GNSS permanent stations. Many seismogenic areas are monitored in this way. As an example, one can mention the Southern California Integrated GPS Network (SCIGN) that has been completed in 2001 and consists of more than 250 stations (Hudnut et al. 2002).

R. Barzaghi (✉) · B. Betti · C.I. De Gaetani
DICA-Politecnico di Milano, Piazza Leonardo da Vinci 32, 20133 Milan, Italy
e-mail: riccardo.barzaghi@polimi.it

B. Betti
e-mail: barbara.betti@polimi.it

C.I. De Gaetani
e-mail: carloiapige.degaetani@polimi.it

R. Cefalo et al. (eds.), *New Advanced GNSS and 3D Spatial Techniques*,
Lecture Notes in Geoinformation and Cartography,
DOI 10.1007/978-3-319-56218-6_3

In Italy, the Istituto Nazionale di Geofisica e Vulcanologia (INGV) has established the Rete Integrata Nazionale GPS (RING) with more than 180 stations (Avallone et al. 2010) and the Istituto Nazionale di Oceanografia e di Geofisica Sperimentale (OGS) has implemented the FReDNet in the North-East Alpine area (Zuliani et al. 2003).

GNSS permanent stations for deformation analysis are carefully monumented to properly detect crustal deformations. Deep-drilled brace are frequently used in order to couple the GNSS antenna to ground in a stable way (http://www.unavco.org).

Besides a careful monument setting, a detailed data analysis must be carried out in order to properly estimate the crustal movements.

The most common parametric model that is used in analysing the coordinate components $\underline{X} = (x_1, x_2, x_3) = (N, E, Up)$ of the GNSS daily time series is

$$x_i = a + bt + \sum_{k=1}^{N} [A_k \cos(\omega_k t) + B_k \sin(\omega_k t)] + \sum_{j=1}^{M} c_j H(t - t_j) + \varepsilon_i(t) \quad i = 1, 2, 3 \tag{1.1}$$

This model has been proposed by different authors (see e.g. Nikolaidis 2002). The linear term accounts for the station velocity while harmonic components are included to model annual, seasonal and higher frequency time dependent phenomena. Possible discontinuities due to instrument/software and/or reference frame changes are modelled by the terms containing the Heaviside function $H(\cdot)$. By least squares adjustment, the model parameters are estimated assuming different models for the coloured noise $\varepsilon_i(t)$. The most common stochastic models for $\varepsilon_i(t)$ are those presented in Williams (2003) with further implementations in Williams (2008). In these papers, $\varepsilon_i(t)$ is assumed to have a power spectrum that depends on the frequency f according to the formula

$$P(f) \approx f^k \tag{1.2}$$

Based on the value of k, different stochastic process can be described with this model. If k is in the range $-1 \leq k \leq 1$, $\varepsilon_i(t)$ is a stationary stochastic process. For $|k| > 1$ $\varepsilon_i(t)$ is non-stationary (Mandelbrot 1967). Particular cases are for $k = 0$, $k = -1$ and $k = -2$ for which the $\varepsilon_i(t)$ process is, respectively, a White Noise process, a Flicker Noise process or a Random Walk process.

A different time-domain approach has been proposed by Barzaghi et al. (2004) where $\varepsilon_i(t)$ is assumed to be a second order stationary process, ergodic in the mean and in the covariance.

In this case, the parameters estimation is done in a two steps procedure. The first least squares iteration is accomplished by considering that $\varepsilon_i(t)$ is White Noise. The $\varepsilon_i(t)$ least squares residuals are then computed and their stationarity is tested using the generalized KPSS-test (Hobijn et al. 2004). If stationarity condition is satisfied (which currently happens in the authors' experience when removing the linear, annual and semi-annual terms in (1.1)), the empirical auto-covariance of $\varepsilon_i(t)$ is

estimated and then modelled with a proper positive definite model function. Least squares adjustment is then repeated using the derived covariance structure.

Furthermore, using this approach, collocation can be applied for filtering the residuals $\varepsilon_i(t)$. This can be done in order to detect and describe possible high frequency effects that are present in the GNSS coordinates time series (Borghi et al. 2016). In the following this filtering procedure is detailed and applied to GNSS coordinate time series of the FReDNet network.

2 Filtering the GNSS Time Series

The filtering procedure of the GNSS coordinate time series that is proposed in this paper is developed in subsequent steps. At first, a usual outliers rejection is set up and known discontinuities due to e.g. instrumental changes are removed.

The parametric model (1.1) is then estimated assuming White Noise behaviour of $\varepsilon_i(t)$. Least squares residuals are then checked for stationarity by means of KPSS test. As already stated, using a proper parametric model, stationarity of the residuals is ensured. The empirical auto-covariance function is then estimated and fitted with a proper model covariance function, i.e. a positive definite function (Barzaghi and Sansò 1983).

The final estimate of the model parameters is then accomplished in a further least square step that is performed using the proper covariance structure as defined by the model covariance function. Thus, the parametric model is optimally estimated taking into account the existing time correlations.

Starting from the second step least squares residuals, a filtering procedure can be applied. We assume that the residuals $\varepsilon_i(t)$ can be modelled as the sum of a time correlated weakly stationary signal $s_i(t)$ and a white noise (uncorrelated) component $n_i(t)$, independent from $s_i(t)$

$$\varepsilon_i(t) = s_i(t) + n_i(t) \quad i = 1, 2, 3 \tag{2.1}$$

As already pointed out, under these hypotheses, the empirical covariance function of $\varepsilon_i(t)$ can be estimated and modelled. Collocation filtering method (Moritz 1980) can be applied to the residuals in order to estimate the signal component as

$$\hat{s}_i(t) = \sum_{j,k=1}^{N} C(|t - t_k|)[C + \sigma_n^2 I]_{kj}^{-1} \varepsilon_j(t_i) \quad i = 1, 2, 3 \tag{2.2}$$

The filtered component allows defining some coherent behaviour of the residuals that could be related to some crustal deformations (see Fig. 1).

Although this filtering procedure is quite effective, a further smoothing could be required to enhance the low frequency components of the filtered signal. It is in fact

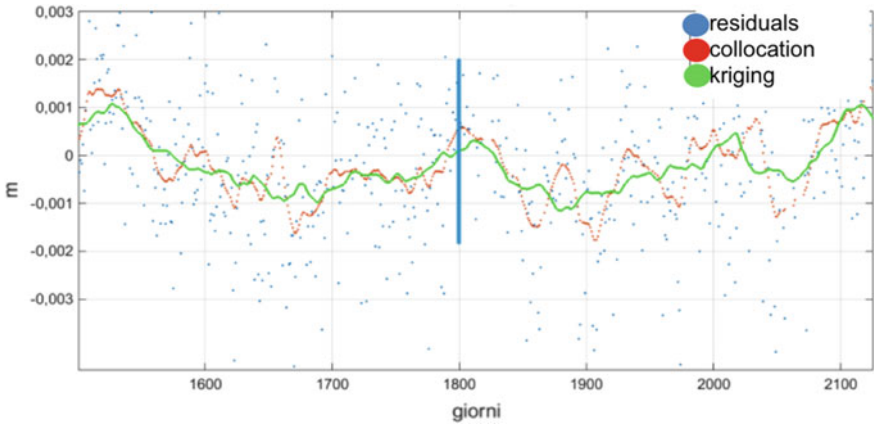

Fig. 1 The least squares residuals and the filtered signals

expected that possible inter-seismic crustal deformations have a smooth behaviour in time. In order to enhance the low frequency component in $\hat{s}_i(t)$ a moving average operator can be applied. As it is well known this is equivalent to low pass filtering in the frequency domain (Bracewell 1986).

This low-pass filtering procedure can be accomplished by kriging moving average (Wackernagel 2003). We considered an amplitude of the sliding time window equal to twice the correlation length of the covariance function $C(\cdot)$ of $\hat{s}_i(t)$ (the correlation length is the distance at which the covariance function is half its value in the origin). The mean value of the signal over each sliding window is computed as

$$\hat{m}_s = \sum_{j=1}^{N} \omega_j \hat{s}_i(t_j) \quad i = 1, 2, 3 \tag{2.3}$$

where N is the number of $\hat{s}_i(t)$ values in the window and the ω_k weights are given as the solution of the system

$$\begin{cases} \sum_{j=1}^{N} \omega_j C(t_i - t_j) - \eta = 0 \\ \sum_{j=1}^{N} \omega_j - 1 = 0 \end{cases} \qquad i = 1, \ldots, N \tag{2.4}$$

The low pass-filtered signal is thus smoother than the original values as it is shown in Fig. 1 (green line).

By using such regularized residuals, analyses on possible transient crustal deformations can be performed effectively since most of the noise sources have been eliminated from the $\varepsilon_i(t)$ residuals. In the following section, the application of this procedure to the FReDNet GNSS time series is discussed.

3 The FReDNet Case Study

The FReDNet network, as already mentioned, is a GNSS network that has been established for estimating the crustal deformation in the Eastern Alpine area. Most of the stations have been recording data for a long time period. In our analysis, we selected thirteen stations that have more than three years of data. They are plotted in Fig. 2 (red stations) together with those having a shorter acquisition period (white stations).

The filtering procedure described in Sect. 2 has been applied to the coordinate components of each station and the filtered residuals in (2.3) have been estimated. In order to investigate if spatially correlated phenomena can be seen in these values, the Principal Component Analysis (PCA) has been applied (Jolliffe 2002). This analysis has been performed on the horizontal components only. For each component, the following matrix Y^k has been set up

$$Y^k = \begin{bmatrix} \hat{m}_1^k(t_1) & \hat{m}_2^k(t_1) & . & . & \hat{m}_p^k(t_1) \\ \hat{m}_1^k(t_2) & \hat{m}_2^k(t_2) & . & . & \hat{m}_p^k(t_2) \\ . & . & . & . & . \\ . & . & . & . & . \\ \hat{m}_1^k(t_N) & \hat{m}_2^k(t_N) & . & . & \hat{m}_p^k(t_N) \end{bmatrix} = \begin{bmatrix} y_{11}^k & y_{12}^k & . & . & y_{1p}^k \\ y_{21}^k & y_{22}^k & . & . & y_{2p}^k \\ . & . & . & . & . \\ . & . & . & . & . \\ y_{N1}^k & y_{N2}^k & . & . & y_{Np}^k \end{bmatrix} \tag{3.1}$$

where k is the component index ($k = 1$ for the North component and for $k = 2$ for the East component), p is the number of considered stations and N the number of days in the time series ($N > p$). By Singular Value Decomposition (SVD) of Y^k one can get

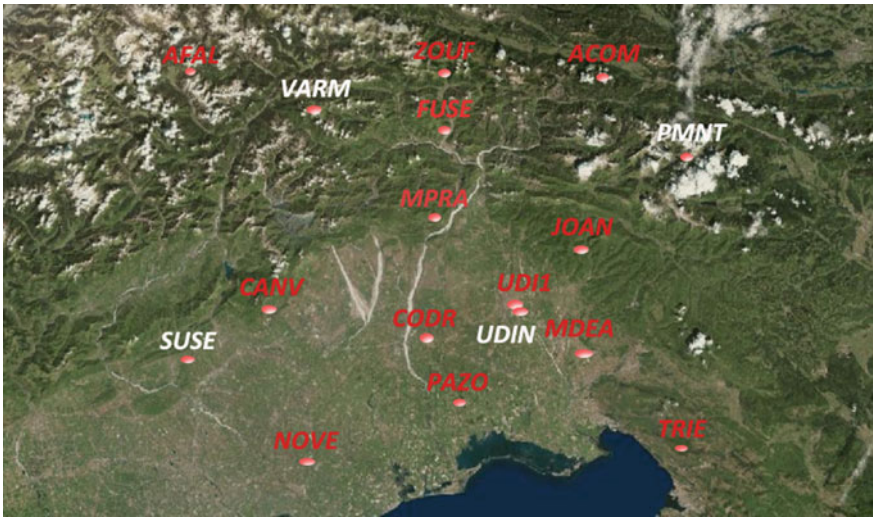

Fig. 2 The stations selected for the analysis (in *red*)

$$Y^k = U^k L^k (V^k)^t \tag{3.2}$$

where U^k and V^k are suitable orthogonal matrices and L^k is a diagonal matrix having dimension equal to the rank r of Y^k. The columns of U^k and V^k are called left and right singular vectors for Y^k and the diagonal elements in L^k are called singular values of Y^k.

By virtue of (3.2), one can write for each component of (3.1)

$$y_{ij}^k = \sum_{m=1}^{r} u_{im}^k l_m^k v_{jm}^k \tag{3.3}$$

Also, by considering only the first most relevant $m < r$ singular values one can obtain the approximation of the elements of Y^k as

$$(\tilde{y}_{ij}^k)^m = \sum_{n=1}^{m} u_{in}^k l_n^k v_{nj}^k \tag{3.4}$$

The PCA is intimately related to SVD of Y^k since it can be proved that U^k, V^k and L^k define also the spectral decomposition of the covariance matrix of Y^k. Thus, by considering the larger m singular values one "explains" most of the variability contained in the covariance matrix of Y^k. In turn, by (3.4) one can also give an estimate of the signals implied by these singular values and see how they reproduce the original y_{ij}^k in (3.1). If some of the y_{ij}^k are properly reproduced using the selected larger singular values, one can also check if they are spatially clustered. In this way, by applying this analysis, one can find cluster of stations (if any) that mainly contribute to the overall variability. Since the signals considered in (3.1) refer to coordinate variations in time, this means that by virtue of this approach clusters of stations with "highly" variable coordinates can be found. Once we are able to detect these clustered stations, a cross-check can be performed with known seismic events and/or known fault systems which can account for this "high" coordinates variability.

The PCA analysis on the selected stations led to the singular values that are plotted in Fig. 3 for the North (left panel) and the East (right panel) components.

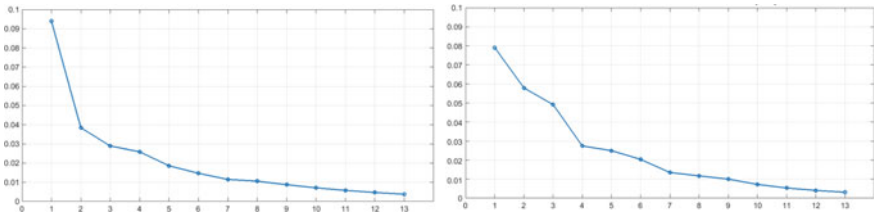

Fig. 3 The PCA singular values for the considered FReDNet stations (North component on the *left*, East component on the *right*)

It can be seen that the first two values in each component are much larger than the remaining (this is particularly true for the North component). If we consider only these values, the signal in (3.4) can reproduce in a very detailed way that of one station only, namely the signal of the CANV station. In Fig. 4, the CANV signal and its approximation (3.4) obtained with the first singular value are represented: the agreement of the two signals is striking.

The same doesn't hold for the remaining stations. As an example, the signals of the NOVE station are displayed in Fig. 5.

Thus, the main variation in the covariance matrices is then given by the CANV station. This means that, in the analysed period, this station has highly varying coordinates. In recent studies, it has been proved that this variability is given by a local effect related to groundwater storage in the Cansiglio plateau area (Devoti et al. 2015). Hence, the proposed analysis proved to be effective since one physical phenomena was spatially related to a given station.

If we now remove the CANV station and repeat the same analysis on the twelve remaining stations, we have no sharp differences among the singular values. The filtered signals based on the larger singular values don't cluster so clearly in a specific area. There are however some (weak) indications of a better fit between the original signals and the filtered ones (using only the two larger singular values in each component) in the SE area where an earthquake occurred on December 6th, 2011 (the Gradisca d'Isonzo 0.8-magnitude seismic event).

If the original signals of the stations clustered in the PCA analysis are inspected, one can see that on that date, some coordinate variations are present. As an example, the East components of MDEA and TRIE (which are the closest stations

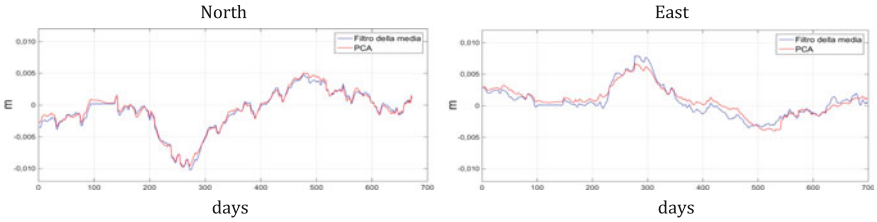

Fig. 4 The PCA analysis on the CANV station signals (*blue* original values; *red* PCA signal)

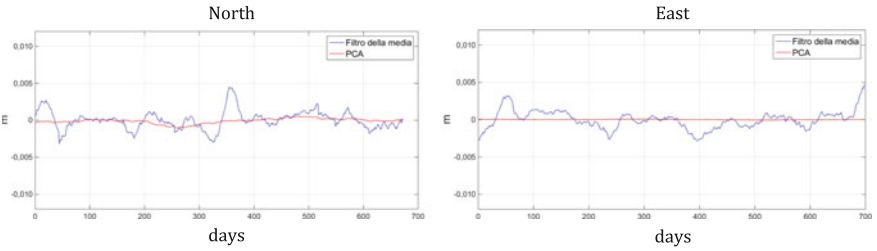

Fig. 5 The PCA analysis on the NOVE station signals (*blue* original values; *red* PCA signal)

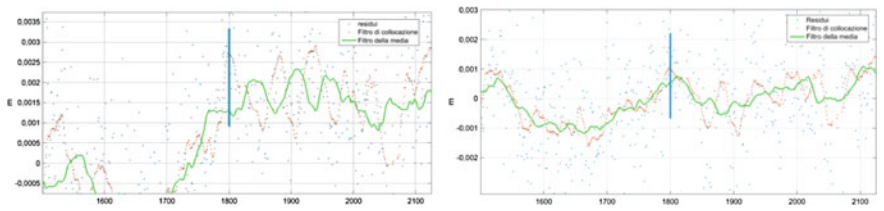

Fig. 6 The TRIE (*left panel*) and MDEA (*right panel*) filtered East component residuals and the Gradisca d'Isonzo seismic event (*blue line*)

to Gradisca d'Isonzo) are plotted in Fig. 6. On December 6th, 2011 (blue line), they both display a common high signal variability.

4 Conclusions

In the last twenty years, GNSS technology has opened new perspectives in the geophysical investigations. Particularly, the crustal deformations can be nowadays estimated with high accuracy and precision. In this respect, an invaluable role is played by the GNSS permanent stations designed for monitoring crustal movements. The analysis of the coordinate time series allows describing the entire seismic cycle in seismogenic areas. The filtering procedure that has been proposed in this paper proved to be effective and able to spatially cluster permanent stations having common behaviour. In the FReDNet case study, two different physical phenomena were identified. In the first analysis step, a groundwater storage effect in the Cansiglio area has been evidenced. The subsequent analysis allowed identifying a cluster of stations possibly related to a 0.8-magnitude seismic event in the Gradisca d'Isonzo area. Further investigations are needed to prove that this procedure can reveal other geophysical relevant phenomena related to the inter-seismic phase such as, e.g., aseismic transient slip events.

Acknowledgements The authors wish to thank Dr. David Zuliani and Dr. Giuliana Rossi of the National Institute of Oceanography and Experimental Geophysics (OGS) for providing the FReDNet GNSS time series data.

References

Avallone A, Selvaggi G, D'Anastasio E, D'Agostino N, Pietrantonio G, Riguzzi F, Serpelloni E, Anzidei M, Casula G, Cecere G, D'Ambrosio C, De Martino P, Devoti R, Falco L, Mattia M, Rossi M, Tammaro U, Zarrilli L (2010) The RING network: improvement of a GPS velocity field in Central Mediterranean. Ann Geophys 53:2

Barzaghi R, Sansò F (1983) Sulla stima empirica della funzione di covarianza. Bollettino di Geodesia e Scienze Affini, n. 4

Barzaghi R, Borghi A, Crespi M, Pietrantonio G, Riguzzi F (2004) GPS permanent network solution: the impact of temporal correlation. In: Sansò F (ed) International association of geodesy symposia, vol 127, pp 179–183

Borghi A, Aoudia A, Javed F, Barzaghi R (2016) Precursory slow-slip loaded the 2009 L'Aquila earthquake sequence. GJI. doi:10.1093/gji/ggw046

Bracewell RN (1986) The Fourier transform and its applications. McGraw-Hill Book Company, New York

Devoti R, Zuliani D, Braitenberg C, Fabris P, Grillo B (2015) Hydrologically induced slope deformations detected by GPS and clinometric surveys in the Cansiglio Plateau, Southern Alps. Earth Planet Sci Lett 419(2015):134–142 (Elsevier)

Hobijn B, Franses PH, Ooms M (2004) Generalization of the KPSS-test for stationarity. Stat Neerl 58(4):483–502

Hudnut KW, Bock Y, Galetzka JE, Webb FH, Young WH (2002) The Southern California integrated GPS network (SCIGN). In: Fujinawa Y, Youshida Y (eds) Seismotectonics in convergent plate boundary. Terra Scientific Publishing Company (TERRAPUB), Tokyo

Jolliffe IT (2002) Principal component analysis, 2nd edn. Springer-Verlag, New York, Berlin, Heidelberg

Mandelbrot B (1967) Some noises with 1/f spectrum, a bridge between direct current and white noise. IEEE Trans Inf Theory 13(2):289–298

Moritz H (1980) Advanced physical geodesy. Herbert Wichmann Verlag, Karlsruhe

Nikolaidis R (2002) Observation of geodetic and seismic deformation with the global positioning system. Ph.D. thesis

Zuliani D, Battaglia M, Murray M, Marson I (2003) FReDNet: a Continuous GPS geodetic network monitoring crustal deformation in NE Italy. EOS 84(28)

Wackernagel H (2003) Multivariate geostatistics: an introduction with applications, 3rd edn. Springer-Verlag, Berlin

Williams SDP (2003) The effect of coloured noise on the uncertainties of rates estimated from geodetic time series. J Geodesy 76:483–494

Williams SDP (2008) CATS: GPS coordinate time series analysis software. J Geodesy 12 (2/March). doi:10.1007/s10291-007-0086-4

The Actual Perspectives of GNSS Multi-constellation Services and Receivers for Kinematic Applications

Raffaela Cefalo, Mauro Calderan, Francesco Filippi, Cristoforo Montefusco, Andrea Piemonte and Tatiana Sluga

Abstract 11 years ago, on 28 December 2005, was launched the Europe's very first navigation satellite, GIOVE-A (Galileo In-Orbit Validation Element-A), thus starting the deployment of Galileo, the EU's own global satellite navigation system. The deployment phase of Galileo suffered of many difficulties and delays but recently the Programme has been accelerated and, in the last months, the pace of deploying Europe's own satellite navigation system continued to increase with the launch of the 18th Galileo satellite, on 17 November 2016. It is expected that the system will be fully operational by 2020, with actual implementation costs in the range of 5.23 billion of euros and 7 billion foreseen till 2020 for EGNOS e Galileo Projects. The excellent performances of Galileo satellites, as measured on the ground, "allows Europe to join the club of the worldwide providers of satellite navigation services". Galileo will be integrated by EGNOS (European Geostationary Navigation Overlay service). Consisting of three geostationary

R. Cefalo (✉) · M. Calderan · T. Sluga
GeoSNav Lab, Department of Engineering and Architecture,
University of Trieste, via Valerio 6/2, 34127 Trieste, Italy
e-mail: raffaela.cefalo@dia.units.it

M. Calderan
e-mail: mauro.calderan@iuav.it

T. Sluga
e-mail: tatiana.sluga@gmail.com

F. Filippi
Department of Engineering and Architecture, University of Trieste,
via Valerio 6/2, 34127 Trieste, Italy
e-mail: francesco.filippi@dia.units.it

C. Montefusco
Enav S.p.A, via Salaria 716, 00138 Rome, Italy
e-mail: cristoforo.montefusco@enav.it

A. Piemonte
Department of Civil and Industrial Engineering, University of Pisa,
Largo Lucio Lazzarino 1, 56122 Pisa, Italy
e-mail: andrea.piemonte@unipi.it

R. Cefalo et al. (eds.), *New Advanced GNSS and 3D Spatial Techniques*,
Lecture Notes in Geoinformation and Cartography,
DOI 10.1007/978-3-319-56218-6_4

satellites and a network of ground stations, EGNOS achieves its aim by transmitting a signal containing information on the reliability and accuracy of the positioning signals sent out by GPS. It allows users, in Europe and beyond, to determine their position to within 1.5 m (1σ). Since the first signals became available to users, demonstrations have shown the usefulness of EGNOS services in every type of kinematic application, in the aerial, maritime and terrestrial domain. As part of 'GIANT' (GNSS Introduction in the AviatioN sector), tests have proved the benefits of EGNOS when landing at airports with fewer aids or when helicopters make emergency landings. The integrity data provided by EGNOS is particularly suited for applications driven by stringent safety constraints during critical navigation phases such as landing aircraft, manoeuvring ships in narrow channels, and tracking the precise locations of trains. Actually many applications are based on EGNOS, and the Open Service (OS), available since October 2009, is widely used in the agricultural world, where it has proved valuable for reducing the use of fertilisers, thus helping to protect the environment. The accuracy of the Open Service has also proved useful to guide blind people in the city via mobile phones—like car drivers using GPS. Towards the certification of the Safety of Life service, many tests have been performed in the aviation, maritime and rail sectors. Mapping of fixed assets, controlling mining machinery and other professional uses are potential applications that could benefit from the EGNOS Commercial Data. Demonstrations showing the potential of EGNOS have been performed in many other sectors and many applications are just waiting to be thought of, such as for rail, road and maritime users. The European Commission (EC) estimates that 6–7% of European GDP (Gross Domestic Product)—around 800 billion by value—is already dependent on satellite navigation. Any GNSS device available on the marked is able to receive GPS, GLONASS and EGNOS signals and globally 40% of GNSS receivers are ready to receive Galileo signals. Multi-constellation services and receivers are used by millions of persons in the world, being part of their daily life, towards a future where geo-localisation of persons and things will become essential for safety and well-being. In this paper the current trend and benefits of multi-constellation services and receivers as well as innovative kinematic research applications, carried out by GeoSNav Lab, Department of Engineering and Architecture, University of Trieste, research team, using multi-constellation receivers, are presented.

Keywords GNSS · Galileo · Multi-constellation · Kinematic · Cable cars

1 Introduction

GNSS is used around the globe for many type of professional and safety-critical applications, each requiring different service levels (Open Service, Safety of Life, Search and Rescue), with 3.6 bln GNSS devices in use in 2014. By 2019, this is forecasted to increase to over 7 bln—for an average of one device per person on the planet (GSA Market Report, issue 4, March 2015). In Fig. 1 a prediction of the

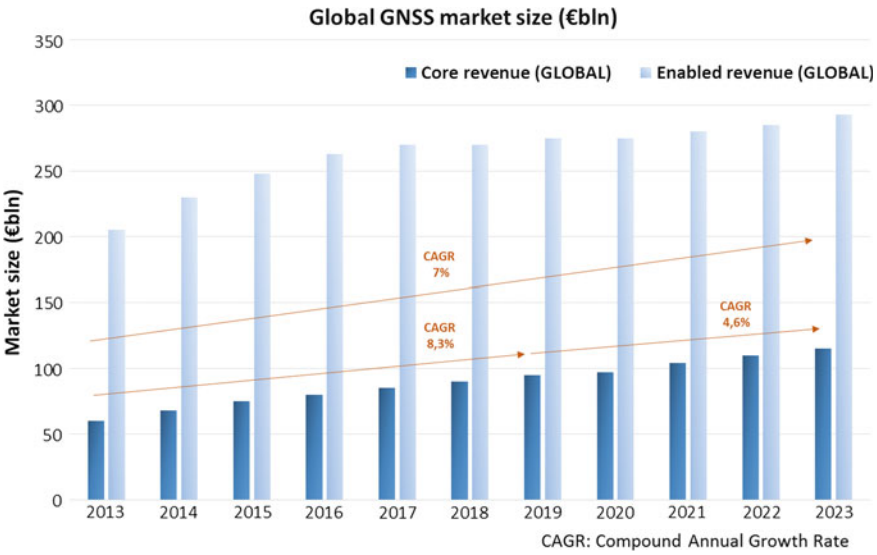

Fig. 1 Global GNSS market in €bln for core and enabled revenues; the mean CAGR (Compound Annual Growth Rate) estimated in 10 years (2013–2023) is in the range of 7% (adapted from: GSA Market Report, issue 4, March 2015)

Global GNSS market size in €bln for core and enabled global revenues, is presented: the mean CAGR (Compound Annual Growth Rate) estimated in 10 years (2013–2023) is in the range of 7%. A higher growth rate in the range of 8.3% has been estimated for the period 2013–2019 and a lower growth rate of 4.6% for the period 2019–2023 (GSA Market Report, issue 4, March 2015).

Thanks to its easy implementation for various smart mobility and LBS (Location-Based Service) applications, GNSS is supporting the smart cities concept. GNSS delivers location information regardless of the environment, can be part of autonomous driving solutions, travel optimisation and automatic transactions. Novel technologies, like IoT (Internet-of-Things) could provide a significant knock-on demand for GNSS capabilities in several market segments.

Applications in LBS and road segments dominate the cumulative revenue, with a total combined of more than 91% (GSA Market Report, issue 4, March 2015) (Fig. 2).

The LBS market continues to grow, with high-end devices now commonly making use of multi-constellation and hybrid positioning, obtained integrating GNSS with other positioning sensors, in particular dead reckoning/INS systems.

More advanced GNSS receivers also use inertial sensors and odometry information to improve the positioning solution, particularly in adverse environments.

GNSS multi-constellation RTK techniques allows real time kinematic applications in difficult environments (urban canyons, strict or partially covered areas, etc.) in different fields: road cadaster, construction sites and archaeological areas (Datta 2016; Li et al. 2015; Mattos and Pisoni 2014; GNSS User Technology Report, issue 1, European GNSS Agency 2016).

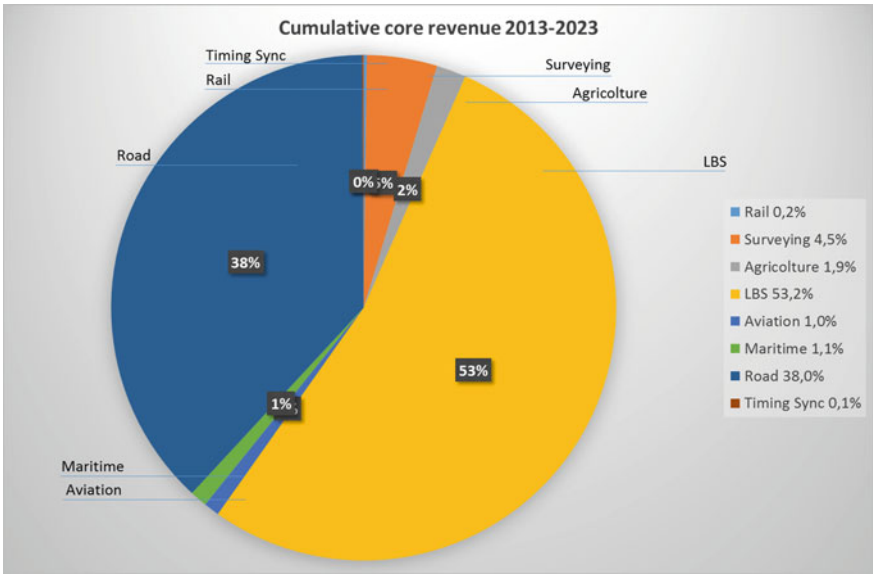

Fig. 2 Cumulative GNSS core revenue 2013–2023 in different sectors (adapted from: GSA Market Report, issue 4, March 2015)

The top four benefits of using signals from more than one GNSS are: increased accuracy, integrity, service availability and continuity of service.

In challenging environments, such as urban areas, many signals suffer no good reception or multipath interference. With multi-constellation GNSS, the best signals may be selected for a navigation solution, thus increasing the accuracy.

Moreover, multi-constellation GNSS brings a significant improvement in the proportion of space and time over which sufficient signals are available without interruption to compute a position solution.

Signal diversity and redundant measurements, together with better geometry from multiple GNSS satellites, allow improved receiver-based integrity monitoring to be carried out, including the detection of multiple satellite/signal failures. The ability of a GNSS receiver to handle multiple frequencies from multiple constellations in the calculation of position is essential to optimal error resolution (Datta 2016; Multi-GNSS Integration, NovAtel Inc.; Multi-Constellation and Multi-Frequency; Groves 2012).

These terms are equally applicable across all domains, starting from terrestrial, maritime and aerial navigation to ionospheric and tropospheric advanced studies.

A multi-constellation receiver can access signals from several constellations: GPS, GLONASS, BeiDou and Galileo for example. The use of other constellations in addition to GPS, results in there being a larger number of satellites in the field of view, which has the following benefits:

– Reduced signal acquisition time.
– Improved position and time accuracy.
– Reduction of problems caused by obstructions such as buildings and foliage.
– Improved spatial distribution of visible satellites, resulting in improved PDOP (Positioning Dilution of Precision) parameters.

When a receiver utilizes signals from a variety of constellations, redundancy is built into the solution. If a signal is blocked due to the working environment, the receiver can use a signal from another constellation, thus ensuring solution continuity. While extremely rare, if a GNSS system fails, there are other systems available.

To determine a position in GPS-only mode, a receiver must track a minimum of four satellites. In multi-constellation mode, the receiver must track five satellites, at least one of which must be from a satellite in the other constellation, so the receiver can determine the time offset between constellations.

Today nearly half of all available mobile applications use location information, a trend that will continue to increase in the near future.

Nearly 65% of GNSS receivers available today are multi-constellation, with more than 20% supporting four constellations. More than 60% of receivers also include SBAS (Satellite Based Augmentation System), either for higher accuracy or integrity.

New signal designs bring significant benefits: improved accuracy, improved multipath mitigation and improved sensitivity.

GSA (European GNSS Agency) together with ESA (European Space Agency) organized a test campaign of GNSS chipsets, highlighting the performance improvements enabled by multi-constellation capability (GNSS User Technology Report, issue 1, European GNSS Agency 2016).

In the following paragraph, some recent developments carried out at the Department of Engineering and Architecture, University of Trieste, using multi-constellation GNSS receivers will be presented.

2 An Experimental Innovative Multi-constellation Architecture Implementation and Related Kinematic Applications

2.1 GeoSNav Experimental System (GES) and User Application Software (UAS)

The implementation of the EGNOS Message Server (EMS) and the opportunities at the beginning offered by the SISNeT (Signal-In-Space through the InterNet) (Torán-Martí and Ventura Traveset 2002; Torán-Martí et al. 2002) and actually by EDAS technology (Torán-Martí and Ventura Traveset 2005) have encouraged the development of a number of applications within the GNSS users community.

One possible application is to provide GNSS users with the best available correction data for their GPS measurements within the area of operations. Corrections can be based on: SBAS, RTCM (Radio Technical Commission Maritime) and RTK (Real Time Kinematic) (RTCA 2001) data.

The aims are to make all correction data available on a Data Server, allowing GNSS users to access this server through a communication link and download the desired corrections. In this way GNSS users, depending on the application and on the operation area, can always benefit of the best available corrections.

An experimental Data Server making available at the same time the EGNOS augmentation messages as well as RTCM and RTK differential corrections computed by dedicated GNSS receivers located at a known reference position, has been initially set up at GeoSNav Lab (Geodesy and Satellite Navigation Laboratory), Department of Engineering and Architecture, University of Trieste, Italy in 2006 (a first prototype of this architecture was presented in Calderan et al. 2004 and Calderan and Cefalo 2005) (Fig. 3). Recently, new functionalities have been added (and partially presented in: Cefalo et al. 2014).

The experimental Data Server, located at GeoSNav Lab, University of Trieste, receives the data from two Novatel MiLLennium GNSS (GPS + EGNOS) receivers, connected by a splitter to the same geodetic choke-ring antenna. The antenna is located on the roof of a building at the Department of Engineering and Architecture, at a georeferenced and stable position.

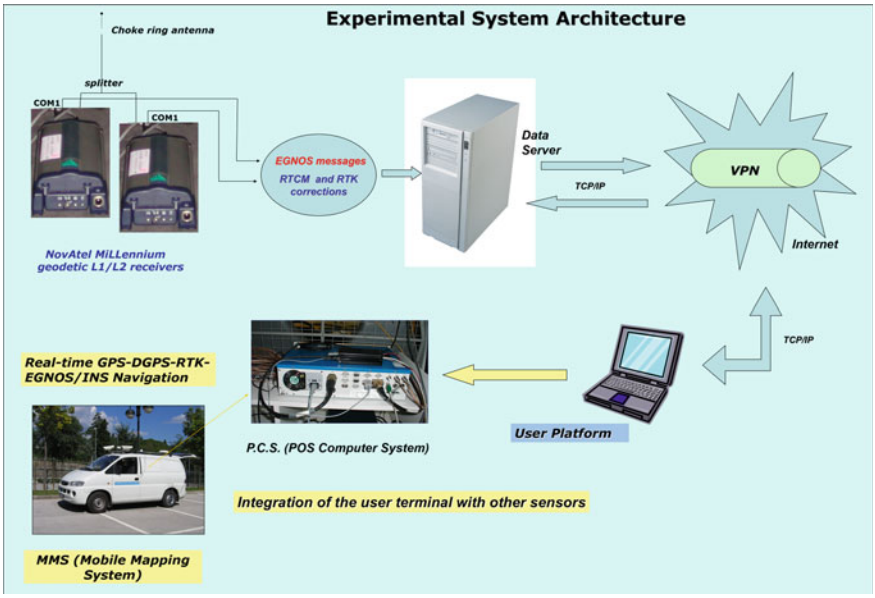

Fig. 3 The GeoSNav Experimental System (GES) Architecture implemented at GeoSNav Lab, Department of Engineering and Architecture, University of Trieste, Italy

All the corrections available on the Data Server are made accessible via VPN (Virtual Protected Network) through the Internet to authorized users equipped with an integrated GPS/GPRS terminal.

Depending on the operational conditions and on the operation area (distance from reference stations/visibility of EGNOS satellites), the user can choose the augmentation to be included in the computation of position, velocity and time.

The research project encompassed the following steps:

- Implementation of a UAS (User Application Software) capable to access the EGNOS WADGNSS (Wide Area Differential GNSS) messages downloaded by geostationary satellites and send these messages to another device via a VPN (Virtual Protected Network) Internet connection;
- Development of the GeoSNav Lab Data Server and optimization of the user terminal;
- Tests on the availability/accessibility of the EGNOS augmentation messages on the Data Server;
- Test on the communication link between the server and the user terminal;
- Static and dynamics tests to assess the navigation performances of the user terminal and the integration of the user terminal with other sensors;
- New kinematic tests to assess navigation performance improvements and GNSS/INS integration.

Two Novatel MiLLennium GNSS (GPS + EGNOS) receivers were connected to GeoSNav EDS (Experimental Data Server) using two different I/O ports (Figs. 3 and 4).

The graphical interfaces showing real-time SV plots, channel tracking status, SNR, azimuth/zenith SV parameters, command control and positioning status (in various different modes: Stand_alone, 3D and 2D DGPS, RTK and SBAS/EGNOS) can be visible on Server screen in Fig. 4.

Detailed analyses on the achievable performances have been carried out by the Authors, comparing the trajectories surveyed using multi-constellation GNSS (GPS + GLONASS + SBAS/EGNOS) devices with the reference trajectory obtained using a MMS (Mobile Mapping System). The MMS was equipped with 2 GNSS L1/L2 receivers and a high accuracy three-dimensional INS (formed by 3 laser gyros, 3 accelerometers and an odometer connected to the back left wheel of the van). GNSS/INS measurements were integrated in real time using Kalman filtering (POS/LV Applanix system).

In Fig. 5 the graphical interfaces of the implemented GeoSNav UAS (User Application Software), developed by the Authors, developed in C++/Bortland environment, are shown. In Fig. 6 an extract of the GPGGA messages computed by the rover GNSS receiver installed on board the MMS, is presented.

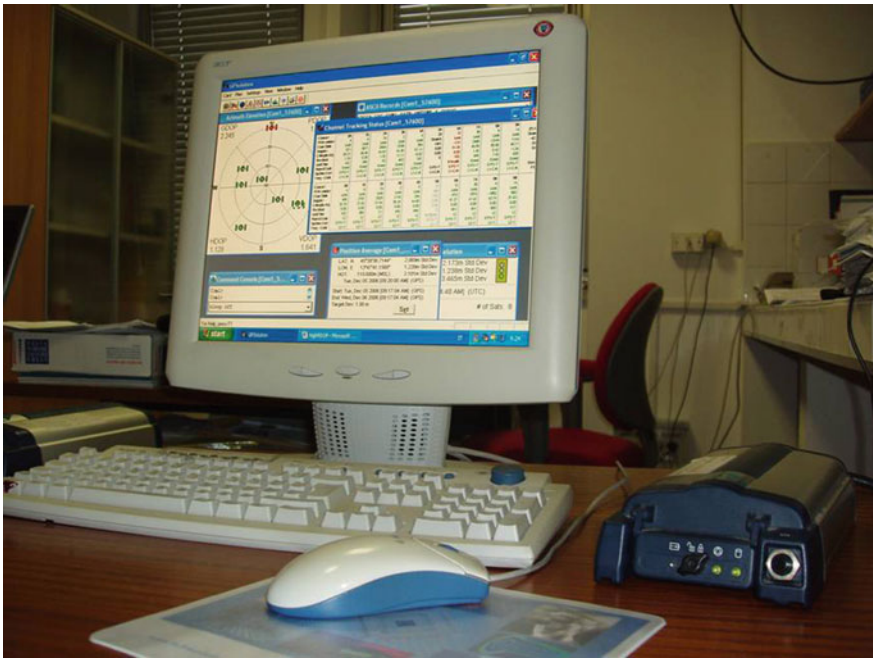

Fig. 4 The Experimental Data Server located at GeoSNav Lab, University of Trieste with the two Novatel MiLLennium GNSS (GPS + SBAS/EGNOS) receivers connected via two I/O ports. On the Server screen are shown the graphical interfaces and the command control and positioning status windows, showing the real-time SV plots, the channel tracking status with azimuth/zenith SV parameters, the signal frequencies, the SNR (Signal to Noise Ratio) parameters, and the tree-dimensional computed coordinates and accuracies

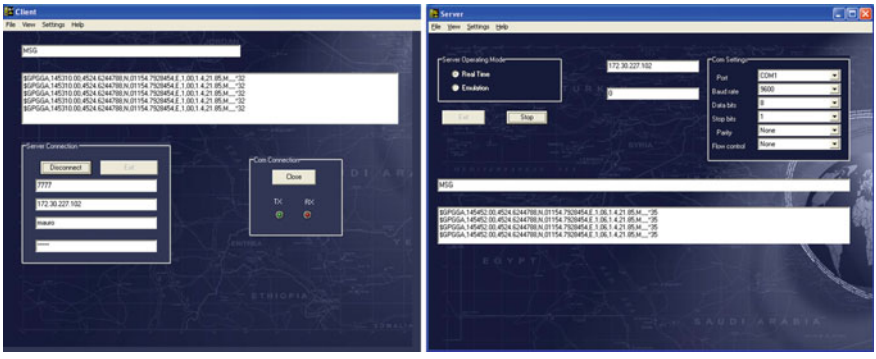

Fig. 5 The Graphical Interfaces of the "GeoSNav COM → TCP SERVER" application implementing the data transfer from the DS to the User Platform

```
$GPGGA,131723.00,4539.6123860,N,01347.6873391,E,9,05,1.6,116.67,M,,,,*04
$GPGGA,131724.00,4539.6122935,N,01347.6872930,E,9,05,1.6,116.82,M,,,,*08
$GPGGA,131725.00,4539.6122765,N,01347.6872205,E,9,05,1.6,117.01,M,,,,*05
$GPGGA,131726.00,4539.6122583,N,01347.6871378,E,9,05,1.6,117.35,M,,,,*03
$GPGGA,131727.00,4539.6122169,N,01347.6871607,E,9,05,1.6,117.59,M,,,,*05
$GPGGA,131728.00,4539.6121151,N,01347.6871835,E,9,06,1.6,118.04,M,,,,*09
$GPGGA,131729.00,4539.6121016,N,01347.6872149,E,9,05,1.6,118.35,M,,,,*0A
$GPGGA,131730.00,4539.6120948,N,01347.6872013,E,9,06,1.6,118.91,M,,,,*02
```

Fig. 6 An extract of the GPGGA messages computed by the rover receiver ("**9**" code means SBAS/EGNOS positioning mode)

2.2 Real Time and Post-processing Applications to Terrestrial Navigation

Jupiter SL 869 and GSM/GPRS GE 910 GNSS (GPS + GLONASS + SBAS/EGNOS) devices, developed by Telit Communications SpA have been installed on board the MMS Gigi-one (GeoSNav Lab, University of Trieste) with their external antennas mounted on the roof of the vehicle. The two tested devices operated in Stand Alone, Assisted and SBAS/EGNOS mode. The location of the external antennas have been accurately georeferenced using a Leica TS30, with a 0.1 mg on angular accuracy (1σ) and 1 mm + 1 ppm accuracy relative to distance measurements.

Several parameters have been computed and analyzed: e.g. TTF (Time to First Fix), 3D coordinates (latitude, longitude, ellipsoidal height then transformed to Gauss-Boaga Easting, Northing coordinates and geoidal heights—EGM96), GDOP (Geodetic Dilution of Precision) and latencies.

These test have been carried out in the framework of the Project "Integration of GALILEO positioning Services into M2M communication systems" coordinated by Telit Communications SpA, to which the Authors took part starting from 2014 until 2016.

In Fig. 7 a detail of the three obtained trajectories, superimposed, after reference system transformations, on Regional (Friuli Venezia Giulia) technical digital cartography (CTRN, nominal scale 1:2000) is presented. In Fig. 8, the trajectories of a new survey were superimposed on remote sensed images using ©Google Earth Web-GIS platform.

The performed tests highlighted the multi-constellation receivers performance benefits in terms of urban canyon availability and accuracy (MMS 3D accuracies in the range of $5 \div 10$ cm, 1σ).

As an example, Fig. 9 plots the Easting, Northing and height differences versus time (s) between the GeoSNav MMS reference trajectory and that one computed using the GNSS (GPS + GLONASS + SBAS/EGNOS) Jupiter SL869 device, for a part of the performed survey.

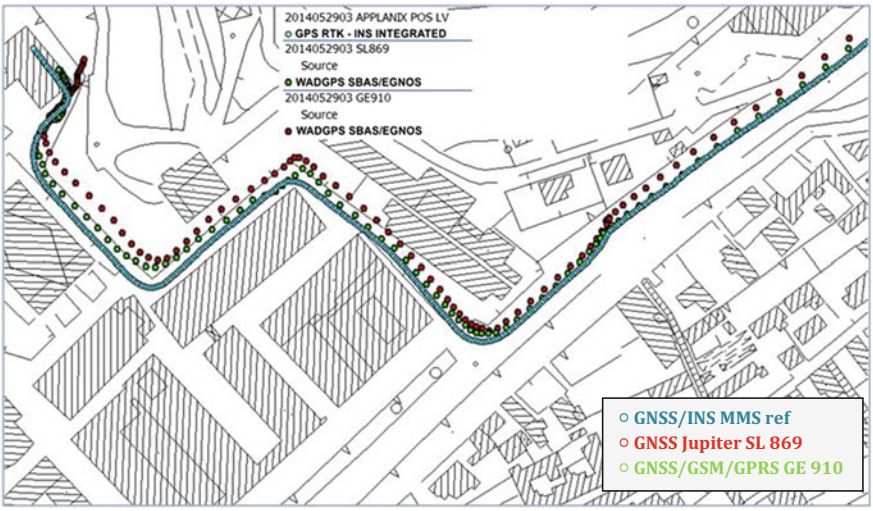

Fig. 7 Superimposition of the three obtained trajectories on Regional Technical Cartography (in *light blue* the GeoSNav Lab MMS reference trajectory, in *red* the trajectory obtained using Telit GNSS Jupiter SL 869 device, in *green* the one obtained using the GNSS/GSM/GPRS GE 910 device)

Fig. 8 A detail of the trajectories simultaneously surveyed using GeoSNav MMS (*green* trajectory), GNSS Jupiter SL869 STD device (*red* trajectory), customized GNSS Jupiter SL869 (*blue* trajectory) and GNSS/GSM/GPRS GE910 (*purple* trajectory) superimposed on ©Google Earth image

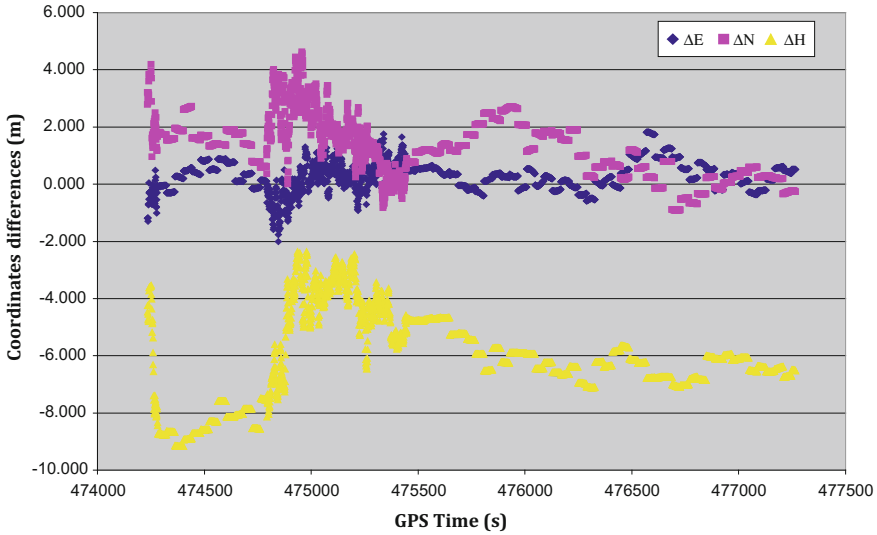

Fig. 9 Positioning data analysis—Easting, Northing and height differences versus time (s) between the GeoSNav MMS reference positions and the ones computed by the GNSS (GPS + GLONASS + SBAS/EGNOS) Jupiter SL869 device

3 Innovative Experimental GNSS/INS Applications to Cable Cars Plants Monitoring for Passengers Safety and Comfort

An innovative and interesting application of kinematic multi-constellation GNSS is related to the study of the dynamic oscillations of cable cars plants, with the aim of analyzing passenger's safety and comfort.

This original research has been developed by the Authors and performed in the framework of a National FRA Project titled "Applications of innovative GNSS/INS technologies to the monitoring of cable car plants for passengers safety", co-funded by the University of Trieste, Italy, during 2013–2015.

Different plants in Friuli Venezia Giulia and Veneto regions, Italy, were surveyed together with technicians and researchers of the Department of Engineering and Architecture, University of Trieste and the Department of Civil and Industrial Engineering, University of Pisa, Italy (Cefalo et al. 2013).

GNSS measurements, in a further step integrated by high accuracy INS, gave the instantaneous 3D positioning of the cabins so to reconstruct the catenary shape (Fig. 10) and the cabins vertical oscillations due to sudden breaks (Fig. 11). The results obtained in post-processing an in real-time by different geodetic GNSS (GPS + GLONASS) receivers (Topcon Hiper Pro and Legacy, and GS14 Leica receivers) have been compared.

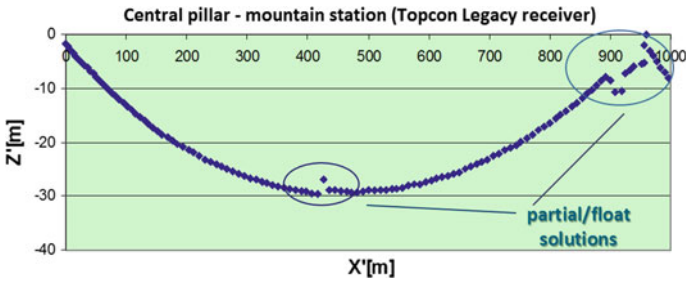

Fig. 10 Funifor cable car plant, Ravascletto (UD), Italy: catenary shape reconstruction of the tract from the plant central pillar to the mountain station, using post-processed 1 Hz GNSS measurements acquired by a Topcon Legacy GPS + GLONASS high frequency receiver. In the *blue ellipses* are shown the partial/float solutions due to signal losses caused by the obstacles (Cefalo et al. 2014)

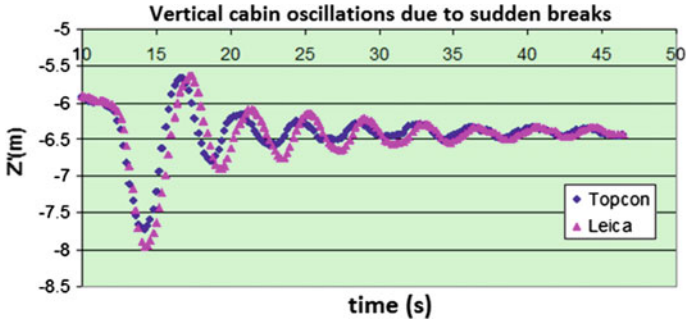

Fig. 11 Real-time and post-processed vertical cabin oscillations due to a simulated emergency break: in *blue* the post-processed trajectory computed using the Topcon Legacy GPS + GLONASS receiver; in *purple* the real-time trajectory computed using a Leica GS14 GPS + GLONASS + BEIDOU receiver (Cefalo et al. 2014)

Due to the stringent norms that need to be fulfilled by these kind of plants, such measurements are important to verify safety parameters during the operative phases and analyze the passenger comfort, in particular dynamic conditions.

As a further development of these researches, the Author will optimize the GNSS/INS/other sensors integration and propose possible updates of the national and European norms, taking full advantage of EGNSS (European GNSS)/INS measurements in order to verify the design solutions and validate different dynamic parameters in real operative conditions.

4 Conclusions

The benefits of GNSS multi-constellation services in different domains is actually evident and will become more and more important in the near future, in particular after the full deployment of the European Galileo System.

The integration of multi-constellation GNSS receivers with other sensors will facilitate the use of satellite techniques in novel application domains, increasing mobility and safety.

Furthermore the decrease in device costs will guarantee the spreading of these technologies between different user categories.

This will encourage novel applications and synergies between GNSS and other European services in different domains (i.e. efficient agriculture, automated machine guidance, precision farming and machine control, surveying and mapping, land and marine survey, cadastral and geodesy, construction and so on) with improved accuracies and performances and increasing consciousness on geo-referencing and timing evolving user needs.

References

An introduction to GNSS—GPS, GLONASS, Beidou, GALILEO and other Global Navigation Satellite Systems—Multi-constellation and Multi-frequency. NovAtel Inc. http://www.novatel.com/an-introduction-to-gnss/chapter-5-resolving-errors/multi-constellation-and-multi-frequency/

Calderan M, Cefalo R (2005) Real time car navigation using WADGPS (wide area differential GPS) corrections through SISNeT (signal in space through internet). In: Proceedings of the EGNOS workshop, Gdynia, Poland, 27–28 Oct 2005

Calderan M, Cefalo R, Montefusco C (2004) From ESTB to EGNOS: overview on the development of the first European Satellite Based Augmentation System. Reports on Geodesy Issue 1-2004—Institute of Geodesy and Geodetic Astronomy, University of Technology Warsaw, Poland, Jan 2004

Cefalo R, Piemonte A, Sciuto G (2013) Applicazione di tecniche topografiche e satellitari per il collaudo di impianti funiviari. BOLLETTINO DELLA SOCIETÀ ITALIANA DI FOTOGRAMMETRIA E TOPOGRAFIA 4(2013):25–34. ISSN: 1721-971X

Cefalo R, Calderan M, Piemonte A (2014) Development and application of an experimental Data Server hosting EGNOS and RTCM/RTK correction data for terrestrial navigation. United Nations ICG/ICTP workshop on GNSS, International Centre for Theoretical Physics, Trieste, 1–4 Dec 2014. http://indico.ictp.it/event/a13233/session/20/contribution/45/material/1/0.pdf

Datta A (2016) Multi-constellation GNSS receivers becoming a standard (2016) Geospatial World, 6 Oct 2016. https://www.geospatialworld.net/multi-constellation-gnss-receivers-norm/

EGNOS for Professionals web site: http://www.esa.int/navigation/egnos-pro

EGNOS web site: http://www.esa.int/navigation

GNSS User Technology Report, issue 1, European GNSS Agency (2016) www.gsa.europa.eu

Groves P, Ochieng W, Feng S, Kale I (2012) Multi-GNSS integration: the challenges of diversity. With GNSS, the more, the merrier—true or false? InsideGNSS, May/June 2012. http://www.insidegnss.com/node/3092

GSA Market Report, issue 4, March 2015, ISBN 978-92-9206-013-8. www.gsa.europa.eu

Li X, Zhang X, Ren X, Fritsche M, Wickert J, Schuh H (2015) Precise positioning with current multi-constellation global navigation satellite systems: GPS, GLONASS, Galileo and BeiDou. Sci Rep 5:8328

Mattos PG, Pisoni F (2014) Quad-constellation receiver: GPS, GLONASS, Galileo, BeiDou. In: GPS world, 1 Jan 2014. http://gpsworld.com/quad-constellation-receiver-gps-glonass-galileo-beidou/

MiLLennium GPSCard Software Versions 4.503 and 4.52, NovAtel Inc, OM-20000053 Rev 2, 2001/01/16, http://www.novatel.com/assets/Documents/Manuals/om-20000053.pdf

RTCA (2001) Minimum operational performance standards for global positioning system/Wide area augmentation system airborne equipment. Ref. RTCA/DO-229C, Nov 2001

Torán-Martí F, Dr. Ventura-Traveset J (2002) EGNOS performances in urban areas using the ESA SISNeT technology: advanced modelling of user masking effects. Doc. Ref. E-TN-PFM-E-0029-ESA, Apr 2002

Torán-Martí F, Dr. Ventura-Traveset J (2005) The EGNOS data access system (EDAS) the access point to the EGNOS products in real-time for multi-modal service provision. In: Proceedings of the GNSS 2005 Munich, Germany, July 2005

Torán-Martí F, Ventura-Traveset J, Chen R (2002) The ESA SISNeT technology: real-time access to the EGNOS services through wireless networks and the internet. In: Proceedings of the ION GPS, Portland, Oregon USA, 24–27 Sept 2002

Monitoring of the Italian GNSS Geodetic Reference Frame

Maurizio Barbarella, Stefano Gandolfi and Luca Tavasci

Abstract In 2011, Italy established a new geodetic reference system, the European Terrestrial Reference System 1989 (ETRS89), which was based upon the ETRF2000 reference frame at epoch 2008.0. In order to maintain this reference, the IGMI defined a permanent GNSS network within the EPN densification project, known as the "Rete Dinamica Nazionale" (RDN) and composed of 99 tracking stations located in and around Italy. Eight years of data are now available and the aim of this work is to estimate the velocities of the official RDN sites. It was necessary to pre-analyze the data accurately because of the incomplete maintenance of the associated repository. The network was calculated using a PPP approach and applying the GIPSY-OASIS II software package, and the solutions were aligned to ITRS using a customized procedure. After they were transformed into ETRF2000, the time series of the solutions were properly analyzed to find discontinuities and solve jumps caused by earthquakes and instrumental changes. Results highlighted the residual velocities with respect to ETRS89, which can reach 5 mm/year in some areas. The velocity field is shown to be very inhomogeneous, with clusters of sites presenting very different behaviours.

Keywords Italian reference network · Deformation models · Precise point positioning · RDN · Italian velocity field

M. Barbarella · S. Gandolfi · L. Tavasci (✉)
DICAM—University of Bologna, Viale Risorgimento 2, 40136 Bologna, Italy
e-mail: luca.tavasci2@unibo.it

M. Barbarella
e-mail: maurizio.barbarella@unibo.it

S. Gandolfi
e-mail: stefano.gandolfi@unibo.it

R. Cefalo et al. (eds.), *New Advanced GNSS and 3D Spatial Techniques*,
Lecture Notes in Geoinformation and Cartography,
DOI 10.1007/978-3-319-56218-6_5

1 Introduction

The need for a geodetic reference frame closely linked to the European standards has led to a new official reference system being defined for Italy. This new reference frame was specified by ministerial decree of November 10, 2011, as a specific implementation of the European Terrestrial Reference System ETRS89, this being ETRF2000 at epoch 2008.0. According to this decree, the reference frame is monitored through a permanent Global Navigation Satellite System (GNSS) network known as the Rete Dinamica Nazionale (RDN). The RDN is a network composed of 99 GNSS tracking stations distributed as homogeneously as possible across the Italian peninsula. These stations were selected from among the 400 or so existing stations owned by scientific institutes and commercial companies, and the GNSS data are acquired by the IGMI (Istituto Geografico Militare Italiano—the Italian Military Geographical Institute) and stored in a specific repository.

Data was collected starting at the very end of 2007, and initially were calculated for 28 consecutive days every six months by three different analysis centres, using the Bernese software package (Dach et al. 2007). The network's official coordinates were published in 2011 and, during that year, the analysis centre of Bologna repeated the calculation using three different software packages: Bernese and Gamit (King and Bock 1999), both based on the differenced approach, and GIPSY OASIS II (Webb and Zumberge 1997), which is based on Precise Point Positioning (PPP). A comparison between the coordinates obtained showed that the results are in accordance at the centimetre level or less for the three software packages, although it should be noted that differences were found even in the calculations obtained using the same Bernese software.

The Reference Frame Sub-Commission for Europe (EUREF) provides the geodetic reference frame ETRF2000 used by European countries, which is based on the ETRS89 reference system and linked to the stable part of the Eurasian plate. This reference frame is monitored and maintained by the European Permanent Network (EPN). EUREF also provide guidelines for EPN densification (Bruyninx et al. 2013), so that more data can be acquired and used to improve the estimation of the evolution of coordinates over time. EUREF has recognised the RDN as an EPN class B densification network.

The Italian peninsula, together with Greece, lies at the southern borders of the Eurasian plate and is thus affected by significant movement compared to the stable part of Europe. The consequence of this is that the ETRF2000 coordinates of these areas are much less stable over time when compared to those of the other European countries. The Fennoscandian peninsula has similar problems due to post-glacial rebound. These points were highlighted by Z. Altamimi at the EUREF Symposium 2012 of Paris (Fig. 1) in order to encourage interest towards addressing this issue.

According to its current definition, the Italian reference frame is a static set of coordinates that relate to a defined epoch with no modelling of the linear movement of the frame points. There are, nevertheless, several reasons for monitoring the RDN network:

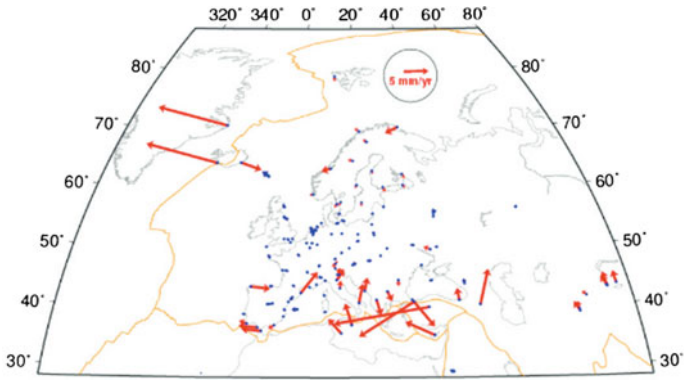

Fig. 1 The chart shows the velocity vectors for the EPN that refer to ETRS89

- The data acquired by each station have to be analyzed and evaluated in order to ensure the good consistency of the results and to highlight any potential problems.
- Because of the crustal movement and earthquakes that affect Italy in particular, the RDN coordinates may change even by several centimetres over a very short time (more than is usual for the ETRF2000 coordinates relating to the stable parts of the Eurasian plate).
- Modern dynamic reference frames, and we must include an official network such as the RDN in this group, must be able to estimate the velocity parameters of their sites. We feel that, after eight years, we have enough confidence in this estimation. Moreover, these velocities are needed for estimating the actual coordinates that refer to the official epoch of reference (2008.0).

For these reasons, the RDN network has been re-calculated using the entire dataset available (2008.0–2016.0), obtaining not only the frame coordinates, but also the velocity vectors of each site. In this paper, we report on the analysis work that has been carried out on data from the 99 official permanent RDN stations, in terms of pre-analysis of the dataset, geodetic calculation in PPP and post analysis of the time series, together with a discussion on the outlook of the Italian reference system.

2 Data Set and Pre-analysis

The list of the 99 official GNSS stations of RDN is available on the official IGMI website and their spatial distribution is given in Fig. 2. The repository containing the related RINEX files has been publicly available since November 2012 (ftp://37.207.194.154/). This repository collects the data obtained from the official RDN stations and from other permanent stations that the IGMI feels could be useful to analyze in consideration of future upgrades to the network.

Fig. 2 The map shows all 99 official RDN sites. *Red dots* represent stations that are no longer sending data to the IGMI repository and *black dots* represent the 78 stations that are still operating and whose data are included in this work

The IGMI does not provide site-log files for the RDN stations, or a report on the consistency of the dataset included in the repository. This information is, nevertheless, fundamental for making correct geodetic calculations, in particular when taking into account aspects concerning the history of the instrumentation and the monumentation of each site.

In consideration of the number of sites to be processed, it was absolutely necessary to develop a procedure to analyze automatically, as far as possible, all and every RINEX dataset, in terms of consistency and metadata included in the file headers. This procedure, known as PAT-NET_GNSS (Gandolfi and Tavasci 2012), was implemented under LINUX using Perl scripts. It provides a complete analysis of the RINEX dataset, allowing the archive to be re-organized into a standard format.

The dataset analysis highlighted that, for some stations, the archive contains no data for the most recent years, indicating that these sites are no longer functional for the purposes of the RDN and thus were excluded from the calculation. Looking at

the remaining sites, other were excluded because of issues connected to the monumentation process that produced an incorrect trend in the time series, a fact highlighted during a previous processing campaign. These sites are marked by red dots in Fig. 2 and were excluded from all successive analyses and calculations. It follows that, in the following, we refer only to the 78 permanent RDN stations indicated by black dots.

Figure 3 shows the percentage of RINEX files contained in the RDN archive relative to each day for the years 2008.0–2016.0. Initially, the IGMI had intended to calculate the network only twice a year, and the data were, therefore, collected only at certain periods.

The EPN stations were constructed and have been maintained following established standards, and EUREF monitors the data produced in terms of stability and integrity. As already mentioned, when the RDN stations were constructed, it was not for the purpose of monitoring the Italian official reference frame and the procedures for archiving data do not strictly follow any international standards. As a consequence, it proved necessary to evaluate the consistency of the dataset to establish whether the RDN is truly comparable with the standard EPN. In order to evaluate the consistency of each GNSS station in terms of available data, and to compare this consistency with the consistency typical of EPN stations, we conceived a specific parameter (Gandolfi and Tavasci 2013) as follows:

$$Q = [A * \%rinex_{ON} + B * \%time\_span + C * (1 - \%interruptions)] * 100$$

where, for each station:

- $\%rinex_{ON}$ is the percentage of RINEX files present in the period between the first and the last days for which station data are available, where 100% means one file for each day in the given time span.
- $\%time\_span$ is the percentage of days in the period between the first and the last days for which station data are available compared to the entire time span analyzed for the relative archive.
- $\%interruptions$ is the percentage of interruptions in the data series, where 100% represents a station working precisely on alternate days.

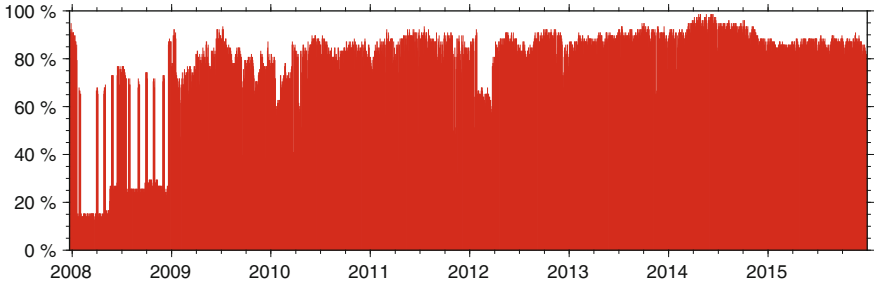

Fig. 3 The graph represents the daily percentage of RINEX files available in the RDN repository. The percentage is calculated for the 78 stations still operating

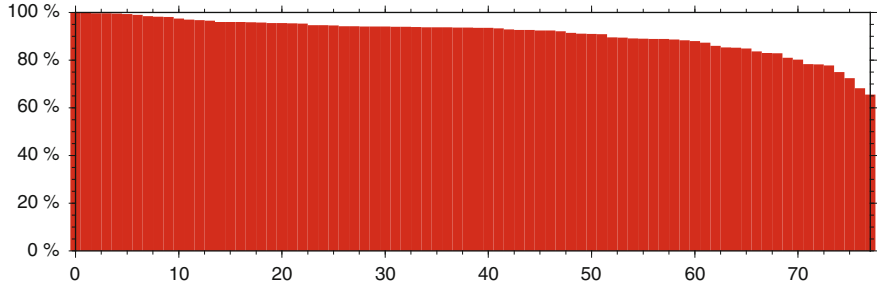

Fig. 4 The graph gives the values of Q calculated for the 78 RDN stations and sorted in decreasing order

The scalars A, B and C are acting as weight for the three parameters, and after a tuning process were fixed to values of 0.4, 0.4 and 0.2 respectively. Q was calculated for the RDN stations under consideration, and a graph showing the results in decreasing order is given in Fig. 4. A previous test on a sub-network of 14 EPN stations located in and around Italy indicated that Q is always greater than 85% while, for 13 of the set of 78 stations considered here, the value of Q is between 85 and 65%. Despite this, we processed data for the 78 stations and considered them all because of the need to retain a homogeneous spatial distribution of the data and, additionally, in consideration of the fact that, over the upcoming years, the data-streams will probably improve in quality even for the 13 stations that today present lower Q values.

Using the PAT-NET_GNSS procedure, the archive was also cleaned from inconsistent or corrupted files that can create problems during the GNSS processing. This procedure was also used to produce ancillary files containing approximate positions and site information necessary for the geodetic calculation of the network.

3 GNSS Processing

Because no significant bias was found in the coordinates when comparing the PPP results with other results obtained through a classical differenced approach, the PPP method was used for all computations. It has been demonstrated that PPP is a powerful tool for accurate and fast calculations on a large dataset (Metois et al. 2015), which in this case contains about 183,000 RINEX files. For this reason, each RINEX file in the dataset was processed following a PPP approach, using GIPSY-OASIS II software, version 6.3. Below are the options selected for the test, where most are the default parameters suggested by JPL for GIPSY users:

- Orbit and clock products: non-fiducial precise FlinnR orbits from JPL, including information to enable single receiver phase ambiguity resolution using GIPSY-OASIS software (WLPB)

- Antenna phase centre variation: IGS absolute phase centre calibration file (igs08.atx)
- Cut-off angle for observations: 7°
- Data rate: 300 s
- Smoother option: static solution
- Number of iterations for ambiguity resolution: 1
- Tide models: solid earth tide (WahrK1, FreqDepLove) (Wahr 1985), polar tide model (PolTid) and ocean tide model (OctTid)—GIPSY default option
- Tropospheric model: VMF-1 (Kouba 2008)
- Troposphere estimation parameters: random walk, set to 3 [mm/sqrt(h)] with wet gradient set to 3.6 [mm/h]—GIPSY default option

The solutions obtained directly from the GIPSY data processing procedure using JPL non-fiducial orbits are not strictly aligned to the IGb08 (Rebischung 2012), this being the most updated release of an ITRS frame until early 2016. These solutions were, therefore, aligned to the IGb08 using the procedure described in Gandolfi et al. (2016). This procedure is based on calculating daily Helmert transformation parameters, which were estimated using data from 14 EPN stations located in and around Italy. It has been demonstrated that the use of regional transformation parameters leads to more precise results and improves agreement between these values and the IGb08 reference. Successively, all the coordinates were transformed into the ETRF2000 reference frame by applying the 14 transformation parameters suggested by EUREF in its memo-V8 (Boucher and Altamimi 2011).

4 Post Processing

The following procedure was performed for each of the 78 considered sites, starting from the ETRF2000 daily solutions:

- The geocentric coordinates of each solution were converted into a local topocentric coordinate system (North, East, Up) to help interpret the ensuing results. The time series of these coordinates were composed and analyzed one by one as set out below. For each solution, the covariance matrix was also propagated in the same topocentric coordinate system.
- The raw time series of the solutions were automatically separated on the basis of the possible discontinuities that had been checked out through the PAT-NET_GNSS procedure, with instrumental changes being taken into account.
- Other discontinuities dependant on earthquakes or local phenomena were checked out by analysing the time series visually.
- For each part of raw time series, the regression lines were calculated together with the related weighted RMS of the solution σ. The inverse of the covariance matrix was considered as a weighting for each solution.

- The solutions with a residual greater than 3σ with respect to the regression line were rejected as outliers. It has to be noted that any solution with outlier values even in a single topocentric component was rejected in all of its components.
- These last two steps were iterated until no more outliers were found.
- Time series which had become separated because of various discontinuities were recomposed after the jumps between the consecutive parts were elaborated by implementing the Heaviside function (Davies 1986). These jumps were calculated as the difference between the coordinates at the epoch of the discontinuity, considering the regression lines of the two parts (Fig. 5).
- The slope m of the regression lines of the recomposed time series were calculated together with the related uncertainty σ_m. These parameters are representative of the mean velocity for each station in the analyzed period.

The velocities calculated in this way can be used for different purposes such as geodesy and geodynamics. When estimating the formal RDN coordinates relating to the epoch 2008.0, which is still the official reference frame for Italy, these velocities can be used to propagate the current ETRF2000 coordinates back in time. Nevertheless, these velocities could be considered when estimating the crustal deformations existing in the Italian territory and its movement with respect to the stable part of the Eurasian plate.

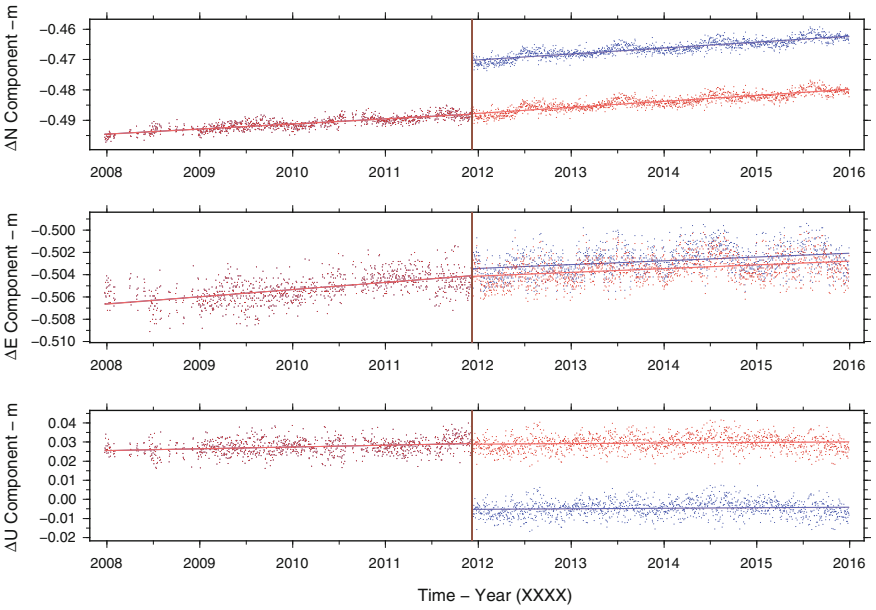

Fig. 5 The graph gives an example of jump in a GNSS time series (*blue dots*) and the relative solution (*red dots*). This example refers to the PRAT station

Table 1 Velocities of the RDN sites expressed in the local topocentric components, North, East and Up respectively, together with the related uncertainties

SITE	V_N	V_E	V_U	σV_N	σV_E	σV_U	SITE	V_N	V_E	V_U	σV_N	σV_E	σV_U
ACOM	0.9	0.0	1.1	0.01	0.01	0.04	MRGE	−0.6	−0.5	1.6	0.02	0.01	0.05
AMUR	4.5	0.7	−0.5	0.01	0.01	0.03	MRLC	4.6	1.3	1.7	0.03	0.02	0.05
AQUI	1.2	−0.2	−1.1	0.02	0.02	0.05	MSRU	3.8	0.4	0.0	0.01	0.01	0.05
BIEL	−0.2	−0.3	0.8	0.01	0.01	0.04	NOT1	4.5	−2.2	−1.5	0.01	0.01	0.04
BRBZ	0.6	−0.2	1.8	0.01	0.01	0.04	NU01	0.2	−0.4	−0.4	0.03	0.03	0.08
BZRG	0.4	−0.1	1.3	0.02	0.01	0.04	PADO	0.9	−0.1	−0.7	0.02	0.01	0.03
CAMP	2.8	−1.4	−0.1	0.03	0.03	0.11	PARM	1.5	1.1	1.3	0.02	0.01	0.06
CARI	1.6	−1.1	−0.6	0.04	0.03	0.11	PASS	0.6	−0.7	0.7	0.02	0.02	0.05
COMO	0.3	−0.3	−0.2	0.01	0.02	0.03	PAVI	0.2	−0.7	0.5	0.02	0.03	0.05
CUCC	2.9	−1.0	1.2	0.02	0.03	0.06	PORD	1.6	−0.4	−0.7	0.01	0.01	0.04
EIIV	2.6	−0.5	0.7	0.02	0.02	0.05	PRAT	1.9	0.5	0.5	0.01	0.01	0.04
ELBA	0.6	−1.1	−0.9	0.02	0.02	0.06	RENO	3.0	0.3	0.3	0.03	0.02	0.09
FASA	4.1	1.0	−0.8	0.01	0.01	0.04	ROVE	0.7	−0.4	0.3	0.01	0.01	0.05
FOGG	3.7	0.9	0.0	0.01	0.01	0.04	RSMN	2.8	1.4	0.8	0.01	0.01	0.04
FRES	2.9	0.9	−0.5	0.01	0.01	0.03	RSTO	3.0	1.6	−1.2	0.01	0.01	0.03
GENO	0.1	0.1	−0.6	0.01	0.01	0.03	SASA	3.8	0.8	−0.8	0.01	0.01	0.04
GIUR	3.7	0.6	−0.9	0.01	0.01	0.04	SASS	0.1	−0.7	0.1	0.02	0.02	0.06
GRAS	0.0	−0.2	−0.3	0.01	0.01	0.03	SERS	2.7	1.4	0.8	0.01	0.01	0.05
GRAZ	0.4	0.6	0.4	0.01	0.01	0.03	SIEN	0.7	−0.2	0.6	0.01	0.01	0.03
GROG	0.4	−0.1	−0.3	0.01	0.01	0.04	SOFI	−2.4	0.3	−0.7	0.01	0.01	0.06
GROT	2.4	−0.2	1.1	0.01	0.01	0.04	STBZ	0.6	0.2	1.6	0.01	0.02	0.05
HMDC	4.4	−1.7	−1.6	0.02	0.02	0.06	SVIN	2.8	0.0	−1.1	0.03	0.03	0.07
IENG	−0.5	0.2	0.0	0.01	0.01	0.03	TEMP	0.1	−0.1	0.2	0.02	0.02	0.06
IGMI	2.0	0.0	−0.4	0.02	0.01	0.04	TERM	4.0	−1.2	−0.9	0.05	0.03	0.13

(continued)

Table 1 (continued)

SITE	V_N	V_E	V_U	σV_N	σV_E	σV_U	SITE	V_N	V_E	V_U	σV_N	σV_E	σV_U
INGR	1.0	−1.2	−0.1	0.01	0.02	0.03	TGPO	1.9	−0.2	−4.8	0.02	0.01	0.04
ISCH	3.9	1.0	−0.6	0.02	0.01	0.05	TGRC	2.8	0.7	0.4	0.02	0.02	0.06
LAMP	2.0	−1.4	−1.3	0.02	0.02	0.06	TORI	−0.3	0.2	1.5	0.01	0.01	0.04
LASP	0.5	0.1	−0.1	0.01	0.01	0.04	TREB	3.9	1.0	0.8	0.01	0.02	0.05
LAT1	0.9	−0.6	1.2	0.01	0.01	0.05	TRIE	2.5	−0.4	−0.5	0.01	0.02	0.04
M0SE	0.5	−1.7	−1.0	0.01	0.01	0.03	UDI1	1.9	−0.6	−0.2	0.01	0.01	0.04
MABZ	0.4	0.1	2.2	0.01	0.01	0.04	UGEN	3.8	0.6	−0.9	0.01	0.01	0.04
MACO	0.4	−0.4	0.4	0.02	0.02	0.07	UNOV	0.8	−1.4	4.3	0.13	0.14	0.48
MADA	0.8	0.0	−1.5	0.01	0.01	0.05	UNPG	1.7	−0.1	−0.4	0.01	0.01	0.03
MALT	4.3	−1.8	−0.6	0.01	0.01	0.06	VAGA	2.6	−0.4	1.7	0.06	0.04	0.05
MAON	0.6	−0.8	−0.3	0.01	0.01	0.04	VERO	0.3	−0.2	0.3	0.02	0.01	0.04
MATE	4.3	0.7	−0.1	0.01	0.01	0.03	VITE	0.4	−0.6	0.1	0.04	0.07	0.08
MEDI	2.4	1.1	−2.1	0.02	0.02	0.03	WTZR	0.1	0.1	1.0	0.01	0.01	0.03
MOCO	3.7	0.8	0.0	0.02	0.01	0.05	ZIMM	0.3	−0.2	1.6	0.01	0.01	0.03
MOPS	3.1	1.2	−0.8	0.01	0.01	0.03	ZOUF	0.9	0.2	0.8	0.02	0.01	0.04

All the values are expressed in mm/year

5 Results and Comments

Table 1 contains the residual mean velocities with respect to ETRF2000 for the 78 RDN sites considered here. The rows shown in Fig. 6 represent the velocity field for Italy that can be obtained from the permanent RDN stations.

Very different mean movements are evident if considering clusters of sites with similar velocities. In particular, the movement of the North-West and Sardinia seems to be well modelled by the ETRS89 and the residual velocities are very small. On the other hand, the South-East of the peninsula runs in North-East direction with a magnitude of more than 4 mm/year, while Sicily and parts of central-southern Italy have drifts in other directions.

Figure 7 shows the vertical velocity field obtained from the data relative to the RDN sites. It has to be noted that the area in the North-East is defined by a negative vertical velocity of about 4 mm/year, due to subsidence.

Fig. 6 Velocity vectors map in ETRS89 estimated for the 78 analyzed RDN sites overlapped to the main tectonic boundaries in the area

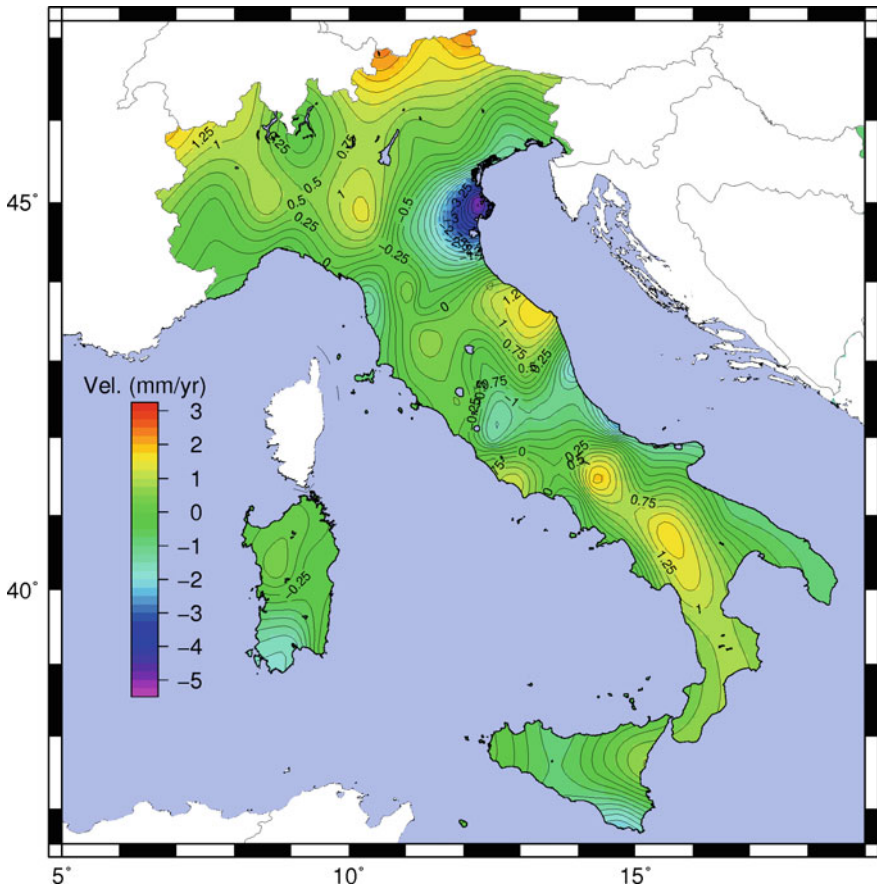

Fig. 7 Vertical velocity field in ETRS89 estimated using 78 RDN sites

According to the data obtained from the official reference network, this calculation confirmed two main factors: Italy is subject to a strong movement relative to the ETRS89 RS, which reaches 5 mm/year in some areas; the Italian velocity field is quite irregular and difficult to connect to a common drift. The modelling of the southern borders of the Eurasian plates is still a challenging issue, and official data from the Greek peninsula are also needed if our intension is to define clusters of sites with common behaviour. The present work should be the basis for the future development of a detailed model where the plate movement at the borders between Africa and Europe can be represented better. This is important if the aim is to reduce the changes to coordinates over time, and obtain residual vectors that are as near as possible to those found in the stable areas of Europe.

References

Boucher C, Altamimi Z (2011) Memo: specifications for reference frame fixing in the analysis of a EUREF GPS campaign. http://etrs89.ensg.ign.fr/memo-V8.pdf

Bruyninx C, Altamimi Z, Caporali A, Kenyeres A, Lidberg M, Stangl G, Torres JA (2013) Guidelines for EUREF densifications. ftp://epncb.oma.be/pub/general/Guidelines_for_EUREF_Densifications.pdf

Dach R, Hugentobler U, Fridez P, Meindl M (2007). Bernese GPS software version 5.0, vol 640. Astronomical Institute, University of Bern, p 114

Davies J (1986) Statistics and data analysis in geology. Wiley, NY

Gandolfi S, Tavasci L (2012) L'analisi di consistenza di archivi di reti di stazioni permanenti GNSS per la valutazione della qualità di un servizio di posizionamento in tempo reale: PAT-NET_GNSS, Atti 16a Conferenza Nazionale ASITA, Fiera di Vicenza 6–9 novembre 2012 (ISBN 978-88-903132-5-7), pp 717–722

Gandolfi S, Tavasci L (2013) Procedure per l'analisi di consistenza e qualità di archivi di reti di stazioni permanenti GNSS: applicazione alla nuova rete dinamica nazionale RDN. Bollettino SIFET (ISSN 1721-971X), 2013, 1:55–66

Gandolfi S, Tavasci L, Poluzzi L (2016) Improved PPP performance in regional networks. GPS Solut 20:485. doi:10.1007/s10291-015-0459-z

IGMI "La Rete Dinamica Nazionale e il nuovo Sistema di Riferimento ETRF2000" available on line, http://host154-194-static.207-37-b.business.telecomitalia.it/rdn/rdn_download.php. Accessed 20 Oct 2016

King RW, Bock Y (1999) Documentation for the GAMIT GPS analysis software. Massachusetts Institute of Technology, Cambridge, MA

Kouba J (2008) Implementation and testing of the gridded Vienna mapping function 1 (VMF1). J Geod 82(4–5):193–205

Metois M, D'Agostino N, Avallone A, Chamot-Rooke N, Rabaute A, Duni L, Kuka N, Koci R, Georgiev I (2015) Insights on continental collisional processes from GPS data: dynamics of the peri-Adriatic belts. J Geophys Res Solid Earth 120(12):8701–8719

Rebischung P (2012) [IGSMAIL-6663] IGb08: an update on IGS08. https://igscb.jpl.nasa.gov/pipermail/igsmail/2012/007853.html

Wahr JM (1985) Deformation induced by polar motion. J Geophys Res 90:9363–9368. doi:10.1029/JB090iB11p09363

Webb FH, Zumberge JF (1997) An introduction to GIPSY/OASIS-II. JPL Publication D-11088, Jet Propulsion Lab, Pasadena

Interoperability of the GNSS's for Positioning and Timing

Alessandro Caporali and Luca Nicolini

Abstract Since 2014.0 we monitor 31 European multiGNSS sites with 5 different receivers (Javad, Leica, Septentrio, Topcon, Trimble), and various combinations of antennas and firmware. We work both in Single Point Positioning (SPP) mode (ionofree combination of pseudoranges, broadcast ephemeris), as a real time user would, and in Precise Point Positioning (PPP) mode (ionofree combination of carrier phases, SP3 precise ephemeris), as a post processing user would, using our MATLAB based, ***multiGNSS*** software. We simultaneously process pseudorange and/or phase data from GPS, Glonass, Galileo, Beidou, QZSS, NAVIC (formerly IRNSS) and SBAS/GAGAN in different combinations, depending on availability and receiver tracking capability. We estimate at each epoch by least squares three coordinates, one Tropospheric Zenith Delay and n_{GNSS} sums of the receiver time offset and the offset of the time scale of each GNSS relative to a common, interGNSS time scale, where n_{GNSS} is the number of tracked GNSS constellations. Differentiation of such offsets relative to the GPS data yields epochwise for each receiver estimates of the time offset GNSS to GPS. Comparing across different receivers we find that such offsets can be biased relative to each other by as much as several tens of nanoseconds. We arbitrarily select the average of six Septentrio receivers as reference, and estimate the receiver biases relative to the average Septentrio. We find that for a given receiver brand, the bias relative to Septentrio for the various GNSS is very repeatable, with a few exceptions. We show that updating the firmware version does affect the GNSS dependent receiver bias. We finalize our work with a table of 'mean' calibrations, for each GNSS, of comparable receivers, whenever their bias to Septentrio is within one standard deviation, and a subtable of 'individual' calibrations for those receivers which fall out of the mean by more than one standard deviation.

Keywords MultiGNSS interoperablity · Position Velocity Timing (PVT) estimates · Inter system bias · Receiver dependent bias · Mean and type receiver calibration

A. Caporali (✉) · L. Nicolini
University of Padova, Center for Space Activities CISAS 'G. Colombo', Padova, Italy
e-mail: alessandro.caporali@unipd.it

R. Cefalo et al. (eds.), *New Advanced GNSS and 3D Spatial Techniques*,
Lecture Notes in Geoinformation and Cartography,
DOI 10.1007/978-3-319-56218-6_6

1 Introduction

As part of the contribution of the University of Padova to the MGEX program (http://mgex.igs.org/) and to the activities of the MultiGNSS Working Group within EUREF (http://www.euref.eu/euref_twg), we monitor since 2014.0 31 European GNSS sites with 5 different receivers (Javad, Leica, Septentrio, Topcon, Trimble) (Fig. 1).

We focus on two issues which are critical for the interoperability of the different GNSS constellations, from the user viewpoint (Chen et al. 2013).

- Offset among the time scales of different GNSS constellations: are the reference time scales of the various GNSSs synchronized among each other? Note: 10 ns (1 ns = 10^{-9} s) relative offset in the time scales ⇔3 m range bias;
- Do different receivers measure different offsets? Does the receiver dependent offset change subject e.g. to firmware update?

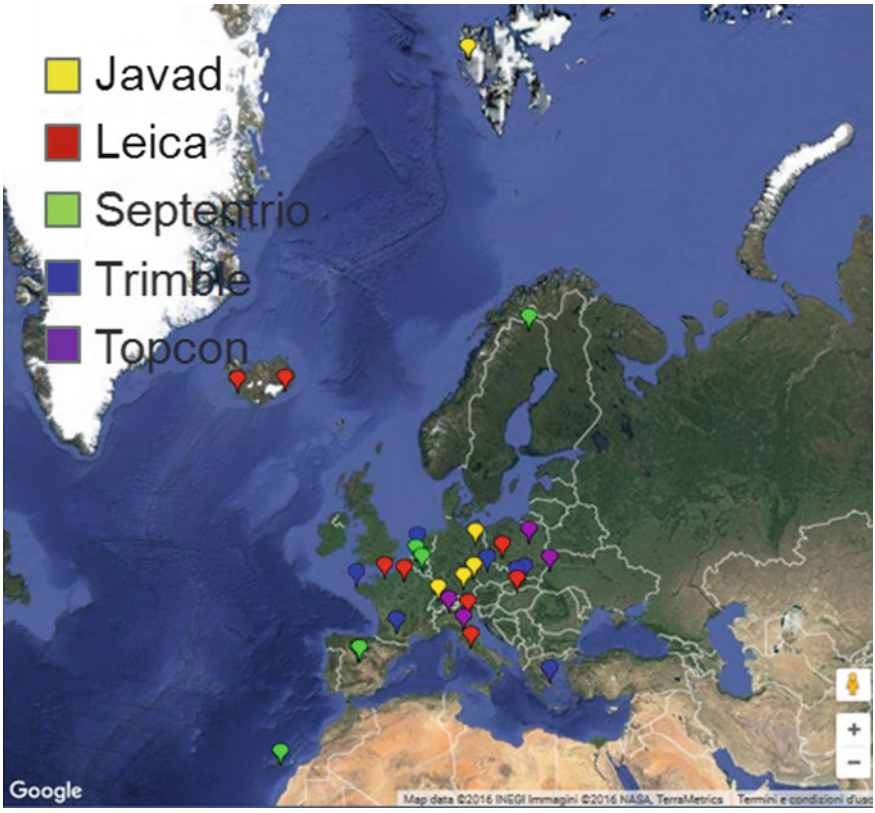

Fig. 1 Map of the analyzed European multiGNSS sites grouped according to receiver type

For these purposes we use our MATLAB based *multiGNSS* software (Dalla Torre and Caporali 2015). We focus on GPS, Glonass, Galileo and Beidou. For some receiver at higher latitudes (e.g. Kiruna–KIRU, Sweden, Wroclaw–WROC, Poland, Ny Alesund–NYA1, Svalbard) QZSS data are also available. A Septentrio receiver has also delivered data from the Indian NAVIC (formerly IRNSS) constellation. As to SBAS, we have data from S27 and S28, both belonging to the Indian overlay system GAGAN in geostationary orbits. No data usable for positioning are instead available for other SBAS, such as for instance EGNOS.

As to the orbits, satellite clocks and other ancillary data (e.g. quality flags), we use broadcast ephemeris in Rinex format downloaded from the MGEX ftp servers, and SP3 orbits/clocks and DCB's (Differential Code Biases) from the German Research Centre for Geosciences (GFZ) and the Center for Orbit Determination in Europe (CODE). We use RINEX 3.x data for all receivers except Topcon, for which the provided RINEX 2.x are converted to RINEX 3.x with the utility *gfzrnx* of GFZ (http://semisys.gfz-potsdam.de/semisys/scripts/download/).

2 Input Data and Model of the Observations

Several codes are available in the carriers at several frequencies, for the different GNSS constellations. It is not the purpose of this paper to provide an extensive analysis with all the possible combinations of codes modulated on the carriers. We rather concentrate, particularly for Galileo, on that combination which is more regularly available in the data, that is I/NAV (OS-SIS-ICD 2015), and use accordingly the related navigation message. Table 1 summarizes the types of signals found in the RINEX data, coded according to the latest RINEX conventions (IGS 2015). Dual frequency code/phase combinations are generated in order to remove first order ionospheric delays.

Table 1 Frequency and codes available in the RINEX data for different GNSSs

System	Carrier/frequency [MHz]		Coding in RINEX 3.03		
GPS	L1 (1575.42)	L2 (1227.60)	C1C	C2W	
Galileo	E1 (1575.42)	E5b (1207.14)	C1	C7I/C7Q/C7X	I/NAV
	E1 (1575.42)	E5a (1176.45)	C1	C5I/C5Q/C5X	F/NAV
BeiDou	B1 (1561.098)	B2 (1207.14)	C1I	C7I	
QZSS	L1 (1575.42)	L2 (1227.60)	C1C	C2S/C2L/C2X	
NAVIC (former IRNSS)	L5 (1176.45)	S (2492.028)	C5A	C9A/C9B/C9C	
SBAS (GAGAN)	L1 (1575.42)	L5 (1176.45)	C1C	C5I	

The model of the pseudorange $p(t)$ is described in Eqs. 1–3. Table 2 contains the explanation of the variables.

$$p^i(t) = range^i + c \cdot dt^i\left(t^{'}\right) + c \cdot (TSC_X + dT_{REC}) + \frac{TZD}{\sin(El^i)} + DCB^i \quad (1)$$

$$range^i = \sqrt{[X^i(t') + \omega_e \cdot Y^i(t - t') - x]^2 + [Y^i(t') - \omega_e \cdot X^i(t - t') - y]^2 + [Z^i(t') - z]^2} \quad (2)$$

$$dt^i(t') = a_0 + a_1 \cdot (t' - T_{oc}) + a_2 \cdot (t' - T_{oc})^2 - \frac{2\sqrt{\mu a}}{c^2} e \cdot \sin(E(t')) + LS \quad (3)$$

The vector of the unknowns consists, at each epoch, of three station coordinates, one TZD and as many (TSC_X + dT_{REC}) as the number of GNSSs constellations in the analysis. These variables are the sum of a first term dependent on the GNSS but independent of the receiver and a second term independent of the GNSS and dependent on the receiver. To monitor the GNSS specific time bias it is convenient to take TSC_G as reference time scale (subscript G stands for GPS) and evaluate the difference (TSC_X + dT_{REC}) − (TSC_G + dT_{REC}), with X referring to all the GNSSs different from GPS (Odijk et al. 2016; Jiang et al. 2016; Chen et al. 2016). Table 3 lists these GNSS specific variables, which will be referred to later on.

Table 2 Explanation of symbols and variables used in Eqs. 1–3

Symbol	Meaning
$Range^i$	Geometric range between satellite *i* and receiver
c	Speed of light
dt^i	Satellite clock error plus leap seconds (LS), see Eq. 3
t'	Time of transmission
T	Time of reception
TSC_X	Time system correction of the X GNSS system (G = GPS; R = GLONASS; E = Galileo; C = Beidou; S = SBAS; J = QZSS; I = NAVIC; N = GAGAN)
dT_{REC}	Receiver clock error
TZD	Tropospheric Zenith delay
El^i	Elevation of satellite *i*
DCB^i	Differential code bias of satellite *i*
X^i, Y^i, Z^i	Earth-centered earth-fixed (ECEF) coordinates of satellite *i*
ω_e	Earth rotation rate (nominal values are defined in the ICD of the various GNSSs)
x, y, z	ECEF coordinates of receiver

Table 3 Definition of the epochwise offsets of the GNSS time scales relative to GPS: in the order Glonass, Galileo, BeiDou, QZSS, NAVIC and GAGAN

Time offset	Definition
GLGP	$(TSC_R + dT_{REC}) - (TSC_G + dT_{REC})$
GPGA	$(TSC_G + dT_{REC}) - (TSC_E + dT_{REC})$
BDGP	$(TSC_C + dT_{REC}) - (TSC_G + dT_{REC})$
QZGP	$(TSC_J + dT_{REC}) - (TSC_G + dT_{REC})$
NAGP	$(TSC_I + dT_{REC}) - (TSC_G + dT_{REC})$
GNGP	$(TSC_N + dT_{REC}) - (TSC_G + dT_{REC})$

3 Data Preprocessing/Smoothing for PPP Processing

Single point positioning is affected by multipath and uncertainties in the arrival time of the centroid of the wave packet. Working with ionofree linear combinations of carrier phases reduces considerably these error sources, but one has to calibrate the phase pseudoranges and correct for cycle slips (Bisnath 2000). The intrinsic precision of these measurements dictates the use of precise ephemeris and DCB's (Gao and Chen 2004; Montenbruck et al. 2014; Li et al. 2012). For the combined solution with GPS, Glonass, Galileo and BeiDou, for which precise ephemeris are available from CODE and GFZ, we constructed phase smoothed pseudoranges in an iterative manner:

First iteration: phase smoothing and cycle slips repair

- Detection of passes: we consider a new pass if the time gap between two observations is greater than 180 s.
- Calculation of L_1, L_2 ($L_i = \lambda_i \cdot \Phi$) in metric units, where λ_i and Φ_i are wavelength and phase measurements of frequency i.
- Calculation of geometry-free Linear Combination: $L_4 = L_1 - L_2$. It has to be noted that this combination only contains differential ionospheric delay and initial phase ambiguities (Dach et al. 2015).
- Detection of cycle slips within each pass: we compute $\delta L_4(t_i) = L_4(t_i) - L_4(t_{i-1})$. It is reasonable to consider the ionospheric delay as a constant between two consecutive epochs, which means that δL_4 contains only the initial phase ambiguities (Banville and Langley 2009; Xiaohong and Xingxing 2012; Zhang et al. 2016). A new cycle slip is detected whenever δL_4 is larger than λ_1.
- Cycle slips divide a single pass into arcs, for each of them we consider the ambiguity as a constant. The ambiguity is estimated as the mean value of differences between carrier phases L_1, L_2 and code measurements C_1, C_2, respectively.
- Iterate if necessary.

Second iteration: after repair of all cycle slips, the ionofree combination of calibrated carrier phases provides preliminary postfit residuals for each pass. We fine tune the ambiguities for each arc:

- For each arc, the mean value of the post-fit residual (μ_{PF}) is calculated.
- Reset of L_3: $L_3 \rightarrow L_3 - \mu_{PF}$, where L_3 is the iono-free linear combination of calibrated carrier phases.

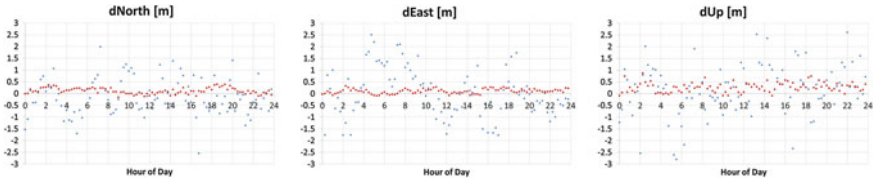

Fig. 2 PPP (phase smoothed pseudoranges, precise ephemeris) versus SPP (pseudoranges, broadcast ephemeris) at 15 min for a combined analysis of GPS, Glonass, Galileo and BeiDou satellites. *From left to right* we plot epochwise offsets of the North, East and Up coordinate relative to nominal. *Blue dots* refer to SPP and *red dots* to PPP

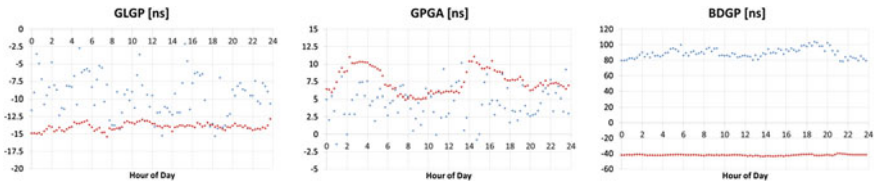

Fig. 3 System time offsets. For SPP (*blue dots*) we use broadcast time polynomials, for PPP (*red dots*) we use the common SP3 time scale. Note the difference in scale of the BeiDou plot (third plot) relative to Glonass and Galileo (first two plots), due to the marked offset of the BeiDou broadcast time relative to the GPS time

Table 4 Comparison of epochwise solutions RMS in PPP and SPP mode

	RMS (PPP) [m]	RMS (SPP) [m]
dNorth	0.13	0.82
dEast	0.10	1.04
dUp	0.21	1.27
TZD	0.08	0.33

We present in Figs. 2 and 3 and example of the increase in stability and overall accuracy when processing data in PPP mode versus SPP mode. Table 4 report the values of Root Mean Squares (RMS) obtained in SPP and PPP mode. Results are relative to KIRU (Kiruna, Sweden) station for day 2016/02/22. For PPP analysis GFZ precise orbits were used.

4 Results

We present in Fig. 4 the offsets of the time scales of the various GNSSs relative to GPS, for the several (up to 31) receivers in our analysis. From the user point of view it is clear that for the various GNSSs be interoperable with GPS, a synchronization between their time scales and the GPS time scale is needed. The time offset between Glonass and BeiDou on the one hand and GPS on the other hand is

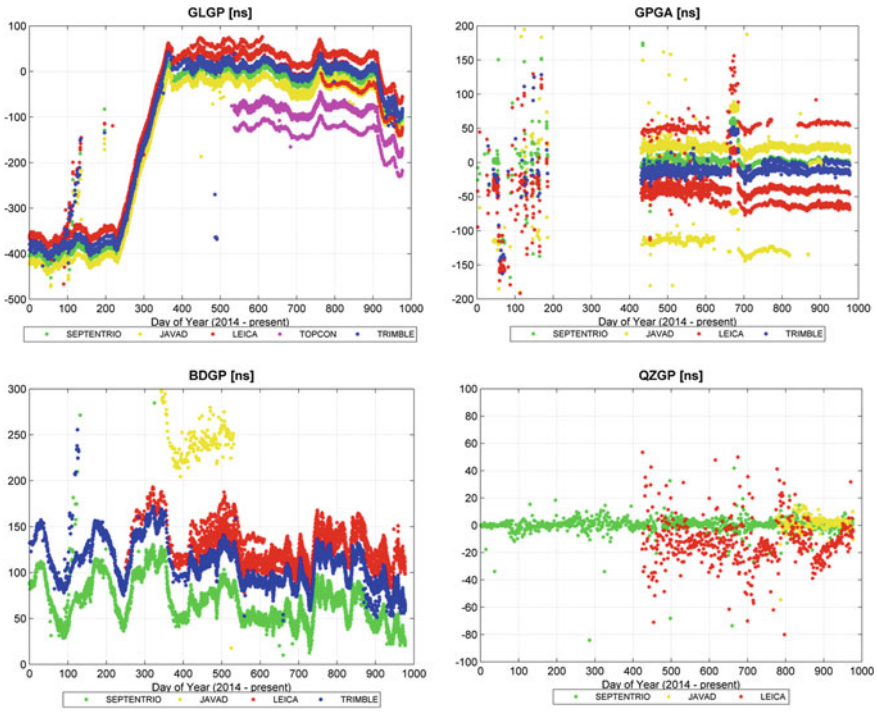

Fig. 4 Time series since 2014.0 of offsets of the Glonass, Galileo, BeiDou and QZSS time scales relative to GPS, using broadcast ephemeris and pseudoranges in ionofree combination

time dependent. Galileo and QZSS time scales maintain a relatively more stable relationship to GPS. Ignoring these time offsets would bring measurement errors of the order of tens to hundreds of meters, resulting in lack of interoperability. Another important aspect is that the synchronization offset is different for different receiver types. For a given receiver type we report several examples of change in offset whenever the firmware is updated.

To best highlight the receiver dependent nature of certain time biases, we have taken the mean of the GNSS_to_GPS time offsets of six Septentrio receivers a reference and analysed the time offsets of the remaining receivers relative to this reference. Figure 5 exemplifies our analysis for the Galileo to GPS time offset of non-Septentrio receivers relative to the mean Septentrio: we find that in correspondence to firmware updates of e.g. WTZZ, PADO or M0SE, the time bias changes. This fact is symptomatic of a lack of standardization on the one hand, and —on the other hand—of the need to monitor these temporal changes of constellation dependent, receiver biases, for appropriate receiver calibration. Table 6 summarizes our findings for the receivers we processed, and provides a first example of mean/individual calibration for multiGNSS receivers.

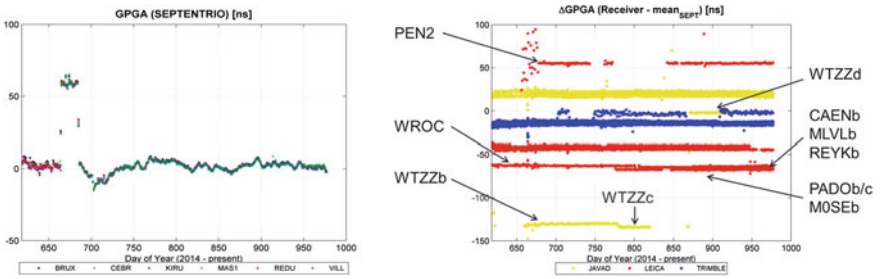

Fig. 5 (*left*) time series of the GPS to Galileo Time Offset (GPGA) for six different Septentrio receivers, showing the excellent consistency among them. (*Right*) Differenced GPGA of non-Septentrio receivers relative to the average of the Septentrio GPGA, showing receiver dependent offsets

Our multiGNSS solution includes, whenever available, the two Indian constellations NAVIC and GAGAN. The first consists of 4 satellites in Geosynchronous inclined (29°) orbit, and 3 satellites in Geostationary orbit. The second consists of two SBAS overlay satellites which in the RINEX files are labeled S27 and S28. Figure 6 on the left shows that the NAVIC time polynomials in the broadcast ephemeris is offset to the GPS time by some 75 ns, whereas both GAGAN and Galileo time scales are reasonably well aligned to GPS time, as it can be seen on the right. The graph on the left is based on an hourly RINEX, day 2016/06/15, of a Septentrio receiver. The one on the right is referred on daily RINEX of WTZZ (Bad Koetzting, Germany) station, day 2016/08/21. Mean values and RMSs of NAGP

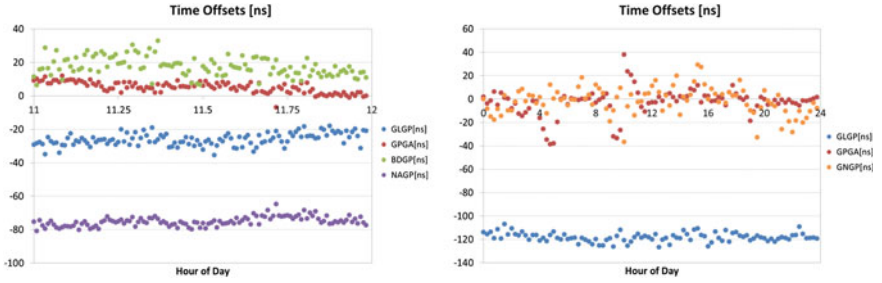

Fig. 6 Time series of the time offsets of NAVIC (*left*) and GAGAN (*right*) to GPS. For NAVIC we used 1 h of data in combination with GPS, Glonass, Galileo and BeiDou, whereas GAGAN was processed in conjunction with GPS, Glonass, and Galileo for one full day

Table 5 Mean values and RMS of IRGP and GNGP

Time offset	Mean [ns]	RMS [ns]
NAGP	−74.99	2.76
GNGP	−1.44	11.60

and GNGP are reported in Table 5. We find that the broadcast time scale of NAVIC is offset to the GPS time scale of -75 ± 3 ns, whereas broadcast time scale of GAGAN is synchronous with GPS within one standard deviation.

Figure 7 shows the postfit residuals of Septentrio receiver, obtained with a combined analysis of GPS Glonass Galileo Beidou NAVIC, and Fig. 8 shows GAGAN postfit residuals of WTZZ, obtained analyzing GPS Glonass Galileo SBAS/GAGAN.

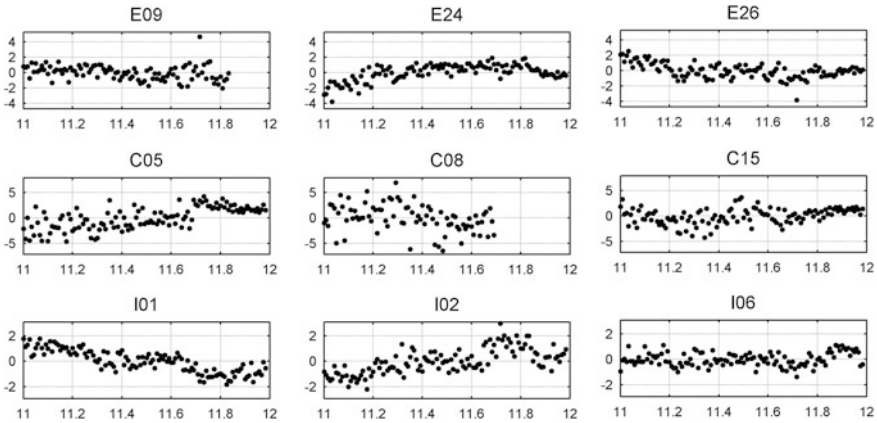

Fig. 7 Post Fit residuals (meters vs. hours) of Galileo (E), BeiDou (C) and NAVIC (I), *from top to bottom*, to highlight the consistency of the solution. GPS and Glonass data were also used in the solution but the plot are not shown. Broadcast ephemeris and satellite clock are taken from the navigation message. Ionofree pseudoranges were processed at 30 s solving epochwise for coordinates, TZD and constellations clock offset

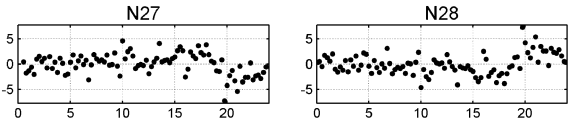

Fig. 8 Post Fit residuals (meters vs. hours) of GAGAN. Broadcast ephemeris and satellite clock are taken from the navigation message. Ionofree pseudoranges were processed at 900 s solving epochwise for coordinates, TZD and constellations clock offset

Table 6 Individual calibration

Station		Receiver			Antenna		Calibration [ns]		
ID	Date	Receiver	Type	Firmware	Type	Radome	dGLGP	dGPGA	dBDGP
GOP7a	2014/01/01	JAVAD	TRE_G3TH DELTA	3.5.1	LEIAR25.R4	LEIT	−19.0 ± 1.3		
NYA2	2014/01/01	JAVAD	TRE_G3TH DELTA	3.5.10	JAV_RINGANT_G3T	NONE	−29.1 ± 0.8	19.0 ± 1.0	
OBE4	2014/01/01	JAVAD	TRE_G3TH DELTA	3.5.10	JAV_RINGANT_G3T	NONE	−30.9 ± 0.6	22.4 ± 1.1	
POTS	2014/01/01	JAVAD	TRE_G3TH DELTA	3.5.10	JAV_RINGANT_G3T	NONE	−21.8 ± 0.9	16.8 ± 1.1	
WTZ3	2014/01/01	JAVAD	TRE_G3TH DELTA	3.6.1b1-68-7da1	LEIAR25.R3	LEIT	−17.8 ± 2.3	20.2 ± 2.0	
WTZZa	2014/01/01	JAVAD	TRE_G3TH DELTA	3.6.4B1-57-AB7E	LEIAR25.R3	LEIT	−14.7 ± 1.7	−117.1 ± 1.0	
WTZZb	2015/09/13	JAVAD	TRE_G3TH DELTA	3.6.4B1-57-AB7E	LEIAR25.R3	LEIT	−16.1 ± 0.8	−130.6 ± 1.8	
WTZZc	2016/02/16	JAVAD	TRE_G3TH DELTA	3.6.4 JAN,12,2016	LEIAR25.R3	LEIT	−12.2 ± 1.0	−133.7 ± 0.8	
WTZZd	2016/05/19	JAVAD	TRE_G3TH DELTA	3.6.6 APR,27,2016	LEIAR25.R3	LEIT	−15.3 ± 0.6	−2.2 ± 0.4	
ZIMJa	2014/01/01	JAVAD	TRE_G3TH DELTA	3.4.9 Apr,18,2013	JAVRINGANT_DM	NONE	−20.6 ± 1.9	21.9 ± 1.8	
ZIMJb	2016/05/12	JAVAD	TRE_G3TH DELTA	3.5.12 Nov,12,2015	JAVRINGANT_DM	NONE	−24.4 ± 0.5	19.8 ± 0.9	
CAENa	2014/01/01	LEICA	GR25	3.11	TRM57971.00	NONE	41.5 ± 3.2	−42.1 ± 1.1	68.0 ± 3.3
CAENb	2016/08/12	LEICA	GR25	3.11	TRM57971.00	NONE	−24.1 ± 0.4	−65.7 ± 0.5	89.6 ± 0.4
HOFN	2014/01/01	LEICA	GR25	3.11.1639/6.403	LEIAR25.R4	LEIT	43.7 ± 4.0	−44.0 ± 0.8	
M0SEa	2014/01/01	LEICA	GR25	3.20/6.403	LEIAR25.R4	LEIT	41.1 ± 4.1		

(continued)

Table 6 (continued)

Station		Receiver			Antenna		Calibration [ns]		
ID	Date	Receiver	Type	Firmware	Type	Radome	dGLGP	dGPGA	dBDGP
M0SEb	2016/02/02	LEICA	GR25	3.22/6.521	LEIAR25.R4	LEIT	−24.9 ± 0.5	−67.4 ± 0.4	
MLVL	2014/01/01	LEICA	GR25	3.11	TRM57971.00	NONE	35.5 ± 11.0	−41.5 ± 6.3	60.3 ± 4.9
PADOa	2014/01/01	LEICA	GR10	3.10.1633/6.403	LEIAR25.R4	NONE	40.7 ± 4.4	−41.4 ± 1.3	53.2 ± 2.2
PADOb	2016/03/15	LEICA	GR10	3.22/6.521	LEIAR25.R4	NONE	−25.3 ± 1.4	−64.7 ± 0.3	77.6 ± 1.8
PADOc	2016/06/15	LEICA	GR10	4.00/6.522	LEIAR25.R4	NONE	−23.5 ± 1.4	−64.4 ± 2.7	77.2 ± 4.4
PEN2	2014/01/01	LEICA	GRX1200 + GNSS	8.51/6.110	LEIAR25.R4	LEIT	41.5 ± 3.3	54.3 ± 5.1	
REYKa	2014/01/01	LEICA	GR25	3.11.1639/6.403	LEIAR25.R4	LEIT	42.8 ± 1.2	−43.9 ± 0.8	62.0 ± 2.4
REYKb	2016/08/08	LEICA	GR25	3.11.1639/6.522	LEIAR25.R4	LEIT	−23.8 ± 0.3	−67.1 ± 0.5	84.0 ± 3.1
WROCa	2014/01/01	LEICA	GR25	3.11.1639/6.403	LEIAR25.R4	LEIT	63.2 ± 1.4		84.7 ± 1.7
WROCb	2015/09/04	LEICA	GR25	3.21/6.403	LEIAR25.R4	LEIT	19.7 ± 1.0	−62.8 ± 0.9	73.1 ± 1.9
WROCc	2016/03/10	LEICA	GR25	3.22/6.522	LEIAR25.R4	LEIT	16.9 ± 1.9	−63.7 ± 0.4	75.6 ± 2.6
BRUX	2014/01/01	SEPTENTRIO	POLARX4TR	2.9.0	JAVRINGANT_DM	NONE	2.8 ± 3.0	0.6 ± 0.6	3.4 ± 3.8
CEBR	2014/01/01	SEPTENTRIO	POLARX4	2.9.0	SEPCHOKE_MC	NONE	−0.4 ± 3.1	0.0 ± 0.6	−3.7 ± 3.1
KIRU	2014/01/01	SEPTENTRIO	POLARX4	2.5.2-esa3	SEPCHOKE_MC	SPKE	−3.2 ± 2.4	−0.2 ± 0.7	2.2 ± 4.3
MAS1	2014/01/01	SEPTENTRIO	POLARX4	2.9.0	LEIAR25.R4	NONE	−1.2 ± 0.4	0.0 ± 0.6	−4.9 ± 2.2
REDU	2014/01/01	SEPTENTRIO	POLARX4	2.5.2-esa3	SEPCHOKE_MC	NONE	0.2 ± 0.4	−0.2 ± 1.0	−0.4 ± 1.3
VILL	2014/01/01	SEPTENTRIO	POLARX4	2.9.0	SEPCHOKE_MC	NONE	2.5 ± 0.4	−0.3 ± 0.9	−0.9 ± 1.1
BOGO	2014/01/01	TOPCON	EUROCARD	2.6.1 Jan,10,2008	ASH700936C_M	SNOW	−117.9 ± 1.1		
COMO	2014/01/01	TOPCON	E_GGD	3.4 Dec,12,2009 p2	TPSCR3_GGD	CONE	−76.3 ± 2.0		
IGMI	2014/01/01	TOPCON	ODYSSEY_E	3.4 DEC,12,2009 P2	TPSCR.G3	TPSH	−69.3 ± 1.8		
SULP	2014/01/01	TOPCON	NET-G3A	4.1 May,31,2013	TPSCR.G5	TPSH	−76.4 ± 0.9		
BBYSa	2014/01/01	TRIMBLE	NETR9	4.81/4.71	TRM59800.00	NONE	16.5 ± 2.7		44.4 ± 2.8
BBYSb	2014/05/03	TRIMBLE	NETR9	4.85/4.71	TRM59800.00	NONE	10.7 ± 0.9	−12.5 ± 1.0	39.9 ± 1.9
BRST	2014/01/01	TRIMBLE	NETR9	4.85	TRM57971.00	NONE	11.2 ± 1.2	−12.2 ± 1.6	38.6 ± 1.9

(continued)

Table 6 (continued)

Station		Receiver			Antenna		Calibration [ns]		
ID	Date	Receiver	Type	Firmware	Type	Radome	dGLGP	dGPGA	dBDGP
DLF1a	2014/01/01	TRIMBLE	NETR9	4.81	LEIAR25.R3	LEIT	23.6 ± 1.8		44.8 ± 1.4
DLF1b	2016/06/17	TRIMBLE	NETR9	5.14	LEIAR25.R3	LEIT	17.5 ± 0.7	−16.3 ± 0.9	42.0 ± 1.4
DYNG	2014/01/01	TRIMBLE	NETR9	5.14	TRM59800.00	NONE	12.5 ± 1.7	−13.2 ± 1.5	38.6 ± 2.6
GANPa	2014/01/01	TRIMBLE	NETR9	4.81/4.29	TRM55971.00	NONE	13.0 ± 2.6		40.5 ± 1.5
GANPb	2014/05/30	TRIMBLE	NETR9	5.10/5.02	TRM55971.00	NONE	9.4 ± 2.5	−15.8 ± 1.3	37.0 ± 2.0
GOP7b	2015/08/21	TRIMBLE	NETR9	5.01	LEIAR25.R4	LEIT	10.5 ± 3.4	−6.8 ± 4.7	36.5 ± 3.1
TLSE	2014/01/01	TRIMBLE	NETR9	5.14	TRM59800.00	NONE	15.2 ± 1.5	−14.3 ± 1.5	43.7 ± 1.9

5 Conclusion

We have shown that the constellations GPS, Glonass, Galileo, BeiDou, QZSS, NAVIC and GAGAN can be used altogether or in separate combinations for positioning, provided that the time scales are appropriately synchronized and type/individual calibration tables such as Table 6 are used. The time offsets are variable in time, and not well predictable, particularly for Glonass and BeiDou. Moreover the offsets depend on the receiver type, implying that a standardization in the receiver firmware is still lacking. Software receivers could represent an alternative, if the processing speed can be sufficiently increased.

References

Banville S, Langley R (2009) Improving realtime kinematic PPP with instantaneous cycle slip correction. In: Proceedings of ION GNSS 2009, 16–19 Sept, GA, USA

Bisnath S (2000) Efficient automated cycle slip correction of dual frequency kinematic GPS data. In: Proceedings of ION GPS 2000, Salt Lake City, Utah, 19–22 Sept, pp 145–154

Chen J, Xiao P, Zhang Yize, Wu B (2013) GPS/GLONASS system bias estimation and application in GPS/GLONASS combined positioning. In: Sun J et al (eds) China satellite navigation conference (CSNC) 2013 proceedings, Lecture Notes in Electrical Engineeringm, vol 244, Springer, Berlin. doi:10.1007/978-3-642-37404-3_29

Chen J, Wang J, Zhang Y, Yang S, Chen Q, Gong X (2016) Modeling and assessment of GPS/BDS combined precise point positioning. Sensors 16(7):1151. doi:10.3390/s16071151

Dach R, Lutz S, Walser P, Fridez P (eds) (2015) Bernese GNSS software version 5.2. In: User manual, Astronomical Institute, University of Bern. Bern Open Publishing. doi:10.7892/boris.72297; ISBN:978-3-906813-05-9

Dalla Torre A, Caporali A (2015) An analysis of intersystem biases for multi-GNSS positioning. GPS Solution 19(2):297–307

European GNSS Open Service (2015) Signal in space interface control document (OS-SIS-ICD), Issue 1.2. Nov 2015

Gao Y, Chen K (2004) Performance analysis of precise point positioning using real-time orbit and clock products. J Glob Positioning Syst 3:95–100

IGS and RTCM-SC104 (2015) RINEX—the receiver independent exchange format, Version 3.03, 14 July. International GNSS Service (IGS), RINEX Working Group and Radio Technical Commission for Maritime Service Special Committee

Jiang N, Xu Y, Xu T, Xu G, Sun Z, Schuh H (2016) GPS/BDS short-term ISB modeling and prediction. GPS Solution. doi:10.1007/s10291-015-0513-x

Li Z, Yuan Y, Li H, Ou J, Huo X (2012) Two-step method for the determination of the differential code biases of COMPASS satellites. J Geod 86(11):1059–1076

Montenbruck O, Hauschild A, Steigenberger P (2014) Differential code bias estimation using multi-GNSS observations and global ionosphere map. Proceedings of ION-ITM-2014. Institute of Navigation, San Diego, CA, pp 26–28

Odijk D, Nadarajah N, Zaminpardaz S, Teunissen PJG (2016) GPS, Galileo, QZSS and IRNSS differential ISBs: estimation and application. GPS Solution. doi:10.1007/s10291-016-0536-y

Xiaohong Z, Xingxing L (2012) Instantaneous re-initialization in real-time kinematic PPP with cycle slip fixing. GPS Solution 16:315–327. doi:10.1007/s10291-011-0233-9

Zhang W, Lou Y, Gu S, Shi C, Haase JS, Liu J (2016) Jpint estimation of GPS/BDS real-time clocks and initial results. GPS Solution. doi:10.1007/s10291-015-0476-y

Improvements in Geodetic Surveying Using GNSS Radio Occultation Observations

Francesco Vespe, Elisa Rosciano and Giuseppe Vizziello

Abstract The coordinates of a static Global Navigation Satellite System (GNSS) station placed on the ground are estimated together with the delay suffered by the incoming satellite signals through the atmosphere. The tropospheric delay (TD) is shaped as the product of the zenith total delay (ZTD) times a slant factor or mapping function (MF) depending on the sine of elevation angles. In processing chain ZTD is just estimated together with the coordinates; while the MF is modeled apart, in an independent way, by using atmospheric profiles retrieved with balloon observations (RAOB) as done for the Niell (1996) or provided by climate or Numerical Weather Prediction (NWP) models as in the Vienna MFs. The several space missions devoted to GNSS-RO (e.g. COSMIC-FORMOSAT, METOP, CHAMP, GRACE end others) are providing a huge amount of data which makes worthwhile to be attempted the reconstruction of a new mapping function (MTMF) based on such kind of data. First results have been achieved merging GNSS-RO data with model. The merging is made necessary because often the GNSS-RO profiles don't reach the ground. The validation activity however has pointed out not meaningful improvements. Thus we have changed algorithms just to minimize the impact of external data provided by the model. We have performed of course comparisons and validation activities as already done, working with data of GNSS stations spread in the Mediterranean area. In particular formal errors and repeatability of ZTD, coordinates and baselines estimated with the MTMF will be compared with those achieved applying the Niell mapping function. In validation activities we have implemented new MTMFs in bernese software.

F. Vespe (✉) · E. Rosciano
Centro di Geodesia Spaziale, Agenzia Spaziale Italiana, Rome, Italy
e-mail: francesco.vespe@asi.it

E. Rosciano
e-mail: elisa.rosciano@est.asi.it

G. Vizziello
Consorzio INNOVA, Maniago, Italy
e-mail: vizziello@consorzio-innova.it

R. Cefalo et al. (eds.), *New Advanced GNSS and 3D Spatial Techniques*,
Lecture Notes in Geoinformation and Cartography,
DOI 10.1007/978-3-319-56218-6_7

Keywords Global navigation satellite systems · Atmosphere · Geodetic surveying · Geophysics

1 Introduction

Currently GNSS is recognized for its contributions to atmospheric research in both weather prediction and climate change. It is well known that GNSS capabilities to provide coordinates with an accuracy within few millimeters, have made the system a powerful tool suitable for scientific investigations in the field of Geodesy, Geophysics, Atmosphere (Hoffmann-Wellenhof et al. 2001) as well as Fundamental Physics (Ashby 2003). These applications are currently feasible because the modelling and the estimation strategies of the bias due to the atmosphere, namely tropospheric and ionosphere delay, have been more and more refined. The ionospheric bias can be mitigated using dual frequency receivers. Unlike the ionospheric bias, the troposphere effects cannot be removed using the same procedure because it is not dispersive. Compensation for the tropospheric bias is often carried out using a standard (TD) model. The tropospheric delay is a function of elevation and altitude of the receiver, and is dependent on many parameters such as atmospheric pressure, temperature and relative humidity.

The GNSS signal arrives to the receiver from a direction that forms an arbitrary angle with the zenith direction. Thus the most comfortable way to model the TD is to express it as the product between the ZTD and a Mapping Function (MF). The MF is essentially a slant factor which provides the number of air masses crossed by the signal through the atmosphere as a function of the elevation angle E. MF = 1 for the zenith direction; while MF = 1/sin(E) for other directions, assuming flat the layers of the atmosphere. But the atmosphere layers are not flat! Thus it was proposed by Marini (1972) and Marini and Murray (1973) to express the MF in terms of a nested function in the following fashion:

$$MF_w(E) = \frac{1}{\sin(E) + \frac{a}{\sin(E) + \frac{b}{\sin(E) + \frac{c}{\sin(E)\ldots}}}} \tag{1}$$

The coefficients involved in Eq. (1) are usually estimated using independent data, namely profiles retrieved with RAOB. The coefficients could be function of some atmospheric parameters such as surface pressure and temperature, latitude, longitude, the Day Of the Year (DOY), topography and/or tropospheric height etc. according to the proposed model. The calculation of more and more refined MF: Lanyi 1984; Davis et al. 1985; Herring 1992; Niell 1996; Ifadis 2003; resulted in significant advances in the accuracy of the geodetic observations in the last three decades. Anyway, the Niell mapping function (NMF) among the Marini-Murray-like

MF showed to be most accurate and based on strongly relevant parameters (i.e. height, latitude and DOY).

Bar-Saver et al. (1998) proposed to add to Eq. (1) the so called gradient term:

$$\Delta D = m_{\Delta}(e) \cdot \cot(e)[G_N cos\phi + G_E sin\phi] \quad (2)$$

where ϕ is the azimuth angle measured Eastward from North.

This term, formulated by MacMillan (1995) for Very Long Baseline Interferometry, is added to the wet and dry MF terms just to take into account horizontal variations of the TD. The $G_{[x]}$ terms in Eq. (2) are just the coefficients of the azimuth gradient of TD. The horizontal term improves the site coordinates estimation. The improvements on the coordinates estimation when the horizontal gradient is applied, are more significant for low elevation angle (5°–10°) as widely demonstrated in Bar-Sever et al. (1998).

In the last years it was proposed to use directly the values of pressure, humidity and temperature provided by climatological (the Global Mapping Function: GMF) and/or Numerical Weather Prediction (the Vienna Mapping Function: VMF_1) models as in Boehm et al. (2006a, b) and Boehm et al. (2009). These last two updated MF, anyway provide coefficients organized in a Marini-Murray fashion as done for the last but one MFs. An important conclusion of these last analysis was that MF achieved using local weather information are more precise than global one. MTMF can be classified among the local MF.

Thus the goal of our work is to re-estimate the NMF coefficients by using the huge amount of data coming from GNSS-RO space mission instead of RAOB and/or the model profiles. In particular, we have used about 1,500,000 events since 2000, exploiting SAC-C (see http://www.conae.gov.ar/satelites/sac-c/SAC-CPUBLI200208.pdf), CHAMP (Wickert et al. 2001) and COSMIC (Anthes et al. 2008) data. Anyway more than 90% of data have been provided by COSMIC space mission. COSMIC is a joint Taiwan-USA/UCAR mission which consists of 6 satellites fully devoted to GNSS-RO. It is capable of retrieving about 2000 of RO events/day and has proven to be of extremely high quality because its satellites are equipped with a receiver with high gain antenna which implements open loop tracking channels. New data retrieved with the GRAS GNSS-RO receivers onboard METOP/ESA satellites (Von Engeln et al. 2011) can be added to our large database. This subject was already tackled by the authors merging GPS-RO observations with models provided by NCEP and ECMWF (Vespe 2013). The merging is made necessary because often the GNSSS-RO profiles don't reach the ground. The validation activity however has pointed out not meaningful improvements (Vespe 2013). Thus we have changed algorithms just to minimize the impact of external data provided by the model. In particular in this new approach we reconstruct the whole profiles, i.e. down to the ground, applying our BPV method (Vespe and Persia 2006; Vespe 2016). With the BPV we select the CIRA86aQ model (Dach et al. 2009) which fits at the best the GNSS-RO bending angles (BA) profile through the cold atmosphere (i.e. from the upper troposphere to the stratopause). Then we use the selected CIRA86aQ (Kirchengast et al. 1999) model itself to perform the merging

we previously did with NCEP/ECMWF data (Vespe 2013, 2016). Thus we will describe the approach applied to estimate the coefficients of the new MF in Sect. 2. In the third the ray-tracing technique (R-T) applied to GPS ground data to extract the coefficients of the MF is fully described. In the 4th section, the results of the experiments performed are discussed and, finally, some conclusions will be drawn.

2 The Calculation of the Matera Mapping Function

We recall the needed steps to reconstruct our MTMF (Vespe and Persia 2006). The tropospheric delay, looking at Fig. 1, which helps us to understand the geometry suitable to estimate the MTMF, is

$$TD = L - L_0 \tag{3}$$

where L is the path of the signal through the atmosphere and L_0 is the pure geometrical path in vacuum. We apply the ray—tracing formula to estimate L:

$$L = \int_{R_E+h}^{R_{atm}} \frac{n^2(r) \cdot r}{\sqrt{n^2(r) \cdot r^2 - a^2}} dr \tag{4}$$

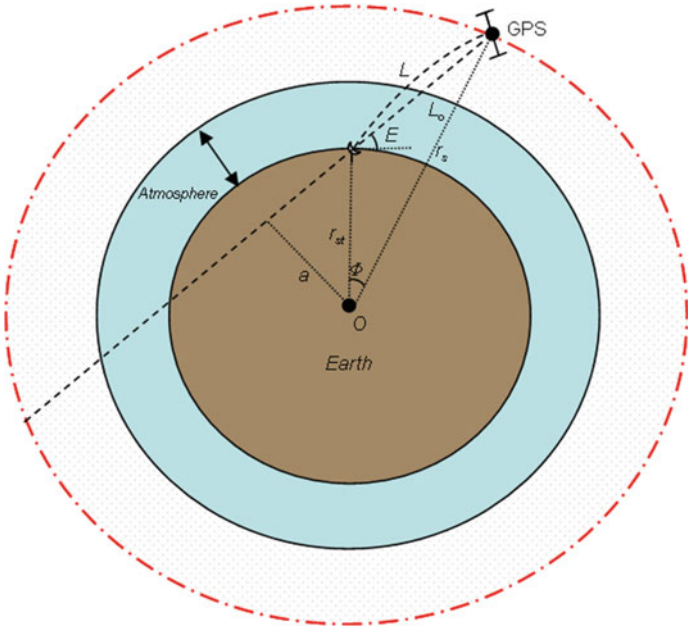

Fig. 1 GNSS acquisition geometry

where R_E is the Earth radius, h is the height above the geoid, a is the impact parameter, n(r) is the refractive index and R_{atm} is the radius of the atmospheric bulge measured from the upper level where the GNSS-RO profile is retrieved.

Thus, L_0 can be expressed as:

$$L_0 = \int_{R_E+h}^{R_{atm}} \frac{dr}{sin(E)} = \frac{h}{sin(E)} \tag{5}$$

so that the elevation angle E is:

$$E = \arcsin\left(\frac{h}{L}\right) = \arcsin\left(\frac{h}{(R_E+h)^2 + R_{atm}^2 - 2R_{atm}\cdot(R_E+h)cos\Phi}\right) \tag{6}$$

where the elevation angle is computed applying the Carnot theorem to the triangle whose vertices are the GPS satellite, the GPS receiver and the Earth centre (see Fig. 1). The angle Φ is computed by applying R-T equation:

$$\Phi = a \int_{R_E+h}^{R_{atm}} \frac{1}{\mathrm{r}\sqrt{n^2(r)\cdot r^2 - a^2}} dr \tag{7}$$

Now, we can apply the following relationship:

$$MF_{[x]}(E) = \frac{L_{[x]} - L_0}{Z[X]D} \tag{8}$$

where

$$Z[X]D = 10^{-6} \int_{R_E+h}^{R_{atm}} N_{[x]}(r)dr \tag{9}$$

In Eq. (8) [X] stands for "W" when we handle the wet component of delay; while "D" is used for the dry component.

According to the NMF (Niell 1996) the variables involved in Eqs. (1) and (8) are: latitude, height, DOY. We have used the same criterion. The parameters to be solved by least squares minimization using as observables the GNSS-RO data are, of course, the coefficients of the Marini-Murray function, truncated at the third order, both for the dry and wet component, and the Niell coefficients for the heights, as shown in Eqs. (10) and (11).

$$MF_d(E) = \frac{\frac{a_d}{1+\frac{b_d}{1+c_d}}}{\sin(E)+\frac{a_d}{\sin(E)+\frac{b_d}{\sin(E)+c_d}}} + \left(\frac{1}{\sin(E)} - \frac{1+\frac{a_h}{1+\frac{b_h}{1+c_h}}}{\sin(E)+\frac{a_h}{\sin(E)+\frac{b_h}{\sin(E)+c_h}}}\right)\cdot h \quad (10)$$

$$MF_w(E) = \frac{\frac{a_w}{1+\frac{b_w}{1+c_w}}}{\sin(E)+\frac{a_w}{\sin(E)+\frac{b_w}{\sin(E)+c_w}}} \quad (11)$$

We have computed the MTMF coefficients according the 3D grid. The main drawback in using the GNSS-RO data is that almost the profiles do not reach the ground. Hence we have selected only the profiles which stop at a height ≤ 1 km. This strict filtering of the data is crucial in our approach because we are forced to merge them with other source of data needed just to have profiles down to the ground. Profiles cut at higher altitudes would weight more the other source of data involved in merging. So the benefits in using GNSS RO observations could vanish.

In the previous approach (Vespe 2013, 2016) we performed a merging with NCEP data (see http://www.emc.ncep.noaa.gov/), applying a sort of optimal approach:

$$N(h) = k(h)\cdot N(h)_{RO} + (1-k(h))\cdot N(h)_{NCEP} \quad (12)$$

where h is the height, $k = 1$ around the lowest value of GNSS RO profile or $k = 0$ for heights close to the ground. Figure 2 shows how the merging of two sets of data works (Table 1).

The green line (Fig. 2a) is the result of merging between the extrapolated behaviour of GNSS-RO refractivity appearing in the first term of Eq. (12) and the model profile. On the contrary when we use BPV approach and select the right CIRA86aQ model (see Fig. 2b) (in our case we sum both dry and wet refractivity provided by the tables) we don't need to apply Eq. (12) because there is no discontinuity between the lower part of real data of GNSS-RO and the model itself. We have selected indeed just the model closest to the real data of GNSS-RO (blue line in Fig. 2b) to reconstruct the profile (see Vespe and Persia 2006; Vespe 2016;

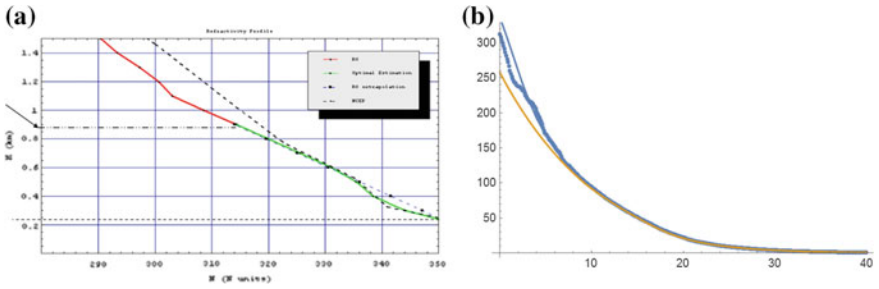

Fig. 2 Merging of refractivity model and GNSS-RO data. In **a** the merging of GNSS RO and model is shown. In **b** the *yellow line* is the BPV dry model, the *blue dot* plot is the same as in Fig. 2a while the *blue line* is the profile we achieve applying BPV and wet models of CIRA-86aQ

Table 1 Features to compute the MTMF coefficients

Latitude gridding	180°/degree of the selected harmonic
Longitude gridding	360°/degree-order of the selected harmonic
Nr of epochs of the year	8 (45 days)
Layers selected to estimate the dry parameters as in Eq. (7)	Up to 2000 m with steps of 400 m starting from sea level About 50 different values of the elevation angle have been selected for fitting

Kirchengast et al. 1999). The only risky action of this approach remains the extrapolation down to the ground of the selected model.

Also in this case the values of the MTMF coefficients have been organized in terms of spherical harmonics (SH) as already proposed and done in Boehm et al. (2006):

$$\begin{aligned} a(\varphi,\lambda,t) &= \sum_{n=0}^{n=?}\sum_{m=0}^{n} P_{nm}\sin(\varphi)\cdot\left(C(t)_{nm}\cos(\lambda)+S(t)_{nm}\sin(\lambda)\right) \\ b(\varphi,\lambda,t) &= \cdots c(\varphi,\lambda,t) = \cdots \end{aligned} \tag{13}$$

Also in this case we have truncated the expansion to the 18th degree as already assessed in Vespe (2013).

3 Results

After having computed the values of the parameters of the MTMF using GNSS-RO data for each of the 8 different epochs of the year (Vespe 2013), we have performed an operational test. Figure 3 shows the network of 8 EUREF GNSS stations to perform the validation. It is the same of that investigated in Vespe (2013). Table 2 shows a brief description of the involved stations. The ZTDs of the 8 stations selected were estimated together with the coordinates using the Bernese software. The minimum coordinates constrained solution approach was applied (Dach et al. 2009). This is the default analysis strategy that Bernese usually applies.

In this way we can tune the strength of the constraints working on the a priori sigmas to give to the stations. The station coordinates are given in IGS05 reference system. The cut off elevation angle was fixed at 5°. The absolute corrections of the phase center variations of the antenna were applied. The coordinates together with hourly ZTD were the output of the computation. The analysis strategy is summarized in Table 3.

We launched an additional data processing session to those already performed (Vespe 2013). In this third sessions we have used the new MF (Hereafter **Cmt**) computed using CIRA86aQ model determined with BPV approach. We recall that the first two solutions were achieved applying in turn the NMF and MTMF adopting just the same input set up and processing strategy as shown in Table 3.

Fig. 3 Network of stations involved in the validation

Table 2 Description of the stations shown in Fig. 3

Station	Location and DOMES
BRUS	Brussel, Belgium. 13101M004
FFMJ	Frankfurt, Germany. 14279M001
MATE	Matera, Italy. 12734M008
ONSA	Onsala, Sweden. 10402M004
PPTB	Braunschweig, Germany. 14234M001
VILL	Villafranca, Spain. 13406M001
ZIMJ	Zimmerwald, Switzerland. 14001M008
ZIMM	Zimmerwald, Switzerland. 14001M004

Table 3 Analysis strategy

Strategy	Minimum constrained network adjustment
Data handling	3 months of data. 8 permanent stations
Satellite orbits	IGS precise
ERP	IERS—IGS
Station coordinates	IGS05
Datum	
Cut-off elevation	5°
Antenna PCV	Relative
Sampling rate	30″
Estimated parameters	Coordinates, satellite and clocks, phase ambiguities, ZTD

The analysis was performed for 3 months of GPS data (Vespe 2013): from January 1th 2007 to April 1th 2007. For every pair of stations baselines their repeatability have been computed according to (Niell 1996):

$$\sigma = \sqrt{\frac{\sum_{i=1}^{n}(b_i - b_0)^2}{n-2}} \tag{14}$$

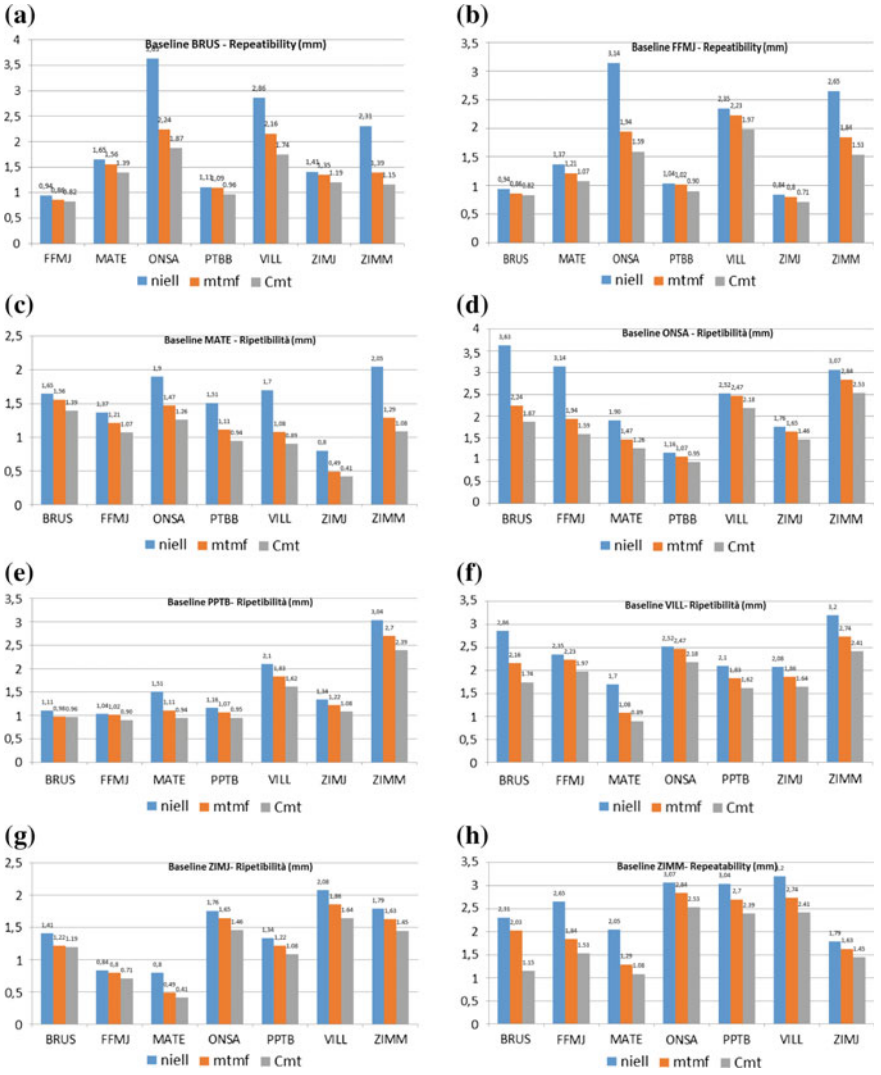

Fig. 4 **a–h** The *blue*, *orange* and *gray* histograms show the results of repeatability achieved with the three processing chain changing the MF: NMF, MTMF and **Cmt**

For each baseline the repeatability is the standard deviation of the n estimates b_i with respect to the mean value b_0 computed on a linear regression. Figure 4a–h shows the repeatability comparison (NMF, MTMF and Cmt) for every baselines.

Then for each station, the ZTD has been estimated for the three sessions as well. Figure 5a–c shows the comparison for 3 stations (BRUS, ONSA and ZIMM) on 1th January 2007 and for 24 h. Analysing 2 weeks the results are the same in term of improvements.

The results achieved show that the application of the new mapping function MTMF improves the level of the baseline repeatability of a mean value of up to 15% and the formal errors of the ZTD up to 20%. It seems that the new **Cmt** proposed to overcome in a more elegant fashion the lack of GNSS-RO data close to the ground, has an even better performance.

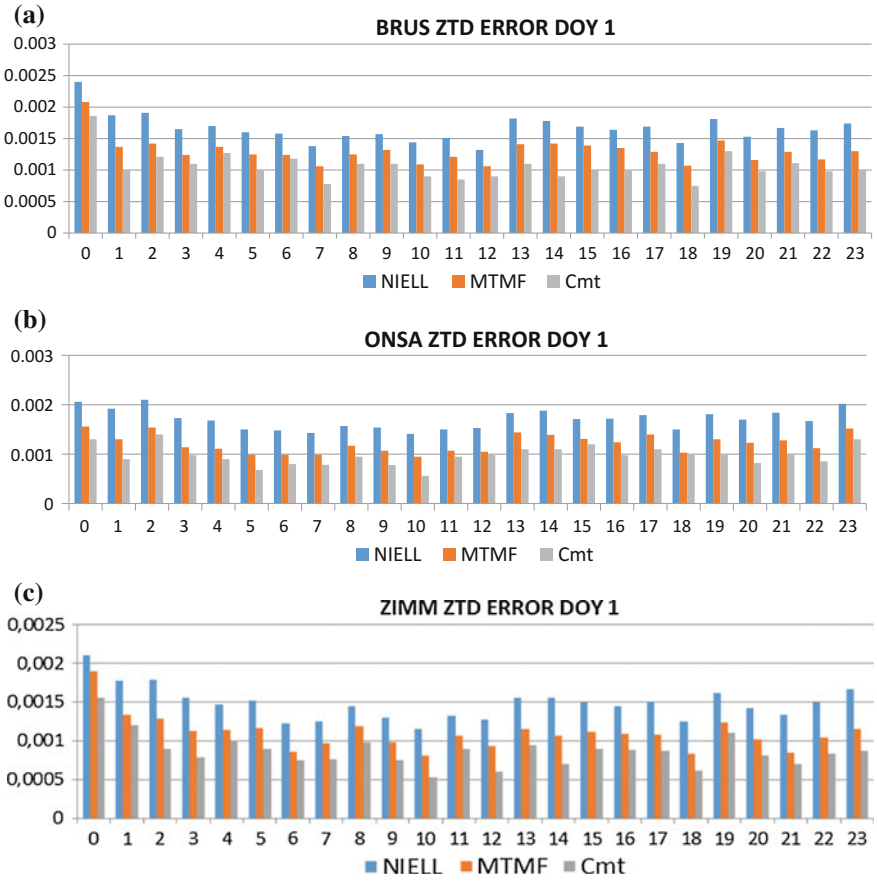

Fig. 5 **a–c** The *blue*, *orange* and *gray* histograms show errors on the estimates of the zenith total delay achieved with the three processing chain with three different MF: NMF, MTMF and Cmt

We would stress that the results achieved regards only a relatively small network centered in Europe. The NMF was indeed built mainly with RAOB observations flying over America and, therefore, particularly tailored for that atmosphere.

4 Conclusions

We have proposed with the present work the use of the huge amount of GNSS-RO data currently available to build new mapping functions: the MTMF and **Cmt** following the same approach as in Niell (1996). The main advantage in using such kind of data concerns the uniform and global distribution of GNSS-RO all over the world and over the oceans. Such advantage, together with the robust statistics due to the huge number of profiles, makes the use of the MTMF as well as **Cmt** particularly promising.

The coefficients of our MFs were computed, indeed, for 8 different epochs of the year and organized in terms of spherical harmonic expansion. The main drawback in using these big amount of GNSS-RO data is that the most of the retrieved atmospheric profiles are truncated before to touch down. In the first release of our work (Vespe 2013, 2016) we have merged in an "optimal estimation fashion" GNSS-RO data with models, as described by Eq. (12) and Fig. 2, in order to overcome such trouble. Looking at Fig. 2a it emerges anyway that often a big discontinuity occurs between the model and the real GNSS-RO occultation at the point on which the profiles are truncated. So it occurs that when we merge the profiles their final behaviour can be strongly, unrealistically warped. So we have conceived a second release of our approach just to avoid such big discontinuity. In this second release (**Cmt**) we apply the BPV approach (Vespe and Persia 2006) to select the model of CIRA86aQ (essentially we estimate the DoY and the Latitude of the refractivity profile to select) which fits at the best the BA profiles provided by GNSS-RO. The model so built agrees better with the real data at the lower end of the GNSS-RO profiles. Thus in the present work we have compared the performances of three different MF: NMF, MTMF and **Cmt**. The results have been summarized in Figs. 3 and 4. We have tested their performances selecting a small network of 8 stations all over the Europe working on time repeatability of the measured baselines three months long and the uncertainties we have in the estimate of ZTD. The improvement achieved with the implementation of the new **Cmt** is of the order of 30–35% with respect the same solutions given by the NMF.

Anyway the results achieved must be tackled with care! The two new proposed MF need indeed to be more deeply validated and we plan to introduce in the computation of the MF coefficients the dependence on the longitude too that till now has been neglected. The validation must be performed for different kind of network and for a wider area of the globe.

Furthermore, a comparison has to be performed with the Global (Boehm et al. 2006a, b) and Vienna MF (Boehm et al. 2009) which are currently the state of art MF currently in use.

Finally, it would be interesting to apply the MTMF to VLBI and DORIS observations as well just to perform a comparison of the ZTD retrieved with different geodetic techniques and test if the agreement of the solutions improves (Snajdrova et al. 2006).

References

Anthes RA, Bernhardt PA, Chen Y et al (2008) The COSMIC/FORMOSAT-3 mission: early results. Bull Am Met Soc 89(3)

Ashby N (2003) Relativity in the global positioning system. Living Rev. Relativ 6

Bar-Sever YE, Kroger PM, Borjesson JA (1998) Estimating horizontal gradients of tropospheric path delay with a single GPS receiver. J Geophys Res 103(B3):5019–5035

Boehm J, Niell A, Tregoning P et al (2006a) Global mapping function (GMF): a new empirical mapping function based on numerical weather model data. Geophys Res Lett 33(7):L07304. doi:10.1029/2005GL025546

Boehm J, Werl B, Schuh H (2006b) Troposphere mapping functions for GPS and very long baseline interferometry from European Centre for Medium-Range Weather Forecasts operational analysis data. J Geophys Res 111:B02406. doi:10.1029/2005JB003629

Boehm J, Kouba J, Schuh H (2009) Forecast Vienna mapping functions for real-time analysis of space geodetic observations. J Geod 86(5):397–401

Dach R, Brockman E, Schaer S et al (2009) 2009: GNSS processing at CODE, status report. J Geod 83(3–4):353–365

Davis JL, Herring TA, Shapiro II et al (1985) Geodesy by radio interferometry: effects of atmospheric modelling errors on estimates of baseline length. Radio Sci 20:1593–1607

Herring TA (1992) Modelling atmospheric delays in the analysis of space geodetic data. In: DeMunk JC, Spoelstra TA (ed) Symposium on refraction of transatmospheric signals in geodesy, Netherlands Geodetic Commission Series 36, pp 157–164, Ned. Comm. voorGeod., Delft

Hoffmann-Wellenhof B, Lichtenegger H, Collins J (2001) GPS theory and practice. Springer, Berlin

Ifadis I (2003) The atmospheric delay of radio waves: modeling the elevation dependence on a global scale. Technical. Report 38L. Sch. of El. and Com. Eng., Chalmers Univ. of Techn., Gothemburg, Sweden

Kirchengast G, Hafner J, Poetzi W (1999) The CIRA86aQ UoG model: an extension of the CIRA-86 monthly tables including humidity tables and a Fortran95 global moist air climatology model. Technical Report for ESA/ESTEC No.8/1999

Lanyi G (1984) Tropospheric delay effects in radio interferometry. TDA Prog Rep 42-78, April–June 1984, pp 152–159, JPL Pasadena (CA)

MacMillan DS (1995) Atmospheric gradients from very long baseline interferometry atmospheric modeling improvements. Geophys Res Lett 22(9):1041–1044

Marini JW (1972) Correction of satellite tracking data for an arbitrary tropospheric profile. Radio Sci 7:223–231

Marini JW, Murray CW (1973) Correction of laser range tracking data for atmospheric refraction at elevations above 10 degrees, NASA Tech. Memo, NASA-TM-X-70555, 60

Niell AE (1996) Global mapping functions for the atmosphere delay at radio wavelengths. J Geophys Res 100:3227–3246

Snajdrova K, Boehm J, Willis P et al (2006) Multi-technique comparison of tropospheric zenith delays derived during the CONT02 campaign. J Geod 79(10–11):613–623. doi:10.1007/s00190-005-0010-z

Vespe F (2013) Atmosphere humidity profiles from GNSS radio occultation observations. IV GALILEO Scientific Colloquium, Prague

Vespe F (2016) Retrieval of atmosphere humidity profiles from GNSS radio occultations observation. In: 67th international astronautical congress, IAC-16,B1,IP,31,x33889

Vespe F, Persia T (2006) Derivation of the water vapor content from the GNSS radio occultations observations. J Atmos Oceanic Technol 23(7):936–943

Von Engeln A, Andres Y, Marquardt C, Sancho F et al (2011) GRAS radio occultation onboard of Metop, vol 47(2). doi:10.1016/j.asr.2010.07.028

Wickert J, Reigber C, Beyerle G et al (2001) Atmosphere sounding by GPS radio occultation: first results from CHAMP. Geophys Res Lett 28:3263–3266

Single-Frequency Receivers as Permanent Stations in GNSS Networks: Precision and Accuracy of Positioning in Mixed Networks

Paolo Dabove, Alberto Cina and Ambrogio Maria Manzino

Abstract Continuous Operating Reference Stations (CORSs) are widely used for many purposes including precise positioning, mapping and monitoring. These architectures are composed of a control centre and a number of permanent stations consisting of geodetic antennas and dual frequency receivers. This infrastructure is costly due to the instruments used and has the additional disadvantage in that inter-station distances between CORSs, that are often too high if a single-frequency receiver acts as a rover. This study focuses on the usefulness of permanent single-frequency stations in order to increase density of existing CORSs for monitoring purposes. In this connection, some innovative GNSS networks composed of geodetic and mass-market L1 receivers have been developed and tested, analyzing the performance of rover positioning in terms of quality, accuracy and reliability in real time. Some tests have been carried out considering different types of receivers (geodetic and mass market) and antennas (patch and geodetic), in real-time mode. The results obtained show that with a "classical" network (where the mean inter-station distances between CORSs are about 40 km) an accuracy of about 5 cm can be achieved after fixing the phase ambiguity with a mass-market L1 receiver acting as rover. In addition, the Time-To-Fix period is very short, being less than 2 min. Despite the obvious fact that increased inter-station distance leads to reduced accuracy, the degree of precision obtainable remains useful for many applications, such as mobile mapping and traffic control. In short, the experiments under examination performed with low-cost GNSS receivers will be useful for many types of applications (landslide monitoring, traffic control), especially where the inter-station distances of permanent GNSS stations are around 40 km.

P. Dabove (✉) · A. Cina · A.M. Manzino
Politecnico di Torino, Corso Duca degli Abruzzi 24, 10129 Turin, Italy
e-mail: paolo.dabove@polito.it

R. Cefalo et al. (eds.), *New Advanced GNSS and 3D Spatial Techniques*,
Lecture Notes in Geoinformation and Cartography,
DOI 10.1007/978-3-319-56218-6_8

1 Introduction

Use of GPS/GNSS instruments is today common around the world, both at a commercial level and for academic research. Over the last ten years, CORS networks have been created specifically to achieve the goal of extending classical RTK (real time kinematic) positioning over an area of more than 40 km. Several experiments were made in the past to evaluate the maximum precision obtainable in a CORS network when using either geodetic or mass-market GNSS receivers. With these types of instruments it is possible to achieve accuracies of a few centimeters and a few millimeters in 'Real time' (Bellone et al. 2016) and post-processing (Dabove and Manzino 2014) approaches respectively.

This work takes its starting point from the research described above, in particular focusing on the usefulness of single-frequency multi-constellation GNSS mass-market receivers in NRTK networks as rovers, and also on the use of these kinds of instruments as permanent stations serving to densify existing CORSs, particularly for monitoring purposes. Two different types of CORS network are considered in this paper in terms of real-time positioning: the first is the "small" network and the second is the "large" one, where the mean inter-station distances are about 25/30 (Sass 2007; Snay and Soler 2008) and 50/70 km respectively. Both "small" and "large" networks are useful for many applications (e.g. mobile mapping, precise positioning, cadastral surveying) (Piras et al. 2009) if geodetic instruments are employed but less useful if mass-market instruments are used, or if the inter-station distance between master and rover increases (Won et al. 2015). The use of single-frequency GNSS receivers brings with it certain limits (Bevly 2004) in obtaining a correct fixing of phase ambiguities (Grejner-Brzezinska et al. 2007; Kim and Langley 2002). The aforementioned factors play a crucial role in obtaining centimeter-level positioning in rapid time and with a high degree of reliability (Chen et al. 2015).

Furthermore, the contribution of L1 mass-market permanent stations in CORS networks both for geodetic and low-cost receivers has been investigated; in particular, we describe how the use of network products can improve the accuracy and precision of a rover at distances of 2.5, 5, 10 and 15 km from the nearest station.

2 GNSS L1 Mass-Marker Receivers as Rovers in CORS Networks

Today, when we speak of GNSS Network for Real Time Kinematic (NRTK) positioning, we have in mind a classic network of permanent stations composed of dual-frequency and multi-constellation receivers (hereinafter called a "classic" network). In this context, various studies (Coulot et al. 2014; Dabove et al. 2014) have been conducted in order to estimate precisions and accuracies available with different kinds of instruments. Some tests have also been performed with rover receivers composed of geodetic instruments, while others have examined mass-market instruments (Dabove and Manzino 2014).

First of all, it is necessary to clarify what the Authors mean by the term "mass-market": in this paper we consider to be mass-market GNSS receivers those instruments capable of tracking both pseudorange and carrier-phase measurements on L1 frequencies alone, and which cost less than 500 € (Cina and Piras 2014). On this basis, the u-blox LEA-6T in its evaluation kit mode (EVK-6T) was chosen as being representative of this category, as described in a previous study by Dabove and Manzino (2014). Similarly, for the antenna, a model was chosen that had been tested previously with resultant high-level positioning accuracy. The Garmin GA38 will be considered as our rover antenna because of its very low cost (about 50 €) and since it is, nevertheless, able to track both GPS and GLONASS satellites, thus allowing multi-constellation positioning. As mentioned in the introduction, two different CORS network configurations have been considered (Fig. 1). Both networks are managed by two currently available network software packages: the Leica GNSS Spider v.4.3.0.4633 provided by Leica Geosystems® and the GNSMART v. May 2015 provided by Geo++®, in combination with the two differential corrections available today for single-frequency receivers: the Virtual Reference Station (VRS®) and the Nearest (NRT). To perform NRTK positioning, the RTKLIB v.2.4.2 software was used (Takasu and Yasuda 2006): in particular the RTKNAVI tool was utilized, as described in Takasu and Yasuda (2006), Manzino and Dabove (2013). This software package makes it possible to fix phase ambiguity thanks to the ratio test: in this case the threshold value is equal to 3. This means that if the phase ambiguities are fixed as integer values, centimeter accuracy can be obtained and one may speak of fixed (FIX) positions. In contrast, with no ambiguity fixing, one speaks of the float (FLT) solution which only provides sub-meter accuracy. The coordinates of TEST point (Fig. 1) and all reference stations were estimated through a post-processing approach using a geodetic receiver and antenna

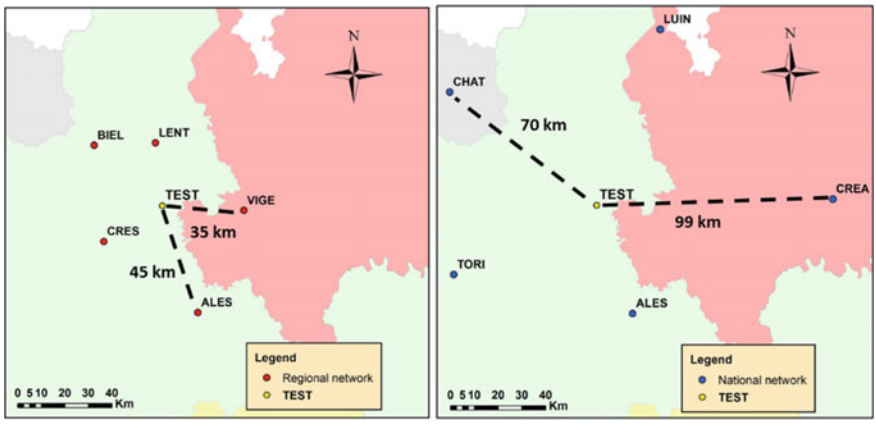

Fig. 1 Inter-station distances of "small" (*left*) and "large" (*right*) networks

Table 1 Results obtained considering the "small" and "large" network and the mass-market receiver as rover

		Small network	Large network	
RTKNAVI Config	Differential correction	2D accuracy at 95% (m)	3D accuracy at 95% (m)	2D accuracy at 95% (m)
Kinematic fix and hold	VRS	0.03	0.06	0.11
	NRT (35 km)	~0.04	~0.04	0.18
Static fix and hold	VRS	0.04	0.03 ÷ 0.04	0.07
	NRT (35 km)	~0.03	~0.02	0.15

and considering a static session of 24 h with a sampling rate of 1 s. The accuracy of these coordinates is about 2 mm. In order to determine the precision and accuracy currently available using a single-frequency and multi-constellation (GPS + GLONASS) mass-market receiver, the u-blox EVK-6T with the low-cost Garmin GA38 antenna were installed on the TEST site for 24 days of acquisition, with a rate of 1 s, with a kinematic positioning, resetting the phase ambiguities each time they are declared fixed. Both Spidernet and GNSMART software packages were utilized to estimate the accuracy obtainable with such receivers but no appreciable differences were found between these two software packages in use: the positioning results obtained by the mass-market receiver in a regional network (inter-station distances of about 25–30 km) are very good both in terms of precision and accuracy if the phase ambiguities are fixed, as it is possible to see from Table 1 (the results shown are obtained using GNSMART software). On the basis of previous studies (Dabove and Manzino 2014), this table only presents "fix and hold" method of integer ambiguity resolution. Considering both "static fix and hold" and "kinematic fix and hold" ambiguity resolution methods available in RTKLIB, accuracies are less than 6 cm using GNSS mass-market receivers, which is suitable for a large number of applications (mobile mapping, cadastral survey etc.) (Guarnieri et al. 2013).

No substantial differences are obtained with respect to (Dabove and Manzino 2014) where a single constellation mass-market receiver was employed as a rover to perform positioning within similar networks. In this case (Table 1) the use of a mass-market dual-constellation receiver does not offer any benefits. Notwithstanding this, an accuracy of about 10 cm can be achieved (Table 1) even with a "small" network.

In addition, time to first fix (TTF) analysis was performed, and after 24 days we had obtained more than 17,000 fixed solutions, which means one FIX solution more or less every 2 min (Dabove and Manzino 2016). This value is reasonable: considering the "large" network TTF is about 175 s (less than 3 min) while it is 81 s if a "small" network is considered. In both cases, the best results are obtained with VRS correction.

3 A "Mixed" Network: Test Set-up and Results

In order to test the use of a GNSS L1 mass-market receiver, a new ad hoc network with "medium" inter-station distances (about 45 km) was defined. The tests, like those of the previous section, were performed on a new network, shown in Fig. 2. In this case, the rover is called TEST and its position is about 19 km from the nearest permanent station, called NOVR. Both the coordinates of TEST and all reference stations were adjusted with the Bernese 5.0 software, using a static session of 2 days with a sampling rate of 1 s in this case too. The characteristics of the NRTK positioning are the same as those described previously. Neither in this case (Table 2) are substantial differences in the quality of rover positioning obtained if Spidernet and GNSMART® software packages are employed: the degrees of accuracy obtained are comparable with those achieved previously (Table 1).

In the "medium" NRTK network the TTF period is also estimated: as it is possible to see from Table 3, a generic user must wait at least 3 min for a FIX position if VRS correction is used. At this point, the challenge is to create a "mixed" network where all sites are composed of dual-frequency and multi-constellation receivers and antennas except for TEST, which is equipped with the same mass-market receiver and the low cost antenna previously described.

Both network softwares were tested but with Spidernet it is not possible to consider a single-frequency receiver as a permanent station. Thus, while Spidernet can, in fact, manage pseudorange and carrier phase measurements, these data

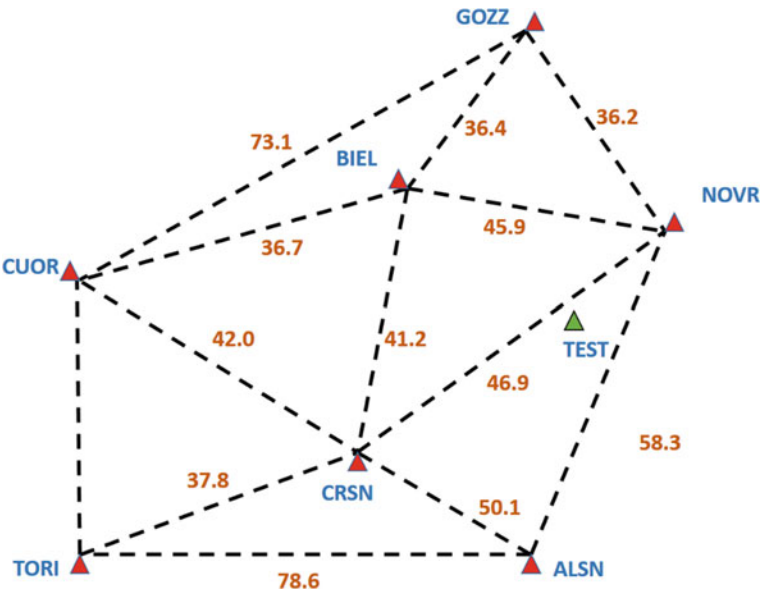

Fig. 2 The new "medium" network: the master stations (*red triangles*) and the rover receiver (in *green*). All distances are in kilometers

Table 2 Accuracies obtainable with the network shown in Fig. 2 and TEST as rover receiver

RTKNAVI configuration	Differential correction	3D accuracy at 95% (m)
Kinematic fix and hold	VRS	0.04
	NRT (19 km)	~0.03
Static fix and hold	VRS	0.03 ÷ 0.04
	NRT (19 km)	~0.02

Table 3 Time to first fix period estimated for different corrections considering the "medium" network shown in Fig. 2 and TEST as rover receiver

Correction type	n° of correct/total FIX	mean TTF	max TTF (s)
VRS	52/78	78 s ± 31 s	183
NRT	41/76	89 s ± 48 s	219

cannot be used for network calculation. GNSMART, on the other hand, exhibits a different behavior. Only in this case can a "mixed" network be examined as both single and dual-frequency receivers can be used as master stations. It is important to stress that the GNSMART software requires approximately 8 min to fix the ambiguity phase for all stations in the network (this is the same time if a network with only geodetic receivers is considered). With a mixed network, and using GNSMART as network software, some tests have been carried out to determine the performances of NRTK positioning with geodetic and mass-market receivers in a mixed network. Test sites 2.5, 5, 10 and 15 km away from TEST have been examined in order to verify precision and accuracy obtainable (Fig. 3).

For these tests, the same instruments installed on TEST site are employed for the rover; different network products, such as VRS and Nearest (NRT) corrections, are used with the RTKNAVI tool for real-time positioning of the mass-market rover receiver, with an updating rate equal to 1 s. The results obtained are somewhat particular: even if the phase ambiguities are fixed for the networks stations, no FIX positions are available for the rover receiver considering all differential corrections, and only float solutions are obtainable. This behavior pertains even where a geodetic (Leica 1230 + GNSS) receiver functions as rover. On the other hand, the float solutions are very good even when the low-cost instrument is employed: the difference between the estimated and the reference positions is about 10 cm if the distance to the nearest station is less than 2.5 km, as it is possible to see from Table 4. In this context, these results are useful only for traffic control purposes or cartographic applications: it could be very interesting to apply this network configuration to real-time monitoring of landslides in order to gain a deeper knowledge of the behavior and movements of the landslide itself.

If the distance between rover and nearest station (also known as the baseline) increases, accuracy does indeed decrease. However, if the difference in distance is in the order of 5 km, the accuracy is in the range of 20 cm, which is useful for many applications, such as mobile mapping, traffic control as well as cartographic applications. The results obtained if the baseline increases are of no particular

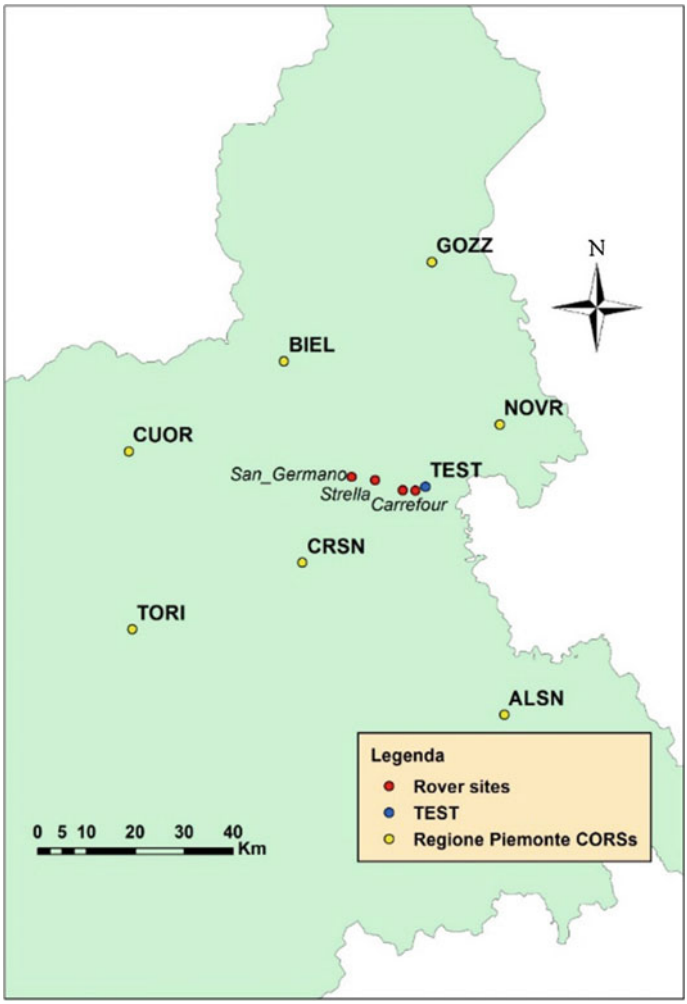

Fig. 3 Rover test sites (in *red*), CORS networks (in *yellow*) and TEST station (in *blue*)

Table 4 Results of mass-market receivers in a mixed network: only FLT solutions are available

Test site	*d* from TEST (km)	Correction	Mass-market	Geodetic
			3D accuracy at 95% (m)	
Carrefour	2.5	VRS	0.09	0.05
		NRT	0.07	0.07
Cascine Strà	5	VRS	0.18	0.15
		NRT	0.22	0.18
Strella	10	VRS	0.53	0.44
		NRT	0.60	0.51
San Germano	15	VRS	0.56	0.50
		NRT	0.61	0.55

interest: in these cases the accuracies obtained are greater than 50 cm, which is not useful for the previously cited purposes. When employing a geodetic receiver as rover (Table 4), good results can also be obtained: if the distance between rover and the nearest station is lower than 5 km, the accuracy is better than 20 cm.

In summary, the results obtained preclude the possibility of performing NRTK positioning in mixed networks as no software currently makes this kind of survey possible. Despite this fact, a new possible solution could be adopted, for example, for landslide monitoring: the idea is to consider all stations (mass-market and geodetic) as masters and analyze the variation of coordinates in order to decide if a displacement occurs. This is possible thanks to GNSMART: the a priori coordinates can be weighted in different ways by the network manager. It is therefore possible to use a stronger constraint weight for geodetic receivers and a looser constraint weight for mass-market ones. At the same time, this software can determine the difference between estimated and a priori coordinates in real time. This is useful because, coupled with some statistical techniques, it makes it the possible to analyze whether a difference is due to measurement noise or represents a real displacement.

54 initializations are made in order to analyze the accuracy of L1 and L1 + L2 CORSs. Some statistical analysis is performed also in order to focus on this aspect: analyzing the behavior of four days of data, after a network initialization of about 8 min, the accuracy of the TEST station is no different from that of the other CORSs, which is to say, about 3 mm in planimetry and 6 mm in altimetry components.

4 Conclusions

The benefits of using a single-frequency receivers are discussed in this paper and their performances in a CORS network were examined.

Two different networks, are investigated with the creation of a “small” and a “large” network. The results obtained using an L1 mass-market GNSS receiver as rover are very good since an accuracy of about 5 cm can be achieved after the fixing of phase ambiguity. Furthermore, TTF is very short: a user need wait no more than 2 min to obtain a fixed solution. If the inter-station distance increases, accuracy does obviously decrease but, notwithstanding this, the precision obtainable is useful for many applications, such as mobile mapping and traffic control.

Subsequently, this kind of receiver has been used as a permanent station, coupled with the same antenna, in an RTK Network with geodetic receivers. In this context, particular results are obtained because no single network software is yet suitable for providing real-time products for “mixed” networks. Nevertheless, as of now, these receivers can be used as masters in real-time network calculation. With GNSMART software it is possible to manage a “mixed” network, and a possible solution could be adopted taking all stations (mass-market and geodetic) as

masters and analyzing the variation of coordinates in order to decide whether a displacement occurs: thus it is possible to compare the difference between estimated and a priori coordinates in real time to analyze whether the difference is due to measurement noise of or constitutes a real displacement.

References

Bellone T, Dabove P, Manzino AM, Taglioretti C (2016) Real-time monitoring for fast deformations using GNSS low-cost receivers. Geomat Nat Hazards Risk, 7(2):458–470. Available at: http://dx.doi.org/10.1080/19475705.2014.966867.

Bevly DM (2004) A low-cost velocity sensor for correcting inertial sensor errors on ground vehicles. J Dyn Syst Meas Control Trans ASME 126(2):255–264

Chen H-Y, Kuo L-C, Lee J-C, Tung H, Su S-H, Yao S-S, Lee H (2015) Reducing distance dependent bias in low-cost single frequency GPS network to complement dual frequency GPS stations in order to derive detailed surface deformation field. Surv Rev 47(340):7–17

Cina A, Piras M (2014) Performance of low-cost GNSS receiver for landslides monitoring: test and results. Geomat Nat Hazards Risk 2014:1–18

Coulot D, Rebischung P, Pollet A, Grondin L, Collot G (2014) Global optimization of GNSS station reference networks. GPS Solution 19(4):569–577

Dabove P, Manzino AM (2014) GPS & GLONASS mass-market receivers: positioning performances and peculiarities. Sensors 2014(14):22159–22179

Dabove P, Manzino AM (2016) An innovative method to predict and to detect the false fixing of the GNSS ambiguity phase. In: International association of geodesy symposia. Springer, Berlin, pp 727–733. ISSN: 0939-9585. doi:10.1007/1345_2015_19

Dabove P, Manzino AM, Taglioretti C (2014) GNSS network products for post-processing positioning: limitations and peculiarities. Appl Geomat 6(1):27–36. ISSN 1866-9298. Available at: 10.1007/s12518-014-0122-3

Guarnieri A, Pirotti F, Vettore A (2013) Low-Cost MEMS sensors and vision system for motion and position estimation of a scooter. Sens 13:1510–1522

Grejner-Brzezinska DA,Kashani I, Wielgosz P, Smith DA, Spencer PSJ, Robertson DS, Mader GL (2007) Efficiency and reliability of ambiguity resolution in network-based real-time kinematic GPS. J Surv Eng 133(2):56–65. doi:10.1061/(ASCE)0733-9453(2007)133:2(56)

Kim D, Langley RB (2002) Instantaneous real-time cycle-slip correction for quality control of GPS carrier-phase measurements. Navig J Inst Navig 49(4):205–222

Manzino AM, Dabove P (2013) Quality control of the NRTK positioning with mass-market receivers. Global positioning systems: signal structure, applications and sources of error and biases. Ya-Hui Hsueh, Hauppauge NY. Chapter 2. pp 17–40

Piras M, Roggero M, Fantino M (2009) Crustal deformation monitoring by GNSS: network analysis and case studies. Adv Geosci 13: Solid Earth (SE) 13, 87

Sass J (2007) Low cost, high accuracy, GNSS survey and mapping. In: Proceedings of the 6th FIG regional conference on strategic integration of surveying services, San José, Costa Rica, 12–15 Nov 2007

Snay RA, Soler T (2008) Continuously operating reference station (CORS): history, applications, and future enhancements. J Surv Eng 134(4):95–104. doi:10.1061/(ASCE)0733-9453(2008)134:4(95)

Takasu T, Yasuda A (2006) Evaluation of RTK-GPS performance with low-cost single-frequency GPS receivers. In: Proceedings of international symposium on GPS/GNSS, Tokyo, Japan, 11–14 Nov 2006; pp 852–861

Won DH, Ahn J, Lee E, Heo M, Sung S, Lee YJ (2015) GNSS carrier phase anomaly detection and validation for precise land vehicle positioning. IEEE Trans Instrum Meas 64(9):2389–2398

Internet Platform for Improving the EGNOS Ionospheric Corrections

Anna Swiatek, Leszek Jaworski and Lukasz Tomasik

Abstract The problem of insufficient accuracy of the EGNOS corrections for the Eastern Poland, located near the border of the EGNOS service area, is well known. The EEI PECS project (EGNOS EUPOS Integration) assumed improving the EGNOS corrections by using the GPS observations from Polish ASG-EUPOS stations. One of important component of the EGNOS correction is ionospheric delay of incoming GNSS signal. In the presented research work, new ionospheric corrections were computed using selected stations located at the eastern and central part of Poland. The new corrections, substituting the original ones for selected grid nodes into original EGNOS corrections in real time, were transmitted by the SiSNet (Signal In Space through Internet) technology to the receivers. The use of regional parameters for the improvement of ionospheric model increased the accuracy and stability of the navigation position, determined during the experiments carried out at Biala Podlaska Airport—located near east border of Poland.

Keywords GNSS · EGNOS · Ionospheric corrections

1 Introduction

The EGNOS-EUPOS Integration PECS project was carried out at Space Research Centre, Warsaw, Poland and was completed by the end of 2012. The main objective of the EEI (EGNOS EUPOS Integration) project was to increase the efficiency and range of application of the EGNOS system, through integration with European Position Determination System (EUPOS). This research problem was investigated by many scholars over the years. However, in their research work they mostly paid attention to accuracy and improvement of navigation positioning by RTK corrections or INS application (Aguilar et al. 2007; Cefalo et al. 2014; Oszczak et al. 2003).

A. Swiatek (✉) · L. Jaworski · L. Tomasik
Space Research Centre P.A.S, Warsaw, Poland
e-mail: ana@cbk.waw.pl

R. Cefalo et al. (eds.), *New Advanced GNSS and 3D Spatial Techniques*,
Lecture Notes in Geoinformation and Cartography,
DOI 10.1007/978-3-319-56218-6_9

The presented project had assumed the improvement of the EGNOS ionospheric corrections only for eastern Poland. The TEC data were obtained from ASG-EUPOS system as sets of values for all available Ionospheric Pierce Points generated for selected permanent stations.

The Ranging and Integrity Monitoring Station (RIMS) network doesn't provide coverage of homogeneous quality correction for the EGNOS service area.

The WRS RIMS site located at Space Research Centre in Warsaw is the most eastern station in the central Europe. This causes the quality of EGNOS corrections in eastern Poland to be lower than in western and central Europe (Grzegorzewski et al. 2012; Jaworski and Swiatek 2009; Jaworski et al. 2013). The EUPOS consists of about 900 reference stations located in 18 European countries. The Polish part of EUPOS—ASG-EUPOS consists of about 100 GNSS permanent stations. Those permanent GNSS stations are available to be used in order to complete the network of RIMS sites. Data obtained from additional GNSS permanent stations could be used to improve the EGNOS corrections.

2 Data Analysis

CSIS station was located at the Space Research Centre, in vicinity of RIMS WRS site. It was equipped with Septentrio PolaRx2 receiver and carried out the permanent measurements in navigation mode using the EGNOS correction for single point positioning. The position was collected at 1-second rate. The daily raw data from receiver were used for reference position computation, using the Bernese GNSS software v5.0. Because the geodetic position was computed with centimetre accuracy it could have been used as a reference for navigation position analyses. The analysis of point coordinates show the permanent shift in horizontal and vertical components in respect to reference values (see Fig. 1a, b).

The observed systematic shift suggested that some EGNOS corrections were computed with insufficient accuracy. Therefore authors decided to compute regional ionospheric corrections and check their suitability to improve navigation position accuracy.

3 Ionosperic Corrections

In Satellite-Based Augmentation Systems (SBAS), such as EGNOS, the ionospheric information is transmitted in two messages: the Ionospheric Grid Point (IGP) Mask and Ionospheric Delays (respectively messages 18 and 26) (RTCADO-229D MOPS 2006).

For the project purpose, as a source of GNSS observation for ionospheric corrections computation, the permanent stations of ASG-EUPOS were used.

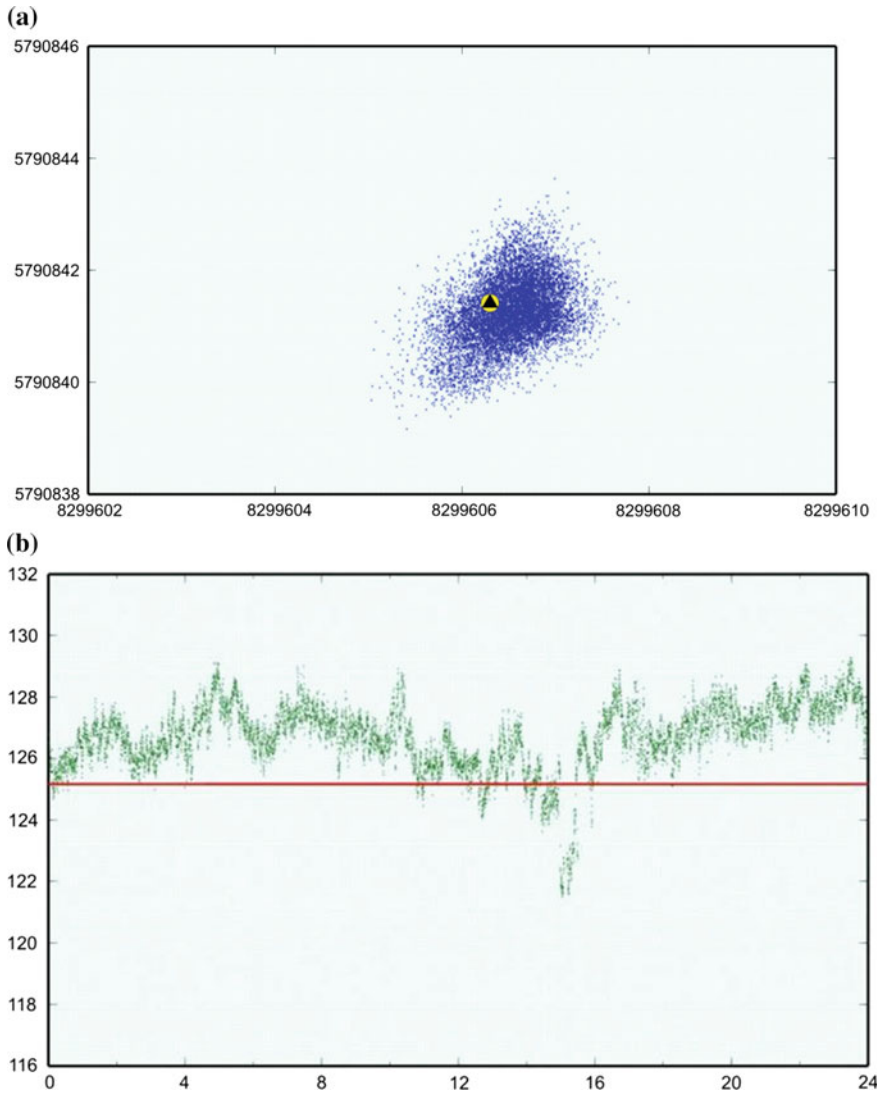

Fig. 1 **a** Horizontal position (in ITRF2005), computed by receiver for station CSIS. The *triangle* indicates the reference horizontal position. **b** Vertical position (ITRF2005) computed by receiver for station CSIS. *Red line* indicates the reference height value

For corrections computation only few selected stations of that system were used (see Fig. 2). The stations were chosen in locations that guaranteed a best coverage of IGP mask corresponding to eastern Poland, and gave an average of 60 TEC values per measurement.

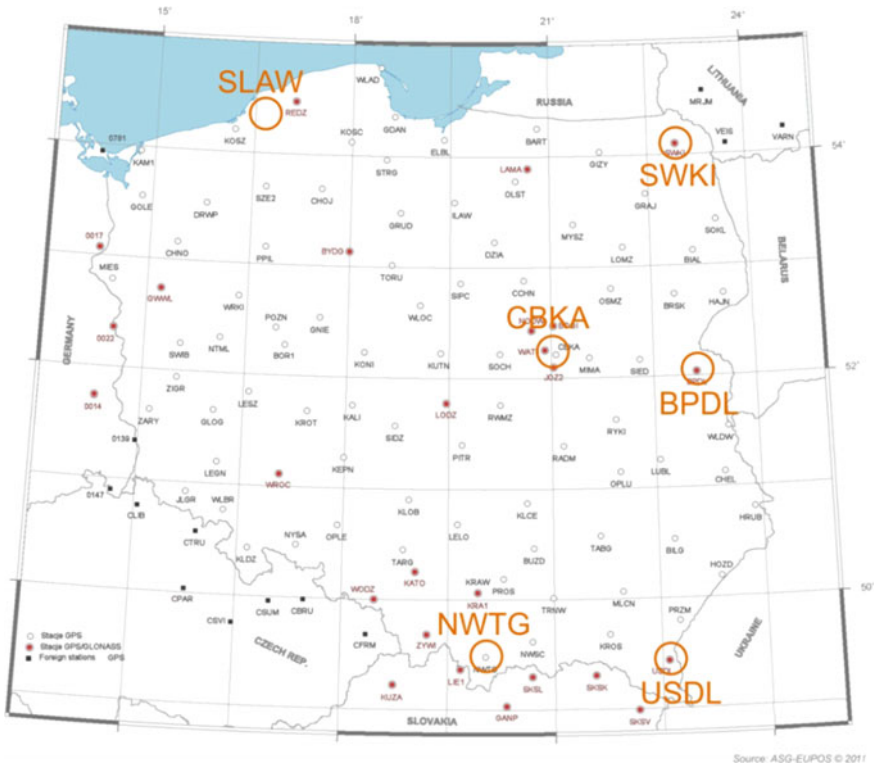

Fig. 2 The location of the ASG-EUPOS permanent stations. The stations selected for ionospheric corrections computation are marked in *orange*

The selected permanent stations delivered, through VRS3Net system, the TEC (Total Electron Content) data for computation of new EGNOS ionospheric correction. For the purpose of the project these new corrections were named 'improved'.

Vertical TEC values calculated for each station and for each observed satellite, generate the field of vertical TEC (VTEC) values. Based on that data the VTEC values are interpolated for selected grid points using a modified method described elsewhere (Juchnikowski and Zbyszynski 1991; Stanislawska et al. 2000).

That procedure puts the same value on the discrete points of known value and interpolates the new values for selected points proportionally to the square of the distance between the points of known values. For interpolated VTEC values the ionospheric delay for 'improved' EGNOS corrections were calculated.

For comparative analysis, the original EGNOS ionospheric corrections were calculated for the same IPP (Ionospheric Pierce Point) as the 'improved' corrections. Calculations were prepared in the same way as it is done by a receiver for interpolation from ionospheric delays broadcasted for IGP to IPP locations.

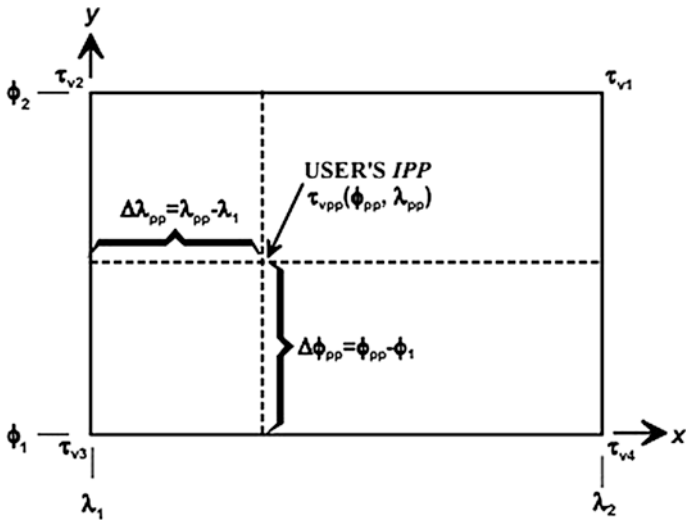

Fig. 3 EGNOS four-point bilinear interpolation algorithm gives an advantage in the speed of calculations and boosts accuracy

For analysed site location the user is surrounded by four nodes of the IGP grid. For the IPP located on a way from a satellite to a receiver, the user interpolates value from those nodes to its pierce point (see Fig. 3).

In this work some restrictions were applied—the four-point bilinear interpolation was applied only when GIVEI (Grid Ionospheric Vertical Error Indicator) value for all four points of the IGP sub mask doesn't equal a "don't use" value.

4 EGNOS Ionospheric Corrections Analysis

Values of ionospheric delay for each IPP were taken for analysis. The set of ionospheric delays obtained from ASG-EUPOS stations data were compared with the corresponding values computed from the EGNOS corrections. The TEC values obtained from ASG-EUPOS were named TEC (ASG) and the values computed from EGNOS were named TEC (EGNOS). For each epoch a set of points with TEC differences was obtained (see Fig. 4).

Because the EGNOS ionospheric correction is expressed in Vertical Delay Estimate (VDE) units [8] all data set was converted to TECU, according to the assumption that 1VDE corresponds to 0.125 m or 0.766 TECU for L1 frequency.

Figure 5 shows that the meridian 21°N is the axis of an asymmetry in the differences between TEC (GNSS) and TEC (EGNOS) for the IPPs. The analysis shows that for all the IPPs the mean difference is −1.85 TECU.

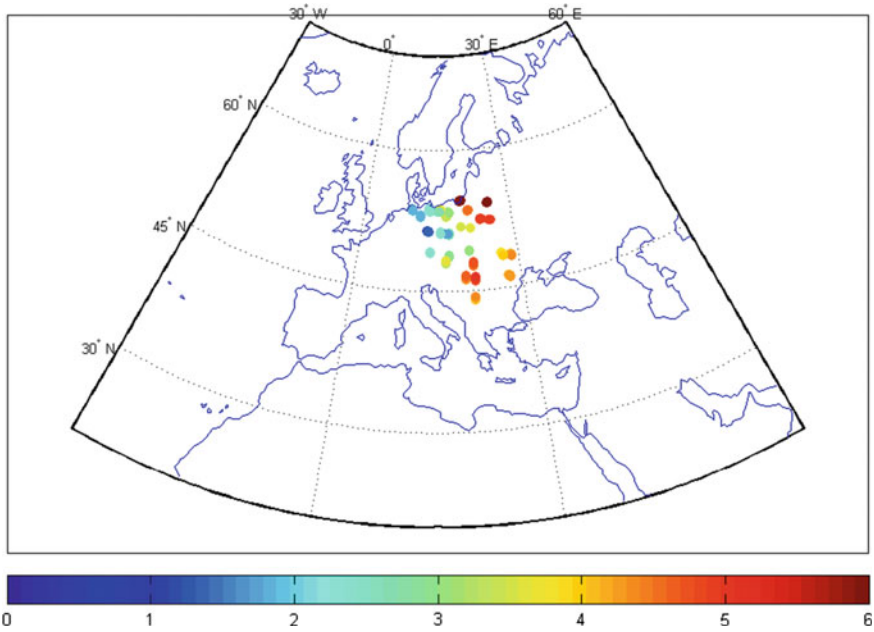

Fig. 4 Example of one epoch asymmetry in TEC differences calculated for observed satellites IPP

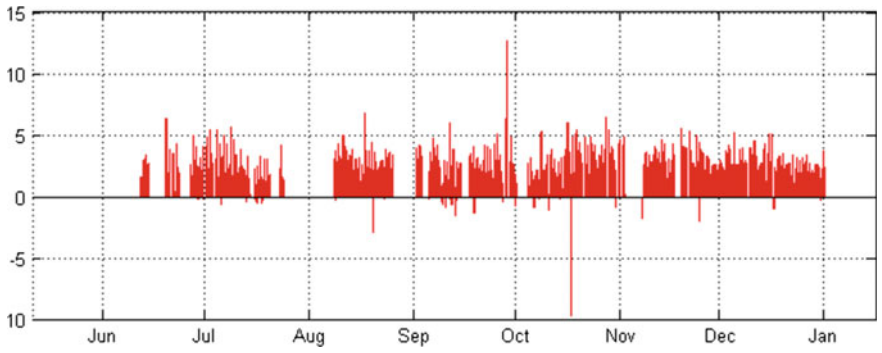

Fig. 5 Differences in the hourly median of ionospheric delays for all the IPPs between TEC (ASG) and TEC (EGNOS)

Analysing the TEC differences for IPPs located west of the meridian 21°N the mean difference is −1.58 TECU, while for those located east of the meridian 21°N, the mean difference is −2.12 TECU.

More than six months of permanent measurements were taken for analysis. ASG-EUPOS and EGNOS data were defined as simultaneous if the time differences between ionospheric corrections computed from ASG-EUPOS and the ones obtained from EGNOS did not exceed 20 s. The hourly median differences between

TEC (ASG) and TEC (EGNOS), computed for all data, gave the 1791 values of ionospheric delays. The obtained values are presented in Fig. 5.

In Fig. 5 permanent shift in difference values between TEC (ASG) and TEC (EGNOS) can be observed. 1731 data points, representing the 96.9% of all the differences, have positive values.

Analysing the absolute values of the TEC differences for the whole analysed period (see Fig. 6a) the Gaussian distribution as well as the shift of about 2 TECU can be observed.

The relative differences in ionospheric TEC (see Fig. 6b) were calculated according to equation:

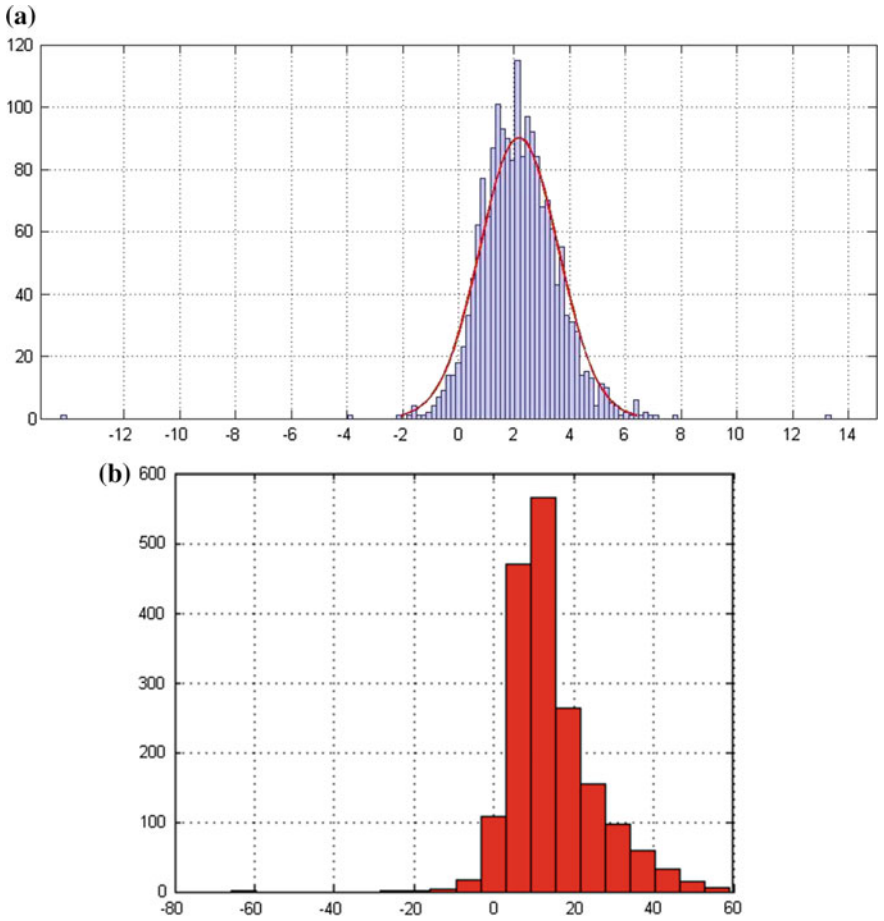

Fig. 6 **a** The ionospheric TEC differences between ASG-EUPOS and EGNOS data (expressed in TECU) for the analysed period. **b** The ionospheric delay relative differences between ASG-EUPOS and EGNOS data (expressed in %) for the analysed period

$$\frac{TEC(ASG) - TEC(EGNOS)}{TEC(ASG)}$$

In Fig. 6b the Chi square distribution is observed. It also confirms the hypothesis of the Gaussian distribution.

All presented analyses show that the EGNOS ionospheric corrections are underestimated. The limited area used for the analyses does not allow to extend this conclusion to the whole system but it can be stated that in Poland, located at east border of the EGNOS service area, there is an asymmetry in EGNOS ionospheric corrections. It could be caused by the insufficient number of satellites used for corrections computation due to the lack of stations located east of Warsaw.

5 Tests of Asis Platform

Presented results of analyses gave the basis for the design of internet platform for a distribution of 'improved' EGNOS corrections. For that purpose ASIS software (Automated SISNet Inspection System) was design. It computed the ionospheric delay corrections in VDE for defined IGP nodes surrounding area of test measurements and substituted the 'improved' values into the original EGNOS message in real time without changing its structure. The 'improved' EGNOS message generated this way was sent to the receiver via Internet (see Fig. 7). The platform was checked using dynamic measurements carried out in the proximity of the east border of Poland on the area of Biala Podlaska Airport. For the test the EGNOS message was received and transmitted after modification using SiSNet (Signal In Space through Internet) technology, described in Torán-Martí and Ventura-Traveset 2004, Torán-Martí and Ventura-Traveset 2003.

The Airport area is the terrain with an open horizon which guarantees optimal conditions for GNSS measurements in the whole test route.

The test measurements were carried out using two identical Septenrtio PolaRx2 receivers connected to one antenna. The antenna was mounted on the roof of the Mobile GNSS Laboratory car, which moved on the airport runways (see Fig. 8).

One of the receivers calculated its positions using the original EGNOS corrections, while the second one applied the 'improved' EGNOS corrections.

The raw data from both receivers were computed in kinematic mode in order to obtain the precise position (x, y and h). In that case flat coordinates x, y and h could be viewed as East, North and Up components respectively. Calculated differences between both receivers did not exceed 1 cm for all components. Those positions were used as a reference for the analysis of navigation positions obtained in the test measurements.

The result differences between navigation and reference position for x, y and height components are presented in Fig. 9. The changes in position for each coordinate are presented together with information about number of observed satellites and satellites with EGNOS correction as well. Red dots define positions

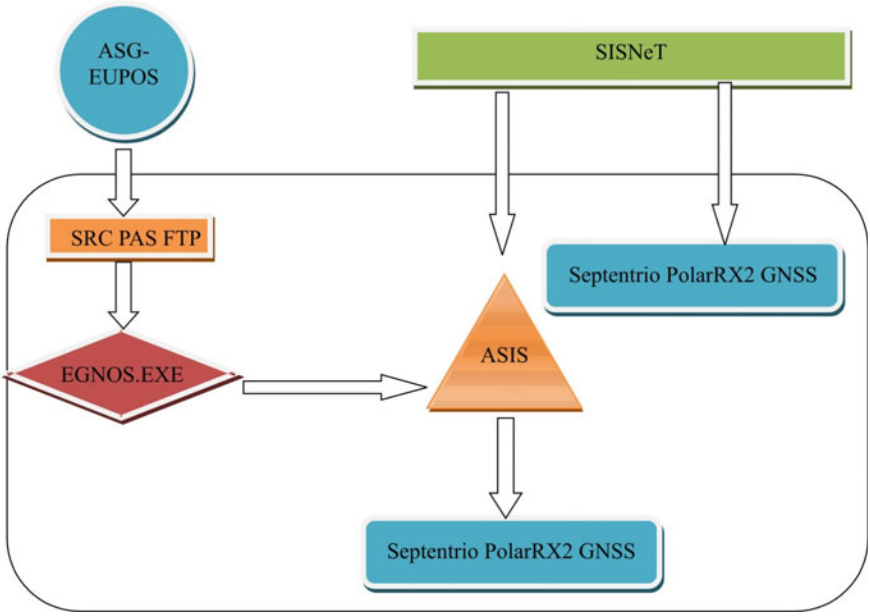

Fig. 7 The scheme of the algorithm of EGNOS message modification

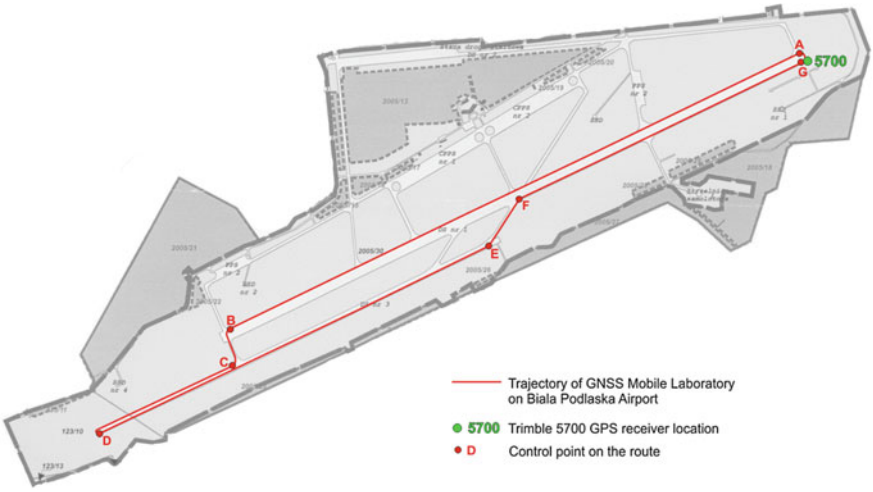

Fig. 8 Reference trajectory established on the Biala Podlaska Airport

computed with the original EGNOS corrections, while blue dots represent positions computed with the 'improved' EGNOS corrections. An improvement in position accuracy for the 'improved' correction can be seen in the graphs.

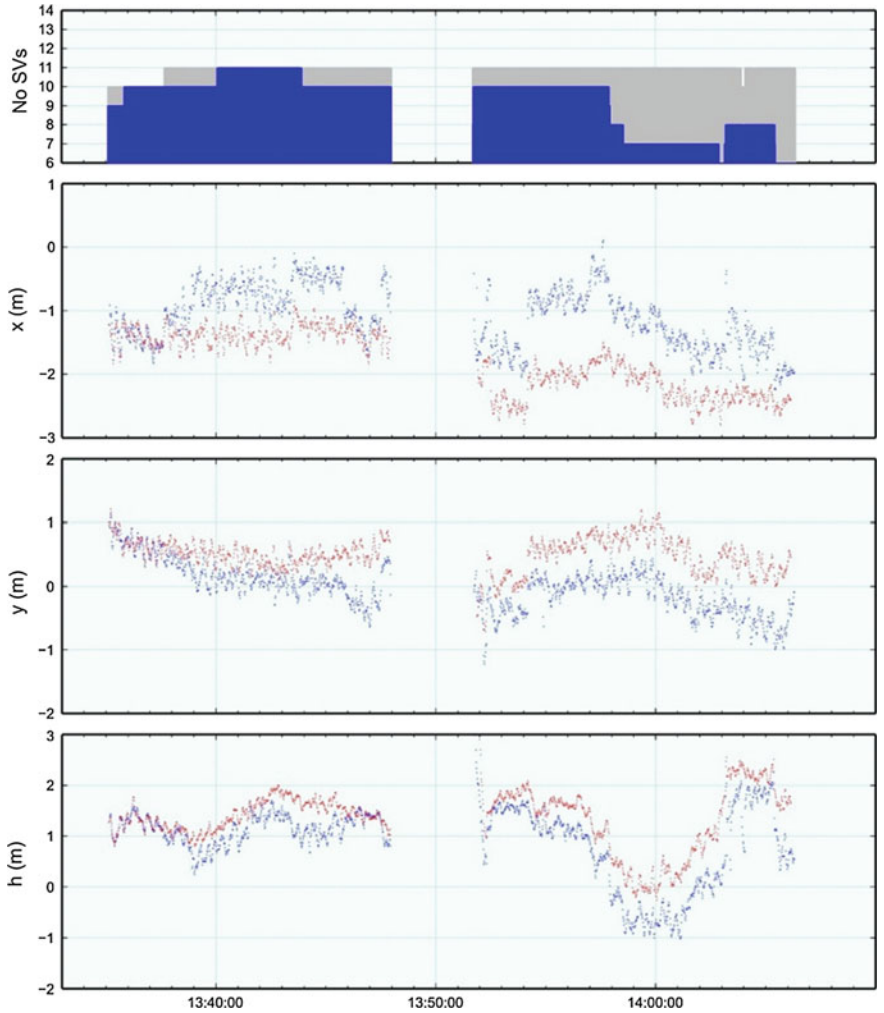

Fig. 9 Differences between navigation and reference positions. *Blue dots* represent differences obtained for 'improved' EGNOS corrections and *red ones* for original EGNOS corrections. *Top graph* presents a number of observed satellites (*grey* shows all observed satellites, *blue* satellites with EGNOS corrections)

6 Conclusions

The TEC analysis shows the general underestimation of the TEC (EGNOS) values near the eastern border of EGNOS service area.

The original EGNOS corrections increase the navigation position errors near the eastern border of EGNOS service area. The experiments carried out at Biala Podlaska Airport showed that EGNOS ionospheric corrections computed by

matching the regional conditions could improve the position accuracy. The regional ionospheric corrections, substituted into the original EGNOS message in real time, improved the obtained position by about 30–40%.

The systematic shift in coordinate components obtained for present SPMS (EGNOS Service Performance Monitoring Support) project shows the area for further improving the accuracy and stability of the position by introduction of another modification of the EGNOS corrections.

Presented results are an interesting material for additional analysis which could be carried out in other border regions of the EGNOS service area. Repeating those test now, after the improvement of ionospheric model adapted in EGNOS system, could deliver a real accuracy of current EGNOS corrections for different areas as well as a real accuracy of navigation positioning.

References

Aguilar ED, Jaworski L, Kolodziejczak M (2007) Accuracy of the EGNOS system during mobile testing, 2007, advances in marine navigation and safety of sea transportation. In: TrasNav 2007 conference proceedings, pp 115–119

Cefalo R, Calderan M, Piemonte A (2014) Development and application of an experimental Data Server hosting EGNOS and RTCM/RTK correction data for terrestrial navigation. United Nations ICG/ICTP Workshop on GNSS, International Centre for Theoretical Physics, Trieste 1–4 Dec 2014. http://indico.ictp.it/event/a13233/session/20/contribution/45/material/1/0.pdf

Grzegorzewski M, Swiatek A, Oszczak S, Ciecko A, Cwiklak J (2012) Study of EGNOS Safety of Life Service during the period of solar maximum activity. Artif Satell 47(4):137–145

Jaworski L, Swiatek A (2009) EGNOS—EUPOS integration project for the territory of Poland, 2009. In: Proceedings of 2ND GNSS VULNERABILITIES AND SOLUTIONS Conference, 2–5 Sept 2009, Baška, Croatia

Jaworski L, Swiatek A, Zdunek R (2013) EGNOS limitations over Central and Eastern Poland—results of preliminary tests of EGNOS-EUPOS integration project. Artif Satell 48(3):93–102

Juchnikowski G, Zbyszynski Z (1991) A modification of foF2 statistical model using vertical sounding data, 1991. In: III PRIME Workshop Proceedings, 12–25 Jan 1991, Rome

Oszczak S, Ciecko A, Bakula M, Popielarczyk D, Balint J, Manzoni G, Cefalo R (2003) Estimation of accuracy of EGNOS system test bed (ESTB) car navigation in central European countries in 2002. In: Proceedings of the GNSS 2003, Graz, Austria, 22–25 Apr 2003, Paper No 222

RTCADO-229D (2006) Minimum Operational Performance Standards for Global Positioning System/Wide Area Augmentation System Airborne Equipment. Prepared by Special Committee 159 (SC-159) and approved by the RTCA Program Management Committee on December, 13 Dec 2006

Stanislawska I, Juchnikowski G, Hanbaba R, Rothkael H, Sole G, Zbyszynski Z (2000) COST251 recommended instantaneous mapping model of ionospheric characteristic—PLES, 2000. Phys Chem Earth 25(4):291–294

Torán-Martí F, Ventura-Traveset J (2004) The ESA SISNeT project: current status and future plans, 2004. In: ESA SISNet Publications—Conference GNSS 2004, Aug 2004

Torán-Martí F, Ventura-Traveset J (2003) The ESA SISNeT technology: real-time access to the EGNOS services through wireless networks and the internet, 2003. In: ESA SISNet Publications ION GPS 2002, 24–27 Sept 2002, Portland, Mar 2003

FReDNet: Evolution of a Permanent GNSS Receiver System

David Zuliani, Paolo Fabris and G. Rossi

Abstract Continuous GNSS networks provide unique information about the crustal dis-placements, of use for studies concerning plate motions, tectonic processes, and earthquake cycle understanding. The Istituto Nazionale di Oceanografia e di Geofisca Sperimentale—OGS, since 2002, is responsible for the installation, maintenance, and development of FReDNet (Friuli Regional Deformation Network), the system for crustal deformation monitoring in the Friuli Venezia Giulia Region. The main objective of the network is the detection of tectonic plate movements in this collision area: such movements can give some guidance to quantify the seismic hazard. The infrastructure currently consists of 16 permanent stations located in the Friuli Venezia Giulia and Veneto regions, all equipped with GNSS receiver (Global Navigation Satellite Systems) capable of tracking satellite systems GPS, GLONASS and Galileo. The system includes a central server for collecting, processing and distributing of data and results. FReDNet, furthermore, provides a service for browsing high-precision real-time positioning in the most common differential correction RTK (Real Time Kinematic) modes. The current document will briefly describe the technical implementation of FReDNet in the last years with new stations, new features (high-frequency sampling and monumentation) and upgraded services.

Keywords GNSS · GPS · GLONASS · Galileo · RTK · FReDNet · Friuli · Tectonic · RTK · High-frequency · Crustal deformation · Cost-effective receiver · SBC · Raspberry pi · Single-frequency receiver · Permanent GNSS receiver · CORS · VirtualBox

Continuous GNSS networks provide unique information about the crustal dis-placements, of use for studies concerning plate motions, tectonic processes, and earthquake cycle understanding. The Istituto Nazionale di Oceanografia e di Geofisca Sperimentale—OGS, since 2002, is responsible for the installation,

D. Zuliani (✉) · P. Fabris · G. Rossi
Istituto Nazionale di Oceanografia e di Geofisica Sperimentale—OGS, Trieste, Italy
e-mail: dzuliani@inogs.it

R. Cefalo et al. (eds.), *New Advanced GNSS and 3D Spatial Techniques*,
Lecture Notes in Geoinformation and Cartography,
DOI 10.1007/978-3-319-56218-6_10

maintenance, and development of FReDNet (Friuli Regional Deformation Network), the system for crustal deformation monitoring in the Friuli Venezia Giulia Region. The main objective of the network is the detection of tectonic plate movements in this collision area: such movements can give some guidance to quantify the seismic hazard. The infrastructure currently consists of 16 permanent stations located in the Friuli Venezia Giulia and Veneto regions, all equipped with GNSS receiver (Global Navigation Satellite Systems) capable of tracking satellite systems GPS, GLONASS and Galileo. The system includes a central server for collecting, processing and distributing of data and results. FReDNet, furthermore, provides a service for browsing high-precision real-time positioning in the most common differential correction RTK (Real Time Kinematic) modes. The current document will briefly describe the technical implementation of FReDNet in the last years with new stations, new features (high-frequency sampling and monumentation) and upgraded services.

1 Friuli Regional Deformation Network

1.1 FReDNet History and Motivations

FReDNet: the Friuli Regional Deformation Network is a network of continuously operating GNSS receivers that monitors the Friuli (Northeast Italy) regional distribution of crustal deformation, providing data for earthquake hazard assessment (website http://frednet.crs.inogs.it, Battaglia et al. 2003). Network installation and data analysis began in the summer of 2002 and currently 16 permanent GNSS stations (see in Fig. 1) are up and running. The complete site list is available in Table 1. UDIN has been uninstalled but its data is available at the website up to 2006/09/05. Moreover, ZOUF is part of the European Reference Frame Network (EUREF see at the official website:
http://www.epncb.oma.be/_trackingnetwork/siteinfo4onestation.php?station=ZOUF_12763M001).

The Friuli area has been struck on 6 May 1976 by an earthquake of magnitude 6.4 (Battaglia et al. 2003), and in 1977 OGS started a seismometric network to better monitor the phenomenon (Priolo et al. 2005). OGS, in 2001, has decided to increase the knowledge on the tectonic movements by implementing, in this area, its geodetic network aimed to crustal deformation studies (FReDNet). Since 2002, FReDNet has provided the research community with RINEX data, time series and crustal deformation velocities (Zuliani et al. 2004). Since then, the Centro di Ricerche Simologiche (CRS) of OGS has been in charge of building and of improving the network and its services. In 2006, the infrastructure has been modified and improved, all receivers were upgraded in order to track both GPS and GLONASS constellations, and real-time services (RTK) for a cadastral and topographic application started.

Fig. 1 FReDNet GNSS permanent site map

Table 1 List of FReDNet GNSS permanent sites. Services available are: H hourly data sampled at 1 s, D daily data sampled at 30 s, G GLONASS constellation, I EUREF-IP site, R RTK service

Station	Location	Installation data	Available services			
ACOM	Malborghetto, (UD)	04/07/03	H,D	G	R	
AFAL	Cortina D'Ampezzo, (BL)	17/06/03	H,D	G	R	
CANV	Caneva, (PN)	19/05/04	H,D	G	R	
CODR	Codroipo, (UD)	27/03/07	H,D	G	R	
FUSE	Tolmezzo (UD)	07/09/07	H,D	G	R	
JOAN	Torreano di Cividale (UD)	28/06/07	H,D	G	R	
MDEA	Medea, (GO)	23/01/03	H,D	G	R	
MPRA	Forgaria del Friuli, (UD)	07/08/02	H,D	G	R	
NOVE	Noventa di Piave, (VE)	27/03/09	H,D	G	R	
PAZO	Palazzolo dello Stella, (UD)	05/12/07	H,D	G	R	
SUSE	Collalto di Susegana, (TV)	18/02/11	H,D	G	R	
TRIE	Sgonico, (TS)	05/02/03	H,D	G	R	
UDI1	Cussignacco, (UD)	04/04/06	H,D	G	R	
UDIN	Cussignacco, (UD)	12/06/02				
VARM	Forni di Sopra, (UD)	03/08/12	H,D	G	R	
ZOUF	Cercivento, (UD)	11/06/02	H,D	G	R	I

1.2 Purposes and Products

Up to now all the products yielded with FReDNet are free of charge and offered on a public website:

- RESEARCH: data and solutions for crustal deformation studies, GNSS data, displacement time series and crustal deformation velocities are available at website and ftp site:
  - http://frednet.crs.inogs.it
  - ftp://www.crs.inogs.it/pub/gps/
- SERVICES: real-time GNSS services (RTK) for land monitoring are reachable at the following CASTER addresses:
  - http://158.110.30.81:2110/
  - http://158.110.30.81:2111/

  The full set of RTK services is available at port 2110 (46 mount points), port 2111 includes a small subset with network solutions only (VRS, MAC, FKP and Nearest) and it is used for a simpler access. Ports and their services are described in detail at FReDNet web site.

Main servers, located inside the CRS building, collect the raw receiver data and format them daily (and hourly) according to a common format called Receiver Independent Exchange (RINEX V 2.3, both observation and navigation messages). Finally, data are checked with the true quality check program QC (released by UNAVCO). Data files can be found on the FTP server in conformity with the international naming conventions (like SOPAC and EUREF data centers).

Moreover, daily and hourly RINEX data from the ZOUF site are forwarded to some GNSS data centers (ASI, BKG, SOPAC).

Currently, besides the standard ftp service, there is a new method to access the GNSS data. This last has been developed to help people that sometimes deal with the GNSS data like engineers, land surveyors, architects. These users usually do not want to spend much time to pack an uncommon set of data, and usually, they do not need the standard set of hourly or daily data which is available on the ftp site (most of the time used by scientists and researchers). A web interface leads the user to build up his own package in a very simple way. The new feature allows the user to create a set of data that covers a fraction of an hour or more than an hour, with the preferred sample rate (1 s, 2 s, 3 s, 4 s, 5 s, etc.) and from one or more sites (see Fig. 2).

The velocities maps are obtained from a monthly elaboration of FReDNet GPS data set. To calculate the velocities two different reference frames are used:

– International Reference Frame (ITRF08): is the most recent and accurate realization of the International Earth Rotation Service (IERS). It is a non-inertial reference system rigidly fixed to the Earth, the origin of the XYZ Cartesian

Fig. 2 A web interface can be used to exctract data from the whole FReDNet database. Session length, site, and sampling rate can be set by the user

system is the Earth's center of mass; the Z-axes passes through the North Pole, the X- and Y-axes lie on the equatorial plane.

– European Reference Frame (Altamimi et al. 2012): it is an Eurasian reference frame determined by setting the "a priori" velocities of a given number of European station to a specific value. Figure 3 reports the velocities within this last reference frame.

Furthermore, several papers (Rossi et al. 2016, Devoti et al. 2015, Caporali et al. 2013, Bechtold et al. 2009, D'Agostino et al. 2005) improved the knowledge of the investigated area, by using the FreDNet data. Finally, CRS, based on the expertise and knowledge gained, has started new activities as landslide monitoring with cost-effective GNSS receivers (Zuliani et al. 2016).

2 Instruments and Software

All the GNSS permanent CORS belonging to FReDNet include professional dual frequency (L1 and L2) multiple-constellation GNSS (at least GPS and GLONASS) receivers and choke ring antennas. Each site is built keeping in mind the crustal deformation aims, particular care is taken for the monumentation used to anchor the antenna to outcrop rock or to soft soil. Here some hints are given in order to keep alive the whole infrastructure. The strategy used is described from the following point of views:

- HARDWARE (GNSS receivers and antennas);
- MONUMENTS (style and performance);
- SOFTWARE (open source or commercial);

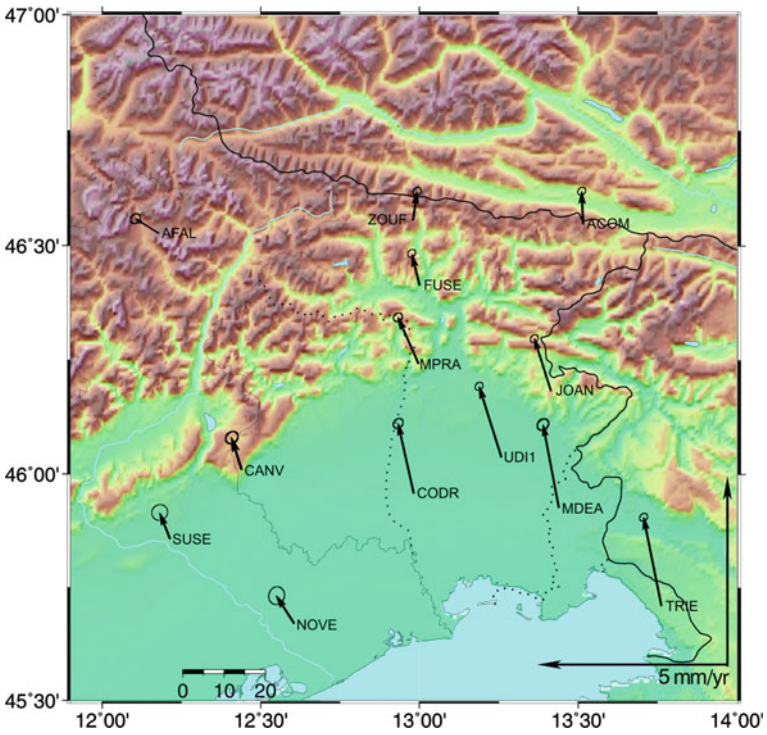

Fig. 3 Crustal deformation velocities (European Reference Frame as defined in Altamimi et al. 2012) of FReDNet GNSS sites

- SERVERS (the system backup nightmare);
- TECHNOLOGY (the aging factor and the best device);

2.1 Hardware: GNSS Receivers and Antennas

GNSS hardware includes the instrumental part of each GNSS CORS: receiver and antenna. To keep alive the infrastructure during decades, maintenance and upgrade are the main and most expensive issues to be taken into account. As a first stratagem, for all the sites, a single GNSS receiver brand is adopted in order to reduce the number of spare parts (and so to reduce the costs). Furthermore, this solution helps to realize all the sites in the same manner (same connectors, power supply, etc.) making upgrades easier and uniform (e.g., firmware update). Even exchanging instruments (possible for the receivers, but not suggested in any case for the antennas) among the sites is less demanding. This operation is sometimes needed when a broken devices belongs to an important remote sites (e.g. ZOUF which is

Fig. 4 GNSS receivers and antenna belonging to FReDNet

part of EPN). In that case a very fast change must be done, and a working devices, belonging to a less important site can be used, as a temporary spare part. As a result, the whole system is more efficient even from the server side, where scripts, made on a single brand/model basis, are optimized to download data and to redirect services and data flows. However, if devices coming from different brands are chosen, retailers tend to be more competitive and they try to offer better products at lower prices. For this reason, in the last years, a balance between single and multiple brand solutions has been chosen: 85% of FReDNet is made with the same receiver brand, while the remaining 15% is a mixture of other brands. The positive effects of this choice are:

- precious expertise is gained to improve network functionalities;
- new application fields have been explored;
- hardware prices have been decreased.

For instance, even if the receivers belonging to FReDNet are mainly Topcon, a new Leica GR25 device has been tried. GR25 includes a recent technology called VADASE (Benedetti et al. 2014). VADASE is an algorithm implemented inside the GR25 firmware to provide autonomous processing capability that does not require additional hardware or infrastructure for differential processing. This is an interesting solution in the seismological field to measure directly co-seismic displacements during an earthquake. In Fig. 4 some of the hardware used inside FReDNet. All the GNSS sites belonging to FReDNet adopt Choke RING antennas. Site configuration files, including history, are available at FReNet web site.

2.2 Monuments: Style and Performances

GNSS antenna anchoring is the most important issue of a permanent site built for crustal deformation analysis. Different terrains must be taken into account, and each of them needs a different solution. During 14 years of activity, a lot has been learned from the Berkeley Seismological Laboratory (BSL) that manages the Bay Area Deformation Network (BARD) in California, from the crustal motion geodesy group lead by Michael Bevis at the Ohio State University, and from the Politecnico of Milano, which helped in starting and upgrading the OGS GNSS network. CRS staff also performs semi-permanent GNSS campaigns, and different solutions were adopted for both permanent and semi-permanent sites as showed in Fig. 5:

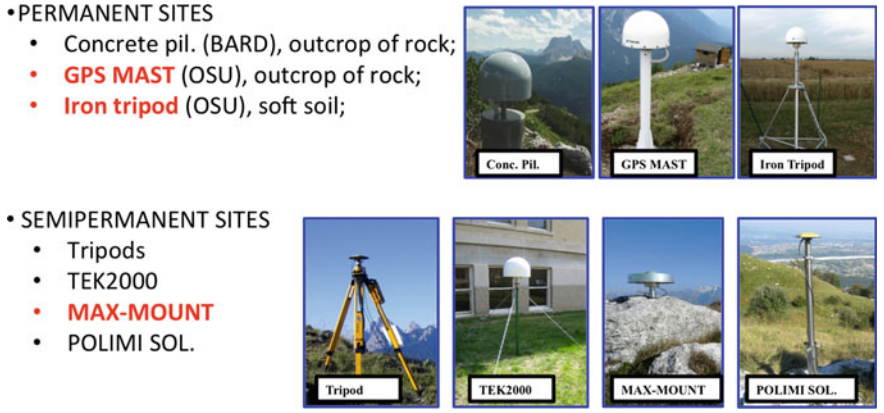

Fig. 5 Anchoring methods adopted for both permanent (FReDNet) and **semi** permanent **sites (GNSS periodical campaigns)**

Concrete pillar anchoring (adopted from BARD of BSL) is a good performance solution in terms of monument stability, but it is expensive (man hours) and tends to degrade over the years. GPS MAST (OSU monument style) is more expensive at the beginning (hardware manufacturing cost is about 500€**),** but it is easier to install (2 workers, 4 h each) and to maintain too. Currently, GPS MAST is the preferred solution for FReDNet outcrop rock anchoring.

Regarding soft soils other issues need to be taken into account: the requirement of a good coupling between the antenna and the surface without an outcrop rock, the monument must be light, to avoid sinking, and inexpensive. There are some expensive solutions, for instance UNAVCO (http://www.unavco.org) implements the expensive Deep Drilled Braced Monument (7500$–15,000$) but we think that the Iron Tripod developed by OSU is a good compromise between performance and cost (less than 500€).

Regarding the semi-permanent campaigns, in the beginning wooden tripods (not so stable and they need a particular care to be correctly installed) were used, but some other solutions arose during the years:

- TEK2000 by OSU (see at: http://kb.unavco.org/kb/article.php?id=202);
- MAX-MOUNT (Italian patent num. BO2004A000404, University of Bologna);
- Politecnico of Milano MAST (Barzaghi et al. 2016).

TEK2000 is the most adaptable; it can be used both for outcrop rock and soft soil installations, and it can be coupled with almost every kind of benchmark. MAX-MOUNT and the MAST from the Politecnico of Milan are more stable, but they require their own benchmark, and they are not suitable for soft soils.

2.3 Software: (Open Source or Vendor-Provided Software?)

The software is one of the main tools to handle the process that transform a raw dataset into a scientific product or service. All steps (control, data downloading, quality check, data elaboration, and publication of results) involve the use of one or more computer programs. The key issue regards the choice between an Open Source and vendor-provided solution. Both of them have advantages and disadvantages.

Branded or vendor-provided software is really efficient and easy to be used but only in its own environment (i.e., it can control a single receiver brand perfectly, but it is limited with the others). Moreover, for the final user it is difficult to make changes or to add new features, and fees and licenses are needed with not so marginal cost.

Regarding Open Source software license costs are minimal or null and everything is under the management staff control but the whole system is more complex to be maintained and much time (human resources) is spent to gain knowledge and expertise.

The experience gained with FReDNet suggests a mixed solution:

- **Linux shell scripts** for site control, data download, quality check and web site (homemade code based on open source software);
- **GNSMART** (see at http://www.geopp.de/gnsmart/) a Geo ++ product for real time GNSS networks and RTK services (commercial software);
- **GAMIT/GLOBK** for GNSS elaboration and post-processing products (displacement time series, crustal deformation velocities). GAMIT/GLOBK (Herring et al. 2008) has been developed by MIT, Scripps Institution of Oceanography, and Harvard University with support from the National Science Foundation and it is a free software for universities and government agencies;
- **RTKLIB** for both RTK and post-processing GNSS issues, RTKLIB is open software and distributed under a BSD 2-clause license and additional exclusive clauses available at: http://www.rtklib.com/. Users are permitted to develop, produce or sell their own non-commercial or commercial products utilizing, linking or including RTKLIB as long as they comply with the license.

2.4 SERVERS: The System Backup Nightmare

The system manager is always worried about backups and, nowadays, well-tested packages (i.e., rsync) are available under different Operative Systems (O.S.) (Linux, Windows, Mac OSX, or BSD) to perform such operation. Moreover, the availability of dedicated hardware devices such Network Attached Storage (NAS) makes the system manager life easier. Backups are usually aimed to have a precious safe copy of GNSS data, but what about the full running O.S?

At CRS a different strategy has been implemented to solve both problems.

The GNSS dataset backup is the easiest part and involves a NAS device and the rsync package running under Linux. rsync is governed by a shell script that synchronizes the official GNSS data set, always online and available to the final user, and a copy stored in a NAS device. The Linux shell script is run automatically every two days.

The less easy part is the O.S. backup. Usually, the O.S. runs on a server and, in the case of a hardware failure, it is not easy to reactivate it in a short time, even if a hard disk copy is available on NAS. A motherboard crash usually needs new hardware and adapting the old O.S. from the NAS backup is challenging and time-demanding. Even keeping a spare part of everything (motherboards, memory, hard disk, etc.) is expensive and inefficient. The strategy implemented for FReDNet is different and based on a virtualization software called VirtualBox. Virtualization software allows a single **host** computer (hardware) to create and run one or more virtual environments. Each virtual environment emulates a complete computer system to allow a **guest** operating system (software) to be run, for example allowing Linux to run as a guest on top of a PC that is natively running a Microsoft Windows operating system (or the inverse, running Windows as a guest on Linux). When the guest O.S. is shut down it ia a simple file saved inside the **host** file system, and it can be copied to a NAS device for backup issues or can be moved and started inside another host which, probably, runs a different O.S. FReDNet main server is a guest virtual machine running Linux Debian ver. 3.2.73 over a MacMini hardware host from Apple running OS X Yosemite 10.10.5. and virtualization software is VirtualBox 5.0.26 from Oracle. This solution is platform independent, makes the O.S. backup as easy as GNSS data set backups, and reduces dramatically the time to reactivate a crashed O.S.

2.5 TECHNOLOGY: The Aging Factor

GNSS receivers tend to obsolescence for different reasons: tracking capabilities, connectivity, and storage issues but usually, because of the costs, the units are not replaced until they are broken. When a new device is bought to replace a broken one it is suggested to buy the best and more update hardware; probably the costs are higher at the beginning, but money will be saved in the long term because the device life cycle will be longer. In that case replacing is wiser than fixing but one cannot replace the entire network in one go. For FReDNet the strategy to keep alive the eldest, but still working, devices has been to use low-cost single board computer (SBC) such raspberry to:

- implement remote low power backups NAS. They are perfect for storing directly GNSS data recorded by a receiver at high frequency (at least 1 Hz or higher. Usually, GNSS permanent sites used for crustal deformation studies are set to record every 30 s, which is enough for long-term crustal surface motion,

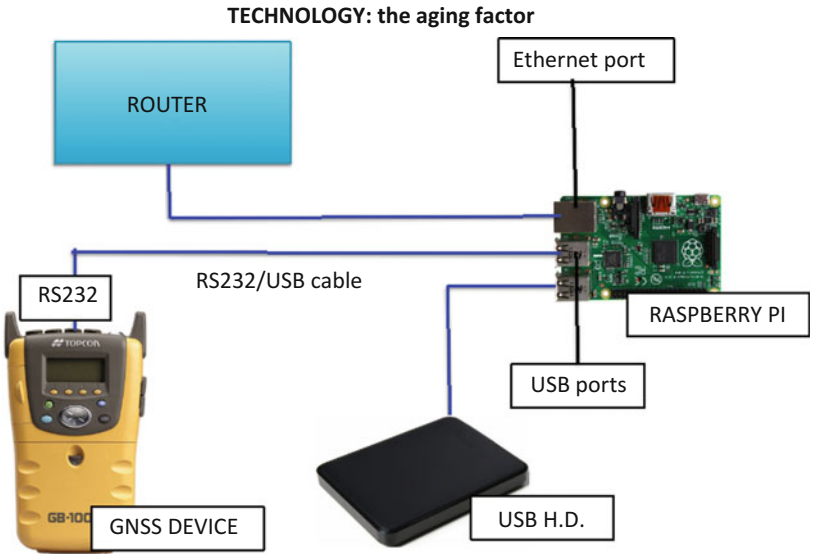

Fig. 6 How to plug an old GNSS receiver to a ``raspberry pi'' to gain new storage capacity and an ethernet connection

but in some areas of the world (Rogers et al. 2003) tremors (1–5 Hz) are observed, accompanying GPS-signal accelerations: "episodic slip and tremors", or ETS. The old receivers are not provided with high capacity storage device, while in this way precious data, needed to reveal ETSs, are saved;

- stream data from device provided with just a serial RS22 without a network interface. SBC can act as a RS232 to ETHERNET device and also can stream the data directly inside the NAS (as above, see Fig. 6).

Raspberry is not alone: other interesting devices can be used, such Intel Edison or Arduino, and they all can be used to improve the remote GNSS receivers limitations or to add new features.

2.6 TECHNOLOGY: The Best Device

Every time a new GNSS hardware is needed, for instance, to expand an existing network or to replace a broken device, the problem is to find out the best parameters to well evaluate the new purchase. Vendors usually tends to highlight or to focus the attention only on the hardware performances such:

- number of constellation tracked (GPS, GLONASS, Galileo, BeiDou, SBAS);
- numbers of GNSS channels simultaneously available (e.g. 452 or more);

- sampling frequency (20 Hz, 50 Hz or even 100 Hz are important to retrieve detailed coseismic motions (Yidong et al. 2014);
- number and types of beat frequencies such L1, L2 and L5.

These characteristics are important, but are they really needed for any kind of application? For FReDNet every device has been chosen with the aim of monitoring long-term crustal deformation, and for this reason, expensive devices have been taken into account. For instance, each device can track at least L1 and L2 beating frequencies that are then combined to remove the unwanted ionospheric delay (Hofmann et al. 1997). Taking into account the ionosphere effect is crucial when the distance between two site, belonging to a GNSS network, is bigger than 5 km (Heunecke et al. 2011). FReDNet is a regional network where each GNSS site is at least 20 km apart from the other, and so dual frequency devices are strictly needed. There are different applications, where the distances between sites are less than 5 km, and so the expensive dual-frequency devices are not needed (Janssen et al. 2003). CRS, since 2015, manages a network of single frequency GNSS receivers (Zuliani et al. 2016) to monitor a landslide located in central Friuli, near the Tolmezzo municipality, the system used is called SENDAS. Good results have been

Fig. 7 SENDAS single frequency GNSS site for landslide monitoring

Fig. 8 LONE, single frequency GNSS device developed by OGS for RTK applications

achieved even with single frequency devices (see Fig. 7) but with a third of the dual frequency device costs.

Even precise GNSS real-time positioning techniques, RTK (Hu et al. 2003), could benefit from cost-effective single frequency devices. In this case, a GNSS receiver called "Rover" can reach a centimetric precision in real time with the aid of some RTK services such VRS, MAC or FKP (Landau et al. 2002). In this application, the Rover receives all the needed correction (double-differences approach) from a virtual reference station (i.e. a VRS services) placed less than 5 km away. The rover, for the reasons mentioned above, can be again a single frequency device. CRS is currently developing and testing its proprietary cost-effective GNSS system called LONE (see Fig. 8). Two different devices are taken into account; the first one is based on a Raspberry platform and a NVS (see at http://drfasching.com/) single frequency GNSS receiver, the second one is based on the emlid platform (https://emlid.com/) which uses a Intel Edison SBC and a u-blox single-frequency receiver. (Figs. 7 and 8)

Up to now, only dual frequency solutions have been available for all the above applications and only recently the market is in ferment for the huge potential of single frequency GNSS devices.

3 Conclusions

Maintaining and upgrading a system of GNSS permanent network receivers such FReDNet is a sensitive issue. There are no definitive or optimal solutions, but everything is a compromise between performance and cost. Luckily enough the market is offering a huge amount of devices such SBC or single frequency GNSS receivers to overcome hardware limitations, to add new features or to be applied efficiently, in some contests, instead of more expensive devices. Even Virtualization software systems are now really performing and they can be used to simplify the system manager work.

Acknowledgements I want to acknowledge the CRS staff: Giorgio Durì, Fausto Ponton, Elvio Del Negro, Michele Bertoni, Sandro Urban, Cristian Ponton and Paolo Di Bartolomeo for their continuous support during FReDNet installation and maintenance. I want to thank Dr. Enrico Priolo (OGS), Dr. Alberto Michelini (Istituto Nazionale di Geofisica e Vulcanologia INGV), Prof. Maurizio Battaglia (Sapienza University of Rome), Prof. Bruno Della Vedova (University of Trieste), Prof. Mike Bevis (OSU), Eng. Dana Caccamise (NOAA's National Geodetic Survey—NGS) and Prof. Mark Murray (New Mexico Tech) for their precious teaching and suggestions.

Bibliography

Altamimi Z, Metivier L, Collilieux X 2012 ITRF2008 plate motion model. J 830 Geophys Res, p 117, B07402, doi:10.1029/2011JB008930

Barzaghi R, Betti B, Biagi L, Pinto L, Visconti M (2016) Estimating the baseline between CERN target and LNGS reference points. J Surv Eng, 10.1061/(ASCE)SU.1943-5428.0000173, 04016012

Battaglia M, Zuliani D, Pascutti D, Michelini A, Marson I, Murray MH, Burgmann R (2003). Network Assesses Earthquake Potential in Italy's Southern Alps. EOS 84 (28), pp 262–264, 15 July 2003, doi:10.1029/2003EO280003

Bechtold M, Battaglia M, Tanner DC, Zuliani D (2009) Constraints on the active tectonics of the Friuli/NW Slovenia area from CGPS measurements and three-dimensional kinematic modeling, J Geophys Res Atmos, 114, B03408, doi:10.1029/2008JB005638

Benedetti E, Branzanti M, Biagi L, Colosimo G, Mazzoni A, Crespi M (2014) Global Navigation Satellite Systems Seismology for the 2012 Mw 6.1 Emilia Earthquake: exploiting the VADASE algorithm, Seismological Research Letters Vol 85, Number 3 May/June 2014, pp 649–656, doi:10.1785/0220130094

Caporali A, Neubauer F, Ostini L, Stangl G, Zuliani G (2013) Modeling surface GPS velocities in the Southern and Eastern Alps by finite dislocations at crustal depths, Tectonophysics 04/2013 590. doi:10.1016/j.tecto.2013.01.016

D'Agostino N, Cheloni D, Mantenuto S, Selvaggi G, Michelini A, Zuliani D (01/2005). Strain accumulation in the Southern Alps (NE Italy) and deformation at the north-eastern boundary of

Adria observed by CGPS measurements. Geophys Res Lett, 32(19). doi:10.1029/2005GL024266

Devoti R, Zuliani D, Braitenberg C, Fabris P, Grillo B (2015) Hydrologically induced slope deformations detected by GPS and clinometric surveys in the Cansiglio Plateau, southern Alps, Earth and Planetary Science Letters, pp 134–142, doi:10.1016/j.epsl.2015.03.023

Herring TA, King RW, McClusky SC (2008) Introduction to GAMIT/GLOBK, report, 944 Mass. Inst Technol, Cambridge

Heunecke O, Glabsch J, Schuhbäck S (2011) landslide monitoring using low cost GNSS equipment—experiences from two alpine testing sites. J Civ Eng Archit, 5(8):661–669. ISSN 1934–7359, (Serial No. 45), USA

Hofmann-Wellenhof B, Lichtenegger H, Collins J (1997) Springer Verlag, Wien New York, fourth, revised edition

Hu GR, Khoo HS, Goh PC, Law CL (2003) Development and assessment of GPS virtual reference stations for rtk positioning. J Geodesy 77:292–302. doi:10.1007/s00190-003-0327-4

Landau H, Vollath U, Chen X (2002) Virtual reference station systems. J Glob Positioning Syst 1(2):137–143

Priolo E, Barnaba C, Bernardi P, Bernardis G, Bragato PL, Bressan G, Candido M, Cazzador E, Di Bartolomeo P, Durì G, Gentili S, Govoni A, Klinc P, Kravanja S, Laurenzano G, Lovisa L, Marotta P, Michelini A, Ponton F, Restivo A, Romanelli M, Snidarcig A, Urban S, Vuan A Zuliani D (2005) Seismic monitoring in Northeastern Italy: a ten-year experience, Seismol Res Lett, Vol 76, Number 4, July/August 2005, 446–454, doi:10.1785/gssrl.76.4.446

Rogers G, Dragert H (2003) Episodic tremor and slip on the Cascadia subduction zone: the chatter of silent slip. Science 300(5627):1942. doi:10.1126/science.1084783

Rossi G, Zuliani D, Fabris P (2016) Long-term GNSS measurements from the northern Adria microplate reveal fault-induced fluid mobilization, Tectonophysics, article in press, doi:10.1016/j.tecto.2016.04.031

Rossi G, Zuliani D., Fabris P (2017) Corrigendum to: long-term GNSS measurements through Northern Adria microplate reveal fault-induced fluid mobilization. Tectonophysics, 694, 486–487, doi: 10.1016/j.tecto.2016.10.035

Volker Janssen, Chris Rizos (2003) A mixed-mode GPS network processing approach for deformation monitoring applications, Surv Rev 37:287, 2–19, doi:10.1179/sre.2003.37.287.2

Yidong Lou, Weixing Zhang, Chuang Shi, Jingnan Liu (2014). High-rate (1 Hz and 50 Hz) GPS seismology: application to the 2013 Mw 6.6 Lushan earthquake, J Asian Earth Sci Vol 79, Part A, 5 January 2014, pp 426–431, doi:10.1016/j.jseaes.2013.10.016

Zuliani D (2004) The FReDNet database, Centro di Ricerche Sismologiche, OGS 2004, Annual Report, pp 100–101

Zuliani D, Fabris P, Del Negro E, Bertoni M, Durì G (2016) Il sistema di monitoraggio GNSS di Esri Italia SENDAS: il case history della frana di Tolmezzo (UD), Conferenza Esri Italia, pp 20–21 Aprile 2016 Roma, doi: 10.13140/RG.2.1.3782.6966

Joint Use of Image-Based and GNSS Techniques for Urban Navigation

Diana Pagliari, Noemi Emanuela Cazzaniga, Livio Pinto, Mirko Reguzzoni and Lorenzo Rossi

Abstract The use of position-based devices is constantly increasing with a wide spectrum of applications, e.g. the continuous demand of mapping services based on user's location. Depending on the specific application, a different level of accuracy could be requested, going from room level to few centimeters of error. The navigation problem is typically faced by using Global Navigation Satellite Systems (GNSS), but this technique cannot efficiently work in case of poor sky visibility, as happens in urban areas. An option could be the combination of image-based and GNSS solutions. Two different assisted photogrammetry techniques are here presented and discussed. First, an image-based navigation solution constrained by using ground control points (GCPs) extracted from urban maps is presented. It was tested considering a set of different scenarios, reaching accuracies of the order of 0.20 m. A second outdoor navigation solution has been realized by integrating the data acquired by a Microsoft Kinect device (RGB and depth images) and a GNSS receiver through a proper Kalman filter. Also in this case the achieved accuracy is of the order of 0.20 m.

Keywords GNSS · Photogrammetry · Navigation · Kinect · Kalman filter

D. Pagliari (✉) · N.E. Cazzaniga · L. Pinto · M. Reguzzoni · L. Rossi
DICA—Department of Civil and Environmental Engineering,
Politecnico di Milano, Milan, Italy
e-mail: diana.pagliari@polimi.it

N.E. Cazzaniga
e-mail: noemi.cazzaniga@polimi.it

L. Pinto
e-mail: livio.pinto@polimi.it

M. Reguzzoni
e-mail: mirko.reguzzoni@polimi.it

L. Rossi
e-mail: lorenzo1.rossi@polimi.it

R. Cefalo et al. (eds.), *New Advanced GNSS and 3D Spatial Techniques*,
Lecture Notes in Geoinformation and Cartography,
DOI 10.1007/978-3-319-56218-6_11

1 Introduction

The development of applications based on an accurate positioning has been increasingly grown during the last years. For instance, considering the demand of content and information based on users' location. Sometimes, a rough positioning solution (e.g. room level) could be sufficient, but in the majority of cases a higher accuracy is required (e.g. few millimeters or even less). However, in most cases an accuracy of some decimeters is sufficient and the present paper is focused on this order of magnitude.

The most common method for outdoor navigation is GNSS (Global Navigation Satellite System) positioning, which has been spread during the last decades (Hofmannn-Wellenhof et al. 2008) because of its easiness of use, cost affordability, combined with the possibility of estimating trajectories with centimetric accuracies. However, in order to get such accuracies, a GNSS receiver has to capture the signal from at least four satellites for a sufficient amount of time to fix the phase ambiguities and to solve the positioning problem. This condition is hardly guaranteed in urban areas because of the presence of obstacles (for instance buildings, dense foliage, tunnels, etc.) that prevent the signal reception, degrade the signal quality or drive to a poor spatial distribution of the visible satellites. In these situations, an interesting solution is represented by HS-GNSS (High Sensitive GNSS). These systems are characterized by a higher level of sensitivity, but the measurement error is usually larger (MacCougan 2003), leading often to unacceptable positioning errors. For the near future, we expect that the number of visible satellites will increase thanks to the use of new constellations, such as Galileo and BeiDou. Usually, GNSS antennas are coupled with INS (Inertial Navigation Systems), to bridge the gaps due to GNSS leakages. This coupling allows estimating position, velocity and vehicle orientation relying on Newton's second law of motion. Because the navigation solution is computed by performing time integrations, INS systems are affected by a consistent drift error if they are used in stand-alone mode or in case of absence of GNSS signal, even for relatively short time interval (usually commercial devices lead to errors of the order of some decimeters after 15 min). Often GNSS and INS are combined to realize MMS (Mobile Mapping Systems), whose cost can increase significantly in case they aim at providing decimetric positioning accuracies (Al-Hamad and El-Sheimy 2014).

An alternative solution could be the use of self-tracking total stations. These instruments are quite expensive but allow reaching millimeters accuracy (Böniger and Tronche 2010). However, they requires a clear and constant visibility between the station point and the tracked object and distances have to be lower than their operative range (usually in the order of few hundreds of meters), conditions that can be hardly satisfied in urban areas.

For all these reasons, photogrammetry could represents an interesting trade-off, for overcoming GNSS drawbacks in urban areas without increasing too much the system cost. However, the use of a pure image-based solution could be unsuccessful in case of bad-textured surfaces, and in any case requires both an

appropriate scale and georeferencing information. Therefore, the idea of integrating photogrammetry and complementary data has to be pursued and is here investigated by some experiments. For instance, a joint use of images and GNSS observations allow to simultaneously solving both the mentioned problems.

2 Photogrammetry Based Navigation

Photogrammetry is increasingly used in a number of different fields, allowing obtaining different levels of accuracies, depending on the used camera and lenses. The recent widespread of image-based techniques is due to several factors; among them, the most remarkable one is the huge automatization of the imaging process that has been achieved in the last years, combined with the improvement of algorithms used for the homologous point search and the personal computer performances. Nowadays, photogrammetry is commonly used in many fields, e.g. from optical metrology applications for surface inspection or reverse engineering, requiring sub-millimetric level accuracy, to mass-market applications for pedestrian positioning, requiring a much lower accuracy, namely of the order of tens of meters. The use of image-based solutions has already been discussed by many authors (see for instance Mautz 2012, Barzaghi et al. 2016; Al-Hamad and El-Sheimy 2014; Roncella et al. 2005) for a plenty of different applications, for both indoor and outdoor environments. However, a photogrammetric solution requires also some additional information to correctly scale the problem (at least the baseline between of a stereo-couple has to be known) and some further constraints, such as Ground Control Points (GCPs) to correctly georeference the computed solution. Optical based navigation systems can be classified according to the source used to obtain this a priori knowledge. A complete review, with a focus on indoor applications is given in Mautz (2012). The data used to assist the photogrammetric solution can be stored in a previously populated database and matched one-to-one with the corresponding points on the images, see e.g. data extract from urban maps in Barzaghi et al. (2016). A different solution can be the a priori knowledge of some information, such as the vehicle attitude and position using an INS/GNSS system. This is quite common for Mobile Mapping Applications (Al-Hamad and El-Sheimy 2014). The use of image-based techniques for bridging GNSS outages has been discussed in Chaplin (1999) and Tao et al. (2001). In both the cases, the authors assumed that the coordinates of the starting point can be determined using an INS/GNSS. Roncella et al. (2005) proposed a pure photogrammetric solution based on the automatic extraction of tie points on the image block, in correspondence with the GNSS outages. The trajectory is then recovered from the estimated EO (External Orientation) parameters. Unfortunately, the proposed method can suit only in case of short period of GNSS absence. In fact, the experienced drift was in the order of 1.5 m along a 300 m path, because of the absence of GCPs. These errors could be reduced by adding further constraints (Eugaster et al. 2012) in suitable locations along the survey.

Especially in case of autonomous navigation, it is very important to compute a real-time solution and often there is no a priori knowledge about the explored environment. This is the main issue of SLAM (Simultaneous Location And Mapping), whose objective is to localize the camera position and attitude, creating at the same time the 3D model of the surrounding space. A number of SLAM image-based solutions can be found in literature and usually they are enforced by integrating data characterized by a different nature. Ramos et al. (2007) proposed to combine visual and laser data, allowing to reach RMS in the order of 6–8 m. The use of laser range systems has always represented the first choice for autonomous navigation; however, these systems are quite expensive. A significant change has been registered with the release of the Microsoft Kinect sensor. This device combines passive and active imaging data, having a low cost and allowing using a single device for robotic navigation and mapping purposes (see for instance Suarez and Murphy 2012; Omara and Sahari 2015; Frankhauser 2015). Often, the investigated solutions are based on RGB-D SLAM algorithm (Izadi et al. 2011; Endres et al. 2012). On the large majority of cases, the Kinect has been used for indoor applications. Nevertheless, the second generation of this device is capable of acquiring data also outdoors, as better detailed in Sect. 4.

3 Outdoor Positioning with Urban Maps

The first proposed example of assisted image-based solution has been realized in the frame of the UMALS project (High Speed 3D Underground Utilities and Automatic Electrical Laying System), which final objective was the automatic laying of medium voltage cables. In order to complete this task, it is necessary to localize and define the geometry of all buried infrastructures (e.g. ducts, cables, pipes). When no external information is available (which is usually the case), it is requested to perform an ad hoc GPR (Ground Penetrating Radar) survey. This instrument is usually pulled by hand or attached to a vehicle and it requires to be externally georeferenced with a horizontal accuracy of 0.20–0.30 m. As pointed out before, this task can be hardly solved using a GNSS solution in urban areas. An INS/GNSS solution would not work properly because the GPR antenna has to be moved slowly to fulfil its sampling requirements, meaning that an inertial solution will be affected by significant drifts even along short paths. Moreover, the GNSS can remain in areas characterized by a bad visibility of the sky for long periods, because the GPR acquisitions are performed along parallel lines.

Photogrammetry could represent an interesting solution, useful for overcoming GNSS signal weakness in urban areas. As stressed before, image-based methods require introducing additional information to correctly scale and georeference the computed results. The idea is to use GCPs extracted from large-scale urban maps and GNSS positions when available, such as at intersections or squares. The proposed solution requires installing one or more digital cameras and a GNSS antenna on the same vehicle used to pull the GPR antenna. The trajectory is computed from

the EO parameters estimated during the bundle block adjustment of the images acquired from the cameras located on the vehicle roof, pointing at the roadside. The GCPs are extracted from large-scale urban maps of the investigated areas in correspondence with building corners. Typically, the framed objects are building façades, which allow to automatically extract tie-points with a high multiplicity. The GPR position can be then computed since all the instruments are rigidly attached to the vehicle and the rigid 3D Helmert transformation from the navigation systems to a vehicle-fixed reference system is estimated during the geometric calibration phase.

3.1 Preliminary Tests

In order to evaluate the feasibility of the proposed inverse photogrammetric approach, a series of simulation and preliminary tests were realized. Barzaghi et al. (2009) investigated the accuracies that can be reached using the discussed solution. Furthermore, other tests were realized to evaluate the behaviour of different algorithms for automatic tie-point search, considering different conditions (e.g. plastered or stony walls, intersections, presence of vehicles or obstacles). Also the impact of various acquisition geometries (nadiral vs. convergent) and a different number of GCPs have been evaluated, together with the impact of image pre-processing (i.e. image filtering to enhance the local contrast). A first complete preliminary test has been realized and discussed in Cazzaniga et al. (2012), in conditions very similar to the ones expected for the operational phase. The vehicle (see Fig. 1) was equipped with two slightly convergent Nikon D70s digital cameras (using a fixed focal length

Fig. 1 The vehicle equipped with two cameras and two GNSS antennas used for the tests

equal to 20 mm) and two GNSS antennas. The second antenna was used to simulate the presence of the GPR, and its trajectory has been used as a reference solution for evaluating the goodness of the proposed photogrammetric approach.

The test was realized acquiring 220 images along a 350 m straight path, in Via Golgi (Milan, Italy). The image-based solution has been georeferenced using 11 GCPs extracted from the urban maps (1:1000 scale) in correspondence with building corners. The vehicle trajectory has been computed by solving the bundle block adjustment, obtaining residuals in the order of 0.20 m. However, the obtained results were affected by a systematic error, probably due to an insufficient accuracy in the calibration stage, combined with a degraded GNSS signal.

3.2 *Cremona Test*

The results obtained during the simulations and the preliminary tests proved the feasibility of the investigated approach and the possibility of georeferencing the GPR with the required tolerance. However, the quality of the photogrammetric solution is strongly tied to the quality of the GCPs extracted from the urban map, thus obtaining very different accuracies depending on the specific block. Moreover, the solution could be corrupted by the presence of outliers due to restitution errors. The integration of some GNSS information, in terms of estimated point positions, within the photogrammetric solution is expected to be helpful in identifying and removing these outliers, making the solution more robust and at the same time more accurate. The GNSS positions can be easily acquired in areas with a good sky visibility (e.g. at the beginning or at the end of the survey or in correspondence with open areas, like squares or intersections). The area selected for the second kinematic test is located in a residential block in the town of Cremona, Italy (see Fig. 2; Pagliari et al. 2015). It has been chosen in order to have only low buildings and small houses, with the aim to acquire a GNSS reference solution during the whole test.

In order to have an auto-consistent photogrammetric block (i.e. to reduce all the drift effects) the images have been acquired following only closed trajectories. Also in this case, the vehicle has been equipped with two Nikon D70s cameras (with a fixed focal length equal to 20 mm) and two GNSS antennas. The GNSS positioning solution computed using data acquired by the first antenna was added as pseudo-observations in the bundle block adjustment, while the data of the second one were used as a reference solution (i.e. simulating the position of the GPR). The effect of the further constraint of the Relative Orientation (RO) between the two cameras was considered too. The processed photogrammetric block was composed by 600 images and 52 GCPs extracted from the urban map (1:1000 scale) and identified in correspondence of building corners, shelters or pitches. The latter type of points was very important to improve the block geometry and constrain the estimates along the height direction.

Four different scenarios have been considered during this test. First of all, a pure photogrammetric solution has been computed, using as constraints only the GCPs

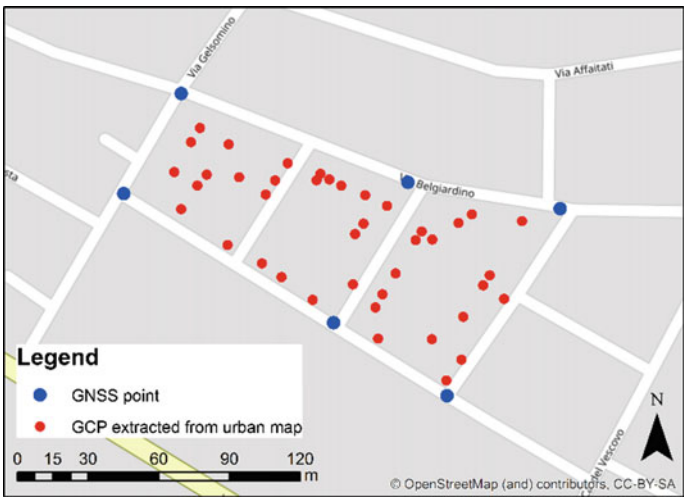

Fig. 2 The residential block used for the Cremona test. The selected GCPs are represented in *red*, while the GNSS pseudo-observations are represented in *blue*

extracted from the digital map. The bundle block adjustment has been computed using the commercial software PhotoModeler® and then refined with the scientific software Calge (Forlani 1986), which allows introducing further constraints such as GNSS pseudo-observations or RO between cameras. The tie point search has been realized by using the software EyeDEA (Roncella et al. 2011). The second scenario has been realized by adding the further constraint of the RO between the two cameras to the previous solution. As for the third scenario, 6 GNSS positions acquired in correspondence with the intersections were introduced in the computation. These GNSS positions were obtained via phase double differences and were characterized by an accuracy of few centimeters. In the last scenario, the combination of both the RO constraint and the integration of GNSS data has been considered. The computed EO positions have been moved to the second GNSS antenna (the one simulating the presence of the GPR) using the lever-arms between the GNSS antenna phase center and the camera projection centers. Their components were estimated during the geometric calibration phase that was realized before the survey. This phase consisted in the simultaneous acquisition of images of a calibration polygon together with the corresponding GNSS positions. The polygon was a building façade on which 7 GCPs were measured using classical topographic methods.

In Table 1 the Root Mean Square Errors (RMSE) computed for the residuals between the photogrammetric solutions and the reference one (i.e. the position derived from the second GNSS antenna interpolated at the shooting time) are shown.

The statistics reported in Table 1 clearly underline how the use of further constraints helps in improving the photogrammetric solution. In particular, the

Table 1 RMSE of the differences between the photogrammetric solutions and the GNSS reference trajectory

Scenario	N [m]	E [m]	h [m]
52 GCPs	0.180	0.311	0.260
52 GCPs + RO	0.195	0.261	0.248
52 GCPs + 6 GNSS points	0.148	0.140	0.128
52 GCPs + 6 GNSS points +RO	0.124	0.092	0.153

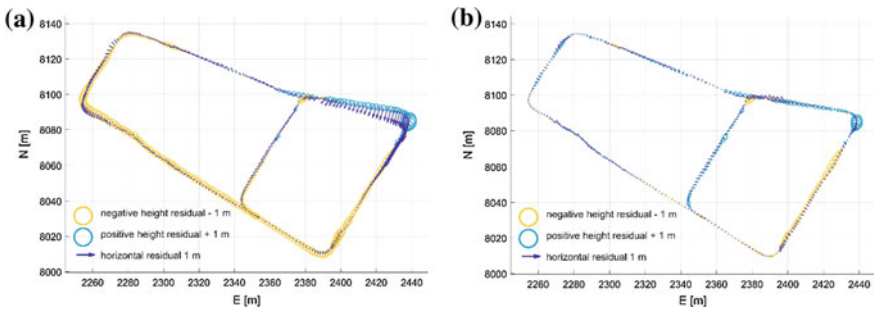

Fig. 3 The residuals between the photogrammetric solution and the GNSS reference trajectory, interpolated at the shooting time: **a** Only 52 GCPs extracted from the urban map. **b** 52 GPSs extracted from the urban map plus 6 GNSS points plus the RO constraint

introduction of few GNSS observations allows improving the results, reaching accuracies of the order of 0.15 m. This result was further improved considering also the RO constraint between the cameras, reaching horizontal accuracies of the order of 0.10 m. A graphic representation of the residuals is shown in Fig. 3.

4 Outdoor Positioning with the Kinect

The Microsoft Kinect (see Fig. 4) has revolutionized the navigation task for robotics applications, allowing to access a depth camera, as well as RGB images, at a cost of about 200$. The Kinect has encountered a great success in the scientific and research community because of the complementary nature of the delivered data, together with the possibility of interacting with the data streaming (up to 30 fps) thanks to the release of official and third part libraries. Some authors have proposed navigation and mapping solutions based on the use of this device (Oliver et al. 2012; Endres et al. 2012; Omara and Shari 2015; Suarez and Murphy 2012). The large majority of the studies has been realized by exploring indoor environments, mainly because the first generation of this device was not capable of acquiring data when disturbed by the direct sunlight. In 2014, a second generation of the Kinect

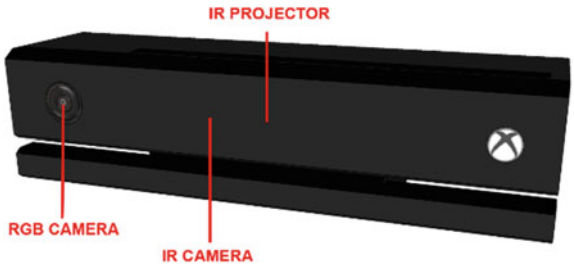

Fig. 4 The second generation of Kinect device; the position of the imaging sensors and the IR projector are shown

device has been sold and a new dedicated Software Development Kit (SDK) has been released. The same set of sensors that composed its predecessor is assembled in the new device: an IR camera co-registered with a depth camera, an IR projector, a RGB camera, a microphone array and a 3-axis accelerometer. The data resolution has been improved and the new device delivers HD images. Moreover, the depth measurements are performed by using a different principle (time of flight instead of triangulation), allowing to acquire data even outdoors under the sun influence.

The second generation of Kinect can acquire HD RGB and IR images, respectively with a resolution of 1920 × 1080 pixels and 512 × 424 pixels. The IR camera delivers different outputs: grey scale images depending on the ambient lighting, active gray scale images independent from the ambient lighting and depth images. In the last case, each pixel is associated with the corresponding distance measurement between the Kinect and the investigated object. Details about the Kinect operation principles can be found in Sell and O'Connor (2014). The new time-of-flight depth measurement principle allows acquiring data even outdoors, with a level of accuracy comparable to indoor acquisitions, say of the order to 0.02 m within the range 0.45–4.00 m (see Pagliari and Pinto 2015; Pagliari et al. 2015).

4.1 RGB-D and GNSS Integration

The approach here presented is based on the combined use of the visual and depth data delivered by the Kinect. These data are used to reconstruct a first approximated trajectory, which is then refined using a Kalman filter that integrates the image-based solution with the GNSS data. The bridge between the different data sources is given by the PC (Personal Computer) acquisition time. As pointed out before, the Kinect delivers data with a frame rate of about 30 fps, so the acquired data were downsampled considering the correspondences between visual and depth images, ensuring a sufficient baseline between two subsequent datasets. RGB and depth images are characterized by a complementary nature, and they can reciprocally overcome their limits. In order to use all the information included in these data, RGB-D images have been created. An RGB-D image consists of a six-dimensional array, composed by the RGB image and the point cloud generated

from the simultaneous depth acquisition. The algorithm implemented for the trajectory recovering is based on the alignment procedure developed by Xiao et al. (2013). Two RGB-D images are taken as input and the rototranslation between them is computed by combining the SIFT keypoints (Lowe 2004) selected from the RGB channels and the information extracted from the point clouds. The algorithm detects the SIFT correspondences that are used to estimate an initial alignment subsequently refined by applying the ICP (Iterative Closest Points) to the point clouds. In case that the ICP solution drifts over a threshold value, it is discarded and only the SIFT alignment is used. The final trajectory is computed incrementally, meaning that the error accumulates over time. This can cause drifts and loop closure problems. For these reasons, the image-based trajectory is integrated with the GNSS observations in a Kalman filtered solution (see e.g. Realini and Reguzzoni 2013).

4.2 The Implemented Kalman Filter

The proposed Kalman filter has been realized under some simplified assumptions. Both the GNSS antenna phase center and the center of projection of the RGB camera are considered coincident with the center of mass of the vehicle, meaning that the motion between subsequent epochs is approximated as a pure translation and the system is schematized as a point. The resulting state vector $\boldsymbol{x}_i = \boldsymbol{x}(t_i)$ at the epoch $t_i = i = 1, 2, \ldots N$ is

$$\boldsymbol{x}_i = \begin{bmatrix} \boldsymbol{r}_i \\ \dot{\boldsymbol{r}}_i \end{bmatrix} \tag{1}$$

where $\boldsymbol{r}_i$ and $\dot{\boldsymbol{r}}_i$ are respectively the position and the velocity vector at epoch i.

The motion between two epochs is assumed to be uniform and linear. A velocity model error $\boldsymbol{\varepsilon}_i$ that allows changes of direction is used:

$$\boldsymbol{x}_{i+1} = \mathrm{T}_i \cdot \boldsymbol{x}_i + \boldsymbol{\varepsilon}_i \tag{2}$$

where T_i is the non-stationary transition matrix between the two epochs t_i and t_{i+1}, described as:

$$\mathrm{T}_i = \begin{bmatrix} \mathrm{I}_3 & \Delta t_{i,i+1} \cdot \mathrm{I}_3 \\ 0 & \mathrm{I}_3 \end{bmatrix} \tag{3}$$

where I_3 is a 3×3 identity matrix and $\Delta t_{i,i+1}$ is the time interval between two acquisition epochs of either the Kinect or the GNSS receiver.

The deterministic model of the observation vector $\boldsymbol{y}_i$ is modelled as:

$$\boldsymbol{y}_i = \mathrm{H}_i \cdot \boldsymbol{x}_i \tag{4}$$

where H_i is the transformation matrix.

The developed Kalman filter integrates two different kind of observations (i.e. Kinect and GNSS). For this reason two different transformation matrices were implemented. The Kinect observations are the displacements of two RGB-D acquisitions between the epochs t_k and t_{k+1} (with $\{t_k\} \subseteq \{t_i\}$), meaning that the design matrix corresponding to an acquisition time t_k is described as:

$$\mathrm{H}_k = [\,\mathrm{I}_3 \quad \Delta t_{k,k-1} \cdot \mathrm{I}_3\,] \tag{5}$$

where $\Delta t_{k,k-1}$ is the time interval between each Kinect acquisition and the previous one.

In case of GNSS observations the single estimated positions and not the raw observations have been used (Brovelli et al. 2008). The design matrix H_j, corresponding to any acquisition epoch t_j (with $\{t_j\} = \{t_i\} \backslash \{t_k\}$) is modelled as:

$$\mathrm{H}_j = [\,\mathrm{I}_3 \quad \mathrm{O}_3\,] \tag{6}$$

where O_3 is a 3×3 null matrix.

4.3 Andrea Cascella's Fountain Test

The proposed solution for the Kinect outdoor navigation has been tested by realizing an experimental acquisition around Andrea Cascella's fountain (Piazza Leonardo da Vinci, Milan) (Pagliari et al. 2016). The Kinect has been installed on a cart, together with a GNSS antenna and a reflective prism, used to acquire the reference trajectory by means of a self-tracking total station. The self-tracking total station has been georeferenced in the GNSS reference frame, by means of a GNSS static survey in two points. A supply battery for the Kinect and a PC have been located on the same cart (see Fig. 5). The survey has been realized by moving the vehicle at crawl velocity around the fountain, maintaining a distance from it lower than the Kinect operative range (4 m).

During the survey, we acquired RGB and depth images, GNSS positions and the PC time associated to both Kinect and GNSS acquisitions. The images delivered by the Kinect have been processed by using an in-house software written in Matlab®, which embedded the alignment function developed by Xiao et al. (2013). The processed dataset was composed by 218 couples of visual and depth images, acquired over a path about 50 m long. The rototranslation that minimizes the discrepancies between the GNSS and the Kinect trajectory has been estimated by least-squares adjustment, with the aim of comparing the solutions obtained with the different sensors. In order to simulate mass-market receiver performances, the GNSS observations have been degraded adding a white noise with a standard

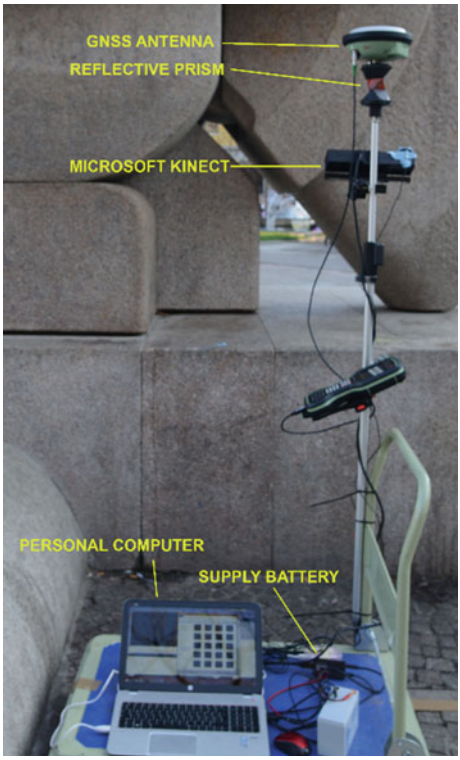

Fig. 5 The cart used for the experimental test with all the installed instruments

deviation equal to 0.30 m. The image-based Kinect and the GNSS trajectories have been used as input for the developed Kalman filter. The GNSS observations are given with the corresponding error covariance matrices, which are revised accordingly to the degradation mentioned before. The Kinect solution is not supplied by covariance matrices, so they have been modeled as diagonal matrices with a standard deviation representative of the outdoor performances of the Kinect depth measurements. The dynamics error was empirically defined, discriminating between corners and straights. A stronger constraint was considered along the height direction, for the whole path. In Fig. 6, the computed solutions are shown. From the test, it comes out that the Kalman filtered solution allowed to correct the drift error accumulated along the Kinect trajectory, being at the same time less disperse than the GNSS one. In Table 2 the standard deviations computed by comparing the different solutions with the reference trajectory are shown. The final solution based on the proposed Kalman filter is characterized by an accuracy of the order of 0.20 m along horizontal coordinates and less than 0.10 m along the vertical one. This represents an improvement over the Kinect solution, which was characterized by horizontal errors of about 0.50 m and height errors of about 0.20 m. It also represents an improvement with respect to the GNSS trajectory whose standard deviation was 0.30 m along all directions.

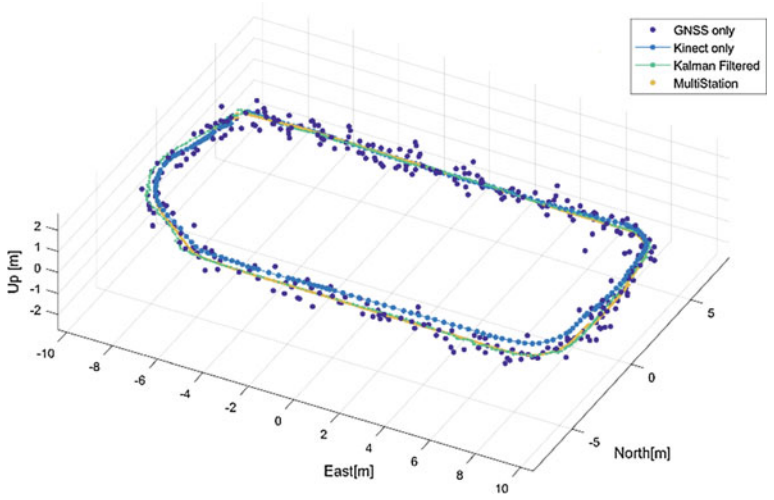

Fig. 6 The computed solutions for the experimental test

Table 2 Standard deviations between the computed solutions and the reference trajectory measured with the self-tracking total station

Solution	North [m]	East [m]	Up[m]
GNSS only	0.280	0.307	0.323
Kinect only	0.524	0.545	0.206
Kalman filtered	0.183	0.195	0.067

5 Conclusions and Final Remarks

In this paper, the use of photogrammetric-aided techniques for urban navigation has been investigated. Two different case studies have been discussed, focusing on the integration of image-based techniques and GNSS. In the first test, the use of photogrammetry, constrained using GCPs extracted from large-scale urban maps, has been tested for georeferencing a slow moving vehicle, reaching accuracies of the order of few decimeters. The effect of introducing GNSS pseudo-observations within the bundle block adjustment, together with the further constraint of RO between the two cameras, was assessed showing accuracies of the order of 0.10 m in all directions. As for the second case study, the use of the new generation of Microsoft Kinect has been tested for outdoor navigation. A Kalman filtered solution has been developed for integrating the Kinect trajectory (computed combining the information that can be derived from depth and RGB images) and the GNSS points. Even if the Kalman filter was written under a number of simplified hypothesis (i.e. the vehicle is modelled as a point, the motion between subsequent epochs is modelled as a pure translation), accuracies in the order of 0.20 m for the horizontal direction and below 0.10 m for the height one have been reached.

References

Al-Hamad A, El-Sheimy N (2014) Smartphones based mobile mapping systems. Int Arch Photogramm Remote Sens Spatial Inf Sci 40(5):29

Barzaghi R, Carrion D, Cazzaniga NE, Forlani G (2009) Vehicle positioning in urban areas using photogrammetry and digital maps. In: Proceedings of the ENC-GNSS09, Napoli

Barzaghi R, Cazzaniga NE, Pagliari D, Pinto L (2016) Vision-based georeferencing of GPR in urban areas. Sensors 16(1):132

Böniger U, Troncke J (2010) On the potential of kinematic GPR survey using self-tracking total station: evaluating system crosstalk and latency. IEEE Trans Geosci Remote Sens 28 (10):3792–3798

Brovelli MA, Realini E, Reguzzoni M, Visconti MG (2008) Comparison of the performance of medium and low level GNSS apparatus, with and without reference networks. Int Arch Photogramm Remote Sens Spatial Inf Sci XXXVI (part 5/C55):54–61

Cazzaniga NE, Pagliari D, Pinto P (2012) Photogrammetry for mapping underground utility lines with ground penetrating radar in urban areas. Int Arch Photogramm Remote Sens Spatial Inf Sci XXXIX-B1, Melbourne, Australia

Chaplin B (1999) Motion estimation from stereo image sequences for a mobile mapping system. Msc. Thesis, Department of Geomatics Engineering, University of Calgary

Endres F, Hess J, Engelhard N, Sturn J, Cremer D, Burgard W (2012) An evaluation of RGB-D SLAM system. In: 2012 IEEE international conference on robotics and automation, River Centre, Saint Paul, Minnesota, pp 1691–1696

Eugster H, Huber F, Nebiker S, Gisi A (2012) Integrated georeferencing of stereo image sequences captured with a stereovision mobile mapping system—approaches and practical results. Int Arch Photogramm Remote Sens Spatial Inf Sci XXXIX-B1:309–314

Fankhauser P, Bloesch M, Rodriguez D, Kaestner E, Hutter M, Siegwart R (2015) Kinect v2 for mobile robot navigation: evaluation and modeling. In: 2015 international conference on advanced robotics (ICAR), Istanbul, pp 388–394

Forlani G (1986) Sperimentazione del nuovo programma CALGE dell'ITM. In: Bollettino SIFET, pp 63–72 (in Italian)

Hoffmann-Wellenhof B, Lichtenegger B, Walse E (2008) GNSS-Global navigation satellite systems. Springer, Berlin

Izadi S, Kim D, Hilliges O, Molyneaux D, Newcombe R, Kohli P, Shotton J, Hodges S, Freeman D, Davison A, Fitzgibbon A (2011) Kinect fusion: real-time 3D reconstruction and interaction using a moving depth camera. In: Proceedings of ACM symposium on user interface software and technology (UIST'11)

Lowe D (2004) Distinctive image feature from scale-invariant. Int J Comput Vision 60(2):91–110

MacGougan GD (2003) High sensitive GPS performance analysis in degraded signal environments. M.Sc Thesis. Department of Geomatics Engineering, University of Calgary

Mautz R (2012) Indoor positioning technologies. Habilitation Thesis at ETH Zurich, 127 p, Swiss Geodetic Commission, Geodetic-Geophysical Reports of Switzerland, no. 86, ISBN 978-3-8381-3537-3

Oliver A, Kong S, Wünsche B, MacDonald B (2012) Using the Kinect as a navigation sensor for mobile robotics. In: Proceedings of the 27th conference on image and vision computing (IVCNZ'12), pp 505–514

Omara HIMA, Sahari KSM (2015) Indoor mapping using kinect and ROS. Agents, Multi-Agent Systems and Robotics (ISAMSR), 2015 International Symposium on, Putrajaya, pp. 110–116

Pagliari D, Cazzaniga NE, Pinto L (2015) Use of assisted photogrammetry for indoor and outdoor navigation purposes. Int Arch Photogramm Remote Sens Spatial Inf Sci 40(4):113

Pagliari D, Pinto L (2015) Calibration of Kinect for Xbox one and comparison between the two generations of Microsoft sensors. Sensors 15(11):27569–27589

Pagliari D, Pinto L, Reguzzoni M, Rossi L (2016) Integration of Kinect and low-cost GNSS for outdoor navigation. Int Arch Photogramm Remote Sens Spatial Inf Sci, 565–572

Roncella R, Re C, Forlani G (2011) Comparison of two structure from motion strategies. Int Arch Photogramm Remote Sens Spatial Inf Sci, vol XXXVIII, 5-W16

Roncella R, Remondino F, Forlani G (2005) Photogrammetric bridging of GPS outages in mobile mapping. In: Electronic Imaging International Society for Optics and Photonics

Ramos FT, Nieto J, Durrant-Whyte HF (2007) Recognizing and modelling landmarks to close loops in outdoor SLAM. In: 2007 IEEE international conference on robotics and automation, pp 2036–204

Realini E, Reguzzoni M (2013) goGPS: open source software for enhancing the accuracy of low-cost receivers by single frequency relative kinematic positioning. Meas Sci Technol 24 (11):115010

Sell J, O'Connor P (2014) The Xbox one system in a chip and kinect sensor. Micro IEEE 34 (2):44–53

Suarez J, Murphy RR (2012) Using the Kinect for search and rescue robotics. In: 2012 IEEE international symposium on safety, security, and rescue robotics (SSRR), College Station, TX, pp 1–2

Tao CV, Chapman MA, Chaplin BA (2001) Automated processing of mobile mapping image sequences. ISPRS J Photogramm Remote Sens 55:330–346

Xiao J, Owens A, Torralba A (2013) SUN3D: a database of big spaces reconstructed using SfM and object labels, ICCV

Part II
New Advanced GNSS and 3D Spatial Techniques—Photogrammetry and Remotes Sensing

Part II reports some chapters relating to advanced topics in photogrammetry and remote sensing.

The first chapter of the part is characterized by three photogrammetric contributions. The first chapter is entitled "Procrustean Photogrammetry: From Exterior Orientation to Bundle Adjustment" by Fabio Crosilla, Eleonora Maset and Andrea Fusiello, DPIA—University of Udine, Italy. It reviews some recent research results of the photogrammetry and computer vision group. In particular, the paper shows how the so-called *anisotropic row-scaling Procrustes analysis algorithms* can be applied to easily solve the image exterior orientation and the bundle block adjustment problems without any linearization or approximated values of the unknown parameters. The solution is iteratively updated without any equation system solution. The only analytical request is given by the eigenvalue–eigenvector computation of 3 x 3 matrices and the adaptation, at each iteration, by a block relaxation scheme (involving rotation, anisotropic scaling and translation) of the image points to their 3D control values or to their corresponding tie point centroids.

The second chapter is entitled "Evaluation of 3D Reconstruction Accuracy in the Case of Stereo Camera-Pose Configuration" by Xuan Zhang[1], Gang Qiao[1] and Marco Scaioni[2], [1]Tongji University, College of Surveying and Geo-Informatics, Shanghai, P.R. China, and [2]Politecnico Milano, DABC (Department of Architecture, Built Environment and Construction Engineering), Italy. The aim of the work is to provide some hints for the application of stereo pairs, available for classical normal configurations and for convergent images as well, according to some theoretical and experimental evaluations of the obtainable accuracy. The results can be of great interest for practical image orientation, tie point extraction and dense matching 3D surface reconstruction problems.

The third photogrammetric chapter, entitled "Towards Surveying with a Smartphone" by Francesca Fissore, Andrea Masiero, Marco Piragnolo, Francesco Pirotti, Alberto Guarnieri, Antonio Vettore, Interdepartmental Research Center of Geomatics, Padua University, Italy, shows the potential improvement, in terms of

reliability and accuracy, obtainable for the structure from motion 3D reconstruction, when information provided by navigation systems is available. The technique is validated for a building reconstruction, using images and navigation information acquired with a standard smartphone.

Some Metric Documentation of Cultural Heritage in Poland by Spherical Photogrammetry by G. Fangi, Università Politecnica delle Marche— Ancona— Italy, describes a new photogrammetric technique making use of the so-called spherical panoramas obtained taking pictures from the same station point covering up to 360°. A software package called Sphera and developed by the author is presented.

The last chapter is devoted to remote sensing technologies and satellite data analysis: "Doing Science with Nano-Satellites", by Anna Gregorio[1,2,3], Alessandro Cuttin[1,4], Mario Fragiacomo[2], Mauro Messerotti[3,2], [1]University of Trieste, Department of Physics, Italy; [2]PicoSaTs Srl, Trieste, Italy; [3]INAF, Osservatorio Astronomico di Trieste, Italy; [4]University of Trieste, Department of Engineering and Architecture, Italy.

The opportunity of using a constellation or a network of nano-satellites (PicoSaTs) as a new generation of telecommunication (e.g. for mobile applications) or navigation systems is explored. This peculiarity could enable the transmission of large amount of data, currently accessible only by larger satellites.

Procrustean Photogrammetry: From Exterior Orientation to Bundle Adjustment

Fabio Crosilla, Eleonora Maset and Andrea Fusiello

Abstract This work reviews the anisotropic row-scaling variant of the Procrustes analysis algorithms applied to develop new analytical tools for solving classical photogrammetric Computer Vision problems. In Garro et al. (Solving the pnp problem with anisotropic orthogonal procrustes analysis, 2012) the anisotropic row-scaling Procrustes analysis was first applied to perform the *exterior orientation* of one image. Moreover Fusiello and Crosilla (ISPRS J Photogrammetry and Remote Sens 102:209–221, 2015) provided a Procrustean formulation of the photogrammetric *bundle block adjustment* problem. Procrustean methods do not require any linearization nor approximated values of the unknown parameters and the results obtained are comparable in terms of accuracy with those given by the state-of-the-art methods.

Keywords Anisotropic extended orthogonal procrustes analysis · Exterior orientation · Photogrammetric bundle block adjustment

1 Introduction

Procrustes analysis is a well known least squares technique used to directly perform transformations among corresponding point coordinates belonging to a generic k-dimensional space. Applied at first in multifactorial analysis, shape analysis and geodesy (Crosilla 1999), in the last decade it was also proposed in Photogrammetry (Akca 2003), e.g., for matching different 3D object models from images (Crosilla and Beinat 2002). In this case the authors applied the so called

F. Crosilla · E. Maset (✉) · A. Fusiello
DPIA, University of Udine, Via Delle Scienze, 208, 33100 Udine, Italy
e-mail: maset.eleonora@spes.uniud.it

F. Crosilla
e-mail: fabio.crosilla@uniud.it

A. Fusiello
e-mail: andrea.fusiello@uniud.it

R. Cefalo et al. (eds.), *New Advanced GNSS and 3D Spatial Techniques*,
Lecture Notes in Geoinformation and Cartography,
DOI 10.1007/978-3-319-56218-6_12

Extended Orthogonal Procrustes Analysis (EOPA) model, that considers the direct similarity transformation between two matrices, and the Generalized Procrustes Analysis (GPA) to simultaneously match more than two coordinate matrices of corresponding points expressed in different reference systems. These models will be briefly reviewed in Sect. 2.

The anisotropic row-scaling variant of the Procrustes Analysis represents instead the basic tool for an alternative solution of other classical photogrammetric problems. The analytical solution of the Anisotropic Extended Orthogonal Procrustes Analysis (AEOPA) with row-scaling, recalled in Sect. 2.3, was first derived by Garro et al. (2012), who applied it to perform the exterior orientation of one image without any a priori information. In Fusiello et al. (2015) the point-line registration problem, which generalizes absolute orientation to point-line matching, was formulated as an instance of the AEOPA model, and its solution was derived. The same formulation solves the Non-Perspective-n-Point camera pose problem, that in turn generalizes exterior orientation to non-central cameras, i.e., generalized cameras where projection rays do not meet in a single point. A generalized version of AEOPA leads instead to the Procrustean solution of the classical bundle block adjustment, derived by Fusiello and Crosilla (2015), also in its robust version (Fusiello and Crosilla 2016). These algorithms will be described in detail in Sect. 3.

The main advantage of the Procrustes methods is that they furnish a simple and compact solution without any linearization of the original equations, and without any approximate value of the unknown parameters.

2 The Mathematical Tool: Procrustes Analysis

Let us start this section by summarily recalling the solutions of the isotropic Procrustes analysis and of its generalized version, which are helpful to introduce the anisotropic variant, on which the entire Procrustean Photogrammetry is based.

2.1 Extended Orthogonal Procrustes Analysis (EOPA)

EOPA allows to directly recover the least squares similarity transformation between two point sets. Let us consider two matrices P and S containing two sets of numerical data, e.g., the coordinates of n points of $\mathbb{R}^3$ by rows. EOPA allows to directly estimate the unknown 3×3 rotation matrix R, the translation vector $\mathbf{c}$ and the global scale factor ζ that solves:

$$\underset{\zeta,\mathbf{c},R}{\text{minimize}} \quad \left\| S - \zeta PR - \mathbf{1}\mathbf{c}^{\mathrm{T}} \right\|_F^2 \tag{1}$$

subject to the orthogonality constraint $R^{\mathrm{T}}R = RR^{\mathrm{T}} = I$, where $\mathbf{1}$ is the all-ones vector and $\| \cdot \|_F$ denotes the Frobenius norm. As demonstrated in Schönemann and Carroll (1970), the rotation matrix that solves problem (1) is given by $R = U\,\mathrm{diag}(1, 1, \det(UV^{\mathrm{T}}))V^{\mathrm{T}}$, where U and V are determined from the SVD

decomposition $P^{\mathrm{T}}\left(I - \mathbf{1}\mathbf{1}^{\mathrm{T}}/n\right)S = UDV^{\mathrm{T}}$. The $\det(UV^{\mathrm{T}})$ normalization guarantees that R is not only orthogonal but has positive determinant. Then the scale factor can be determined by:

$$\zeta = \frac{\mathrm{tr}\left(R^{\mathrm{T}}P^{\mathrm{T}}\left(I - \mathbf{1}\mathbf{1}^{\mathrm{T}}/n\right)S\right)}{\mathrm{tr}\left(P^{\mathrm{T}}\left(I - \mathbf{1}\mathbf{1}^{\mathrm{T}}/n\right)P\right)} \tag{2}$$

and finally the translation can be computed as $\mathbf{c} = (S - \zeta PR)^{\mathrm{T}}\mathbf{1}/n$.

2.2 Generalized Procrustes Analysis (GPA)

Generalized Procrustes Analysis (GPA) (Gower 1975) is a well-known technique that generalizes the classical EOPA (Schönemann and Carroll 1970) to the alignment of more than two point sets, represented as matrices. It minimizes the following least squares objective function:

$$\underset{\zeta_i,\mathbf{c}_i,R_i}{\text{minimize}} \quad \sum_{i=1}^{m}\sum_{j=i+1}^{m} \left\|\left(\zeta_i P_i R_i + \mathbf{1}\mathbf{c}_i^{\mathrm{T}}\right) - \left(\zeta_j P_j R_j + \mathbf{1}\mathbf{c}_j^{\mathrm{T}}\right)\right\|_F^2 \tag{3}$$

subject to $R_i^{\mathrm{T}}R_i = R_i R_i^{\mathrm{T}} = I$, where $P_1, P_2, \ldots, P_m$ are the m matrices that contain (by rows) the same set of n points in m different coordinate systems. The degenerate solution $\zeta_i = 0\ \forall i$ must be avoided by imposing some constraints on ζ_i.

The GPA objective function has an alternative formulation in terms of the centroid. Let $P'_i = \zeta_i P_i R_i + \mathbf{1}\mathbf{c}_i^{\mathrm{T}}$, the following equivalence holds (Commandeur 1991):

$$\sum_{i<j}^{m} \|P'_i - P'_j\|_F^2 = m\sum_{i=1}^{m} \|P'_i - \hat{S}\|_F^2, \tag{4}$$

where $\hat{S} = \frac{1}{m}\sum_{i=1}^{m} P'_i$ is the centroid of the group of matrices, or mean shape: its rows are the coordinates of the geometric centroid of corresponding transformed points.

By comparing formula (4) with the objective function (3), it is possible to define a solving criterion based on iterative computation of the centroid, that leads to great advantages in terms of simplicity and efficiency. In summary, these are the only two steps that are repeated until stabilization of the centroid $\hat{S}$:

(a) solve for the similarity transformations for each matrix P'_i with respect to the centroid $\hat{S}$;
(b) compute the centroid $\hat{S}$ following the sequential updating of matrices P'_i.

Step (a) is a simple EOPA model, whose solution was formulated in Sect. 2.1.

2.3 Anisotropic EOPA (AEOPA)

A first extension of the EOPA with anisotropic scaling along space dimensions was proposed by Bennani Dosse and Ten Berge (2010). Another variant is the one known as AEOPA with row scaling, where each data point or measurement can be scaled independently of the others. In this case, the isotropic scale factor that characterizes EOPA is substituted by an anisotropic scaling represented by a $n \times n$ diagonal matrix Z of different scale values.

The model is the following

$$S = ZPR + \mathbf{1}\mathbf{c}^{\mathrm{T}} \tag{5}$$

and the unknowns R, $\mathbf{c}$ and Z can be retrieved solving the problem:

$$\underset{Z,\mathbf{c},R}{\text{minimize}} \quad \|S - ZPR - \mathbf{1}\mathbf{c}^{\mathrm{T}}\|_F^2 \tag{6}$$

under the orthogonality constraint $R^{\mathrm{T}}R = RR^{\mathrm{T}} = I$. Whereas in the classical solution of the EOPA problem one can recover first R, that does not depend on the other unknowns, then the isotropic scale ζ and finally $\mathbf{c}$, in the anisotropic case the unknowns are entangled in such a way that one must resort to the so called *block relaxation* scheme, where each variable is alternatively estimated while keeping the others fixed. The algorithm can be therefore seen as iterating between two stages, namely:

- assuming known Z, apply the EOPA solution to find $R = U\mathrm{diag}(1, 1, \det(UV^{\mathrm{T}}))V^{\mathrm{T}}$, with $ZP^{\mathrm{T}}\left(I - \mathbf{1}\mathbf{1}^{\mathrm{T}}/n\right)S = UDV^{\mathrm{T}}$, and $\mathbf{c} = (S - ZPR)^{\mathrm{T}}\mathbf{1}/n$;
- given R and $\mathbf{c}$, solve for

$$Z = \left(I \circ PP^{\mathrm{T}}\right)^{-1}\left(PR(S^{\mathrm{T}} - \mathbf{c}\mathbf{1}^{\mathrm{T}}) \circ I\right) \tag{7}$$

where $\circ$ represents the Hadamard, or element-wise, product.

The rigorous derivation of the above formulas can be found in Garro et al. (2012), where problem (6) is rewritten in terms of a Lagrangian function F and solved by setting to zero the partial derivatives of F with respect to the unknowns.

However, expression (7) for the depth matrix Z can be derived in an alternative and more intuitive way, as follows. Assuming that R and $\mathbf{c}$ are known and defining $Y = R\left(S^{\mathrm{T}} - \mathbf{c}\mathbf{1}^{\mathrm{T}}\right)$, (5) becomes

$$P^{\mathrm{T}}Z = Y. \tag{8}$$

Exploiting the Khatri-Rao product, denoted with $\odot$, and its property involving diagonal matrices and the vec operator,[1] Eq. (8) can be written as

$$(I \odot P)\mathrm{diag}^{-1}(Z) = \mathrm{vec}\, Y \tag{9}$$

where diag^{-1} returns a vector containing the diagonal elements of its argument. In the over-determined case, the least squares solution of (9) is given by

$$\mathrm{diag}^{-1}(Z) = \left[(I \odot P)^{\mathrm{T}}(I \odot P)\right]^{-1}(I \odot P)^{\mathrm{T}}\mathrm{vec}\, Y \tag{10}$$

which is equivalent to the following more compact formulation applying the Hadamard product:

$$\mathrm{diag}^{-1}(Z) = \left(I \circ PP^{\mathrm{T}}\right)^{-1}\mathrm{diag}^{-1}(PY). \tag{11}$$

It is easy to see that (11) corresponds to the original solution (7) reported in Garro et al. (2012).

3 Procrustean Photogrammetry

Some of the most common problems in Photogrammetry, such as the *exterior orientation* and the *bundle block adjustment*, can be formulated in terms of an instance of AEOPA and of its generalized version, as shown in Garro et al. (2012) and Fusiello and Crosilla (2015). In this section, the Procrustes solutions of these problems will be reviewed, highlighting the advantages of Procrustes methods.

3.1 Exterior Orientation

Given at least three control points and their projections, the *exterior orientation* problem, a.k.a. the *Perspective-n-Point (PnP)* camera pose problem in Computer Vision, requires to find a rotation matrix R and a vector $\mathbf{c}$ (specifying attitude and position of the camera) such that the vector form of collinearity equations:

$$\mathbf{p}_j = \zeta_j^{-1} R(\mathbf{s}_j - \mathbf{c}) \tag{12}$$

[1]The vec operator transforms a matrix into a vector by stacking its columns.

is satisfied for some positive scalar ζ_j, where $\mathbf{s}_j$ is the coordinate vector of the jth control point in the external system, ζ_j is a positive scalar proportional to the "depth" of the point, i.e., the distance from the jth control point to the plane containing the projection center and parallel to the image plane, $\mathbf{p}_j$ is the coordinate vector of the jth control point in the camera system, where the third component is equal to $-c$, the principal distance or focal length.

Expressing (12) with respect to $\mathbf{s}_j$ and extending it to n control points $\mathbf{s}_1 \ldots \mathbf{s}_n$, one obtains $S = ZPR + \mathbf{1}\mathbf{c}^{\mathrm{T}}$, where P is the matrix by rows of image point coordinates defined in the camera frame, S is the matrix by rows of point coordinates defined in the external system and Z is the diagonal (positive) depth matrix. One can recognize an instance of the AEOPA model (5) that can be solved using the procedure described in Sect. 2.3. The *Procrustean PnP (PPnP)* algorithm can be therefore summarized as in Algorithm 1.

Algorithm 1 PPnP

Input: control points S and their image coordinates P
Output: position $\mathbf{c}$ and attitude R of the camera

1. Start with any $Z > 0$
2. Compute $R = U\mathrm{diag}(1, 1, \det(UV^{\mathrm{T}}))V^{\mathrm{T}}$ with $UDV^{\mathrm{T}} = P^{\mathrm{T}}Z\left(I - \mathbf{1}\,\mathbf{1}^{\mathrm{T}}/n\right)S$
3. Compute $\mathbf{c} = (S - ZPR)^{\mathrm{T}}\mathbf{1}/n$
4. Compute $Z = \left(I \circ PP^{\mathrm{T}}\right)^{-1}\left(PR(S^{\mathrm{T}} - \mathbf{c}\mathbf{1}^{\mathrm{T}}) \circ I\right)$
5. Iterate from step 2 until convergence

We compared the *PPnP* algorithm to the classical exterior orientation solution, that minimizes the sum of squared image coordinate residuals of the collinearity equations. To carry out the simulation, $n = 30$ 3D points were randomly distributed in a sphere of unit radius centered on the origin. The camera was positioned at a distance of 5 m from the origin and the focal length was chosen so as to yield a view angle of 60° with an image size of 1000 × 1000 pixels. Different values of noise $\sigma_P = \{0, \ldots, 5\}$ [pixel] were added to the image coordinates obtained from the projection of the 3D points. For each setting the test was run 100 times and the mean error norm was computed. In all the experiments the initial depths were set to one. In Fig. 1 (left) the rotation errors are shown, which are computed as $\| \log(R^{\mathrm{T}}\hat{R}) \|_F$, where R is the ground truth, $\hat{R}$ is the actual rotation and $\| \cdot \|_F$ is the Frobenius norm. Results show that the mean error for *PPnP* is only slightly higher than the error achieved by the classical exterior orientation.

Fusiello et al. (2013) provided also a robust version of the *PPnP* algorithm based on Forward Search, which proved to be highly effective and accurate in detecting outliers, even for small data size or high outliers contamination.

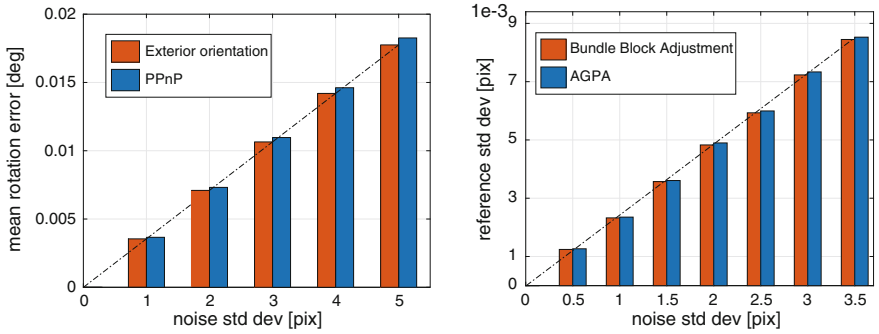

Fig. 1 *Left* Mean rotation error obtained in the exterior orientation of one image versus standard deviation of random noise added to image coordinate. *Right* Root of reference variance of the image coordinate residuals in bundle block adjustment versus standard deviation of random noise added to image tie-point. *Orange* is the error obtained by classical photogrammetric methods, while *blue* is the error achieved by Procrustean solutions. There is no substantial difference in the results obtained by Procrustean and classical photogrammetric methods

3.2 Bundle Block Adjustment

In the *bundle block adjustment* problem it is required to simultaneously find the exterior orientation parameters of multiple images and the tie-points 3D coordinates that minimize a geometric error. Classical photogrammetric bundle block adjustment minimizes residuals in the image plane. Formulating instead the problem in a Procrustes framework (Fusiello and Crosilla 2015, 2016), the geometric error to be minimized belongs to the 3D space and can be expressed as follows:

$$\sum_{i=1}^{m} \|S - Z_i P_i R_i - \mathbf{1}\mathbf{c}_i^{\mathrm{T}}\|_F^2 \tag{13}$$

where each term of the sum represents the difference vector between 3D tie-points (S) and the back-projected 2D points (P_i) based on their estimated depths (Z_i) and the estimated image attitude and position ($R_i, \mathbf{c}_i$) of image i.

The objective function (13) is very similar to the objective function of GPA (4), modulo the substitution of the scalar ζ with the corresponding depth matrix Z. As a consequence, its solution, reported in Algorithm 2, is very similar to the GPA one, with the difference that the isotropic scale factor computation (Sect. 2.2) is substituted with the anisotropic scale formula borrowed from the AEOPA (Sect. 2.3). For this reason, the algorithm is called *Anisotropic Generalized Procrustes Analysis (AGPA)* (Fusiello and Crosilla 2016).

Algorithm 2 AGPA

Input: a set of 3D models $P_i \quad i = 1 \ldots m$
Output: translation $\mathbf{c}_i$, attitude R_i and scale Z_i of each model

1. Initialize $Z_i = I$ and $P_i^{'} = P_i \quad \forall i$
2. Compute centroid $\hat{S} = \frac{1}{m}\sum_{i=1}^{m} P_i'$
3. Register each model P_i to $\hat{S}$:
   (a) Compute $R_i = U\,\mathrm{diag}(1, 1, \det(UV^{\mathrm{T}}))V^{\mathrm{T}}$ with $UDV^{\mathrm{T}} = P_i^{\mathrm{T}} Z_i \left(I - \mathbf{1}\mathbf{1}^{\mathrm{T}}/n\right)\hat{S}$
   (b) Compute $\mathbf{c}_i = \left(\hat{S} - Z_i P_i R_i\right)^{\mathrm{T}} \mathbf{1}/n$
   (c) Compute $Z_i = (I \circ P_i P_i^{\mathrm{T}})^{-1}(P_i R_i(\hat{S}^{\mathrm{T}} - \mathbf{c}_i \mathbf{1}^{\mathrm{T}}) \circ I)$
   (d) Update $P_i^{'} = Z_i P_i R_i + \mathbf{1}\mathbf{c}_i^{\mathrm{T}}$
4. Iterate from step 2. until convergence of $\sum_{i=1}^{m} \|P_i' - \hat{S}\|_F^2$

In Fusiello and Crosilla (2015), both synthetic and real experiments aimed at assessing the accuracy of the *AGPA* algorithm were performed. For the synthetic case, $n = 96$ 3D tie-points were distributed on the scene, and in each of the $m = 16$ cameras, $p = 36$ points were visible. Increasing random noise with standard deviation $\sigma = \{0, 0.5, 1, 1.5, 2, 2.5, 3, 3.5\}$ [pixel] was added to image points coordinates and 25 trials for each noise level were averaged. In each trial first the Procrustean algorithm was run and then the photogrammetric bundle block adjustment, starting from the output of the former. The output of both methods were compared after a least-squares alignment with the ground-truth 3D points. Results reported in Fig. 1 (right) demonstrate that this new approach to bundle block adjustment based on AEOPA allows to obtain practically the same accuracy of the classical least squares solution, having the advantage of converging to the correct solution in most cases, with zero-information initialization. However, a theoretical proof of convergence is still unknown.

Furthermore, a robust version of the algorithm was introduced in Fusiello and Crosilla (2016). This new scheme, based on Iteratively Reweighted Least Squares (IRLS), achieves reliable results also in the presence of a percentage up to 10% of outliers.

4 Conclusions

Procrustes analysis was proved to be a useful tool to solve photogrammetric problems. Whereas classical OPA seeks transformations in 3D space, the anisotropic extension allows to deal with problems involving a projection to 2D space by introducing an auxiliary unknown, the depth of the points, which makes it possible to back-project 2D points into 3D space, thereby restoring the 3D problem. AEOPA leads to a least squares solution without any linearization of the original equations and it does not require any approximate value of the unknown parameters. Results obtained with Procrustean algorithms in Photogrammetry are comparable in terms of accuracy with those given by state-of-the-art methods.

References

Akca D (2003) Generalized procrustes analysis and its applications in photogrammetry. Internal Technical Report at the Institute of Geodesy and Photogrammetry—ETH, Zurich

Bennani Dosse M, Ten Berge J (2010) Anisotropic orthogonal procrustes analysis. J Classif 27(1):111–128

Commandeur JJF (1991) Matching configurations. DSWO Press

Crosilla F (1999) Procrustes analysis and geodetic sciences. In: Quo vadis geodesia?, vol 1. Department of Geodesy and GeoInformatics, University of Stuttgart, pp 69–78

Crosilla F, Beinat A (2002) Use of generalised procrustes analysis for the photogrammetric block adjustment by independent models. ISPRS J Photogramm Remote Sens 56(3):195–209

Fusiello A, Crosilla F (2015) Solving bundle block adjustment by generalized anisotropic procrustes analysis. ISPRS J Photogrammetry and Remote Sens 102:209–221. doi:10.1016/j.isprsjprs.2015.02.002

Fusiello A, Crosilla F (2016) Fast and resistant procrustean bundle adjustment. ISPRS Ann Photogramm Remote Sens Spat Inf Sci III-3:35–41. doi:10.5194/isprs-annals-III-3-35-2016

Fusiello A, Maset E, Crosilla F (2013) Reliable exterior orientation by a robust anisotropic orthogonal procrustes algorithm. In: Proceedings of the ISPRS workshop 3D-ARCH 2013: 3D virtual reconstruction and visualization of complex architectures, ISPRS Archives, vol XL-5/W1, pp 81–86

Fusiello A, Crosilla F, Malapelle F (2015) Procrustean point-line registration and the NPnP problem. In: International conference on 3D vision (3DV), 2015, IEEE, pp 250–255

Garro V, Crosilla F, Fusiello A (2012) Solving the pnp problem with anisotropic orthogonal procrustes analysis. In: Second Joint 3DIM/3DPVT conference: 3D imaging, modeling, processing, visualization and transmission

Gower J (1975) Generalized procrustes analysis. Psychometrika 40(1):33–51

Schönemann P, Carroll R (1970) Fitting one matrix to another under choice of a central dilation and a rigid motion. Psychometrika 35(2):245–255

Towards Surveying with a Smartphone

Francesca Fissore, Andrea Masiero, Marco Piragnolo, Francesco Pirotti, Alberto Guarnieri and Antonio Vettore

Abstract Photogrammetry is one of the most used techniques for monitoring and surveying. It is widely used in several applications and in different working conditions. Accuracy of photogrammetry reconstruction methods may change depending on the working conditions (e.g. the number of acquired images, lighting conditions, baselines between images), and it is strictly related to the success of the solution of the Structure from Motion problem. Despite its widely spread use and the ever growing improvements to the reconstruction technique, photogrammetry still does not reach the same level of reliability of laser scanning surveying techniques: significant issues may occur in photogrammetric reconstructions when in presence of lighting problems or when the object of interest is not sufficiently textured. However, it relies on the use of much cheaper tools with respect to laser scanning techniques and surveying is usually much faster. This paper aims at showing the potential improvement that can be obtained by introducing information provided by the navigation system in the 3D reconstruction algorithm: the goal is that of making the solution algorithm of the Structure from Motion problem more reliable and accurate. As a side effect, faster reconstruction is typically achieved. The technique is validated on a building using images and navigation information got from a standard smartphone.

F. Fissore (✉) · A. Masiero · M. Piragnolo · F. Pirotti · A. Guarnieri · A. Vettore
Interdepartmental Research Center of Geomatics (CIRGEO), University of Padova,
Viale Dell'Università 16, 35020 Legnaro, PD, Italy
e-mail: fissorefrancesca@gmail.com

A. Masiero
e-mail: masiero@dei.unipd.it

M. Piragnolo
e-mail: marco.piragnolo@unipd.it

F. Pirotti
e-mail: francesco.pirotti@unipd.it

A. Guarnieri
e-mail: alberto.guarnieri@unipd.it

A. Vettore
e-mail: antonio.vettore@unipd.it

R. Cefalo et al. (eds.), *New Advanced GNSS and 3D Spatial Techniques*,
Lecture Notes in Geoinformation and Cartography,
DOI 10.1007/978-3-319-56218-6_13

Keywords Photogrammetry · Monitoring · Surveying · SfM · Smartphone feature descriptor · Matching

1 Introduction

Given the number of natural disasters occurred worldwide in the last decades, the interest for a quick spatial data acquisition system, easy to use and available at low cost is constantly increasingly (Pirotti et al. 2015): the availability of such data can be of interest in order to help the management of such difficult conditions and other several applications (Prosdocimi et al. 2015).

Despite professional devices already available on the market allow to acquire accurate and high resolution spatial descriptions of areas of interest (e.g. terrestrial laser scanning, LiDAR, digital photogrammetry), such devices are typically quite expensive and require a good expertise in order to use them.

This work aims at introducing information provided by a positioning system in the photogrammetric reconstruction. The net effect is that of easing the computation of correspondences in images, in particular when taken by quite different points of view: this way, the probability of occurring in matching errors is significantly reduced, hence easing the use of the system to non-professional users.

Furthermore, while other survey systems are based on the use of expensive devices, this system can be used on a standard smartphone, hence enabling its use to a wide number of users: minimum requirements are the presence of sensors enabling navigation (in order to allow the estimation of device position changes, as shown in Sect. 2) and an embedded camera. It is worth to notice that in order to have quick spatial data acquisition (for instance to facilitate disaster management), several works consider the use of Unmanned Aerial Vehicles (UAVs) (Bendea et al. 2008): despite this field is very interesting, this paper will not deal with it, focusing on smartphone acquisitions only.

Photogrammetric 3D reconstruction with smartphones is a problem that has already been considered in the literature and in certain commercial programs (e.g. Autodesk 123D Catch). However, differently from Autodesk 123D Catch, the integration of navigation information in the reconstruction allows to provide directly a metric reconstruction, without the need of control ground points (which, nevertheless, can be useful to improve the obtained results).

Recently developed photogrammetric reconstruction programs, based on the Structure from Motion approach (SfM, Agarwal et al. 2010), can take advantage from navigation information as well: since commonly used feature descriptors can lead to wrong matches in certain conditions (e.g. when dealing with quite different points of view), several works have been considered in the literature in order to improve feature matching performance [in particular with respect to scale-invariant feature transform (SIFT, Lowe 1999)], in terms of matching ability [e.g. ASIFT (Morel and Yu 2009), A^2SIFT (Lingua 2009)] and speed (SURF, BRICK. FREAK, Bay et al. 2008; Leutenegger et al. 2011; Alahi et al. 2012).

2 Positioning

Positioning system considered here is based on a pedestrian dead reckoning-like approach, being an evolution of that presented in (Masiero et al. 2014): the aim of such system is that of allowing positioning also when GNSS signal (Barbarella et al. 2011; Cefalo et al. 2011) is not available. The rationale is that of combining the use of different sensors embedded in the smartphone (i.e. accelerometer, gyroscope, magnetometer) in order to detect human steps and moving direction (Saeedi et al. 2014): the combined use of these estimates clearly allows to update planar device position with respect to its previous value (this is firstly done considering only 2D positioning):

$$\begin{bmatrix} u_{t+1} \\ v_{t+1} \end{bmatrix} = \begin{bmatrix} u_t \\ v_t \end{bmatrix} + s_t \begin{bmatrix} \sin \alpha_t \\ \cos \alpha_t \end{bmatrix} \tag{1}$$

where (u_t, v_t) is the 2D (planar) position of the device (e.g. smartphone), expressed with respect to the North and East directions (i.e. global reference system), before the t-th step, s_t is the length of the t-th step, and α_t is the corresponding heading direction. Notice that an estimation of the initial position is assumed to be a priori available.

Smartphone is supposed to be carried by the user's hand and the heading direction is assumed to be *approximately* fixed with respect to the local coordinate system: tracking system is designed to estimate and correct device attitude changes, with absolute value lower than 36 degrees, with respect to the conventional orientation. Then, tracking device position is obtained by means of non-linear particle filtering (Masiero et al. 2014): this choice allows to deal with system nonlinearities and with external constraints (e.g. geometric constraints provided by prior knowledge of the environment, such as a building map in indoor navigation). Particle filtering is usually a computational demanding kind of estimation procedure: however, interestingly, the considered particle filtering approach has been shown to work with a relatively small number of particles (e.g. few hundreds), hence enabling real-time tracking.

Barometer measurements are used in the altitude estimation: to facilitate the model parameter learning problem and to make the update of parameter values efficiently adaptive with respect to working conditions, altitude variations are modeled as linearly dependent on pressure variations, i.e.

$$w_{t+1} = w_0 + a(p_{t+1} - p_0) \tag{2}$$

where the device altitude w_{t+1} is expressed as the sum of the initial altitude w_0 (assumed to be known) with a term dependent on the pressure variation $(p_{t+1} - p_0)$ scaled by a factor a. Above Eq. (2) can be integrated in (1) and, furthermore, temporal dynamic of altitude variations can be used in order to make altitude estimation more robust.

3 Matching

This section considers the feature matching problem. Automatically finding corresponding points in different images is the basic step for reconstructing camera and 3D points relative positions (Heyden and Pollefeys 2005): automation in this process is probably the most relevant characteristic in SfM approaches with respect to classical photogrammetry.

Automatic feature matching is based on the characterization of feature points by means of descriptors summarizing the appearance of the regions in the neighborhood of the considered points (e.g. SIFT, Lowe 1999): hypothetical matches are computed by means of similarity considerations between descriptors of different images (Lowe 1999). Similarity is typically measured in terms of distance between descriptor vectors (e.g. Euclidean distance between normalized vectors): furthermore, in order to increase the matching reliability, a match between feature point i and j is usually considered only if the fraction of the distance (i.e. *distance ratio criterion*) between their descriptor vectors and any other distance between i and another feature point is lower than a threshold (e.g. 0.6). An analogous requirement can be requested for j as well.

Appearance-based matching procedures typically generate a certain number of wrong matches, which is an undesirable working condition: wrongly matched features negatively affect the estimation of camera and 3D points values. To reduce the number of wrong matches, epipolar geometry is estimated and then exploited to discard outliers: RANdom SAmple Consensus (RANSAC, Chum et al. 2003) is used to determine an estimate of the Fundamental matrix [or the epipolar matrix, when considering calibrated camera case (Brown 1971; Fraser 1997; Habib et al. 2003; Fusiello and Irsara 2011; Balletti et al. 2014)] which summarizes the geometric relation between two views, then point matches that are not sufficiently well described by the estimated Fundamental matrix are discarded.

Then, several approaches have been proposed in the literature to make feature matching even more robust in difficult working conditions (e.g. when dealing with significant point of view changes, when considering repetitive structures), e.g. alternative feature descriptors (e.g. ASIFT, A^2SIFT, see also González-Aguilera et al. 2016) and other information on the scene (Kurz et al. 2011; Troiani et al. 2014; Masiero and Vettore 2016) can be considered.

Similarly to Kurz et al. (2011), Troiani et al. (2014), Masiero and Vettore (2016) this work introduces information on camera orientation provided by the navigation system in the matching procedure: this change allows to reduce the number of wrong matches while avoiding excessive increase of the computational burden (Sect. 4).

Estimation procedure is based on a two-step RANSAC-like algorithm. Camera is assumed to be calibrated, where an essential matrix estimation and outlier rejection are obtained by means of a RANSAC-like procedure. As shown in Algorithm 1, an initial estimate of the essential matrix is obtained in the outer for loop by using just two point correspondences per time (by using device orientation information

provided by the navigation system), whereas the inner for loop is used to improve the initial estimation by using 5-point essential matrix estimation algorithm (Nistér 2004). N and N_2, used in Algorithm 1, are chosen in order to ensure a sufficiently large probability of estimating the correct model (Chum et al. 2003).

Algorithm 1

for i = 1:N
randomly select two feature matches
estimate essential matrix two-point algorithm
calculate inliers
if number of inliers is greater than previous maximum number
for j = 1:N_2
randomly select three feature matches
estimate essential matrix five-point algorithm
calculate inliers
update best model *if* needed
end
end
end

Furthermore, since the system considered here is designed to be as fast as possible, a comparison of performance changes is considered within the matching procedure proposed in Masiero and Vettore (2016) when dealing with different feature descriptors: indeed, a number of different feature descriptors (e.g. SURF, BRISK and FREAK) have been proposed in the recent years, with the main aim of reducing the computational complexity related to the use of SIFT while ensuring similar matching performance, if possible. Actually, SIFT descriptors are still widely used in the photogrammetry community, but when dealing with (almost) real-time applications or with low computational power (or the need of reducing power consumption, e.g. in mobile devices) the use of computationally more convenient solutions can be quite attractive. Results of this comparison on a specific case study are shown in Sect. 4.

4 Results

This section presents the results obtained with the proposed system in terms of positioning (Sect. 2) and feature matching (Sect. 3) performance.

4.1 Positioning

Experiments on the positioning system have been conducted on three floors of a university building, and in order to make the results statistically more robust, experimental data have been collected by three volunteers, two men and one woman, with heights from 1.65 to 1.85 m, each of them walking for a ten minute walk involving significant changes of altitude: variation of altitude estimation has been tested for range of considered altitudes of approximately 5 m. Building characteristics (e.g. floor altitudes) are assumed to be available to the navigation system (2D spatial positioning as in (1) is integrated with geometric information on the building and low cost barometer measurements), which exploits them to improve positioning performance:

- average altitude estimation error is 0.2 m.
- 20% positioning error reduction with respect to Masiero et al. (2014) (estimation uncertainty is larger when moving on stairs: such uncertainty can be reduced when estimates of variation altitude are available).

4.2 Feature Matching

Efficiency of Algorithm 1 is tested from an estimation accuracy point of view, and then comparing computational burden and percent of correctly matched features for different feature descriptors.

First, effectiveness of Algorithm 1 is tested on its ability in estimating the essential matrix: the goal is that of reducing the sensibility of 2-point essential matrix estimation algorithm (Troiani et al. 2014) and the computational burden of 5-point algorithm for realistic values of the measurement noise (in particular noise on orientation measurement, which is critical for the efficiency of IMU (Inertial Measurement Unit) based algorithms for estimating the essential matrix). Table 1 reports the average accuracy (Frobenius norm of the difference between estimated and correct essential matrix) results on 100 independent Monte Carlo simulations, varying the orientation measurement noise (lowest noise measurement level, σ_0, has been set to the value experimentally measured on Google Nexus 5).

Table 1 Accuracy of the algorithms for estimating the essential matrix varying the magnetometer measurement noise

Noise level	2-point algorithm	5-point algorithm	Algorithm 1
σ_0	0.22	0.33	0.26
$2\ \sigma_0$	0.21	0.18	0.15
$3\ \sigma_0$	0.41	0.15	0.18

Computational burden depends on the probability of finding feature correct matches, being usually significantly smaller for Algorithm 1 than for 5-point algorithm.

Then, comparison of matching performance of different feature descriptors is investigated in the case of 3D reconstruction of a building, which is a clear case of interest in the surveying field (Fig. 1 shows two sample images of the testbed image set). Image samples have been acquired by using a Google Nexus 5, with focus distance set to infinite.

Feature locations have been obtained by using Harris operator and extracting positions of local extrema. Then, descriptors have been computed on the same locations for all the considered alternatives.

First, matches obtained with distance ratio criterion are initially considered: percent of correct matches is reported in Table 2: rows in Table 2 reports:

- number of correct feature matches with respect to the number of detected feature points (both matched and unmatched),
- number of correct matches with respect to the number of features matched (both correctly and incorrectly) by the approach.

Since the number of features matched by the distance ratio criterion changes significantly depending on the considered descriptor type, then first and second row in Table 2 show two different aspects of the descriptor performance. As expected,

Fig. 1 Example of two test images (Pentagono building, University of Padova)

Table 2 Average percent of correctly matched features with respect either to the total number of features or to the number of matched ones

	SURF [%]	BRICK [%]	FREAK [%]	SIFT [%]
w.r.to number of features	6.3	6.3	2.3	11.0
w.r.to matched features	85.8	98.4	85.6	98.9

computational burden can be reduced considering alternative descriptors to the SIFT: computational times for computing descriptors and matches with SURF, BRICK and FREAK are 52, 46, and 53% of the time required by SIFT [results are obtained on two images of the considered data set (slightly different results can be obtained changing images, hardware and software implementations, but without affecting overall conclusions on the methods)].

The effect of different descriptor choices is evaluated also on the average uncertainty (e.g. standard deviation) on fundamental matrix estimated by feature matches (similar results can be obtained on the essential matrix, if camera is calibrated), which shall be used both to reject feature match outliers and to compute initial external camera parameter values for bundle adjustment optimization. Table 3 shows the estimated uncertainties for the considered descriptors.

Then, Table 4 shows matching performance of the same descriptors when considering the same number of matches for each descriptor type (i.e. 200 matches).

5 Discussion and Conclusions

The integration of barometer measurements in the navigation system is a viable way in order to provide altitude estimation and reduce indoor positioning accuracy [20% error reduction, approximately, with respect to Masiero et al. (2014)]: in particular, the latter is achieved by reducing positioning error when moving from a floor to another.

Algorithm 1 allows to reduce estimation error of the essential matrix when noisy measurements are provided from the navigation system: this allows to improve feature matching (in terms either of estimation quality or computational time) and outlier rejection procedures. Table 1 shows that the proposed approach is effective when magnetometer measurement noise is intermediate, whereas for very low or very high levels of noise 2-point or 5-point algorithm, respectively, work better. This is actually coherent with intuition:

- when a very good orientation estimate is available (low noise level) it can be proficiently used directly, this however is quite risky because it is not possible to know a priori whether a measurement is good or not,
- when available device orientation estimate is really very poor, its use does not improve significantly performance with respect to RANSAC-based 5-point estimation,

Table 3 Average percent error on the value of the largest component in the fundamental matrix

SURF [%]	BRICK [%]	FREAK [%]	SIFT [%]
25.3	13.7	21.0	6.7

Table 4 Average percent of correctly matched features (among 200 matches)

SURF [%]	BRICK [%]	FREAK [%]	SIFT [%]
90.1	96.9	76.2	99.6

– in all other cases the proposed algorithm can be used to improve system performance.

In agreement with the results shown in Sect. 4 on feature matching performance of different descriptors (Table 2, 3 and 4), SIFT has shown to have optimal (or close to optimal) performance in all the considered criterions with the exception of the computational burden, where it is the slowest. BRICK is very efficient in terms of percent of correctly matched features with respect to hypothetical matches determined by feature appearance only (see Table 2). In our examples, BRICK shows also a small uncertainty in the estimated fundamental matrix (Table 3). SURF and FREAK show similar matching performance with respect to matches determined by feature appearance only (Table 2), however SURF performs better than FREAK in the considered example when dealing with just a fixed number of matches (e.g. best 200 feature matches, Table 4): this is probably due to the lowest number of hypothetical feature matches provided by FREAK (number of feature matches provided by FREAK is sometimes smaller than 200, hence in order to have 200 hypothetical matches the matching threshold has to be less restrictive, causing an increase of wrong appearance based matches in Table 4 with respect to Table 2).

To conclude, the use of descriptors computationally more efficient with respect to SIFT can be interesting for real-time applications: among the considered descriptors, BRICK is particularly interesting in terms of percent of correctly matched features (comparable to SIFT). Despite the percent of correctly matched features of all the considered descriptors is usually quite high, SIFT is still better in terms of total number of correct matches and of uncertainty in the estimated fundamental matrix.

References

Agarwal S, Snavely N, Seitz S, Szeliski R (2010) Bundle adjustment in the large. In: European conference on computer vision (Lecture notes in computer science), vol 6312, pp 29–42

Alahi A, Ortiz R, Vandergheynst P (2012) Freak: Fast retina keypoint. In: 2012 IEEE conference on computer vision and pattern548 recognition (CVPR). IEEE, New York, 2012, pp 510–517

Balletti C, Guerra F, Tsioukas V, Vernier P (2014) Calibration of action cameras for photogrammetric purposes. Sensors 14:17471–17490

Barbarella M, Gandolfi S, Meffe A, Burchi A (2011) Improvement of an MMS trajectory, in presence of GPS outage, using virtual positions. In: ION GNSS 24th international technical meeting of the satellite division, pp 1012–1018

Bay H, Ess A, Tuytelaars T, VanGool L (2008) Speeded-up robust features (SURF). Comput Vis Image Underst 110:346–359

Bendea H, Boccardo P, Dequal S, Giulio Tonolo F, Marenchino D, Piras M (2008) Low cost UAV for post-disaster assessment. Int Arch Photogramm Remote Sens Spatial Inf Sci 37(Part B): 1373–1379

Brown D (1971) Close-range camera calibration. Photogramm Eng 37:855–866

Cefalo R, Cociancich A, Di Bartolomeo M, Ferro F, Iansig M, Manzoni G, Montagner G (2011) Integrated topographic, GNSS, remote sensing and GIS/WebGIS techniques applied to the study of Aquileia river port structures. In: The new technologies for Aquileia

Chum O, Matas J, Kittler J (2003) Locally optimized RANSAC. In: Pattern recognition. Springer, Berlin, pp 236–243

Fraser CS (1997) Digital camera self-calibration. ISPRS J Photogramm Remote Sens 52:149–159

Fusiello A, Irsara L (2011) Quasi-Euclidean epipolar rectification of uncalibrated images. Mach Vision Appl 22:663–670

González-Aguilera D, López-Fernández L, Rodriguez-Gonzalvez P, Guerrero D, Hernandez-Lopez D, Remondino F et al (2016) Development of an all-purpose free photogrammetric tool. ISPRS-Int Arch Photogramm Remote Sens Spatial Inf Sci, 31–38

Habib A, Morgan M (2003) Automatic calibration of low-cost digital cameras. Opt Eng 42: 948–955

Heyden A, Pollefeys M (2005) Multiple view geometry. In: Medioni G, Kang SB (eds) Emerging topics in computer vision. Prentice Hall

Kurz D, Benhimane S (2011) Gravity-aware handheld augmented reality. In: 2011 10th IEEE international symposium on mixed and augmented reality (ISMAR). IEEE, New York, pp 111–120

Leutenegger S, Chli M, Siegwart RY (2011) BRISK: Binary robust invariant scalable keypoints. In: International conference on computer vision, 2548–2555

Lingua A, Marenchino D, Nex F (2009) Performance analysis of the SIFT operator for automatic feature extraction and matching in photogrammetric applications. Sensors 9(5):3745–3766

Lowe D (1999) Object recognition from local scale-invariant features. In: IEEE international conference on computer vision, vol 2, pp 1150–1157

Masiero A, Vettore A (2016) Improved feature matching for mobile devices with IMU. Sensors 16 (8):1243

Masiero A, Guarnieri A, Pirotti F, Vettore A (2014) A particle filter for smartphone-based indoor pedestrian navigation. Micromachines 5(4):1012–1033

Morel J, Yu G (2009) ASIFT: a new framework for fully affine invariant image comparison. SIAM J Imaging Sci 2:438–469

Nistér D (2004) An efficient solution to the five-point relative pose problem. IEEE Trans Pattern Anal Mach Intell 26:756–770

Pirotti F, Guarnieri A, Masiero A, Vettore A (2015) Preface to the special issue: the role of geomatics in hydrogeological risk. Geomat Nat Hazards Risk 6(5–7):357–361

Prosdocimi M, Calligaro S, Sofia G, Dalla Fontana G, Tarolli P (2015) Bank erosion in agricultural drainage networks: new challenges from structure-from-motion photogrammetry for post-event analysis. Earth Surf Proc Land 40:1891–1906

Saeedi S, Moussa A, El-Sheimy N (2014) Context-aware personal navigation using embedded sensor fusion in smartphones. Sensors 14(4):5742–5767

Troiani C, Martinelli A, Laugier C, Scaramuzza D (2014) 2-point-based outlier rejection for camera-IMU systems with applications to micro aerial vehicles. In: 2014 IEEE international conference on robotics and automation (ICRA), pp 5530–5536

Evaluation of 3D Reconstruction Accuracy in the Case of Stereo Camera-Pose Configuration

Xuan Zhang, Gang Qiao and Marco Scaioni

Abstract This paper presents an empirical methodology to assess the quality of camera calibration and to check out the effects of image geometry in 3D photogrammetric reconstruction. The proposed methodology is applied to the simple stereo-pair configuration, but it is also suitable to be extended to larger image block geometries. The basic concept consists in the empirical evaluation of potential effects of biases in camera calibration within the use of a 3D test field. The multiple repetition of the standard camera calibration procedure in order to provide a sample of parameter values to be averaged, is demonstrated to guarantee a better determination of the whole set of calibration parameters. It is also demonstrated that, as the background theory supports, a longer baseline and a small convergence angle between camera stations may furnish the best results in term of accuracy.

Keywords Close-range photogrammetry · Camera calibration · Quality assessment · Accuracy · Stereo configuration

1 Introduction

In Computer Vision and Photogrammetry the fundamental aim is to reconstruct 3D coordinates of features from their projections on digital photos. To achieve this result, suitable configurations for camera stations are adopted, depending on the specific application, on the size of the targeted object, and the accuracy required. The effectiveness of a configuration depends on the intersection angle between rays projecting corresponding points and the average image scale.

X. Zhang · G. Qiao · M. Scaioni (✉)
College of Surveying and Geo-Informatics, Tongji University,
Shanghai, People's Republic of China
e-mail: marco.scaioni@polimi.it

M. Scaioni
Department of Architecture, Built Environment and Construction
Engineering (DABC), Politecnico Milano, Milan, Italy

R. Cefalo et al. (eds.), *New Advanced GNSS and 3D Spatial Techniques*,
Lecture Notes in Geoinformation and Cartography,
DOI 10.1007/978-3-319-56218-6_14

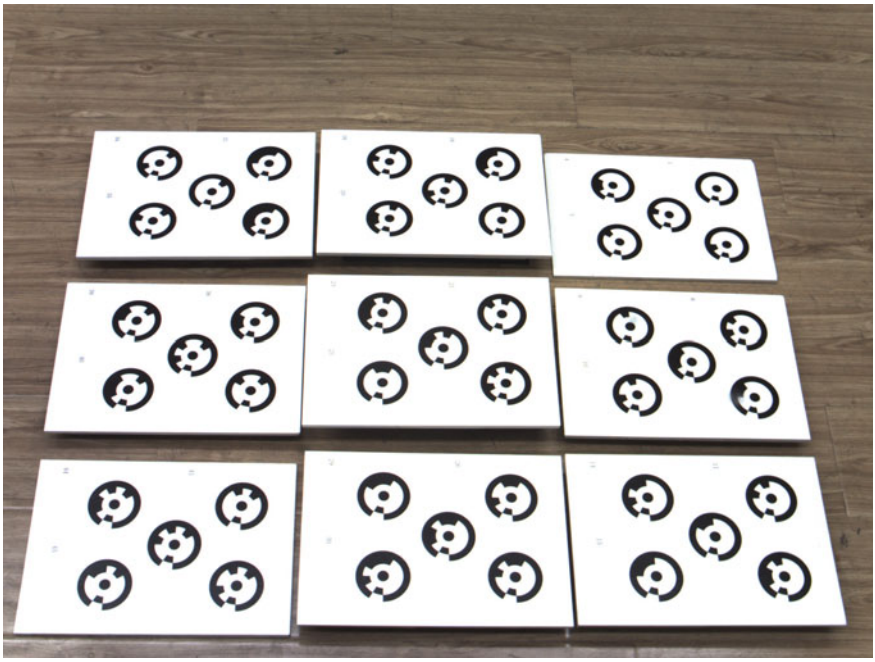

Fig. 1 Calibration panels adopted in the experiment; panels have been placed at different eights from the ground to improve the calibration geometry

The basic camera-pose configuration is made up of two overlapped images, which depict the object from two different perspectives. Such a case, frequently addressed to as *stereo* framework, represents the minimum configuration to obtain 3D coordinates from 2D images (Hartley and Zisserman 2004). This approach is widely used when the reconstruction process has to be used for automatic guiding of moving machines (as in Robot Vision), when the object to observe is moving (like in industrial manufacturing control or in laboratory experiments—see, e.g., Feng et al. 2016), or when a device for the *stereoscopic vision* has to be applied, like in the standard mapping process adopted within the aerial photogrammetric pipeline (Kraus 2008). Generally, the stereo-pair is captured by using two cameras or by moving one camera on two different positions. Generally, camera axes are shifted along a direction parallel to one of both sides of the sensing frame. In such a case, the optical axes result to be parallel between them (in photogrammetry such geometry is referred to as *normal* or *nadiral* configuration, see Kraus 2008). Very often, the optical axes are convergent (see Fig. 1). With this modified geometry, a more homogeneous precision of 3D point reconstruction can be obtained (Fraser 1996).

The stereo configuration has two main advantages. First of all, a minimum number of sensors are involved: two in the case the camera stations have to be kept stable, or even only one in the case the camera is moving (as in aerial photogrammetry missions). Secondly, the 3D reconstruction process basically goes

through the identification of corresponding features between both images, limiting the burden of computing operations. This property makes the stereo case highly competitive in real-time applications, where the automation of this process is required (Hartmann et al. 2016). On the other hand, the stereo configuration suffers from the small redundancy of the observations that makes more difficult the identification of outliers in the observed set of corresponding points (Barazzetti et al. 2011a). In practice, the high risk of errors is compensated for with the use of a large number of features and with the application of robust techniques for estimating those parameters governing the relative geometry of both images (usually called *relative orientation*), see Roncella and Forlani (2015).

In order to enforce the observations' redundancy, other small configurations are used, which are made up of three (*trinocular vision*) and four images, respectively. All images cover a common area where the object to reconstruct is placed. Of course, these frameworks require a more involved camera system, unless the same camera is used at different stations. Anyway, such a solution cannot be pursued in real-time applications or when the object is not stable. The relative positions of camera stations can be based on a strip geometry where the camera axes lie on the same plane, or on a convergent geometry where camera axes do not belong to the same plane. The second solution generally results in a more stable geometry for the detection of errors in the set of corresponding points, which now should be visible on three or four images. Moreover, the convergent geometry also provides more homogeneity in the coordinate precision of 3D points.

Of course, when the object to reconstruct is larger, blocks made up of more numerous photos are used. In such a case, the camera-pose structure cannot be classified into one of the basic configurations, but first the block *external orientation* is computed using *bundle block adjustment* (Triggs et al. 2000), then the object is modelled using some subsets that depict sub-regions of the entire targeted object (see Luhmann et al. 2014). For example, in standard projects of aerial photogrammetry, several stereo-pairs are organized into almost regular strips of overlapping photos, see Kraus (2008). In a similar way, in the popular *Structure from Motion* (SfM) approach (Snavely et al. 2008) a camera is shifted to sequentially collect a sequence of photos that overlap within small subsets of three or four subsequent images.

In the literature less attention has been paid to the estimation of the accuracy that can be achieved from different basic camera-pose frameworks, especially in the Computer Vision community. Owing to this reason, this paper would like to give to the readers an empirical evaluation of the accuracy that can be obtained from the stereo-pair configuration depending on two factors: (1) the influence of camera calibration, and (2) the relative camera poses. This aim is obtained through the repetition of some photogrammetric projects where some reference sets of 3D check points are reconstructed, whose coordinates have been independently measured. By comparing the coordinates of these check points with respect to the reference coordinates when using different configurations, the effects on the accuracy can be determined.

2 Influence of Camera Calibrations Parameters

Camera calibration is an important part for precise 3D points determination and further 3D reconstruction. This topic is largely documented in the literature, whose state-of-the-art has been recently reviewed by Luhmann et al. (2016).

In analogue airborne cameras and in old terrestrial metric or semi-metric cameras a simplified camera calibration model was used, whose parameters consisted of the principal distance (c), the principal point (PP) coordinates (x_0, y_0), and an empirical function to model radial distortion. In addition, the fiducial marks or the "repères" coordinates were adopted to define the *photo coordinate* system and to compensate for film deformations. In such a case, calibration parameters were directly determined in special laboratories using photo-goniometers (Kraus 2008).

In the last two decades, the calibration of non-photogrammetric cameras for metric applications has become widely popular under the impulse given by the spreading of digital sensors. Generally, new models for calibration of generic cameras became quite popular in both Photogrammetry and Computer Vision. These models can compensate for other types of distortions that cannot be neglected in non-photogrammetric cameras, such as decentering and affine distortions.

Generally, today in photogrammetry the *Brown's model* (Brown 1971) is widely adopted either for terrestrial cameras applied in Close-range and UAV (Unmanned Aerial Vehicle), or in multiple cameras integrated in airborne digital sensors. In Brown's model the corrections ($\Delta x, \Delta y$) to the image coordinates of a generic point can be expressed as:

$$\Delta x = (x - x_0)\left(K_1 r^2 + K_2 r^4\right) + P_1\left(r^2 + 2(x - x_0)^2\right) + 2P_2(x - x_0)(y - y_0)$$

$$\Delta y = (y - y_0)\left(K_1 r^2 + K_2 r^4\right) + P_2\left(r^2 + 2(y - y_0)^2\right) + 2P_1(x - x_0)(y - y_0)$$

where:

(x, y)	are the image coordinates of a generic point;
K_1, K_2	are the radial distortion parameters;
P_1 P_2	are the decentering distortion parameters;
r	is the radial distance, $r = \sqrt{(x - x_0)^2 + (y - y_0)^2}$

In the common practice, the calibration parameters of a camera may be determined using two different approaches. In the first one, an independent sensor calibration is operated by acquiring a specific block of images targeting a set of control points. Images are then contemporarily oriented using a bundle block adjustment (BBA) including calibration parameters as additional unknowns. In such a case, a set of ground control points (GCP) with already know coordinates can be used (*field calibration*), or targets may be used as tie points in BBA. In the second approach, targets may be also avoided using *targetless* calibration, as proposed in Barazzetti et al. (2011b). Independent calibration has the advantage to be operated using a

camera geometry very suitable for this task, disregarding the camera pose to be adopted afterwards in the reconstruction projects. The alternative to this method is to compute calibration parameters together within the same BBA adopted for 3D reconstruction (*self calibration*). Of course, the block should feature a suitable geometry for calibration as well (see Luhmann et al. 2016). This solution has become today quite popular because of the diffusion of low-cost fully automatic photogrammetric software packages.

Disregarding the method used for computing camera calibration parameters, these are usually assumed as error-free quantities to be used as constant values in photogrammetric projects. In general, this assumption may not be guaranteed, since their estimate through a BBA involved an uncertainty which then propagate to the accuracy of final 3D point determination. The question posed here is how much the uncertainty of calibration parameters may affect such an accuracy? In order to answer to this question, a set of experiments has been designed and illustrated in next Sect. 2.1.

2.1 Experiment to Assess the Influence of Each Individual Calibration Parameter

In order to assess the influence of any individual calibration parameters, some experiments have been done using an industrial camera CGU-500C CGimagetech (CMOS sensor with 2592 × 1944 pixels, pixel size 2.3 μm) equipped with an 8 mm lens. PhotoModeler Scanner 2013 software has been used (www.photomodeler.com) to compute camera calibration. Nine calibration panels reporting five coded targets each are provided with this photogrammetric software package (see Fig. 1). These targets could be automatically recognized, measured and labelled in the images, to be used as tie points in BBA. According to a common best practice calibration procedure, images have been captured from 4 stations. From each of them, one image in landscape orientation and two rolled images after clockwise and anticlockwise 90° rotations have been recorded. This strategy led to a total number of 12 images per each calibration run. Five calibration run have been repeated under the same conditions, providing five sets of calibration parameters (see Table 1).

To analyze the variability of each parameter, we considered first the mean values of the different repetitions. Table 1 shows the best estimates of the parameter values. Then we considered the values featuring the maximum bias w.r.t. the mean values and we compared them to the standard deviations. For all parameters, absolute largest errors are included in 2σ interval around the mean. If the estimated values are normally distributed, this interval is expected to host approximately 95% of occurrences.

Since in the common photogrammetric practice the calibration is normally computed only once, such worst cases may happen without any chance to be detected. While Table 1 shows how much may be the variability of parameter deviations within diverse repetitions of the calibration procedure, the effect that

Table 1 Estimated camera calibration parameters after five different independent repetitions (the same symbols adopted in Sect. 2 are used here)

	c (mm)	x_P (mm)	y_P (mm)	K_1 (mm^{-2})	K_2 (mm^{-4})	P_1 (mm^{-1})	P_2 (mm^{-1})
1	8.688	2.943	2.426	1.613E-03	−3.113E-05	−6.000E-05	3.724E-05
2	8.696	2.958	2.441	1.603E-03	−3.341E-05	−5.449E-05	1.129E-04
3	8.708	2.958	2.444	1.580E-03	−2.684E-05	−5.457E-05	5.955E-05
4	8.708	2.955	2.445	1.597E-03	−3.159E-05	−5.674E-05	7.540E-05
5	8.704	2.961	2.443	1.632E-03	−3.303E-05	−5.420E-05	8.502E-05
Mean values	8.701	2.955	2.440	1.605E-03	−3.120E-05	−5.600E-05	7.402E-05
Std.dev.	0.0074	0.0063	0.0069	1.724E-05	2.341E-06	2.196E-06	2.529E-05
Absolute largest deviations	0.0126	0.0123	0.0136	2.700E-05	4.360E-06	−4.000E-06	3.888E-05

such deviations may have on the final determination of 3D coordinates in a stereo-pair is evaluated using a test-field of 33 coded targets put on three planar boards at different depth from the camera (Fig. 2). Reference values of such control points have been measured by using a theodolite. Precision of any single reference coordinate is supposed to be approximately ±2 mm.

Just after the calibration runs have been completed, a stereo-pair with 1.5 m-long baseline has been collected from a 3.2 m distance. The conditions are the same as during calibrations, so that we may assume that the same real deformations happened in the images. After reconstruction of relative orientation using the target coordinates on the stereo images, 3D point coordinates have been derived in an arbitrary reference system. In a next step, such 3D coordinates have been transformed into the reference system of the reference framework. Eventually, residuals have been analyzed. Root Mean Square Errors (RMSE) of residuals are reported in Table 2. This procedure has been repeated seven times, each of them using a different calibration set, as described in Table 2. The basic set is composed by the "mean values" of different calibrations, which are shown in Table 1. In the following rows, RMSE's obtained with the same basic set but replacing at any time the "mean value" of one parameter with its largest deviation are shown.

In the first row of Table 2, RMSE of residuals when using the mean calibration values of all parameters follow the behavior that can be predicted using formulas for computing the theoretical precision of the normal case, see Kraus (2008). Table 2 shows that errors in the determination of principal distance and PP can be completely compensated by the use of control points. In fact, these help correct the global scaling due to changes of c, and shifts due to changes of x_P and y_P.

This is what typically happens in BBA, where the positions of photos may be slightly modified to account for inner orientation errors.[1] On the other hand, the effect of errors in symmetric radial distortion parameters (K_1, K_2) are bigger than

[1]The group of calibration parameters including c, x_P and y_P are often referred to as *inner orientation* (Kraus 2008).

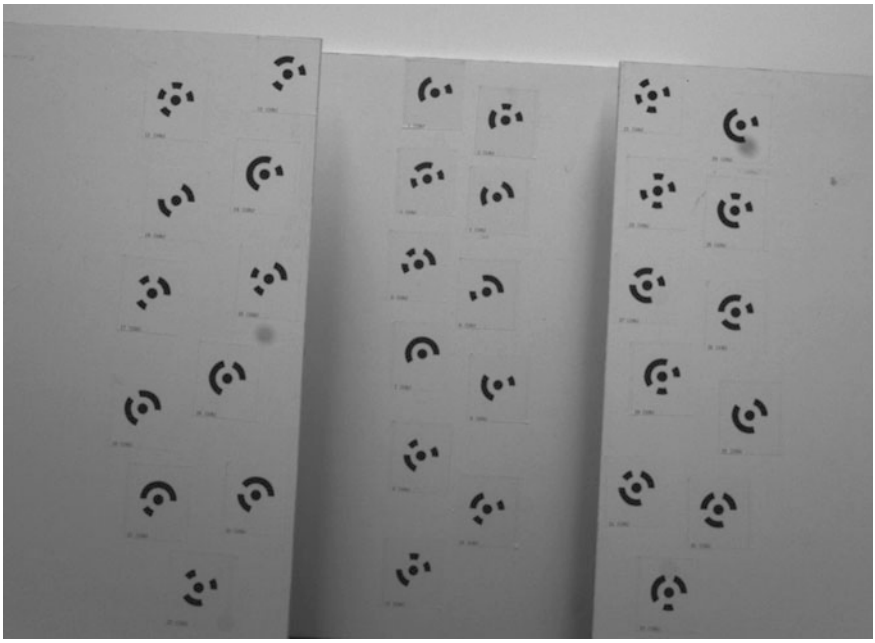

Fig. 2 The reference framework adopted to check out the effects of calibration's largest errors

Table 2 The influence of largest deviations of camera parameters

	RMSE ΔX (mm)	RMSE ΔY (mm)	RMSE ΔZ (mm)	RMSE 3D (mm)
Mean values	0.34	0.33	0.89	1.01
Replace c	0.34	0.33	0.82	0.95
Replace (x_P, y_P)	0.37	0.35	0.85	0.99
Replace K_1	0.36	0.38	1.18	1.29
Replace K_2	0.37	0.41	1.33	1.44
Replace P_1	0.35	0.33	0.89	1.01
Replace P_2	0.38	0.34	0.89	1.03

others, resulting in average biases up to approximately 30 and 45%. Then the influence of radial distortion parameters is quite significant. In many applications of camera calibration, people use only the first term K_1 for modelling symmetric radial distortion. But through our experiment, we found that the influence of K_2 may be also significant. Moreover, the major effects can be found on depth direction. Eventually, the effect of errors in decentering distortion parameters (P_1, P_2) are negligible.

Attention should be paid to the possible presence of high correlations (e.g., when$|\rho| > 0.95$) between estimated calibration parameters. In such a case, the risk

of overparameterization becomes high and one of the correlated parameters should not be used in Brown's model.

3 Influence of Geometric Configuration

Besides camera calibration, the geometric configuration of images is the other main causative reason that may affect the precision of 3D points determination. Limiting the analysis here to the stereo case, the geometric configuration may be parameterized using 2 parameters: stereo-pair baseline (B) and relative convergence angle (α), see Fig. 3.

3.1 Experiments on the Influence of Geometric Configuration

Using the same test-field described in Sect. 2.1, a second group of two experiments have been made by varying the baseline length and the relative convergence angle of an image pair. For excluding the influence of camera calibration, a set made up of the "mean values" of camera calibration parameters found in the previous experiment have been fixed. Four values for the baseline length corresponding to overlaps 55, 65, 75, and 85% have been applied. For each of them, four relative convergence angles have been set: 0°, 10°, 20° and 30°.

3.2 Baseline Length Influence Under Different Relative Convergence Angles

Figure 4 shows the change of total 3D RMSE depending on different overlaps and relative convergence angles between the stereo pair. Of course, since plots in Fig. 4 report empirical results from real tests, some small irregularities can be found, due to the fact that different images are adopted in each configuration, and the measurement of image coordinates has been repeated independently.

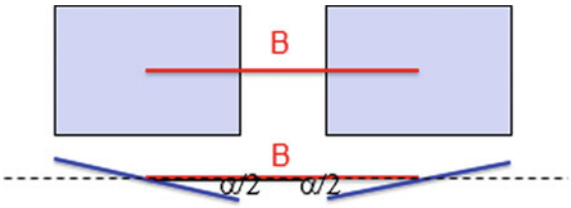

Fig. 3 Scheme of stereo-pair baseline and relative convergence angle

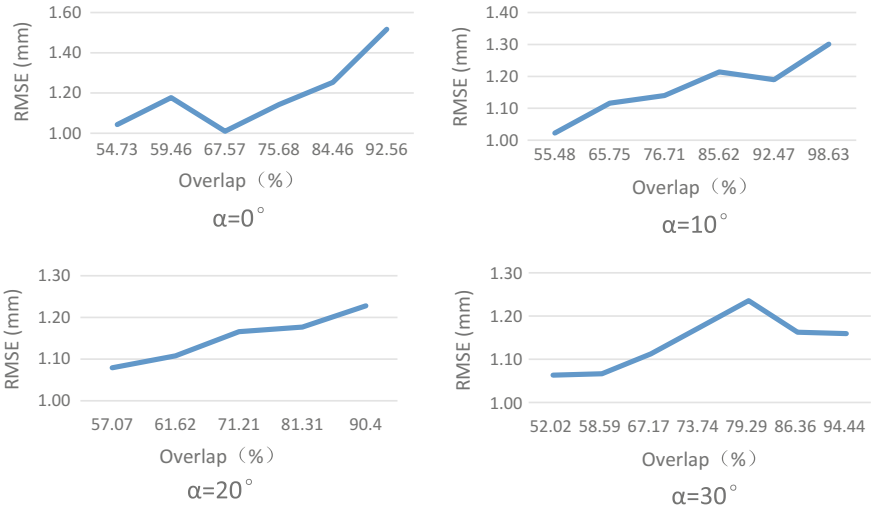

Fig. 4 Plots showing the influence of overlaps *vs* relative convergence angles in the stereo case as obtained from the empirical tests

The plots confirm what is supposed to be from the theoretical background, i.e., the influence of shortening the baseline (and consequently to enlarge the overlap) on 3D point determination may be significant even up to 30%. Generally, the deviations of 3D RMSE are smaller than 15% when the overlap is shorter than 70%. At the same time, changing the relative convergence angle does not have a great influence on 3D RMSE, even though in the convergent cases, the effect of shortening the baseline is mitigated.

3.3 Relative Convergence Angle Influence Under Different Baseline Lengths

Figure 5 shows the change of total 3D RMSE depending on different relative convergence angles and overlaps between the stereo pair. Results are dual with respect to the ones discussed in the previous Sect. 3.2.

In this case, the influence of different relative convergence angles on 3D point determination is lower than the one obtained from the analysis of overlaps. Maximum changes of 3D RMSE are less than 15%. Residuals generally grow with increasing angles, but stabilize between 20° and 30°. Exception to the general trend is made in the case with 85% overlap, when 3D RMSE decreases along with the angle increases. Even though such a case would require further analysis, we retain that here the baseline is too short and consequently results may have been altered.

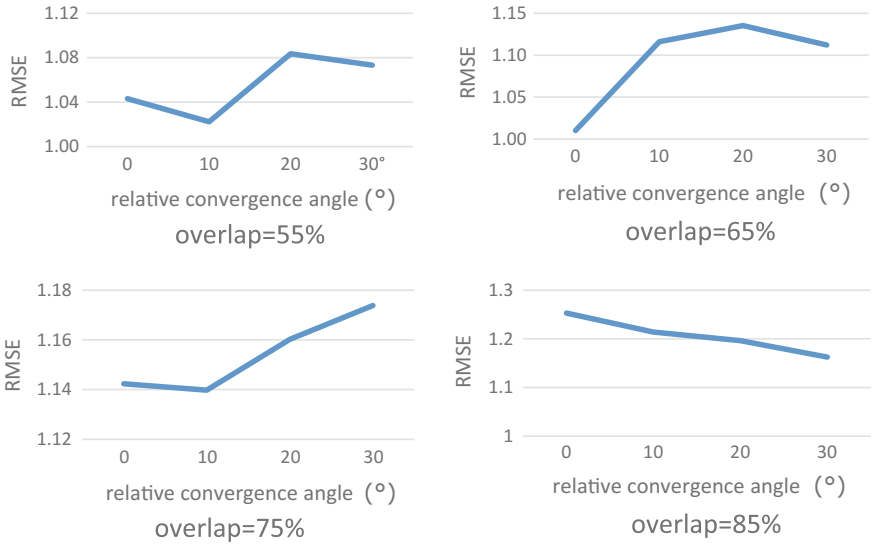

Fig. 5 Plots showing the influence of relative convergence angles vs overlaps in the stereo case as obtained from the empirical test

4 Conclusions and Proposal of Some Best Practices

Precise Close-range Photogrammetry is quickly getting more and more popular. Thus the research on the factors which may affect the precision of 3D point determination is important. This paper focuses on the influence of single camera calibration parameters and geometric configuration on 3D point determination when the stereo-pair configuration is applied.

The paper just reports a few preliminary results to be more focused in the future with the repetition of more numerically consistent experiments, by comparing different sensors, and by following more rigorous statistical analysis, e.g., on the empirical frequency distribution of the results. On the other hand, this paper would like to attract the attention of the readers on the fact that in the case high-precision photogrammetry is pursued (e.g., in image metrology), greater attention should be put on the assessment of camera calibration quality and on the study of image geometry. This paper would like to draw some guidelines about how to operate this kind of assessment on the basis of a simple test-field.

Camera calibration parameters may influence the precision of photogrammetric 3D reconstruction, especially radial distortion, whose effect cannot be compensated for by the use of external constraints as ground control points. In the case of important or high-precision photogrammetric projects, calibration should be repeated to improve the precision and reliability of the final results.

The baseline length is influencing the results up to 30% in terms of increasing 3D RMSE. The effect of relative convergence angles has less influence, although they may mitigate the changes of overlap.

Acknowledgements This research was supported by the National Science Foundation of China (project No. 41201425) and the Fundamental Research Funds for the Central Universities.

References

Barazzetti L, Forlani G, Remondino F, Roncella R, Scaioni M (2011a) Experiences and achievements in automated image sequence orientation for close-range photogrammetric projects. In: Proceedings of SPIE, vol 8085, paper No. 80850F, 13 p

Barazzetti L, Mussio L, Remondino F, Scaioni M (2011b) Targetless camera calibration. International Archives of the Photogrammetry, Remote Sensing and Spatial Information Sciences, Vol 38, Part 5/W16, 8 p

Brown CD (1971) Close-range camera calibration. Photogram Eng 37(8):855–866

Feng T, Mi H, Scaioni M, Qiao G, Lu P, Wang W, Tong X, Li R (2016) Measurement of surface changes in a scaled-down landslide model using high-speed stereo image sequences. Photogram Eng Remote Sens 82(7):547–557

Fraser CS (1996) Network design. In: Atkinson KB (ed) Close-range photogrammetry and machine vision. Whittles Publishing, UK, pp 256–282

Kraus K (2008) Photogrammetry—geometry from images and laser scans. Walter de Gruyter, Berlin

Hartmann W, Havlena M, Schindler K (2016) Recent developments in large-scale tie-point matching. ISPRS J Photogram Remote Sens 115:47–62

Hartley RI, Zisserman A (2004) Multiple view geometry in computer vision, 2nd edn. Cambridge University Press, Cambridge, p 672

Luhmann T, Robson S, Kyle S, Boehm J (2014) Close range photogrammetry: 3D imaging techniques, 2nd edn. Walter De Gruyter Inc., Germany, 684 p

Luhmann T, Fraser C, Mass H-G (2016) Sensor modelling and camera calibration for close-range photogrammetry. ISPRS J Photogram Remote Sens 115:37–46

Roncella R, Forlani G (2015) A fixed terrestrial photogrammetric system for landslide monitoring. In: Scaioni M (ed) Modern technologies for landslide monitoring and prediction. Springer, Germany, pp 43–68

Snavely N, Seitz SM, Szeliski R (2008) Modeling the world from internet photo collections. Int J Comput Vis 80(2):189–210

Triggs B, McLauchlan P, Hartley R, Fitzgibbon A (2000) Bundle adjustment—a modern synthesis. In: International workshop on vision algorithms, Springer, Berlin Heidelberg, paper no. 1883, pp 298–372

Some Metric Documentation of Cultural Heritage in Poland by Spherical Photogrammetry

Gabriele Fangi

Abstract Poland is a country with very rich CH, mainly in architecture. Churches, monasteries, castles, important buildings of noticeable workmanship are spread all over the country. I have made some experiences of metric documentation using a technique called Spherical Photogrammetry. Some projects are fully exploited; some are only at the orientation stage. Nevertheless, the philosophy is to document and build-up an archive: in case of need one can retrieve this documentation and use it to provide information, measurements, and so on. Spherical Photogrammetry is a new photogrammetric technique making use of the so-called spherical panoramas. They are obtained taking pictures from the same station point, partly overlapping, and covering up to 360°. Once downloaded in the computer they are projected on a virtual sphere having with the same center, then stitched together and projected in the cartographic plane with the so-called azimuth-zenith or longitude-latitude projection. The two orientation angles, horizontal direction and zenithal angle, can be measured, like in a theodolite. A software package has been prepared called Sphera. The 3D object extraction is assured, provided two or more oriented spherical panoramas, taken from different station points, by intersecting projective straight lines. The panorama orientation takes place in steps: (1) model formation by coplanarity, (2) absolute orientation, (3) block triangulation with independent models, (4) least constraints block bundle adjustments. The properties of the panoramas are many: FOV up to 360°, covering the entire visible space, the resolution is very large, much bigger than the one of any available commercial camera. Therefore the surveying time on place is short, enabling to produce large documentation projects in an easy and fast manner. Up-to-now no commercial software package is available, but I believe and hope that it will be available eventually. The main difficulty is in that any orientation and plotting is manual, making the procedure slow and difficult in the restitution phase. The examples shown are Saint Florian and Rynek market square, Kociny Palace in Kracow.

G. Fangi (✉)
Università Politecnica delle Marche, Ancona, Italy
e-mail: gabrielefangi@gmail.com

R. Cefalo et al. (eds.), *New Advanced GNSS and 3D Spatial Techniques*,
Lecture Notes in Geoinformation and Cartography,
DOI 10.1007/978-3-319-56218-6_15

Krakow has a large tradition in arquitectural photogrammetry. Untill the years ‘80 the Laboratory of Photogrammetry for Architecture in Krakow was the largest and most important in the world (Krakowskie przedsiebiorstwo geodezyjne).

Keywords Cultural heritage · Spherical photogrammetry · Documentation

1 Short Review of the Spherical Photogrammetry

Panoramas have widely been used to texture 3D models generated from laser scanning, for creating virtual reality tour applications, documenting landscape and cultural heritage sites, advertising real estates and recording crime scenes. The photographs, taken from a single viewpoint, partly overlapping, are projected into a sphere.

The sphere is then mapped in a plane with the so-called equirectangular projection or azimuth-zenith (Fig. 1).

From the image coordinates, one can derive the two direction values.

$$\vartheta = \frac{x}{R} \quad \varphi = \frac{y}{R}$$

Therefore spherical panorama can be regarded as the registration of any possible direction coming from the station point. The Spherical Photogrammetry was developed by the A. since 2007, (Fangi 2010; Fangi and Pierdicca 2012). For the complete treatment of the theory see (Fangi and Nardinocchi 2013) (Fig. 2).

The collinearity equations (1) and those of coplanarity (2) in terms of image coordinates are then used (Figs. 3 and 4).

$$\begin{aligned} x &= r.\left[-\Theta + \arctan\frac{(X - X_0) + d\alpha_y(Z - Z_0)}{(Y - Y_0) - d\alpha_x(Z - Z_0)}\right] \\ y &= r.\arccos\frac{-d\alpha_x(X - X_0) + d\alpha_y(Y - Y_0) + (Z - Z_0)}{d} \end{aligned} \tag{1}$$

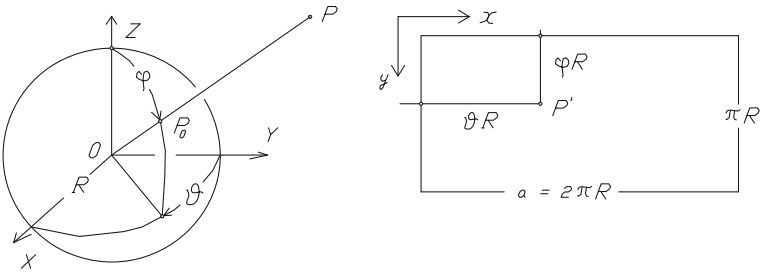

Fig. 1 The equirectangular projection. From image coordinates the two direction angles

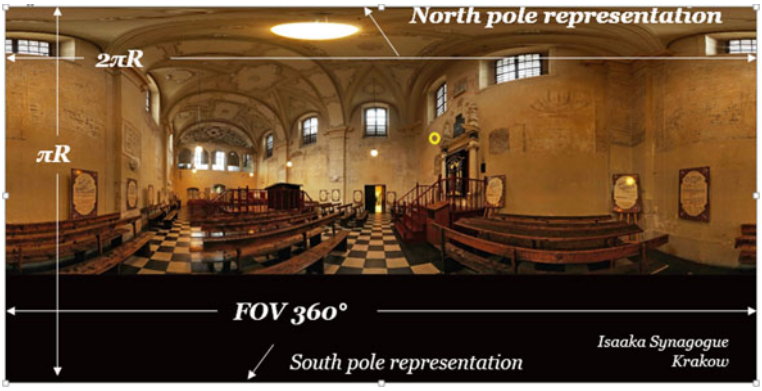

Fig. 2 A spherical panorama of the Isaak Synagogue in Krakow

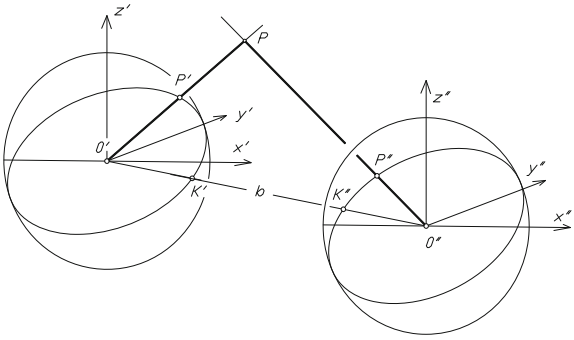

Fig. 3 The arrangement of the two spheres with the intersecting rays

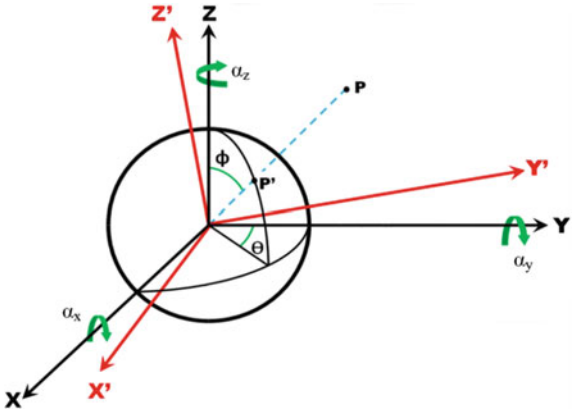

Fig. 4 Two angular corrections da_x, da_y are needed to make vertical the z axis

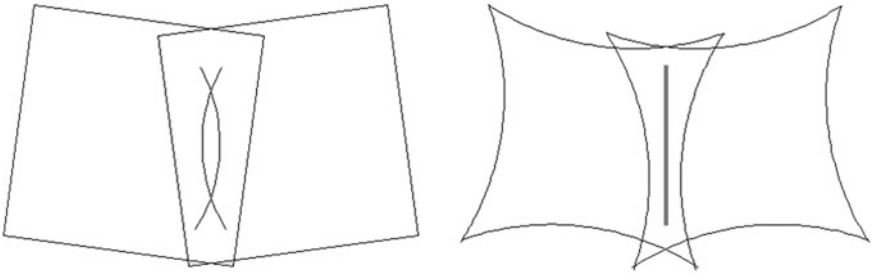

Fig. 5 The correction of the lens distortion

$$g = x'^{\mathrm{T}} V x'' = 0$$
$$[x' \quad y' \quad z'] R'^{\mathrm{T}} \begin{bmatrix} 0 & -bz & by \\ bz & 0 & -bx \\ -by & bx & 0 \end{bmatrix} R'' \begin{bmatrix} x^n \\ y^n \\ z^n \end{bmatrix} = 0 \tag{2}$$

1.1 Low-Cost Photogrammetry and Emergency Photogrammetry

The spherical photogrammetry makes possible the low-cost photogrammetry, the equipment being reduced to the digital camera, the tripod, the spherical head, and a longimeter. The advantages are the low-cost, the high resolution, FOV up to 360°, high speed in the field, very good for iconographic documentation, possibility to produce virtual tours, no or few bureaucracy, no permission, easy and safe transportation. The disadvantages are the plotting fully manual, making the restitution very slow, the difficult orientation, the absence of stereoscopy. The lens distortion is estimated and corrected by merging the overlapping photographs, but the stitching is far to be perfect (Fig. 5).

The high speed of documentation and the very light equipment make possible the "emergency photogrammetry" (Pisa et al. 2010; Cingolani and Fangi 2011). In this manner it was possible to make metric documentation of an impressive amount of CH emergencies in Syria, performed in 2010, before the war, (Fangi et al. 2013).

2 Steps of the 3D-Object Extraction

The orientation proceeds as follows. After the model formation, the absolute orientation takes place, and the following models are linked by model concatenation, ending with Block Bundle adjustment (Fig. 6).

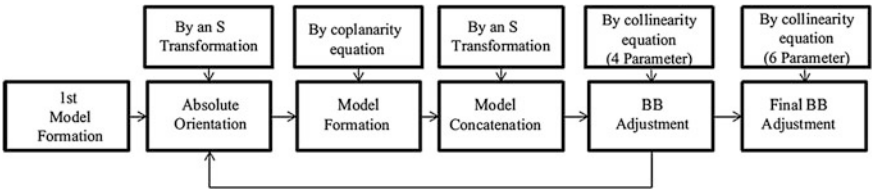

Fig. 6 Lay-out of the orientation procedure

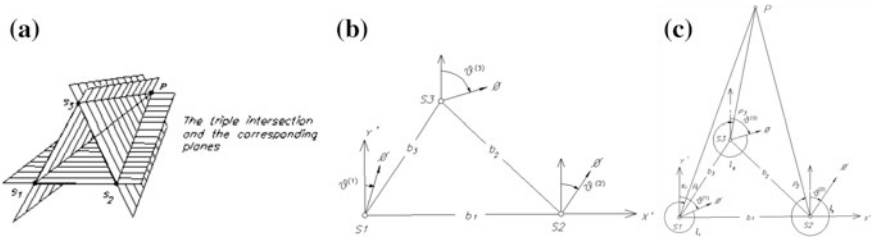

Fig. 7 The trinocular model

The photogrammetric models can be Binocular Model (*three independent parameters*) or Trinocular Model (*seven independent parameters*). The coplanarity condition (2) is developed as follows (Fig. 7):

$$\begin{pmatrix} [\sin\varphi_i \sin(\vartheta_i+\alpha_i)] & [\sin\varphi_i \cos(\vartheta_i+\alpha_i)] & [\cos\varphi_i)] \end{pmatrix} \begin{pmatrix} 0 & b_{z_{i+1}} & -b_{y_{i+1}} \\ -b_{z_{i+1}} & 0 & b_{x_{i+1}} \\ b_{y_{i+1}} & -b_{x_{i+1}} & 0 \end{pmatrix} \begin{pmatrix} [\sin\varphi_{i+1} \sin(\vartheta_{i+1}+\alpha_{i+1})] \\ [\sin\varphi_{i+1} \cos(\vartheta_{i+1}+\alpha_{i+1})] \\ [\cos\varphi_{i+1})] \end{pmatrix} = 0 \tag{3}$$

2.1 The Epipolar Geometry

The epipolar line equation (4), being a, b, c the parameters of the intersecting plane, is Fangi and Nardinocchi (2013) (Fig. 8):

$$y = R.atan\left(-c/(\sin\left(\frac{x}{R}\right) + b.\cos(x/R))\right) \tag{4}$$

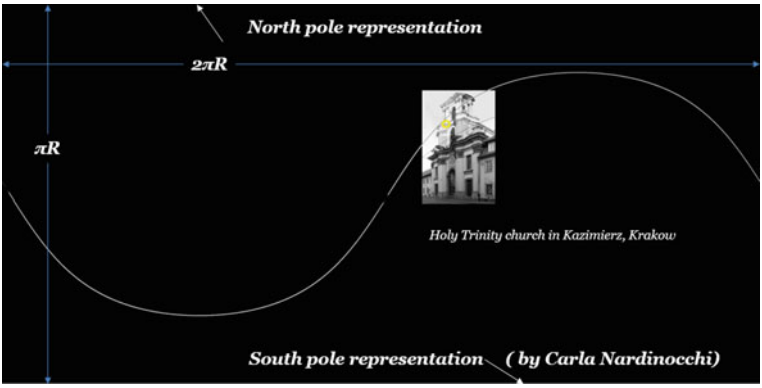

Fig. 8 The epipolar line on a panorama of the Holy Trinity church in Kazimirsk, Krakow

3 The Surveys in Poland

As we did already for many countries, Brazil (Amorim et al. 2013), Vietnam (Fangi et al. 2013), Syria (Fangi et al. 2013), we carried out some photogrammetric documentation also in Poland. The visited cities in 2011 and 2015 are Warsaw, Poznan, Wroclaw and Krakow. Most of the documented arquitectures are still to be plotted. Here the list of the sites: Warsaw—Church of the Holy Cross, Warsaw—Church of Saint Joseph or of the Visitandines, Wraklow—City hall, Poznan Saint Stanislaw Church, Krakow—Church of st Peter and st. Paul, St. Andrea's church (XI c), Krakow—The Barbican, Krakow—Lord's Transfiguration Church, Krakow Church of Carmelites, St. Ann's Church in Krakow, St. Katarina—Kazimisk Krakow, Church St. Michel in Kazimierz, Holy Trinity church in Kazimierz, Synagogue Tempel in Kazimierz, Isaak Synagogue in Kazimierz, Pałac_Dembińskich_Szczekociny, Krakow—Old market square, Rinek our Lady church and the tower of the old city hall, Krakow—Our Lady church, Krakow—Church of saint Florian (Fig. 9).

3.1 Pałac_Dembińskich_Szczekociny, or Kociny Palace

This very important building is now in very bad conditions. It is located near Krakow. It was designed by the architect Franciszek Ferdynand Nax in 1780. The Municipality of Szczekociny plans the restauration and a survey was carried out with twelve spherical panoramas around it (Figs. 10, 11 and 12).

(*model and render by G. Hinna*)

The project has been run in cooperation with prof. Regina Tokarcz, AGH, Krakow.

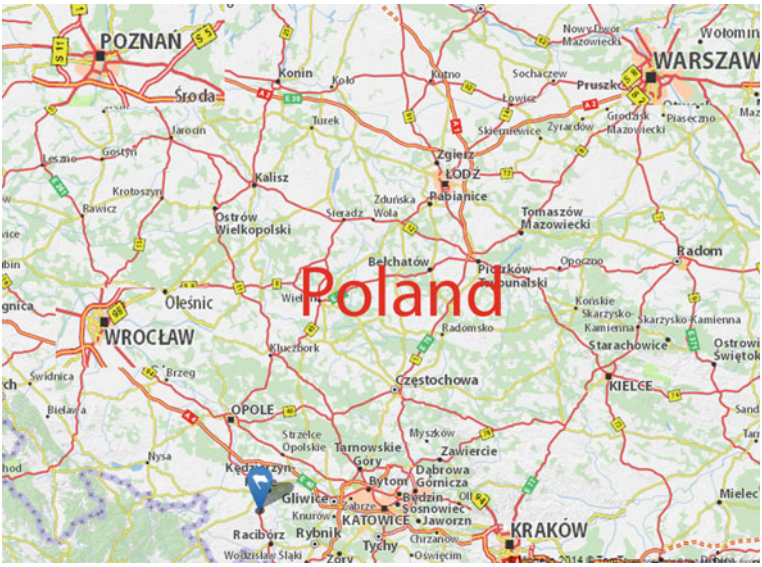

Fig. 9 Poland and the visited cities

Fig. 10 Pałac_Dembińskich_Szczekociny, Plottings, orientation network and thematic map

3.2 Rynek Główny (Square) Project

The square is located in the Kraków Old Town, with the most important sights of the city. It is rectangular and it measures 200 m on each side, and thus the largest medieval square in Europe.

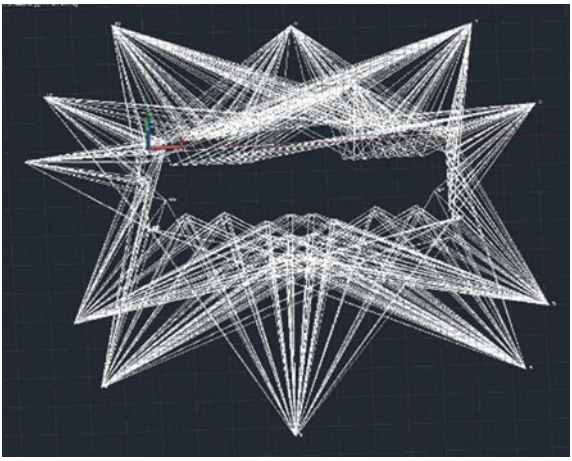

Fig. 11 Pałac_Dembińskich_Szczekociny, Plottings, orientation network and thematic map

Fig. 12 Pałac_Dembińskich_Szczekociny, Plottings, orientation network and thematic map

Planned in 1257 to house the city market. The city Hall remains the clock tower, while on a corner of the square stands the Basilica of our Lady (Figs. 13, 14, 15, 16, 17, 18 and 19).

Fig. 13 Krakow—Old market square, Rynek our Lady Church and the tower of the old city hall

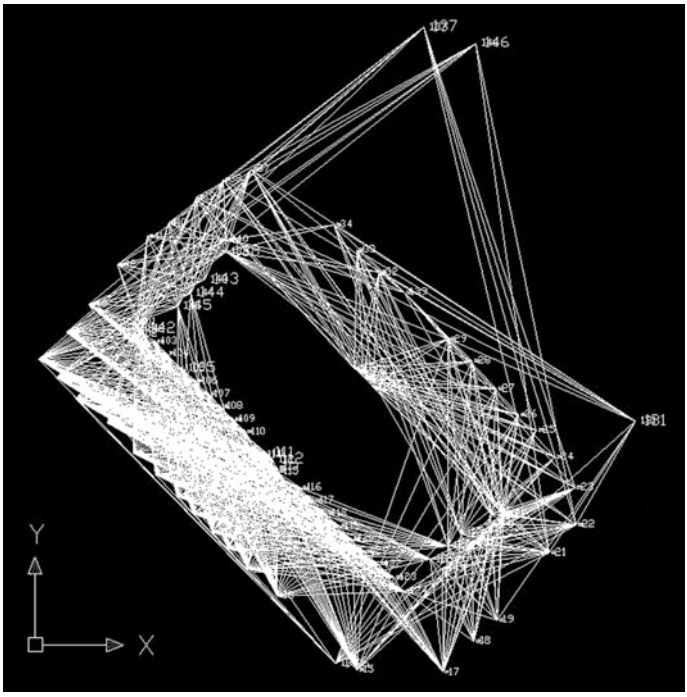

Fig. 14 The orientation network of the old market square

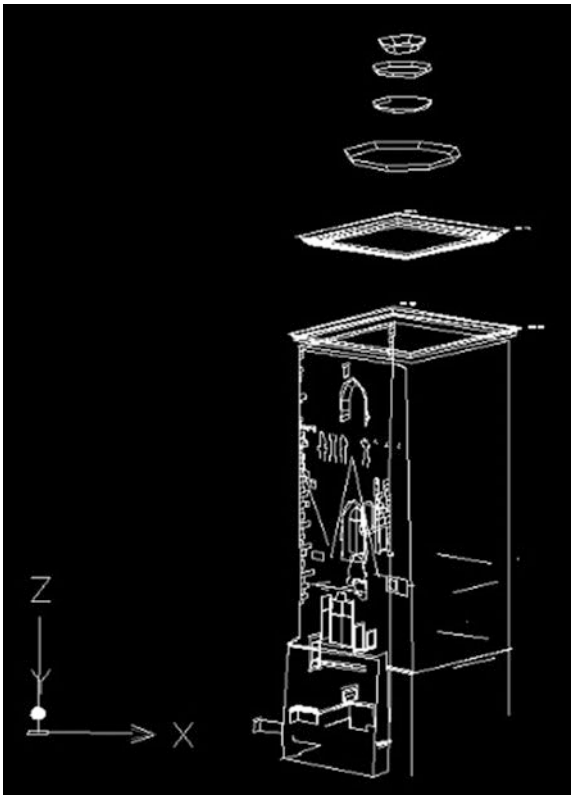

Fig. 15 Wire—frame and orientation network and render of the City Hall Clock Tower

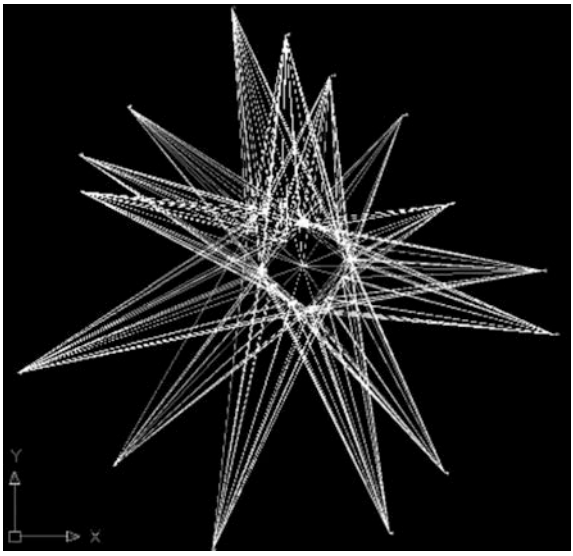

Fig. 16 Wire—frame and orientation network and render of the City Hall Clock Tower

Fig. 17 Wire—frame and orientation network and render of the City Hall Clock Tower

3.3 Krakow—Church of Saint Florian

The church of Saint Florian is the vice-cathedral of Krakow. Saint Florian is the protector of the city and of the fire-brigades. In the years 1950 it was the parish church of Karol Woytila. It was built in XVII c in baroque style.

Fig. 18 Krakow—Our Lady church (14th century) (Model and render by M. Dignani)

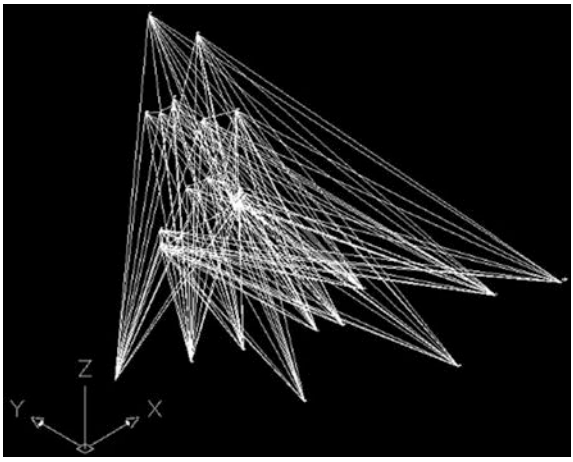

Fig. 19 Krakow—Our Lady church (14th century) (Model and render by M. Dignani)

Fig. 20 Krakow—Church of saint Florian—Orientation network and Wire-frame model (by F. Spedaletti)

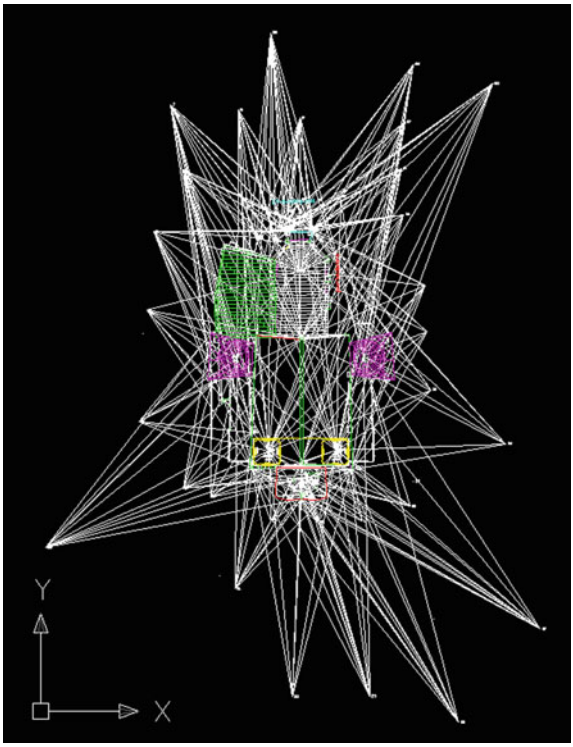

Fig. 21 Krakow—Church of saint Florian—Orientation network and Wire-frame model (by F. Spedaletti)

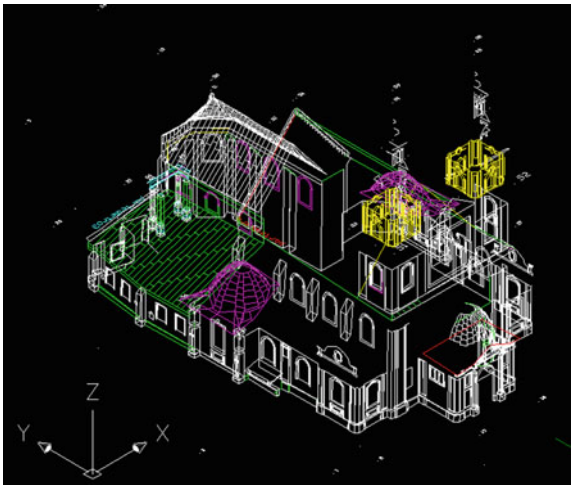

Fig. 22 Krakow—Church of saint Florian—Orientation network and Wire-frame model (by F. Spedaletti)

4 Final Remarks

Making documentation means knowing the history, the customs of a people. I have shown some examples and I could have shown much more, just to underline the main quality of SP: in short time an impressive amount of metric documentation of Cultural Heritage Architecture can be collected with cheap and simple equipment at a very low cost. Any project shown is suitable for reliable measurements. There is a strong need of CH documentation. The technique is most appropriate for applications not requiring dense point clouds, such natural surfaces, or complicated objects, and in situations with limited access to funds or as a quick field method to document many features in a short time. It is not possible that 3D reconstruction from spherical panoramic images will replace traditional close-range photogrammetry or laser scanning; the Spherical Photogrammetry will offer supplementary information to the conventional and modern cultural heritage documentation techniques.

References

Cingolani E, Fangi G (2011) Combined adjustment with spherical panoramas, and non metric images for long range survey, the San Barnaba Spire, Sagrada Familia, Barcelona, Spain. Cipa, Prague 2011, settembre ISSN: 1802-2669 ID 63759

De Amorim AL, Fangi G, Malinverni ES (2013) Documenting architectural heritage In Bahia, Brazil, using spherical photogrammetry. In: XXIV international CIPA symposium—international archives of the photogrammetry remote sensing spatial information sciences, XL-5/W2, pp 219–224. doi:10.5194/isprsarchives-XL-5-W2-219-2013

Fangi G (2010) Multiscale multiresolution spherical photogrammetry with long focal lenses for architectural surveys. In: ISPRS Mid-term symposium, Newcastle, June 2010 ISSN 1682-1777 ID 585

Fangi G (2013) Spherical photogrammetry for cultural heritage metric documentation: a critical examen six years after the beginning. In: A dimensao urbana do patrimonio – Encontro Internacional Arquimemoria 4, 14–17 May 2013, 1 edn, Salvador IAB –BA 360 p (ISBN 978-85-66843-00-2/ISBN 978-85-66843-01-9 DVD - ID 156123)

Fangi G, Malinverni ES, Tassetti AN (2013) The metric documentation of cham towers in vietnam by spherical photogrammetry, ISPRS Ann. photogramm. Remote Sens Spatial Inf Sci II-5/W1, 121–126, doi:10.5194/isprsannals-II-5-W1-121-2013, 2013. ID 155338

Fangi G, Nardinocchi C (2013) Photogrammetric processing of spherical Panoramas. Photogram Rec 28(143): 293–311. doi:10.1111/phor.12031 © 2013 The Remote Sensing and Photogrammetry Society and John Wiley & Sons Ltd. ID 146702 2-s2.0-84883817879

Fangi G, Pierdicca R (2012) Notre Dame du Haut by spherical photogrammetry integrated by point cloud generated by multi view software. Int J Heritage Digit Era 1(3):461–479

Fangi G, Wahbeh W, Piermattei L (2013) Spherical photogrammetry as rescue documentation for the reconstruction of some UNESCO Sites in Syria. Int J Heritage Digit Era 2(3): 335–342. doi:10.1260/2047-4970.2.3.335. Publisher Multi Science Publishing, ISSN 2047-4970 ID 156110

Pisa C, Zeppa F, Fangi G (2010) Spherical photogrammetry for cultural heritage. In: Proceeding of the second workshop on heritage and digital art preservation, Florence, Italy, pp 3–6

Doing Science with Nano-Satellites

Anna Gregorio, Alessandro Cuttin, Mario Fragiacomo and Mauro Messerotti

Abstract Nano-satellites represent a new generation of satellite platforms that is opening its own market niche expanding extremely quickly. These satellites are small and light, thanks to their cubic shape they are also modular and have raised the interest of space operators thanks to their jack-in-the-box concept. Particularly interesting is the Earth Observation and remote sensing segment, that has large potential applications for safety issues, or even more practical applications for agriculture. The possibility of using a constellation or a network of nano-satellites as a new generation of telecommunication (e.g. for mobile applications) or navigation systems seems also very appealing for the next future. Besides the advantages of using nano-satellites, this type of space missions still presents a number of technical issues; one of these is the on-board telecommunication system that, working at low frequencies, provides a very limited data rate preventing the transmission of large amounts of data. Only by improving this system, nano-satellites can become real science space missions.

Keywords Nano-satellites · Earth Observation · Remote Sensing · Telecommunication system · Constellation of satellites

A. Gregorio (✉) · A. Cuttin
Department of Physics, University of Trieste, P.le Europa, 1, 34127 Trieste, Italy
e-mail: anna.gregorio@ts.infn.it

A. Gregorio · M. Fragiacomo · M. Messerotti
PicoSaTs SRL, c/o Area Science Park, Padriciano 99, I, I 34149 Trieste, Italy

A. Gregorio · M. Messerotti
INAF, Osservatorio Astronomico di Trieste, Via G.B. Tiepolo, 11,
I-34143 Trieste, Italy

A. Cuttin
Department of Engineering and Architecture, University of Trieste,
P.le Europa, 1, 34127 Trieste, Italy

R. Cefalo et al. (eds.), *New Advanced GNSS and 3D Spatial Techniques*,
Lecture Notes in Geoinformation and Cartography,
DOI 10.1007/978-3-319-56218-6_16

1 Introduction

Nano satellites represent a new generation of satellite platforms that is opening its own niche, expanding extremely quickly. These satellites are very small, light, and thanks to their cubic shape they are also modular, as Lego® bricks, and have raised the interest of space operators thanks to their jack-in-the-box concept. Born as educational tools, nano-satellites are now becoming real scientific and technological space system, although a number of issues still needs to be solved.

In this paper we want to briefly analyse the status and future of science missions nano-satellites. After a brief introduction on nano-satellites and what has already been achieved with these missions, we will focus on the most significant science topic in this field, Remote Sensing and Earth Observations. Remarks on some technical issues are also given; finally we give some conclusions.

2 Science with Nano-satellites

2.1 Nano-satellites

From the late 90s, with the construction of the first small satellites with very compact mass and size, space technology, an almost exclusive prerogative of large companies specialised in the aerospace field, wants to become a technology available to small companies, facilities and research institutes, historically smaller in terms of personnel and less funded. The design can be complex, given the environment in which such systems have to operate, but it is clear that the so called "CubeSat" systems, initially designed for educational purposes, are being brought to the daily technological and scientific use (Hevner et al. 2011). Over the last decade more than one hundred CubeSats, modular small satellites whose basic element is an Aluminium cubic structure of 10 cm side, have been launched. This number will double very soon and in recent years interest for small satellites has grown considerably also for commercial applications further expanding the potential of these systems.

In recent years the nano-satellite concept of a cubic satellite for educational purposes has evolved and now belongs to a wider class of satellites, building satellites using CubeSat bricks using up to 27 units ($3 \times 3 \times 3$) which provides for the extension of the satellite to larger boxes with mass up to 50 (The CubeSat Program 2014).

A recent study by SpaceWorks Enterprises, one of the world leaders in satellite launch field, presented a comprehensive analysis of trends of small satellites, in the class 1–50 kg. Spaceworks projections, see Fig. 1, based on announced and future

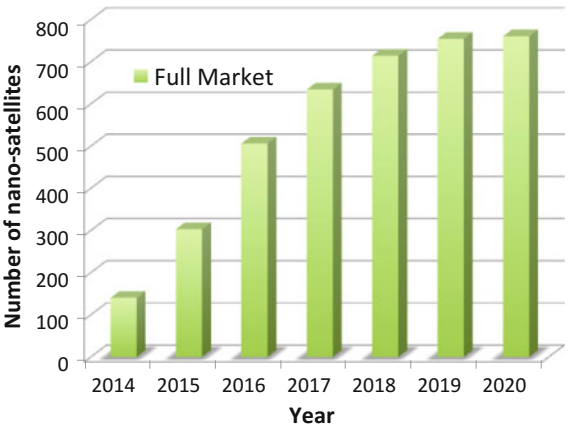

Fig. 1 Number of past and future launches according to SpaceWorks analysis

plans of developers and programs indicate as many as 3000 small satellites to be launched from 2016 through 2022.[1]

According to these projections, applications are diversifying with increased use in the future of Earth Observation and remote sensing missions from less than 40% of the total number of nano-satellites towards almost 75%.

What is not specified in this study is the interest demonstrated by the International Science Community in the space field towards the usage of these platforms for small science missions. Just as one of the most important facts in 2016, in January the International Space Science Institutes in Bern, Switzerland, organized a Forum during which international researchers with active experiences in CubeSats and their development discussed on three major topics:

- Identify suitable CubeSat missions, discuss their feasibility and/or science results already been achieved;
- Identify barriers that limit the science impact of the CubeSat platforms;
- Characterize limitations of a CubeSat platform for science purposes.

One of the results on this forum was the creation of a short internationally focused consensus document, "white paper", summarizing the status of small space missions and the way to go forward, that is being prepared.

Particularly interesting are the Earth Observation and remote sensing fields, with a number of potential applications ranging from safety issues (e.g. water and fire monitoring), to more practical applications for agriculture.

Although it is evident that Remote Sensing and Earth Observations represent the main Science field for small space missions, it is worth mentioning the impressive number of science topics that is being touched by CubeSats with at least one representative mission example:

[1]SpaceWorks Nano Microsatellite Market Forecast http://spaceworksforecast.com/2016-market-forecast/.

- Spaceweather, Meteorology, Atmospheric and Solar Physics: DICE, FireFly, GRIFEX (GEOCAPE ROIC In-Flight Experiment) (Robinson and Moretto 2008; Crowley et al. 2011);
- Astronomy, Astrophysics, Particle and Nuclear Physics: Astro-1, ELFIN (Electron Losses and Fields Investigation), CuSPP (CubeSat mission to study Solar Particles over the Earth's Poles)[2];
- Lunar, Interplanetary and Asteroid missions: Lunar Flashlight, Near Earth Asteroid (NEA) Scout, SIMPLEX, INSPIRE (Interplanetary NanoSpacecraft Pathfinder In a Relevant Environment) (Spangelo et al. 2015);
- Interferometry and Constellation: EDSN (Edison Demonstration of Smallsat Networks)[3];
- Space Debris (Clean Space One, D-Orbit)[4];
- Biology and Human Health: BioSentinel[5];
- Navigation and Telecommunication systems: PhoneSat, ISARA (Integrated Solar Array and Reflectarray Antenna), OCSD (Optical Communications and Sensor Demonstration).[6]

Correspondingly new instrumentation is being miniaturized and can eventually be used as an important test bench for future larger missions:

- Electric and magnetic field instruments, plasma density and temperature instruments, neutral gas pressure gages and wind instruments, mass spectrometers;
- Particle detectors, Gamma and X ray detectors, photometers and spectrometers, hyper-spectral imagers;
- Advanced radio receivers (GNSS receivers, microwave radiometers).

2.2 *Remote Sensing and Earth Observations*

Earth Observation from satellites allows the acquisition of global and synoptic detailed information about the planets (including the Earth) and their environments. Sensors on Earth-orbiting satellites provide information about global patterns and dynamics of clouds, surface vegetation cover and its seasonal variations, surface morphologic structures, ocean surface temperature, and near-surface wind. The rapid wide coverage capability of satellite platforms allows monitoring of rapidly changing phenomena, particularly in the atmosphere.

[2]https://www.nasa.gov/content/goddard/nasas-science-mission-directorate-cubesat-initiative.

[3]https://www.nasa.gov/directorates/spacetech/small_spacecraft/edsn.html.

[4]http://www.deorbitaldevices.com/.

[5]https://www.nasa.gov/centers/ames/engineering/projects/biosentinel.html.

[6]https://www.nasa.gov/directorates/spacetech/small_spacecraft/isara_project.html, https://www.nasa.gov/directorates/spacetech/small_spacecraft/ocsd_project.html.

Remote sensing can significantly contribute to provide a timely and accurate picture of the agricultural sector, as it is very suitable for gathering information over large areas with high revisit frequency. A close monitoring of agricultural production systems is necessary, as agriculture shall strongly increase its production for feeding the nine-billion people predicted by mid-century. This increase in production must be achieved while minimizing the environmental impact of agriculture. Achieving this goal is difficult, as agriculture must cope with climate change and compete with land users not involved in food production (e.g., biofuel production, urban expansion, etc.). The necessary changes and transitions have to be monitored closely to provide decision makers with feedback on their policies and investments. Nano-satellites is already being used in this field (Kramer and Cracknell 2008), instruments like the TMA (Three Mirror Anastigmat) telescope, on board the Proba-V (Francois et al. 2014), a small ESA (European Space Agency) mission for Vegetation studies, is now being miniaturized and brought to CubeSats.

It is worth mentioning that in this context the University of Trieste, with the two departments of Physics and Engineering and Architecture, is developing a new low cost detector, named PicoAgri, dedicated to agriculture monitoring to be used on board nano-satellites. The detection system is made of an optical system and a sensor, the processing unit used by now is by now an Arduino 1, that have been already demonstrated to work in flight although we are analysing the possibility of using a more powerful unit. The system is mostly based on COTS (Commercial Off The Shelf) devices that are being adapted to the requirements of the system. The acquisition of the satellite image is performed via a *multispectral sensor* that cover four spectral bands simultaneously, blue (459–479 nm), red (620–670 nm), near Infrared (841–875 nm) and shortwave infrared (1628–1652 nm). PicoAgri uses four different sensors, one for each spectral band, to reconstruct the spectral image of the soil; the satellite acts as an *along track scanner* (*push-broom scanner*) to obtain the spectroscopic image. The camera consists of an optical system projecting an image onto a linear array of sensors, the CCD array, arranged perpendicular to the flight direction of the spacecraft. We analysed possible COTS components both for the sensor and optical systems; linear CCD systems have been identified, acquired and are now being tested while suitable lenses are not available on the market. A dedicated optical system is in the design phase. The principal advantage of this type of sensor is the lack of mechanical parts, this prevents malfunction and extend the satellite lifetime.

3 Technology Issues

Besides the many advantages of using nano-satellites (cost and time effectiveness, focused objectives, fast turn-around experimental approaches), with respect to large missions nano-satellites intrinsically hold some limitations, mostly related to their physical size, and as a consequence on power and attitude control systems. In addition, nano-satellites still present a few technical issues; one of these is the

on-board telecommunication system that, working in the low frequency radio-amateur band, provides a very limited data rate preventing the transmission of large amounts of data.

In particular Earth Observation and remote sensing space missions produce large amounts of data that directly reflect the quality of scientific data (i.e. image resolution) they produce. For this reason these applications are accessible by now only by larger satellites providing high data transmission rate. Only by improving the telecommunication system of small satellites thus enabling the transmission of large amount of data, nano-satellites can become real science space missions. In this context, the University of Trieste with its recently born spin-off company PicoSaTs, envisages a new generation of nano-satellite communication systems working at high frequencies (Ka band) providing very high data rates.

The constantly growing number of orbiting nanosatellites is not yet followed by an improvement in the communication technology they use, with the obvious exception of those spacecrafts that are launched by companies that have demanding payloads, and address this issue with proprietary solutions. To date, most orbiting CubeSats mount wire antennas and use frequencies allocated in the radio amateur service (Klofas and Leveque 2012).

We assume that the main reason behind this technological gap is that the majority of the organizations face a space mission for the first time, and therefore prefer to use devices that are proven to be reliable.

To satisfy the need for more downloaded data keeping the existing technology, ground station replication is a viable option. Increasing the contact time with a number of known ground station increases the capability of downloading more data in a linear fashion. Some initiatives address this approach with different levels of success (Leveque et al. 2007; Pandolfi et al. 2016; White et al. 2015).

Another option to sustain a demanding data budget is to address the technological issues of providing nanosatellites with the capabilities of using communication systems at higher frequencies, like those in the Ka band. Corresponding wavelengths enable the design of small and directive antennas, and, as a consequence, faster data rates can be obtained.

The importance of equipping CubeSat with performing radios is also enabled by the presence on the market of ADCS with sufficient capabilities to ensure the proper pointing of highly directive antennas. The result of the optimized radiation pattern of the antenna array is shown in Fig. 2.

A proposed solution (Cuttin et al. 2015) consists of an array of microstrip patches, a convenient approach in terms of size, mass, mounting and cost. Otherwise, efficient radiators such as parabolic reflectors, horn antennas, and reflect arrays have demanding requirements in terms of mass or volume requirements (King et al. 2012; Hodges et al. 2013; Sauder et al. 2015).

Thanks to an advantageous algorithm capable of optimizing the far-field of arrays by means of the definition of proper masks (Buttazzoni and Vescovo 2014), as shown in Fig. 2, it has been proved that a small but directive antenna, consisting of a circularly polarized array of 256 patch elements tuned at 37 GHz, can be housed on one face of a CubeSat.

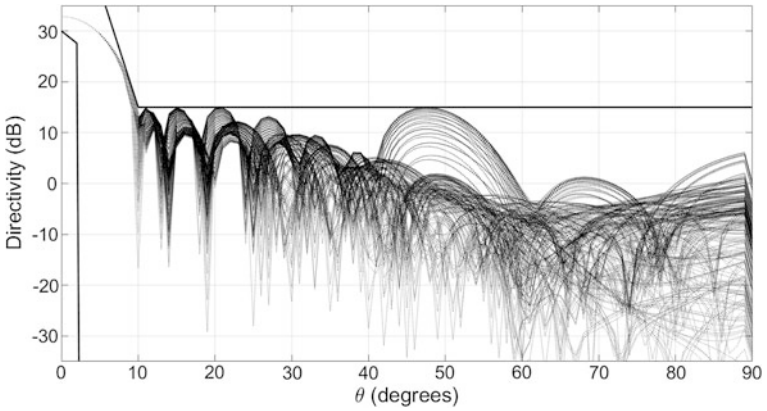

Fig. 2 Optimized radiation pattern of the antenna array

Such antenna could easily be used to perform data downlink at a very fast data rate.

4 Conclusions

In recent years the nano-satellite concept has evolved and now belongs to a wider class of satellites with mass up to 50 that is being brought to the daily technological and scientific use.

With respect to larger satellites, these nano-satellites are agile, meaning cost and time effective, they can focus on specific scientific objectives and, being based on a standard platform, provide a fast turn-around experimental approach mitigating also issues related to measure gaps. Besides that, they still represent an important educational tool that allows creative mission ideas to reach a successful implementation, thus enhancing university participation in space activities, eventually training the next generation of scientists and engineers in space by offering full end-to-end mission experience.

From the scientific and technological point of view, nano-satellites represent a potential tool for advanced research in many science areas. They already demonstrated the capability to cover an impressive number of science topics, ranging from spaceweather, atmospheric and solar physics, astrophysics and particle physics or even dedicated to biology and human health, to sophisticated lunar and interplanetary missions, or even more technological missions for navigation and telecommunication or based on interferometry and constellations.

Particularly interesting are the Earth Observation and remote sensing fields, with a number of potential applications ranging from safety issues (e.g. water and fire monitoring), to more practical applications for agriculture. In this context the

University of Trieste is developing a new low cost detector based on COTS components, named PicoAgri, dedicated to agriculture monitoring to be used on board nano-satellites.

Besides the many advantages of using nano-satellites, with respect to large missions nano-satellites intrinsically hold some limitations, mostly related to their physical size, and a few technical issues. One of these is the on-board telecommunication system that, working in the low frequency radio-amateur band, provides a very limited data rate preventing the transmission of large amounts of data. Only by improving the telecommunication system of small satellites thus enabling the transmission of large amount of data, nano-satellites can become real science space missions. In this context, the University of Trieste with its recently born spin-off company PicoSaTs, envisages a new generation of nano-satellite communication systems working at high frequencies (Ka band) providing very high data rates.

Acknowledgements We acknowledge support by the University of Trieste through FRA (Fondi Ricerca Ateneo) 2014 funded activity "Osservazione e monitoraggio dei terreni: sistema di rivelazione per nano-satelliti".

References

Buttazzoni G, Vescovo R (2014) An efficient and versatile technique for the synthesis of 3D copolar and crosspolar patterns of phase-only reconfigurable conformal arrays with DRR and near-field control. IEEE Trans Antennas Propag 62(4):1640–1651. doi:10.1109/TAP.2014.2308319

Crowley G, Fish C, Swenson C, Burt R, Stromberg E, Neilesen T, Burr S, Barjatya A, Bust G, Lasrsen M (2011) Dynamic ionosphere cubesat experiment (DICE). In: Proceedings of the 25th Annual AIAA/USU Conference on Small Satellites, Logan, UT, USA, Aug 2011. Paper SSC11-XII-6

Cuttin A, Buttazzoni G, Vescovo R, Tenze L (2015) Radiation pattern synthesis of a high gain, circularly polarized rectangular antenna array in the Ka band for CubeSat class satellites. In: Proceedings of the 3rd IAA conference on University Satellite Missions and Cubesat Workshop. International Academy of Astronautics, IAA Book Series, Conference and Symposium Proceedings, Roma

Francois M, Santandrea S, Mellab K, Vrancken D, Versluys J (2014) The PROBA-V mission: the space segment. Int J Remote Sens 35(7):2548–2564. doi:10.1080/01431161.2014.883098

Hevner R, Holemans W, Puig-Suari J, Twiggs R (2011) An advanced standard for CubeSats. In: Proceedings of AIAA/USU conference small satellites, 2011

Hodges R, Shah B, Muthulingham D, Freeman T (2013) ISARA—integrated solar array and reflectarray mission overview. In: Proceedings of AIAA/USU conference small satellites, 2013

King JA, Ness J, Bonin G, Brett M, Faber D (2012) Nanosat Ka-band communications—a paradigm shift in small satellite data throughput. In: Proceedings of AIAA/USU conference small satellites, 2012

Klofas B, Leveque K (2012) The future of CubeSat communications: transitioning away from amateur radio frequencies for high-speed downlinks. In: Proceedings of AMSAT space symposium

Kramer HJ, Cracknell AP (2008) An overview of small satellites in remote sensing. Int J Remote Sens 29(15)

Leveque K, Puig-Suari J, Turner C (2007) Global educational network for satellite operations (GENSO). In: AIAA/USU conference on small satellites

Pandolfi G, Albi R, Puglia J, Berdal Q, DeGroote R, Messina M, Di Battista R, Emanuelli M, Chiuri DE, Capitaine T, Scaringello A (2016) Solution for a ground station network providing a high bandwidth and high accessibility data link for nano and microsatellites. In: 67th international astronautical congress (IAC), Guadalajara, Mexico, 2016

Robinson EM, Moretto T (2008) Small satellites for space weather research. Space Weather AGU J 6

Sauder JF, Chahat N, Hodges R, Peral E, Rahmat-Samii Y, Thomson M (2015) Designing, building, and testing a mesh Ka-band parabolic deployable antenna (KaPDA) for CubeSat. In: Proceedings of AIAA aerospace sciences meet, 2015

Spangelo S, Castillo-Rogez J, Frick A, Klesh A, Sherwood B (2015) JPL's advanced CubeSat concepts for interplanetary science and exploration missions. NASA JPL/Caltech CubeSat Workshop, Logan, Utah, Aug 2015

The CubeSat Program (2014) CubeSat design specification. Retrieved from http://cubesat.atl.calpoly.edu/images/developers/cds_rev13_final.pdf

White DJ, Giannelos I, Zissimatos A, Kosmas E, Papadeas D, Papadeas P, Papamathaiou M, Roussos N, Tsiligiannis V, Charitopoulos I (2015) SatNOGS: satellite networked open ground station. Engineering Faculty Publications. Paper 40. http://scholar.valpo.edu/engineering_fac_pub/40

Part III
New Advanced GNSS and 3D Spatial Techniques Application to GIS, Web-GIS, UAVs, Disaster Management and Cultural Heritage

Part III proposes some interesting utilization of the most recent and advanced tools in digital cartography and field survey.

The first chapter is devoted to the use of GIS and Web-GIS for different applications. The first chapter, entitled "Optimization of a Co-Generative Biomass Plant Location Using Open-Source GIS Techniques. Technical, Economical and Environmental Validation Methodology", by Agostino Tommasi[1], Raffaela Cefalo[1], Aldo Grazioli[2], Dario Pozzetto[3], Yaneth M. Alvarez Serrano[3], Michel Zuliani[4], [1]GeoSNaV Laboratory, University of Trieste, Italy; [2]Department of Engineering and Architecture, University of Trieste, Italy; [3]Department of Electronical, Mechanical and Management, University of Udine, Italy; [4]Carnia Mountain Community, Tolmezzo (UD), Italy, demonstrates how high-level GIS analysis can be carried out using only open-source software. The chapter reports the operations that brought to the identification of the optimal location of a new co-generative biomass plant in the Carnia region (Italy). The authors used a great amount of geo-referenced data to obtain this result, subsequently verified and validated using a methodological approach. The validation process has successfully taken into account the technical, economic and environmental feasibility of the proposed plant solution.

The second GIS-related chapter is entitled "Geography of WWI Sites Along the Italian Front by Means of GIS Tools" by Paolo Plini, Sabina Di Franco, Rosamaria Salvatori, Italian National Research Council, Institute for Atmospheric Pollution Research, Rome, Italy; it illustrates the results of a GIS project focused on the First World War sites along the Italian front. An impressive number of raster maps and vector layers have been obtained from historical documents and old maps. One of the most challenging tasks was the correct reconstruction and geolocalization of place names, taking also in account the different linguistic variants of each place. The final WWI database contains 6600 places categorized by typology and expressed in up to six different languages. A Web-GIS version has been developed and made available for public dissemination.

The following chapter is entitled "A Comparison of Low-Poly Algorithms for Sharing 3D Models on the Web" by Grazia Caradonna, Simona Lionetti, Eufemia Tarantino and Cesare Verdoscia, Politecnico di Bari, Italy.

The aim of the study is to reduce the size and complexity of 3D models in the field of cultural heritage, thus allowing more complex spatial analyses from experts and easing data access for citizens. The Authors, focusing on an historical building of Bari (Italy), developed a PostgreSQL DBMS and a front-end PHP interface to allow users queries and analyses.

The fourth chapter is entitled "Application of Digital Photogrammetry from UAV Integrated by Terrestrial Laser Scanning to Disaster Management. Brcko Flooding Case Study (Bosnia Herzegovina)" by Francesco Cescutti[1], Raffaela Cefalo[1], Franco Coren[2], [1]GeoSNav Lab, Department of Engineering and Architecture, University of Trieste, Italy, [2]INOGS—Istituto Nazionale di Oceanografia e Geofisica Sperimentale, and reports the methodology used for the survey of two landslides located in the Brcko region (Bosnia & Herzegovina). The field operations, carried out in harsh environment, involved UAV (Unmanned Aircraft Vehicle) photogrammetry and laser scanning surveys; the data acquired by the two systems have been successfully integrated and permitted to produce detailed maps of the two landslides.

The fifth chapter, entitled "Kinematic Positioning: From Mobile Mapping Systems to Unmanned Aerial Vehicles at Pisa University", by Gabriella Caroti and Andrea Piemonte, Civil and Industrial Engineering Department, University of Pisa, is a compendium of twenty years of activities in the field of territory mapping by the means of mobile geo-referenced sensors. The authors illustrate the techniques and tools evolution in mobile mapping during the years: from land-based vehicles to unmanned aerial systems, using a wide spread of different sensors.

The sixth and final chapter is entitled "Ionosphere TEC Variations Over Bosnia and Herzegovina Using GNSS Data" by Medzida Mulic and Randa Natras, Geodesy Department, Faculty of Civil Engineering, University of Sarajevo, Bosnia & Herzegovina; it focuses on disaster management and monitoring. In particular, the authors analyze TEC (Total Electron Content) variability using GNSS observation data recorded at Sarajevo (Bosnia & Herzegovina) station. The analyses focused on the earthquakes registered in Sarajevo in February and April 2015, with near-located epicenters. The results indicate that some of the evidenced TEC anomalies are directly linked to the seismic activities.

Optimization of a Co-generative Biomass Plant Location Using Open Source GIS Techniques. Technical, Economical and Environmental Validation Methodology

Agostino Tommasi, Raffaela Cefalo, Aldo Grazioli, Dario Pozzetto, Yaneth M. Alvarez Serrano and Michel Zuliani

Abstract The principal aim of this research activity is to identify, inside the administrative territory of the Carnia Mountain Community, Friuli Venezia Giulia Region, Italy, the optimal location of a new co-generative biomass plant, exploiting georeferenced parameters obtained through an integrated analysis based on open source GIS (Geographical Information System) and DBMS (Database Management System) applications. The parameters used for this analysis are related to naturally available biomass estimation, public and private users distribution, already existing and planned thermal plants, wood industrial activities locations and electrical and road infrastructures. All these georeferenced data have been homogenized and processed together in order to obtain the energetic demand and offer maps. The authors present a methodological approach to verify and validate the GIS based optimal solution, taking into account the thermal requirements of the residential, commercial and industrial settlements potentially connectable inside the cogeneration plant catchment area. It is expected to realize the technical, economic and environmental feasibility related to the different proposed plant solutions

A. Tommasi · R. Cefalo (✉)
GeoSNaV Laboratory, University of Trieste, Trieste, Italy
e-mail: raffaela.cefalo@dia.units.it

A. Grazioli
Department of Engineering and Architecture, University of Trieste, Trieste, Italy

D. Pozzetto · Y.M. Alvarez Serrano
Department of Electronical, Mechanical and Management,
University of Udine, Udine, Italy

M. Zuliani
Carnia Mountain Community, Tolmezzo (UD), Italy

R. Cefalo et al. (eds.), *New Advanced GNSS and 3D Spatial Techniques*,
Lecture Notes in Geoinformation and Cartography,
DOI 10.1007/978-3-319-56218-6_17

(the generation plant of heat and electricity and district heating network), thus allowing to compare the proposed solution with the traditional plants powered by fossil fuels.

Keywords Biomass · GIS · DBMS · Economical analysis · GRASS · QGIS · Feasibility

1 Introduction

Today, when defining any environmental strategy plan, the production and consumption of energy is one of the essential factors and, in recent years, the attention has increasingly focused on the use of renewable sources. Their exploitation is important in order to reach different objectives such as reducing the greenhouse effect, partially replacing the fossil fuels, reducing the need to import energy resources from outer regions and respecting the commitments made by the 1997 Kyoto Protocol (United Nations 1998).

From an environmental and economical point of view, the reduction of the dependence on hydrocarbon consumption is not only a global target, but also a local target. In the search for alternatives, mountain areas emerge as a possible—but partial—solution, thanks to their availability of significant natural resources (Frombo 2009), one being the biomass obtainable from forest exploitation.

Biomass alone will never completely replace oil, but could play an important role in a more complex replacement strategy, involving energy from other renewable sources (IVALSA 2007). The forest-based biomass exploitation is an opportunity to stimulate local economy, and can also provide a new source of heating in the mountain areas not served by natural gas (Chiopris 2006). A sustainable exploitation of the forest, along with other traditional mountain activities such as agriculture and livestock, not only plays an economic role but also ensures landscape and land maintenance, as well as the survival of local knowledge and traditions (Carnia Mountain Community 2011).

This study has the purpose to identify and validate, inside the administrative territory of the Carnia Mountain Community, Friuli Venezia Giulia Region, Italy, the optimal location of a new co-generative biomass plant, using georeferenced data, integrated GIS and DBMS applications and feasibility verification methodologies. The study is structured in two different parts: the first identifies the optimal plant location using GIS and DBMS techniques, and the second verifies and validates the results, taking into account the technical, economic and environmental feasibility of the proposed plant location. A conceptual framework of this study workflow is presented in Fig. 1.

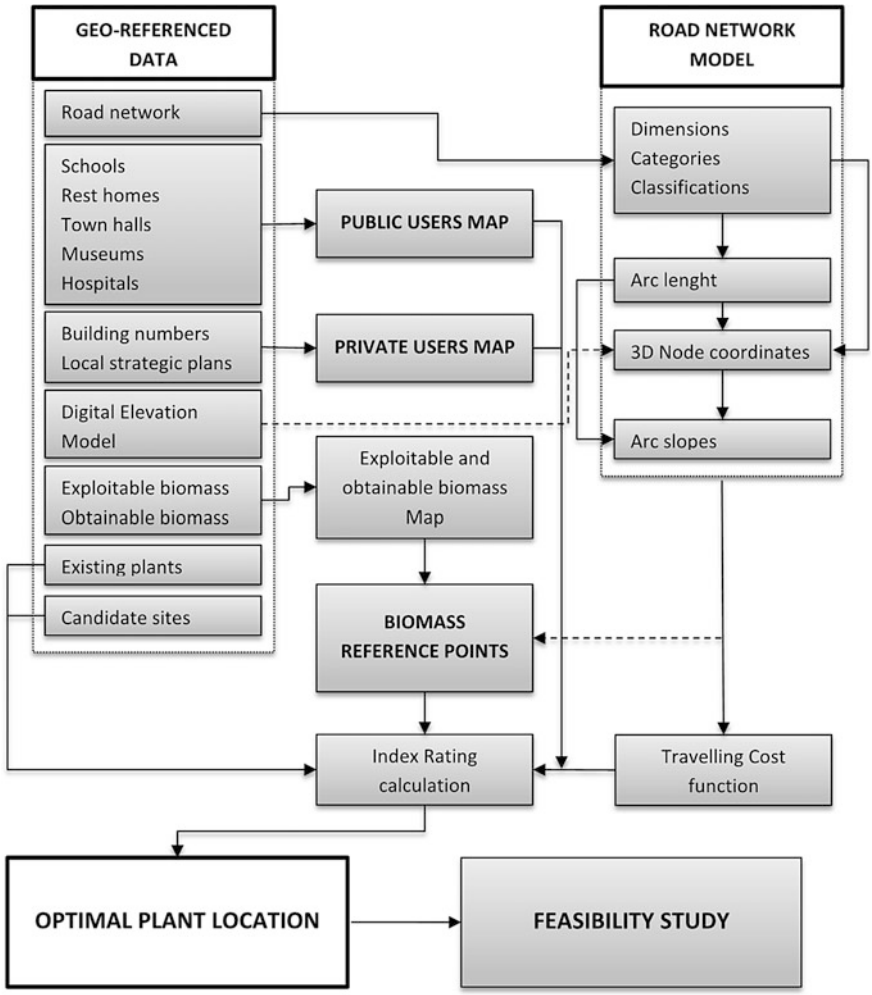

Fig. 1 Conceptual framework of the study

2 Study Area

The area object of this study is the Carnia Mountain Community, an association of 28 Municipalities located in North-East Italy. Carnia is an historical and geographical region of the Friuli Venezia Giulia Region; it includes all of the Carnic Alps, in the northwestern part of the Region. The dominant landscape is alpine, characterized by the alternation of high mountains with valleys shaped by Quaternary glaciation. The Carnia area has a heterogeneous morphology, due to the simultaneous presence of carbonate and other geological formations (Del Favero et al.1998). In the study area,

the forest has an extension of 810 km^2 over 1.221 km^2: this means a forest coverage rate of 67.5%. For this reason, the Mountain Community is promoting the use of wood biomass, with actions designed to increase the quality of production, improve logistics and facilitate the supply of raw materials. Major investments and other incentives have led to the creation of seven biomass plants, fueled with wood chips for heating and, in the case of the Arta Terme plant, capable of electrical energy production. According to the studies made by the Mountain Community of Carnia, all these investments made to promote the energy use of biomass will be amortized from the energy sales revenues. According to the energy plan of the average production of biomass potential from complementary retractable forest biomass (type of biomass for which the ordinary intervention is cost-effective) is 15.906 m^3 corresponding to 13.800 t/year (Marchesin and Vlaich 2005).

According to the Carnia Energy Plan, the already existing wood biomass thermal plants use 6.630 t/year of wood chips and a great part of the timber needed is currently being imported from outside the Region. The exploitation of forest biomass for energy production thus has a great potential.

3 Input Data

This study has taken into account a wide variety of geo-referenced data describing the spatial distribution of the variables needed for the definition of bio-energetic basin.

First it is necessary to define the energy demand, i.e. to identify who are the users, both public (schools, hospitals, etc.) and private (civil homes, industrial facilities, etc.), that may profit from the district heating network or the electric energy production. It is also necessary to define the quantity of energy supply available in the Carnia territory from wood biomass exploitation and how it is spatially distributed. In order to assess the feasibility of the supply chain it is essential to have a complete information on road conditions in Carnia, with a major focus on forest viability. The location of the already existing (or already planned) thermal and power plants should be also taken into account, as their presence can adversely affect the construction of a new power plant.

Another analysis hypothesis is the conversion of some abandoned buildings belonging to the Carnia Mountain Community.

In the past the Carnia Mountain Community has commissioned some studies to obtain an accurate evaluation of forest biomass available for energy purposes; in particular, a study from 2005 (Marchesin and Vlaich 2005) has analyzed the potential production of biomass from the forest. The study estimates a quantity of biomass of 15.906 m^3 which, in terms of weight, corresponds to approximately 13.800 t/year.

For this study, one of the key factors is the knowledge of the Carnia road network characteristics, in order to create an accurate supply chain model.

The Mountain Community has provided an updated and extended vector data of Carnia road network, from which many different types of information can be

extracted. Each road section is identified by its name, is classified according to the type of road (forest, urban, primary, etc.) and has some additional attributes, like arc length. Starting from this geographical information layer, a more complex arc-node road network model was obtained, in order to make advanced GIS network analysis. The model includes new attributes, calculated using GIS and DBMS tools: arc lengths, nodes coordinates, arc slopes and travelling cost.

As a source of wood biomass, the biomass resulting from the waste of primary and secondary processing wood industries has also been considered. In Carnia, the available amount of wood biomass from the compartment of the timber is estimated to be around 7.378 t/year.

As candidate locations for the new biomass power plant, a number of abandoning sites property of the Mountain Community were taken into account, focusing on their reuse. The candidate sites need to present suitable characteristics, as an adequate area extension and arrangement, a good connection to the transport network and the absence of activities.

4 GIS and DBMS Data Processing

The analysis of the geo-referenced data for the localization of a new thermal power plant site has been carried out using various GIS and DBMS open-source tools, the most notables being Quantum GIS (http://www.qgis.org), GRASS GIS (https://grass.osgeo.org) and PostGIS (http://www.postgis.net).

First, all the various data have been homogenized, and grouped into three categories: data about energy demand (public and private users), those concerning energy supply (forest biomass and industrial waste) and those related to the road network. All those georeferenced information layers—except the road network and the biomass polygons—were treated as (and, where necessary, converted to) point features. By estimating a travelling cost and connecting it to the road arcs, the road network has been split in cost isolines (lines with the same travelling cost, calculated from a starting point) for each candidate site. A spatial query based on those cost isolines allowed to compute a rating coefficient for every candidate site.

With regard to public utilities, the following categories have been taken into account: town halls, schools, museums, rest homes and hospitals. Each of these categories has been provided by the Mountain Community of Carnia in the form of points belonging to a shapefile; all those layers have been merged into a single shapefile using SQL query. The spatial points representing the house numbers (for population density estimation) have been grouped for each hamlet, in order to simplify the spatial analysis operations. To define the industrial users, the areas designated for industrial uses has been extracted from the town plans of Carnia municipalities. A structured query provided the substitution of the polygons with their centroids, with the PostGIS ST_Centroid function.

The biomass available for energy purposes in the Carnia territory comes from two primary sources: the forest biomass and wood waste products from the wood

processing companies. A polygon layer containing, as an attribute, the yearly amount of obtainable forest biomass represents the first energy source. Performing a GIS spatial intersection between this vector file and another polygon layer representing the wooded area accessible through the forest roads (which is the result of a dynamic buffer depending from road and territory characteristics (Pizzolito 2010)) a new polygon layer has been generated, representing the annual biomass amount actually obtainable through the forest road network. Starting from this vector file, composed of polygons representing the specific annual quantity of accessible biomass, a new layer was obtained, composed by a set of points, each of them located on a forest road arc and representing the starting points of the supply chain, the ending point being the (hypothetical) biomass power plant. Each one of this point had to be unique for every road arc and every wood polygon. In other words, the goal was to avoid to have more than one point belonging to the same forest polygon or falling on the same road arc. This has been obtained with a structured SQL query, performed with PostGIS. In this way the resulting layer was composed by 411 points, each of them representing the areas of obtainable and accessible biomass, directly linked with the road network.

For the creation of the road network model, the first step was to eliminate all those unnecessary elements, like highway and private roads. The goal is to keep only the most suitable roads for vehicular traffic types of trucks of the logging companies from skidding areas to potential positioning of the power plant sites. It is clear that considering more road types can only slow down the network analysis processes. The next step was to remove the sets of roads not connected to the main Carnia network, as not relevant to the search.

The obtained vector layer has been imported in GRASS GIS for further network analysis, using the Directed Graph Library (DGLib) written by Roberto Micarelli [9]. GRASS network analysis is based on graph theory; a graph is defined as a finite set of logical connections between objects, called vertices. Nodes represent the vertices, and arcs represent the connections between them, with a defined travel direction. For each node, line and travel direction, a different traveling cost can be assumed. Once imported, the vector file has been cleaned from topological errors (v.clean command) and has been prepared for the network analysis (v.net and v.category commands).

Slope is one of the main factors to be considered (especially for forest roads) for the calculation of the travelling cost of each road segment. In this study, the slope has been estimated using the following formula:

$$p_i = \frac{z_{i,2} - z_{i,1}}{L_i} \cdot 100$$

where p_i is the average slope percentage, $z_{i,1}$, $z_{i,2}$ denote vertex elevations and L_i is the length of the i-th arc. In order to apply this formula the length and the three-dimensional coordinates of it's the starting and ending vertices of each arc of the road graph have been calculated. The vertex elevations has been sampled directly (using the v.what.rast command) from a 20 meters DEM (Digital Elevation Model) covering the Friuli Venezia Giulia region. Because this slope value is averaged over the entire arc length, and due to the discretization imposed by the DEM raster format

(formed by 20 × 20 m square cells), the leading results can sometimes be not adherent to reality, requiring a manual intervention from the operator.

At the end of all these operations, a fully functional GRASS vector file representing the Carnia road graph has been obtained, with particular attention to the forest. This graph can serve as a decision-making tool in land use planning, thanks to the large number of information provided in the attribute table. The field of application can vary depending on the necessity, and it is subject to the choice of a criterion for traveling cost calculation. In this case study, the traveling cost has been defined as the time necessary to travel through the road arc, supposing a mean travelling speed (related to road class and slope).

5 Optimal Site Location Identification

The road network permits to evaluate, for every potential power plant site, the amount of annual obtainable biomass, the number of industries from which it is possible to obtain wood processing scraps, the number of possible public and private users, the presence of industrial target users, and the total power of all the interfering thermal power stations. This evaluation is carried out splitting the road graph into cost isolines (travelling time from the starting point—see an example in Fig. 2) and, by the use of a fixed distance buffer, running a spatial query on all the available spatial layers.

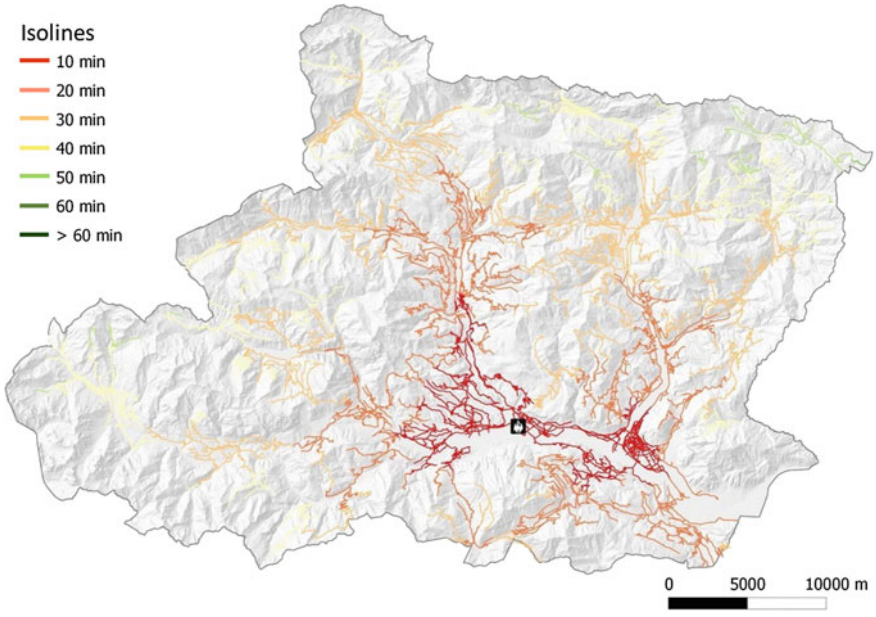

Fig. 2 Cost isolines for the "Ex Marconi" site

The results of this spatial query allow to implement a rating index for every potential plant location (Table 1), enabling an easier comparison between the sites and, therefore, the identification of the optimum one for a new biomass thermal plant location.

The site characterized by the best index is that of the already existing Arta Terme power plant, with a rating index of 8.0. This result confirms the correct choice of the plant's placement, one of the largest of the Friuli Venezia Giulia Region, and is an incentive to lower the proportion of wood fuel imported from abroad in favor of that directly produced in the Carnia area. This goal can only be reached through a strengthening of the short supply chain and its operators. The second ranked site is the "ex Marconi" site in Villa Santina, with a rating index of 7.6. This site looks like the best candidate for the construction of a new biomass power plant, thanks to its strategic location, in the center of the Carnia territory. It is located in an area rich in both public and private potential users and industrial activities, also equipped with good infrastructure connections.

6 Technical Feasibility of the Analyzed System Solution

On the ground of the results presented in the previous section, another study [9] has analyzed the feasibility and sustainability of the power plant implementation. In this study, the Authors carried out the design of a cogeneration plant and district-heating network serving the thermal loads, the economic evaluation of the investment among the other alternatives and, finally, the environmental sustainability of the cogeneration plant and the district heating network compared to conventional systems.

The design of the thermal plant considered the need of a public and private buildings district heating, with 30 W/m thermal load demand evaluation. The project outside temperature is −12 °C (winter season), with 200 days per year of winter heating (considering a 24/24 operativity), thus resulting in a total of 5.200 h of annual heating. The calculated energy required is 28.5 MWt, and the expected energy required is estimated to be 23.6 MWt. Based on outside temperature variation, operative hours of the plant and energy demand variation, the plant's graph of the duration curve of energy demand vs operative hours has been elaborated.

In conclusion, the technical feasibility evaluation has designed a cogeneration plant with steam turbine, with an estimated power of 4 Mwt. The integration and reserve plant is composed of 3 heat generators, 10 Mwt each, with 5.031 h of expected functioning time and a gross power supply of 12.501 Mwh. Other designing variables are: 90 °C input water heat, 70 °C output water heat, 14.144 meters city network length, 400 mm first pipe diameter, a network load loss of 723.7 kPa, 10.018 t/year of wood biomass consumption and 1.254.281 Nm^3 of natural gas consumption.

After the technical feasibility evaluation, the Authors have carried on the economic feasibility evaluation of the plant, using a NPV (Net Present Value)

Table 1 Rating indices for the candidate sites

	Candidate site								
Index	**Arta terme**	**Ex marconi**	**Ex RSU**	**Treppo carnico**	**Verzegnis**	**Ampezzo**	**Forni avoltri**	**Forni di sopra**	**Sauris**
Reachable forest biomass	9.1	9.3	7.0	8.5	5.6	7.3	7.1	3.0	3.7
Wood industries	8.7	9.6	10.0	4.2	7.9	5.5	2.1	1.5	0.6
Private users	6.0	6.2	6.3	10.0	5.4	3.6	1.8	0.7	0.5
Industrial users	8.0	10.0	9.3	4.0	7.8	4.8	4.5	1.0	1.3
Public users	8.6	9.3	10.0	6.3	7.2	5.8	2.4	0.6	1.6
Competition with other plants	7.4	1.0	0.0	2.6	1.3	7.9	9.0	10.0	9.2
Rating	**8.0**	**7.6**	**7.1**	**5.9**	**5.9**	**5.8**	**4.5**	**2.8**	**2.8**

methodology. The result is a negative present value of 8.157.512 €, with a 10 years amortization schedule.

Finally, the environmental sustainability of the whole project has been evaluated using the Life Cycle Assessment (ISO 14040, ISO 14044) methodology. The study confronts the annual CO_2 emitted by the designed plant and a traditional gas system. Using the designed plant and network system, 5.873,2 tCO_2/year of annual emission can be potentially saved.

7 Conclusions

The theme of energy, its production and consumption is essential in the definition of any plan or environmental policy; in particular, in recent times the focus has increasingly concentrated on the production of energy from renewable sources. Among all the different types of renewable sources, biomass plays an important role, thanks to its extensive and homogeneous distribution in the territory object of the study. Despite in Carnia the wood area extension is 72655.38 ha, there is forest under-utilization, lack of forest management and wood accumulation.

For this reason, the Carnia Mountain Community launched a policy for the revival of the mountain by activating an integrated system that promotes the use of biomass, with actions designed to increase the quality of production, improve logistics and facilitate the supply of raw materials. These actions have led to the creation of seven biomass plants fueled with wood chips that provide district heating and, in one case, electrical energy production.

In addition to the existing seven power plants, this study has identified, using GIS applications and open source DBMS, the optimal placement of an additional power plant for district heating/cogeneration powered by solid biofuel (wood biomass).

The implementation of all the available georeferenced data in a GIS road graph tool has led to the development of a rating value for every candidate location, allowing a direct comparison between all the sub-optimum possible sites. This confrontation found that the optimum location of a new thermal power plant using wood is the “Ex Marconi” site, an industrial warehouse in Villa Santina (UD).

Following the identification of the optimal power plant location, technical and economic feasibility and environmental sustainability have been analyzed. The methodology, proposed in detail in another paper (Blazek et al. 2002), allows to test different cogeneration plant localizations as identified above. The results of this feasibility and sustainability test show that all the considered alternatives have technical feasibility and permissible environmental sustainability. The economic feasibility permits to identify the globally acceptable solution, if an investor takes the risk of getting profits only after the tenth year of the realization of the cogeneration plant with the associated district heating network in the municipality of Villa Santina.

The obtained results demonstrate that Geographic Information Systems are a powerful and flexible tool for the study and the analysis of the optimal location of strategic facilities, and in particular of biomass fueled power plants. The use of open-source software, easy accessible but at the same time bringing advanced features, allows to achieve these objectives without direct cost by the user, an important factor in enabling the deployment and use of these applications in the Public Administration.

Concluding, the whole methodology presented in this paper and in (Cefalo et al. 2016) could be easily applied to analogous situations and similar geographical contexts.

References

United Nations (1998) Kyoto protocol to the United Nations framework convention on climate change

Frombo F, Minciardi R, Robba M, Rosso F, Sacile R (2009) Planning woody biomass logistics for energy production: a strategic decision model. Biomass Bioenerg 33:372–383

Ivalsa (2007) Linee guida per lo sviluppo di un modello di utilizzo del cippato forestale a fini energetici. Progetto Sviluppo della filiera foresta-legno-energia attraverso il rafforzamento dell'associazionismo forestale

Chiopris G (2006) La produzione potenziale di energia da biomasse della foresta del Friuli Venezia Giulia. In atti e contributi del convegno: Valorizzazione energetica delle risorse forestali della montagna del Friuli Venezia Giulia. Tarcento, 29 aprile

Comunita Montana Della Carnia, (2011) Relazione della Carta dei valori della Carnia. Servizi di elaborazione della Carta dei Valori della Carnia necessaria per l'azione pilota di pianificazione di Area Vasta prevista dal progetto SUSPLAN Pianificazione sostenibile in aree montane, finanziato nell'ambito del Programma Interreg IV Italia Austria 2007–2013

Del Favero R, Poldini L, Bortoli PL, Dreossi G, Lasen C, Vanone G (1998) La vegetazione forestale e la selvicoltura nella regione FVG. Regione Autonoma FVG, Direzione regionale delle foreste, Servizio della Selvicoltura, Udine

Marchesin M, Vlaich M (2005) Pianificazione delle biomasse forestali della Comunità Montana della Carnia

Pizzolito E (2010) Cartografia a supporto dell'indagine territoriale in materia di bioedilizia per il teritorio carnico. Relazione tecnica. Convenzione Metodi per il monitoraggio ambientale e la pianificazione equilibrata e sostenibile del territorio e dell'ambiente urbano: progettazione e redazione della cartografia a supporto dell'indagine territoriale in materia di bioedilizia

Blazek R, Neteler M, Micarelli R (2002) The new GRASS 5.1 vector architecture. Open source GIS—GRASS users conference 2002, Trento, Italy, 11–13 Sept 2002. University of Trento, Italy, 2002

Cefalo R, Grazioli A, Pozzetto D, Alvarez Serrano YM, Tommasi A (2016) Comparative analysis of technical, economical and environmental feasibility of cogeneration plant using wood biomass. 25th Expert Meeting Komunalna Energetika/Power Engineering, Maribor

Geography of WWI Sites Along the Italian Front by Means of GIS Tools

Paolo Plini, Sabina Di Franco and Rosamaria Salvatori

Abstract In the framework of the commemorations for the First World War, a GIS project was started in order to identify, archive and disseminate the places involved by the war along the Italian front. The GIS operates through a set of raster layers represented by more than 500 raster maps and a set of vector layers dealing with places, catchment basins, front lines, deployment areas. Particular attention has been paid to all the occurrences of place names in order to univocally associate one place name to a set of geographic coordinates, thus creating a specific geodatabase. An online GIS version is available for data search and visualization.

Keywords WWI · GIS · Online GIS · Geographical terminology · Geodatabase

1 Introduction

The memory of historical events and the geographical knowledge linked to those events is quite often connected only to the most relevant among them and there is still a sort of "gap" to fill (Baker 2003); year after year a lot of information vanishes leaving only a trace of the most meaningful places, the so called places of memory that help to anchor collective memories. In the framework of WWI commemorations a renewed interest arose for that places in Italy where the First World War was fought from May 1915 until November 1918, located in a large area including the north-east of Italy, part of the present Austrian and Slovenian Republics and a portion of the French former administrative regions of Lorraine, Champagne-Ardenne and Picardie. Only a few number of places where the fate of the war was decided have been raised to national symbols, while most of the other places simply disappeared from the collective memory leaving a trace only within restricted communities of local experts and researchers.

P. Plini (✉) · S. Di Franco · R. Salvatori
Italian National Research Council, Institute for Atmospheric Pollution Research, Via Salaria km 29.300, 00015 Monterotondo Stazione, RM, Italy
e-mail: paolo.plini@cnr.it

R. Cefalo et al. (eds.), *New Advanced GNSS and 3D Spatial Techniques*,
Lecture Notes in Geoinformation and Cartography,
DOI 10.1007/978-3-319-56218-6_18

Geo-information plays a relevant role to preserve memories and to improve historical knowledge through geographical information (Gregory et al. 2007). It could also enhance the comprehension of strategy, tactics and logistics helping to understand the trend of war events.

WWI historical-geographical studies are still mostly performed consulting textual documents and maps edited without using computer technology, by different authors in different languages and in different times. A validation of geographical content appears mandatory, in order to identify a specific place and its name on the modern official cartography. In fact the huge amount of potential historical-geographical information that can be retrieved on the web is, most of the times, not so straightforward to discover and compare to "present" geographical location.

Even if modern times brought new techniques for the production of maps, global positioning systems, geolocalization, geodatabases, GIS and online GIS, etc. quite often there is a lack of connection with other technologies for the dissemination of historical-geographical information. All those tools and techniques represent undoubtedly an advantage even if the complete automatization could create the risk to lose information. In wider terms, dealing with geographical information i.e. searching for historical places is still a complex task, especially taking into consideration the chronological distance from the facts and the heterogeneity of the textual and cartographic sources, as well as not having a proper digital corpus or a local gazetteer, a geographical dictionary that can be accessed and searched on-line and is a valuable resource for the automatic search of toponyms (Goodchild and Hill 2008; Zhu et al. 2016).

In this perspective an Italian National Research Council (CNR) research project was carried on aiming at developing a Geographic Information System (GIS) to collect and preserve the information about the places where the Italian Army was involved in WWI events, making available this set of information for further uses.

The CNR goal was to build a system where the historical information coming from documents is treated in order to extract the geographical information and store it in different layers taking into account the multitemporal perspective.

Lacking a proper local gazetteer, the search of places, whose names were extracted directly from text and old maps, and their identification on official maps was one of the major issues that arose during this study. Particularly challenging was the search for a correspondence between each name and its position. This particular task made difficult to find in present maps the traces of places destroyed, renamed or nowadays located in different nations and since the present cartography has changed it is also difficult to contextualize the historical events.

2 Documents and Cartography

The collection of WWI geographical data was performed by manually extracting the information from more than two hundred printed and online documents. All these documents, published from 1915 to nowadays, have a very abundant even if heterogeneous content and quite often they lack in geographic accuracy both in term of textual information and map availability.

Twenty-one 1:100,000 sheets of the first Italian national territorial representation (1876–1900) were used. Those maps were referred to the Bessel ellipsoid oriented to the Navy Hydrographic Institute in Genua and compiled according to a poly-centric natural Samson-Flamsteed projection.

Another useful set of maps is represented by the twenty-four 1:100,000 sheets of the "Grande Carta della Guerra Italiana", edited in 1915 by the Italian Touring Club and based on the cartographic products of the Italian Military Geographic Institute.

Thirty-three sheets of the Austro-Hungarian 1:75,000 cartography were used, the so called Spezialkarte der Österreichisch-Ungarischen Monarchie compiled by the K.u.K. Militärgeographisches Institut, completed in 1890 with further integrations dated 1894, that adopted a polyhedral projection referred to Bessel ellipsoid and organized into zones and columns totaling 1060 sheets.

In addition to this official cartography, more than four hundred maps, drawings and sketches edited from the war period to present times and available in digital or printed formats were collected and used to support the research.

Once acquired in digital format in order to made it usable into the GIS this material created very often difficulties due to lacking information concerning scales, projection, North position. This implied a specific work in order to harmonize different coordinate reference systems and scales, referring the whole dataset to the GIS project's reference WGS84 system.

The cartographic base adopted for the GIS project is represented for the Italian territory by the official cartography WGS84/UTM32 N of the Italian Military Geographic Institute (I.G.M.), scale 1:25,000 and for the Slovenian territory by the official Slovenian cartography ETRS89 D96/TM in scale 1:50.000, rescaled.

Within the GIS both the official Italian and Slovenian maps and other useful material such as aerial photos of the Italian territory are accessed through Web Map Service (WMS) from the National Geo-portal. This approach allows to dynamically display raster maps coherent with the adopted projection system.

Being an historical GIS focused on documentary evidence and heterogeneous material, we decided to work within a range of accuracy sufficient to provide univocal information about a certain place (http://www.port.ac.uk/research/gbhgis/aboutthegbhistoricalgis/).

3 GIS and the Geodatabase

In order to handle the collected WWI geographical data, a Geographical Information System (GIS) was implemented to guarantee an accurate positioning of every site, in each and every case. The project has been designed using open sources tools that ensure the availability of a free source code that could be downloaded and updated by the community of users. On the GIS side QGIS -the official project of the Open Source Geospatial Foundation—has been used.

The database of national administrative borders (http://www.gadm.org/country) was downloaded as well as the OpenStreetMap database of places (Haklay and Weber 2008) referred to Italy, Slovenia, Austria and France (http://download.geofabrik.de/). The resulting raw geodatabase contained around 70,000 records, each one having its unique geographical coordinates. Data were organized mainly in point layers even if a limited use of line and polygon layers are represented into the system. Lines and polygon layers were necessary to draw changes of the front line during the war, drainage basins and the national, regional and municipal borders.

The geodatabase was filtered and modified in order to handle all the relevant information, both geographical and historical and to identify WWI place names (Jordan 2009) in the text. In particular in the database some additional columns were created dealing with administrative geography (province, region, state), physical geography (altitude) and history (name of the place during the war, typology and occurrence into official documents).

In addition, the different terminological occurrences (toponym) of WWI place names and the linguistic equivalents in French, German and Slovenian were collected in order to ease the queries performed through the use of an online GIS.

At the end of this process the correct name and its terminological variants are inserted in the WWI geodatabase.

This approach allowed also to highlight the terminological issues related to different forms of geographical names such as use, language, translation, and meaning. Identification of different terminological variants is crucial to ensure accuracy and exactitude which are both key factors to obtain a fully searchable and acceptable geographic information.

The work of harmonization of toponyms, coming from different sources and having different typology, and their geographical coordinates leads, as a side effect, to the creation of a table specifically devoted to the handling of toponyms themselves (gazetteer).

The WWI geodatabase contains at the time of this paper 6600 identified WWI places. Places are categorized in order to distinguish their typology related to physical geography and civilian and military infrastructures (see Fig. 1). Out of these identified places more than 1600 present at least one and up to six different variants totaling more than 12,000 geographical alternative place names.

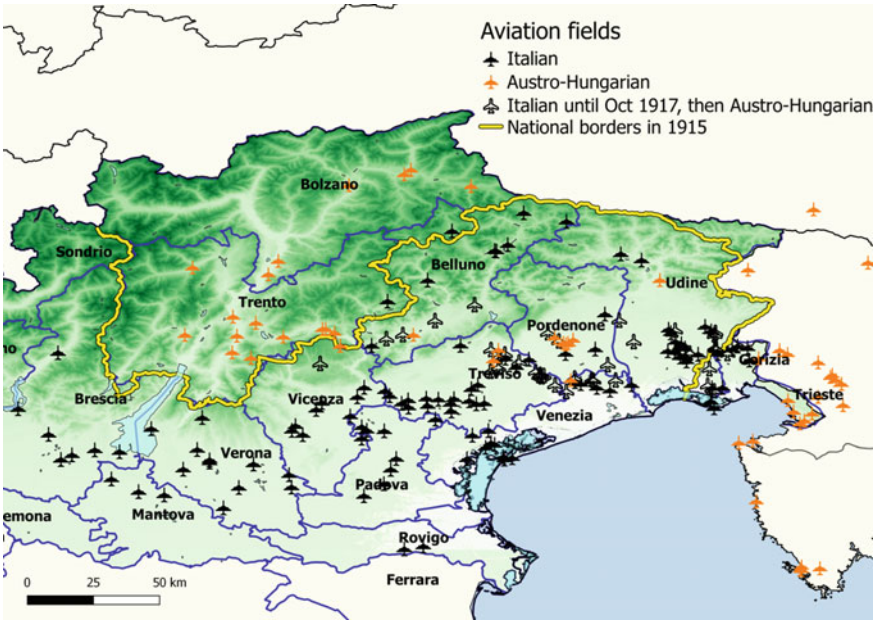

Fig. 1 The border between the Kingdom of Italy and the Austro-Hungarian Empire in 1915 and the aviation fields of both Armies as extracted using a specific query in QGIS, overlapped on a digital elevation model

4 Online GIS

Once reached a satisfactory number of identified places, the development of an online version of GIS was started. Concerning the software to publish spatial data MapServer for Windows 3.0.6 was adopted and the p.mapper 4.3.2 framework was used to set up a MapServer application based on PHP/MapScript.

Visualizations are generated in real time by the server. The user is provided with a set of navigation tools, according to the area to display it is possible to zoom in/out, increase or decrease the layer transparency and switch on/off the different layers. The search function is available on the places' names. Since the geodatabase contains all the available versions of a place name, including variants and equivalents in French, German and Slovenian, it is possible to perform queries using all these forms. The system answers to the queries positioning itself on the area containing the results. If more than one place comes as a result (homonyms) the displayed area includes both results.

The internal search engine is configured in order to accept also part of a name in upper- or lowercase.

Within the online GIS the following materials have been used:

Vector layers referring to places, water catchment, airports, different front lines from 1915 to the end of the war, etc.

Raster layers including some of the ancient maps used for the GIS and the digital elevation model from the Shuttle Radar Topographic Mission.

WMS data including I.G.M. cartography, aerial photographs and OpenStreetMap data

5 Results and Conclusions

Such a research project dealing with the detailed identification and characterization of places linked to WWI events is pretty unique on the international scenario. The work does not take the cue uniquely from official documents whereas it was conducted analyzing an heterogeneous collection of texts and maps.

While collecting the WWI place names, it has been realized that quite often the name of one place was not univocally linked to geographic coordinates and one name not always led to one place.

The analysis of the collected data made it possible to harmonize historical, linguistic and geographical knowledge. This procedure ensured a very high coverage in terms of identified places and a very good coverage concerning their placement into the territory. Out of 6600 places found both in documents and maps only one hundred of them are still lacking of coordinates. The geographical/terminological component enriched the system with valuable hard-to-found information, usually disaggregated into a myriad of different textual and cartographic sources.

The analysis of names' variations produced as a result the creation and maintenance of a local specific gazetteer, where the above mentioned terms are listed, uniquely geolocalised and made available on the web through an online GIS (http://webgis.iia.cnr.it/GGGIS/).

The gazetteer of place names on WWI along the Italian front being one of the products of the research serves as a basis for the online GIS. The place names in this gazetteer are linked to geographical information in such a way that to each name now corresponds one and only one place and the name itself could be used while performing queries providing univocal and unambiguous results.

The analysis of the terminological forms of toponyms represents a huge improvement leading to a better, easier and more effective geographical search. In this work terminological variants usually representing an obstacle during the search since they produce a noise level incompatible with the commonest tools such as search engines, provide an extra value and an additional element to achieve positive results.

After a two-year's work the online GIS appears as an effective tool able to provide precise noise-free and geographically coherent results. If compared with the pre-existing situation, it represents a turning point, able to contain all the collected information, organizing it in a normalized format and allowing a controlled but flexible use.

Each one of the 6600 places currently available is endowed with historical and geographic additional information. This number will surely increase in future but it is sufficient to demonstrate how the territory was influenced by WWI even if in some cases the only remnant of a place is represented by its name.

Acknowledgements The research is being performed in the framework of the activities carried on to commemorate the WWI centenary and is supported by the Italian Presidency of the Council of Ministers (http://www.centenario1914-1918.it/it/2014/04/21/sentiero-della-pace-il-progetto-cartografico).

References

Baker ARH (2003) Geography and history: bridging the divide. Cambridge University Press, Cambridge

Goodchild MF, Hill LL (2008) Introduction to digital gazetteer research. Int J Geogr Inf Sci 22 (10):1039–1044. doi:10.1080/13658810701850497

Gregory IN, Healey RG, Historical GIS (2007) structuring, mapping and analysing geographies of the past. Prog Hum Geogr 31(5):638–653

Haklay M, Weber P (2008) Open street map: user generated street maps. IEEE Pervasive Comput 7(4):12–18

Jordan P (2009) Some considerations on the function of place names on maps. In: ICC proceedings. http://icaci.org/files/documents/ICC_proceedings/ICC2009/html/nonref/12_2.pdf. Accessed 27 Sept 2016

Zhu R, Hu Y, Janowicz K, McKenzie G (2016) Spatial signatures for geographic feature types: examining gazetteer ontologies using spatial statistics. Trans in GIS 20:333–355. doi:10.1111/tgis.12232

A Comparison of Low-Poly Algorithms for Sharing 3D Models on the Web

Grazia Caradonna, Simona Lionetti, Eufemia Tarantino and Cesare Verdoscia

Abstract In recent years, the rising popularity of 3D models in the field of Cultural Heritage has brought additional geo-spatial formats for its documentation, making necessary to test new approaches in managing, publishing and studying heterogeneous data in an integrated way. Nowadays several computer applications and IT instruments are available for the management of cultural, archaeological and environmental heritages. The large size and complex nature of data makes it difficult for heritage experts to manage them for run more complex spatial analyses. Furthermore, it is also more difficult for citizens to access 3D models aimed at tourism and education. In this paper, we analyze recent low-poly methods aimed at reducing the size and complexity of 3D models applied to the case study of an historical building of Bari (Italy). The main idea is to create simple geometries (through low-poly algorithms) to significantly reduce the number of polygons in the reality-based environment and publish the model on the web. After the comparative evaluation of different low-poly algorithms and the generation of a test model, a PostgreSQL DBMS and a front-end PHP interface were developed to allow users to analyze and query the model.

Keywords 3D models · Low-poly algorithms · Architectural heritages

G. Caradonna · S. Lionetti · E. Tarantino (✉) · C. Verdoscia
Politecnico di Bari, Via Orabona 4, 70125 Bari, Italy
e-mail: eufemia.tarantino@poliba.it

G. Caradonna
e-mail: grazia.caradonna@poliba.it

C. Verdoscia
e-mail: cesare.verdoscia@poliba.it

R. Cefalo et al. (eds.), *New Advanced GNSS and 3D Spatial Techniques*,
Lecture Notes in Geoinformation and Cartography,
DOI 10.1007/978-3-319-56218-6_19

1 Introduction

Digital 3D models are used in almost all areas of design and engineering through architectural design optimization techniques. With the advent of new imaging technologies (e.g., advanced proximal sensing systems and consumer 3D cameras), we can now capture models that are both deep and broad in detail (Lu et al. 2016). The displayed 3D object can be either an entity in the real and fantasy world as well. However, creating large-scale models is both challenging and labour intensive. The steps of topographic survey for the development of a 3D representation of cultural heritage are often also very expensive. Furthermore, the enormous number of points and polygons involved are easier to manage through stand-alone software. A 3D model is divided in two categories, one is a solid, and the other is a shell (Galyean 1991). The solid model is more realistic, but also more difficult to build, while the model of a shell is a polyhedral object like a thin eggshell, which represents the object's boundary but not its volume (Liu et al. 2016). When a 3D model is created, a set of points is used to represent the shape. Lines connect these points to form the wireframe and a polygon mesh, which is a collection of vertices, edges and faces, defines the model shape. Nowadays, 3D models are reduced through low-poly algorithms, although similar algorithms have been studied for years. De Carlo et al. (2002) and Wen et al. (2006) generated images into sketch style with bold edges and large areas of constant colour. Olsen and Winnemöller (2006) used a bilateral filter to produce abstract images. Chen et al. (2014) proposed a method to generate stylish images with polygons by Voronoi Tessellation, which look quite like the results of a low-poly style. The purpose of this non-photorealistic rendering is similar, i.e. to render the images into a more abstract result without losing main information such as shape and colour. As for low-poly image rendering, the main difficulty lies in preserving shape and colour information with limited triangles. The polygon mesh is divided into different number of triangles. Generally, a large part of triangles in a polygon makes the shape of a model more detailed but also takes more rendering time. To decrease rending times or to increase frame rate, it is necessary to reduce the number of triangles in the scene. Therefore, low poly is needed for a polygon mesh (Murdock 2012). 3D computer graphics software packages allow users to create models and change mesh of models by adding, subtracting, stretching or re-shaping, according to user needs. Such software can also display a model from a variety of angles at once, and usually its view can be zoomed, rotated, or translated. Most modelling software packages support many different model formats to be imported in other applications for further processing. Currently, the most popular 3D computer graphics software programs in the world include 3ds Max, cinema4D, etc. (Liu et al. 2016; Do and Lee 2010). The 3ds Max, which is formerly known as 3D Studio, was originally released in 1990 for the DOS platform. However, Autodesk's 3D Studio showed its powerful features and stability. Web-based visualization is becoming important in cultural heritage to communicate the results of a project and involve people (Pecchioli et al. 2012; Scianna and Gristina 2016). The usage of this technology can support the objective

of "preventive conservation" of artefacts and diffuse their important historical value using Internet. Recent developments in techniques for modelling, digitizing and visualizing 3D shapes have led to a boom in the number of 3D models available on the Internet and in domain-specific databases. This has led to the development of 3D shape retrieval systems that, given a query object, can retrieve similar 3D objects. For visualization aims, 3D shapes are often represented as a surface, i.e. polygonal meshes, for example in VRML (Virtual Reality Modelling Language) format. These models often contain holes and not enclose with precisely. On the contrary, 3D volume models, such as solid models produced by CAD (Computer Aided Design) systems, or voxels models, enclose a volume properly (Tarantino and Figorito 2011). Therefore, users who want to work with content of distributed databases in the Web need retrieval and visualization methods with special requirements of distributed environments and heterogeneous content (Caradonna et al. 2015; Caradonna et al. 2016). The ability to use content-based retrieval techniques for complex data, like 3D geometry or images, is important when the information provided by metadata is not sufficient or the production of additional metadata is too expensive or not possible at all. Critical problems to be solved include speeding-up the retrieval process, improving the quality of search results using relevance feedback given by the user and reducing the amount of transmitted data needed for the retrieval process (Loffler 2000). However, in delivering 3D models we are faced with a dilemma between narrow network bandwidths and the large volumes of the spatial data sets to be delivered (Yang et al. 2007). To overcome such dilemma, one solution is to implement some algorithms to generate a model version using fewer polygons that look reasonably like the original (Melax 1998). This paper compares algorithms for generating low poly rendering of images related to the case study of the "ex Palazzo della Motta" skyscraper of Bari (Apulia region, Italy). The comparison will be useful for choosing the best performing algorithm to reduce a model and furtherly publish it on the web.

2 The Case Study

The case of study described in this paper is a building known as "Ex Palazzo della Motta" (i.e. the building previously known as Palazzo Motta), one of the oldest buildings in the "Borgo Murattiano" district of Bari, currently home to Apulia administrative offices and characterised by a variety of interesting architectures. The building was first established in 1813 and reworked until 1955. Its site was the starting point for the development of the modern city of Bari and its grid plan. For many years, the building housed a large and popular café called "Bar Motta" and for this reason, it was nicknamed "Palazzo Motta", becoming a meeting point for local citizens (Fig. 1).

Fig. 1 Old pictures of "Palazzo Motta 1955"

3 Method

One of the features of the detailed model of a complex heritage structure is the large number of polygons in a small area. This is very time-consuming for the hardware (on the PC platform) in terms of real-time rendering, which results in an unsatisfactory frame rate. For this purpose, the model needs to be fragmented into logical and smaller elements to be adapted to culling methods. Moreover, the mesh must be optimized by removing duplicated and unwanted faces (Haval 2000; Guarnieri et al. 2010). The most widespread software currently used for 3D modelling includes 3D STUDIO MAX, BLENDER and MESHLAB. The algorithms "Optimize", "Multires" and "Subdivide" are present in 3D STUDIO MAX software. They perform a re-meshing of a model, by reducing the number of polygons and changing its geometry. The algorithms act on the threshold angle between the faces, which will be combined into a single surface. The degraded angles that could be created by the algorithms need to be eliminated. The main drawbacks in the use of this software package are the low level of object optimization, with loss of details, and the fact that it is not completely free. The simplification algorithm tested through the software BLENDER is "Decimate" using "Collada" as model format. When the algorithm is applied, the number of faces increases because all the squares are converted into triangles and each square is decomposed into two triangles. The Decimate modifier reduces the number of polygons of a mesh non-destructively decreasing the number of vertices/faces of a mesh with minimum changes of form. The Decimate modifier is a non-destructively method and can be done interactively and in safety. Even if the software package is free and produces realistic/physically accurate results, it has some major disadvantages: images contain some degree of

noise; flickering occurs between frames in animation; longer render times; low conversion format availability; more stress on the computer's CPU.

Figure 2 shows a view of the Low-poly model of "Palazzo della Motta" created through Blender software. The last open software tested in this study is MeshLab. This software features a mesh viewer application, where a 3D object stored in a variety of formats can be loaded and interactively inspected in an easy way, by simply dragging and clicking on the mesh itself. MeshLab supports an ever-growing variety of 3D formats (all the most common formats are supported) to accommodate the broadest range of users. First, the model was converted into one of the compatible formats available. Most of them demonstrated similar performances. In this case the.obj was chosen due to its file size of 11,338 kb with 97,424 faces of the created model. Three algorithms provided in the MeshLab package were tested on the chosen building: Vertex Clustering, Quadric error metrics and Marching cubes. In the Vertex Clustering algorithm, the clustering process determines a tie closeness of the vertices in the object space, and for those vertices found to be close to one another (which are likely to be mapped onto the same pixel), a new representative vertex is created to replace them (Low and Tan 1997). By applying this algorithm, the number of faces was reduced from 97,424 to 18,738 (Fig. 3).

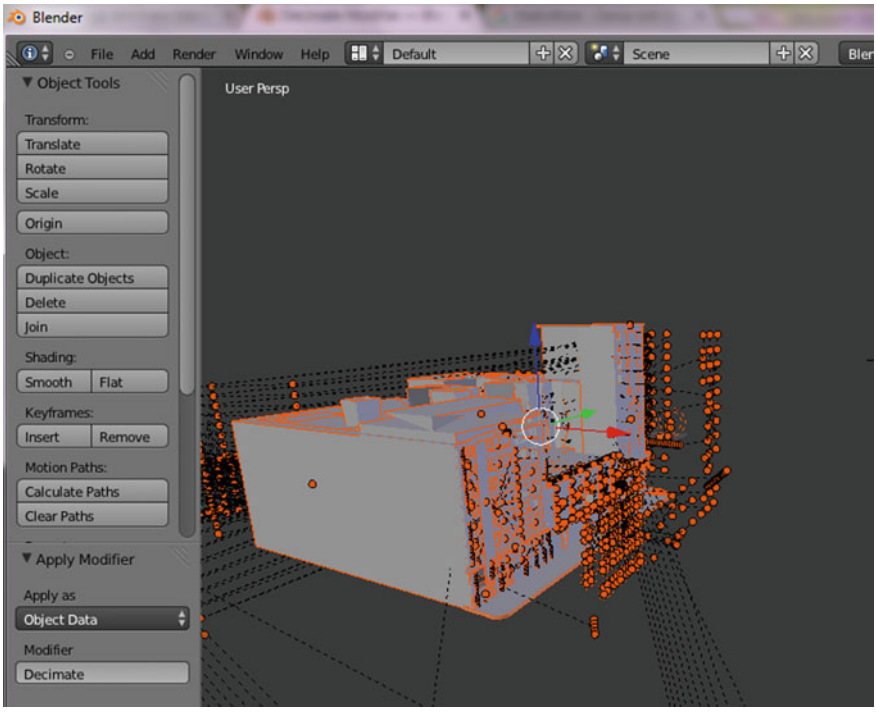

Fig. 2 Low-poly model of "Palazzo della Motta" created through BLENDER software

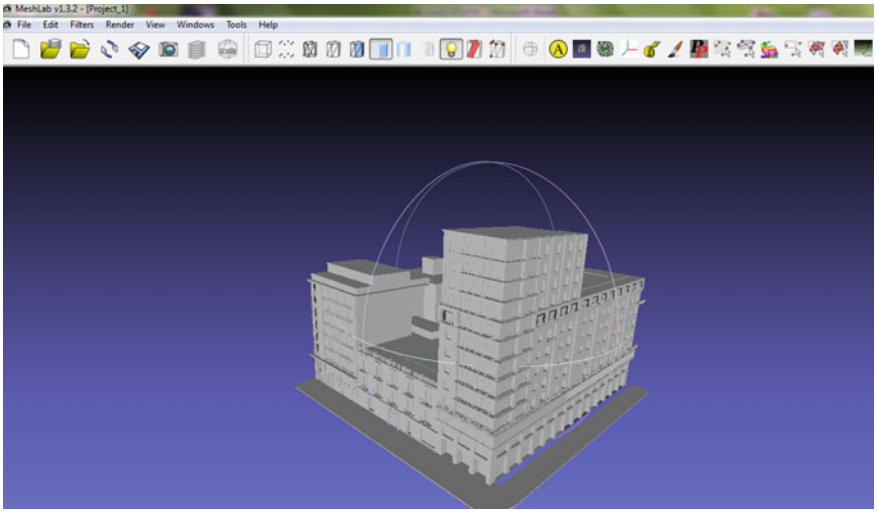

Fig. 3 Low-poly model of "Palazzo della Motta" created through MESHLAB software

The quadric error metrics algorithm produces high quality approximations of polygonal models. The algorithm uses iterative contractions of vertex pairs to simplify models and maintains surface error approximations using quadric matrices. It joins unconnected regions of models facilitating approximations, both visually and in terms of geometric error. To allow topological joining, our system also supports non-manifold surface models (Garland and Heckbert 1997). As the result of this reduction, faces were reduced from 97,424 to 9706, losing greatly in details. The marching cubes algorithm creates triangle models of constant density surfaces from 3D data (Lorensen 1987). The algorithm proceeds through the scalar field, taking eight neighbour locations at a time (thus forming an imaginary cube), then determining the polygon(s) needed to represent the part of the surface that passes through this cube. The individual polygons are then fused into the desired surface. Each vertex of the generated polygons is placed on the appropriate position along the cube's edge by linearly interpolating the two scalar values that are connected by that edge. Because of this reduction, faces were reduced from 97,424 to 57,400. Table 1 summarizes the results of the application of the three MeshLab algorithms. The Quadric error metrics algorithm shows the best results in terms of faces and size, even if the model after the reduction dramatically lost in details. The best

Table 1 Quantitative comparison of vertex clustering, quadric error metrics and marching cubes algorithms provided by MeshLab software

	Faces	Size (kb)
Origin (not reduced) file	97,424	11,338
Vertex-clustering	18,738	1885
Quadric error metrics	9706	1232
Marching cubes	57,400	4519

performance was observed by the Vertex clustering algorithm because the model was easy to manage and detailed at the same time.

4 Conclusions

This paper investigates the possibility of creating 3D models aimed at their further publishing on the web. Open software packages able to reduce 3D objects through low-poly algorithms without loss of significant details were preferred. We compared three software: 3D STUDIO MAX, BLENDER and MESHLAB. The latter proved its reliability for the above purposes and it is suitable for 3D modelling beginners because it is very user-friendly. Further studies are foreseen to test the management of 3D building models in open web systems.

References

Caradonna G, Figorito B, Tarantino E (2015) Sharing environmental geospatial data through an open source WebGIS. In: International conference on computational science and its applications. Springer, Berlin, pp 556–565

Caradonna G, Novelli A, Tarantino E, Cefalo R, Fratino U (2016) A WebGIS framework for disseminating processed remotely sensed on land cover transformations. Rep Geodesy Geoinf 100:27–38

Chen Z, Xiao Y, Cao J (2014) Approximation by piecewise polynomials on Voronoi tessellation. Graph Models 76:522–531

DeCarlo D, Santella A (2002) Stylization and abstraction of photographs. In: ACM transactions on graphics (TOG). ACM, pp 769–776

Do TV, Lee J-W (2010) 3darmodeler: a 3d modeling system in augmented reality environment. Int J Electr Comput Syst Eng 4:145–154

Galyean TA, Hughes JF (1991) Sculpting: an interactive volumetric modeling technique. In: ACM SIGGRAPH computer graphics. ACM, pp 267–274

Garland M, Heckbert PS (1997) Surface simplification using quadric error metrics. In: Proceedings of the 24th annual conference on computer graphics and interactive techniques. ACM Press/Addison-Wesley Publishing Co., pp 209–216

Guarnieri A, Pirotti F, Vettore A (2010) Cultural heritage interactive 3D models on the web: an approach using open source and free software. J Cult Heritage 11:350–353

Haval N (2000) Three-dimensional documentation of complex heritage structures. IEEE Multimedia 7:52–55

Liu T, Zhao D, Pan M (2016) An approach to 3D model fusion in GIS systems and its application in a future ECDIS. Comput Geosci 89:12–20

Loffler J (2000) Content-based retrieval of 3D models in distributed web databases by visual shape information. In: Information visualization. IEEE international conference on proceedings. IEEE, pp 82–87

Lorensen WE, Cline HE (1987) Marching cubes: a high resolution 3D surface construction algorithm. In: ACM siggraph computer graphics. ACM, pp 163–169

Low K-L, Tan T-S (1997) Model simplification using vertex-clustering. In: Proceedings of the 1997 symposium on interactive 3D graphics. ACM, pp 75-ff

Lu Z, Guerrero P, Mitra NJ, Steed A (2016) Open3D: crowd-sourced distributed curation of city models. In: Web3D symposium proceedings

Melax S (1998) A simple, fast, and effective polygon reduction algorithm. Game Developer 11:44–49

Murdock KL (2011) 3ds Max 2012 Bible. Wiley, New York

Olsen SC, Winnemöller H, Gooch B (2006) Implementing real-time video abstraction. In: ACM SIGGRAPH 2006 Sketches. ACM, p 133

Pecchioli L, Pucci M, Mohamed F, Mazzei B (2012) Browsing in the virtual museum of the sarcophagi in the Basilica of St. Silvestro at the Catacombs of Priscilla in Rome. In: 18th international conference on virtual systems and multimedia (VSMM). IEEE, pp 413–420

Scianna A, Gristina S, Sciortino R (2016) Integrazione di sistemi GIS FOSS e modelli dati 3D PDF per la fruizione multimediale di beni monumentali e archeologici: il Castello di Maredolce a Palermo. viii edizione 1

Tarantino E, Figorito B (2011) Extracting buildings from true color stereo aerial images using a decision making strategy. Remote Sens 3:1553–1567

Wen F, Luan Q, Liang L, Xu Y-Q, Shum H-Y (2006) Color sketch generation. In: Proceedings of the 4th international symposium on Non-photorealistic animation and rendering. ACM, pp. 47–54

Yang B, Purves R, Weibel R (2007) Efficient transmission of vector data over the Internet. Int J Geogr Inf Sci 21:215–237

Application of Digital Photogrammetry from UAV Integrated by Terrestrial Laser Scanning to Disaster Management Brcko Flooding Case Study (Bosnia Herzegovina)

Francesco Cescutti, Raffaela Cefalo and Franco Coren

Abstract The recent development of the unmanned aircraft (UAV) in the civil sector has generated a strong interest in the aerial survey industry, especially in sectors where costs and speed of use play a key role. In May 2014, in Brcko region, Bosnia & Herzegovina, torrential rains and flooding of rivers and torrents occurred, thus activating hundreds of landslides. In this paper, the methodology used for the survey of two landslides, identified in the Brcko area, and the obtained results have been described. Photogrammetry from UAV and laser scanning surveys were carried out in June 2015 in the framework of the international no profit Project "Assessment of flood-damaged infrastructures in Bosnia & Herzegovina and Serbia", led and funded by SEG (Society of Exploration Geophysicists) and AGES (Association of Geophysicists and Environmentalists of Serbia). The purpose of this work is to integrate laser scanner data with the ones generated by aerial photogrammetry from UAV, in order to produce detailed maps that can be used by geophysicists to optimize their analysis.

Keywords Laser scanning · UAV · Digital photogrammetry · GNSS · Landslide

F. Cescutti (✉) · R. Cefalo
GeoSNav Lab—Department of Engineering and Architecture,
University of Trieste, Trieste, Italy
e-mail: cescutti.francesco@gmail.com

R. Cefalo
e-mail: raffaela.cefalo@dia.units.it

F. Coren
INOGS—Istituto Nazionale di Oceanografia e Geofisica Sperimentale, Sgonico, Italy
e-mail: fcoren@inogs.it

R. Cefalo et al. (eds.), *New Advanced GNSS and 3D Spatial Techniques*,
Lecture Notes in Geoinformation and Cartography,
DOI 10.1007/978-3-319-56218-6_20

1 Introduction

In May 2014 torrential rains have occurred in Bosnia, Serbia and Croatia. The major ones were recorded along the Sava river, especially in the Brcko District, causing its overflowing and the flooding of large parts of the city and surrounding country.

In the Bosnian region of Brcko District, a large number of landslides occurred, affecting several neighboring villages (Stretti 2015).

SEG (Society of Exploration Geophysicists) and AGES (Association of Geophysicists and Environmentalists of Serbia) funded the international Project "Assessment of flood-damaged infrastructures in Bosnia & Herzegovina and Serbia" in order to investigate the damages caused by these natural events.

This international Project brought together different professional teams in order to produce a detailed geotechnical report to support the authorities in the reconstruction process.

Several methodologies integrated in a time laps manner in order to provide data and information useful to improve the reconstruction efforts and prevent further landslides (Stretti 2015; Rinaudo 2016; Eisenbeiß 2009; Caroti et al. 2015; Snezana 2016).

Due to the disasters, dozens of people died, thousands lost their houses, entire villages were evacuated and many facilities and infrastructures were destroyed or damaged. More than two thousand landslides have been activated by the flood and torrential rain. The danger of landmines and unexploded ordnance aggravated this situation; the flood destroyed the signs of minefields, war remnants of the '90s; with the retreat of the waters, many bombs were carried by the current, thus making cleaning and reconstruction operation more dangerous. During this two-year project different landslides will be surveyed in Bosnia & Herzegovina and Serbia.

Principal objectives are:

- The geophysical assessment and geotechnical investigation of landslides in Bosnia & Herzegovina and Serbia
- The education and training of geophysicist and environmentalists in Bosnia & Herzegovina and Serbia

Seismic and electric surveys have been used to obtain a full set of elastic parameters and a stratigraphic map.

2 Survey Area and Geological Situation

In 2015 and 2016 several tests have been performed in order to investigate possible advancement or landslide shape changes. During this campaign, two landslides located in Brcko surrounding countries, were investigated. The surveys were carried out on 22 and 23 June 2015 (Fig. 1).

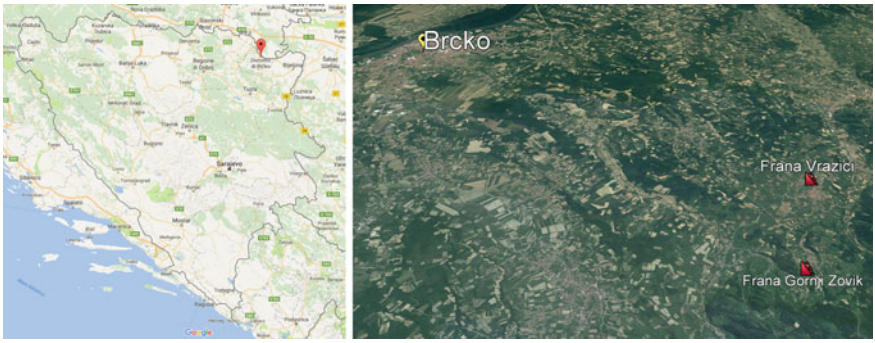

Fig. 1 Bosnia & Herzegovina and Brcko District—© 2016 Google Earth

Fig. 2 Gornji Zovik landslide survey area

The detected areas are characterized by a hilly territory with a low population density; the surrounding land is mainly used for agricultural purposes.

The first landslide is located near the village of Gornji Zovik and involves an area of approximately 600 m × 200 m (Fig. 2); the landslide in its movement has damaged many surrounding buildings making some of them unusable.

The red circles in Fig. 2 represent the areas where the UAV were carried out.

The survey in the village of Gornji Zovik was performed in two consecutive days (Fig. 3).

The second landslide is located in the village of Vrazici, it affects a property consisting of a house and an orchard, nearly 200 m × 80 m.

Fig. 3 Vrazici landslide survey area

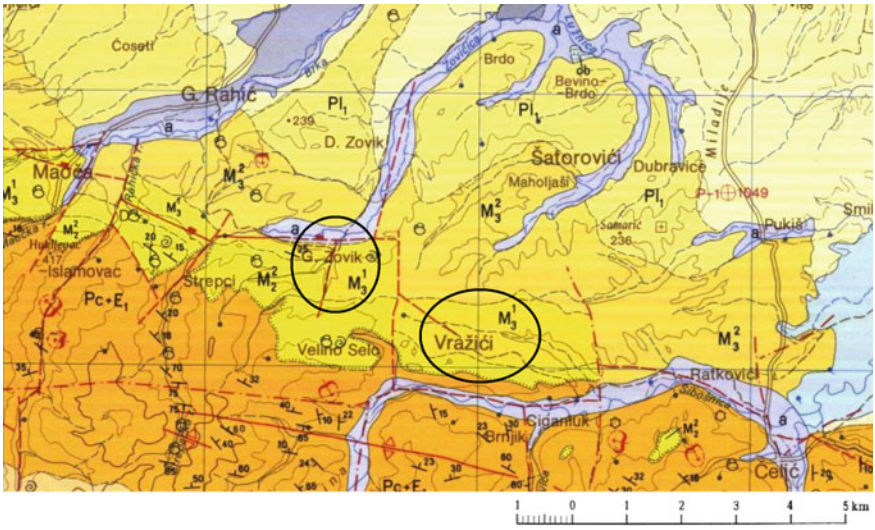

Fig. 4 Geological map of survey areas

Although the survey area is small, the investigation was not easy because of the strong slope of the terrain and the thick cover caused by the canopy of trees (Fig. 4).

The geological map produced by the Bosnian Military Geographic Institute shows in the areas interested by the survey of a soil of M13 type, formed by

sandstone, marl, marl sands, clays and limestones; this terrain originated in the Neogene geological period. The litotype M13 is limited to the north by an area characterized by the presence of litotype M23 (consisting of clay, marl, sandstone and gravel) and to the south by an area with a PC + E1 composition (formed by shales and sandstones).

The soil is mainly composed of:

- Sandstones: it is a sedimentary rock, formed by the cementation of sands in different periods; it can be found in the production of wheels of mills, grinding wheels and it is used in building constructions.
- Marl: is a sedimentary rock, mainly of marine origin, generated by the slow settling of the clay particles, the rock is formed by clay and carbonate. It has a strong hygroscopicity which promotes the degradation process and a strong water imbibition that produces a high variation in the physical and mechanical characteristics of the rock. It is used for the production of cement and hydraulic lime.

The alternating layers of sandstone, marl and clay form the sedimentary complex called Flysch.

This type of soil, due to the intense rains occurred in May 2014, suffered a heavy modification of its mechanical characteristics, coming to full saturation, which caused the annulment of the internal cohesion forces. Only the internal friction thus determined the passive component of the stability forces. This compromised the slope stability in several parts of the area interested by the study, thus producing a series of landslides. Is worth to mention that in addition, in the examined area, many landslides occurred due to erosion at the foot of the slopes, caused by the erosion from water runoff and rivers flooding.

3 Equipment and Methodologies

The aerial survey was conducted using two multirotor (Reg 2010), specifically quadcopters, an obvious choice in wooded areas where it's not possible to have a runway for take-off and landing.

The UAV quadcopter 650-class has a diameter from motor to motor of about 650 mm, it is capable of autonomous flight between waypoints, uses the flight control board APM 2.6 (APM Copter 2016) and has a flight autonomy of about 25 min (Fig. 5; Table 1).

The 250-class UAV quadcopter has a diameter of about 250 mm, it's not capable of autonomous flight (Baseflight Firmware installation 2016) but can transmit real-time videos from an analogic camera installed on board (Fig. 6; Table 2)

Unfortunately, the largest quadcopter couldn't be used for the surveys due to the failure of the control board, so only the smaller one was used.

Fig. 5 650-class quadcopter

Table 1 UAV Quadcopter 650 class specifications

650-class UAV quadcopter	
Flight time	25 min
Battery	2 × 4 s 4000 mha
Propeller	17 × 5.5 inch
Take off weight (TOW)	2.5 kg
Maximum take off weight (MTOW)	3.5 kg
Maximum speed	55 km/h

One Canon A2200 camera was installed on board with CHDK (Canon Hack Development Kit) firmware; this particular type of firmware allows the camera remote control via USB cable and specific scripts implementation (CHDK Script 2016) (Table 3).

The terrestrial laser scanner used in the surveys was a Riegl VZ400 (Riegl laser measurement system 2014, 2016) with an integrated GPS (L1) receiver, it provides scan data acquisition with 5 mm accuracy and 3 mm repeatability (Riegl 2014).

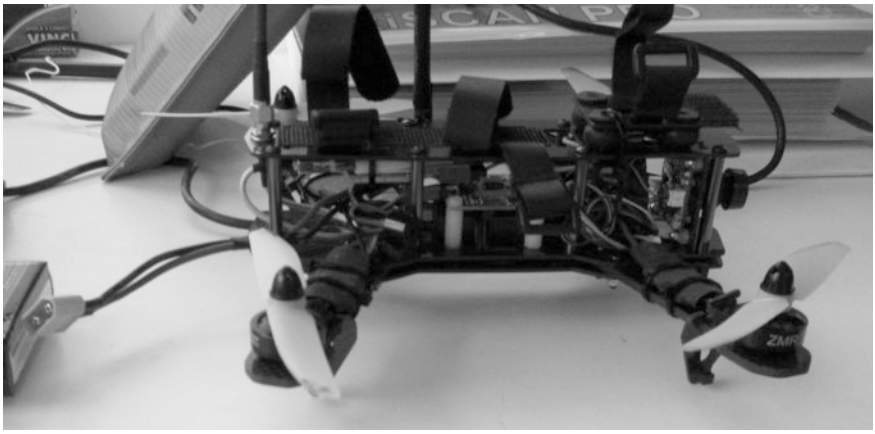

Fig. 6 250-class quadcopter

Table 2 UAV quadcopter 250 class specifications

UAV quadcopter 250	
Flight time	7 min
Battery	3 s 2200 mha
Propeller	5 × 4.5 inch
Take off weight (TOW)	550 g
Maximum take off weight (MTOW)	800 g
Maximum speed	80 km/h

Table 3 Canon A2200 specifications

Canon A2200	
Sensor	14.1 Megapixel, 1/2.3-inch type charge coupled device (CCD)
Focal length	5.0 (W)–20.0 (T) mm (35 mm film equivalent: 28–112 mm)
Maximum aperture	f/2.8 (W)–f/5.9 (T)
Shooting capacity	Approx. 280 shots
Weight	135 g

4 Data Processing

The processing of photographs taken during the flight has been performed using PhotoScan 1.6 (Agisoft 2016) and Surfer v.12 (Golden Software 2016) software.

Photoscan allows the processing of digital images, creating three-dimensional models and orthophotos.

The use of laser scanning system along with aerial photogrammetry allowed a quick recognition of the markers in the laser scanner data, to be used as ground control points (GCP).

For the purpose of this specific campaign and due to the particular operative environmental conditions (mine fields), the geophysicists asked for a relative 3D model, so no geodetic/GNSS surveys were planned in the investigated areas (Fig. 7).

Markers were detected as corners of houses, roofs, light poles, haystacks, rocks and anything else easily visible from above; the coordinates of these points have been obtained from the laser data, then inserted in PhotoScan in the form of markers and then we passed to the recognition of each element in each photo.

Planimetric and altimetric coordinates have been extracted from scanner data. Flight altitudes have been reconstructed using Photoscan and were in the range of about 30 m for each mission (Fig. 8).

The UAV photos were processed using Photoscan software, creating a dense point cloud, the terrain mesh and textures in order to generate the orthophotos.

The point cloud has been filtered with an algorithm present in Photoscan, exporting the ground points into Surfer v.12. This last software was used to produce a custom contour map importing data as Grid; Kriging procedure has been applied with a 0.25 m grid spacing. This processing technique was applied for each survey area.

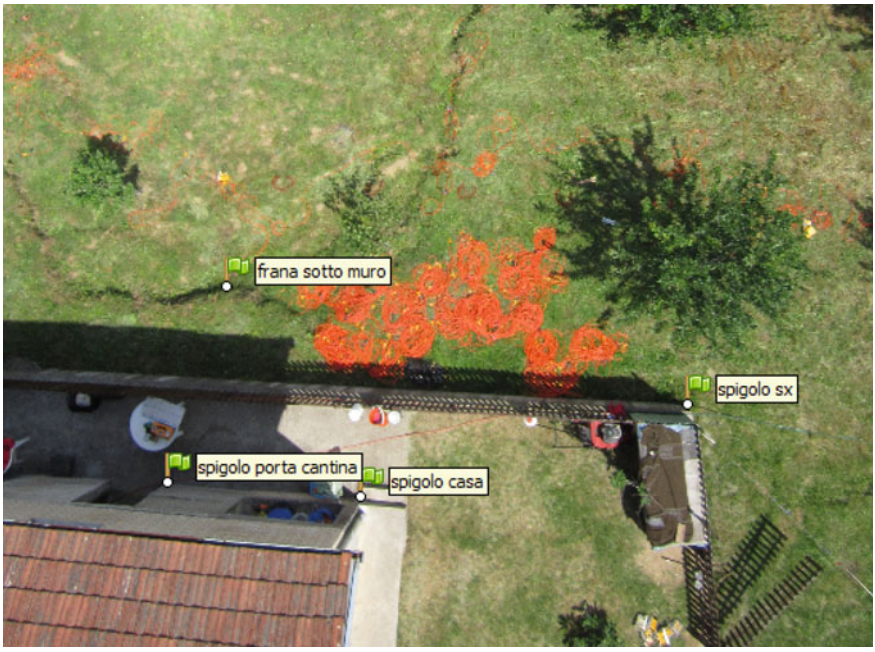

Fig. 7 Example of recognition of GCP

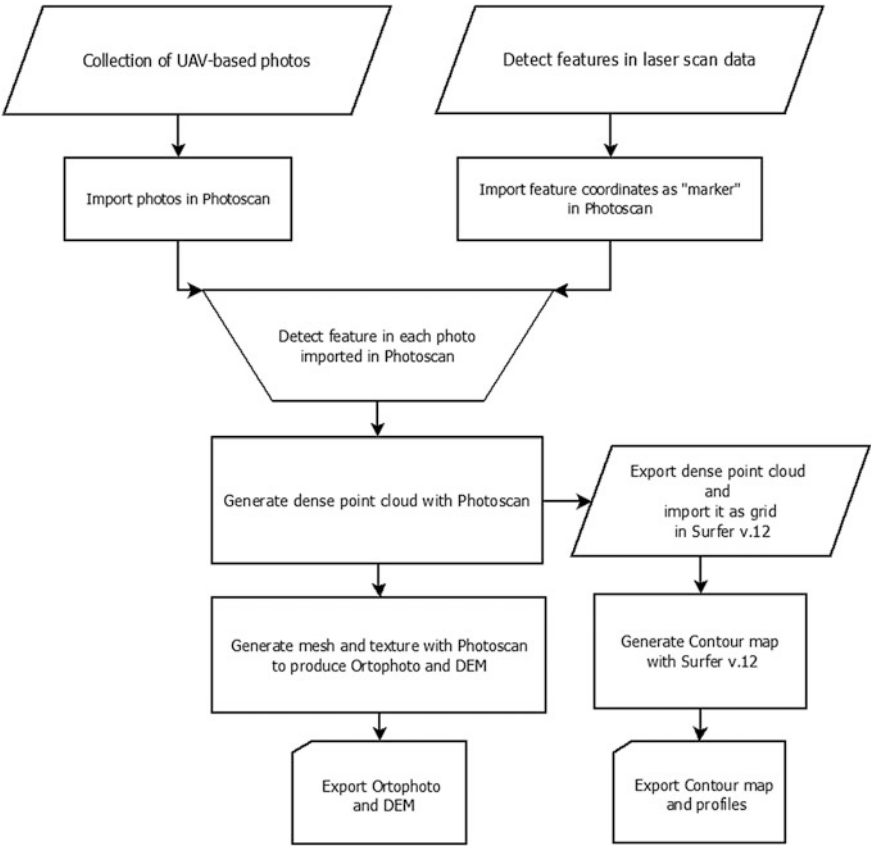

Fig. 8 Workflow elaboration process

The use of the photogrammetric system installed on board the UAV, allowed to cover a large area in a very short time: the surveys relative to this landslide, covering an area of 120,000 m^2, were performed in half day.

It has to be noted that, unlike "classical" approach, once the survey is completed, no "physical" markers had to be collected inside the survey site, thus reducing the operation times. This represent a key factor especially in different areas and in regions as those of Bosnia & Herzegovina that aren't safe from unexploded ordnance.

5 Results

5.1 Gornji Zovik Landslide Survey

640 photos have been collected during this survey, with a mean flight altitude of 30 m, reaching 50 m only in a few points.

Standard deviation parameters were computed for all the used GCPs; the three dimensional standard deviation is 0.23 m, which is acceptable for the purpose of the performed geophysical survey.

In Fig. 9 the orthophoto of Gornji Zovik survey area is presented. Figure 10 shows an elevation profile computed using Surfer v.12 that follows the course and direction of the path tracked by geophysicists (oblique line on the map) during the electrical and seismic surveys.

Due of the presence of dense vegetation, different scans acquired by laser scanner couldn't be properly oriented in the central image area; the lack of information is clearly visible in the right image of Fig. 11 that represents the laser scanner points.

Fig. 9 Ortophoto of Gornji Zovik survey area

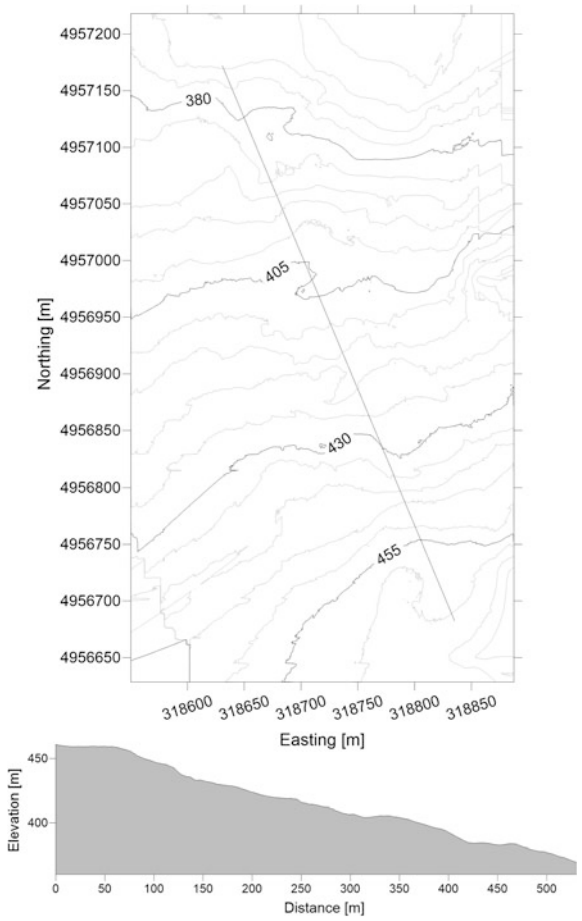

Fig. 10 Gornji Zovik survey area map and terrain profile along the evidenced *oblique line* evidenced

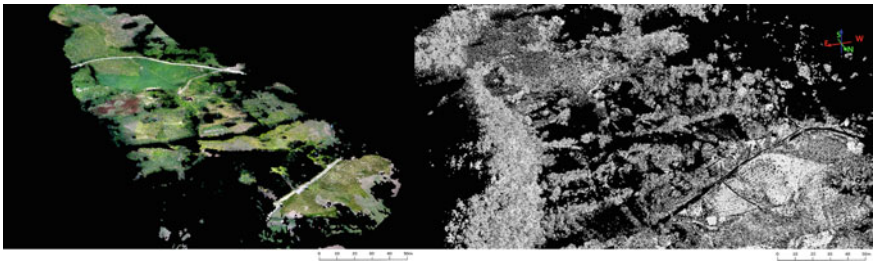

Fig. 11 View of photogrammetric points on *left* and laser scanner data on *right*

In Fig. 12, photogrammetric points obtained from UAV photos fill correctly the empty spaces present in the laser scanner data.

Figure 13 shows in detail the accumulation area (located at 318,800 m, 4,957,150 m—Easting and Northing WGS84-UTM coordinates) of the landslide along with several cracks; the road repairs in the transverse direction can be noticed in the image.

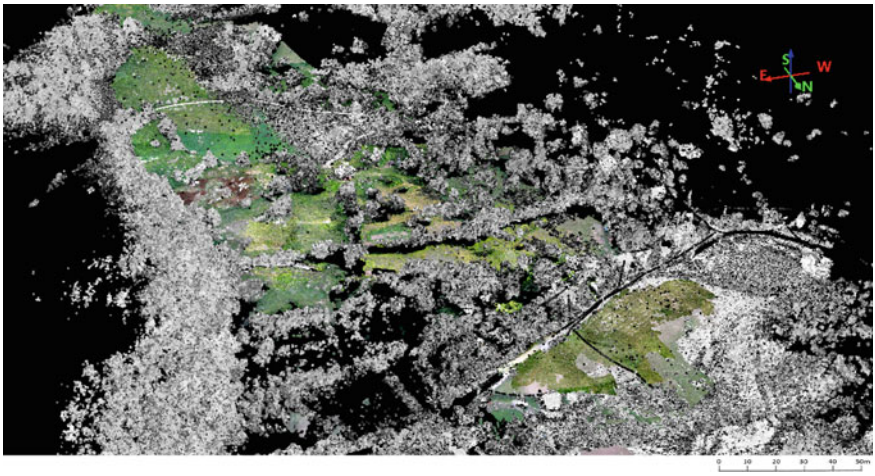

Fig. 12 Overlap of photogrammetric data with laser scanner data

Fig. 13 Orthophoto detail

5.2 *Vrazici Landslide Survey*

See Fig. 14.

During this survey 400 photos were taken, with a 30 m mean flight altitude.

The computed rms error is similar to that obtained for Gornji Zovik landslide, with an uncertainty average of 19 cm, more which could be considered sufficient for the relative positioning of the points surveyed by the geophysicists.

Figure 15 shows an elevation profile that follows the course and direction (corresponding to the oblique line on the map) of the path tracked by geophysicists during the electrical and seismic surveys.

In Fig. 16, the mesh details, especially for the landslide release areas (red lines) and accumulation areas (blue poligons), are clearly visible.

Fig. 14 Orthophoto of Vrazici survey area

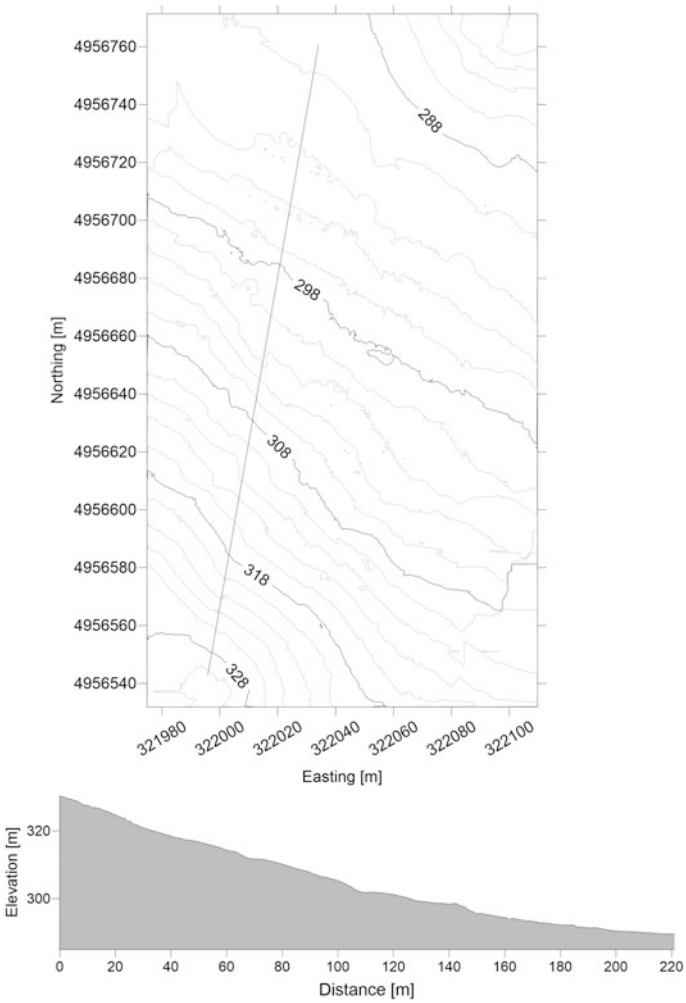

Fig. 15 Map of Vrazici survey area

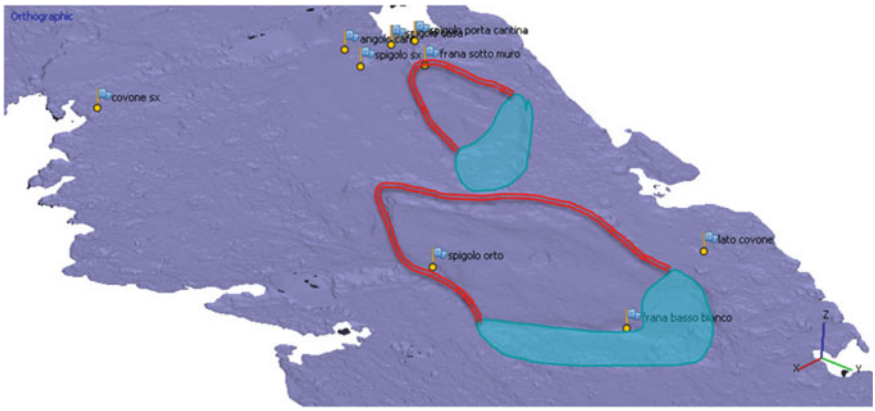

Fig. 16 Mesh details of Vrazicy suvey area

6 Conclusions

Integrating laser scanning and aerial photogrammetric data, the surface of two landslides in Brcko region, Bosnia & Herzegovina, were surveyed in a fast and accurate way.

The performed campaigns allowed creating 3D terrain models of the investigated landslides, thus giving a useful tool to the geophysicist's teams to better analyze seismic and electric surveys.

Unlike the "classical" approach, once the survey has been completed, no "physical" markers was collected inside the survey site, thus reducing the operation times.

This represent a key factor especially in areas like Bosnia & Herzegovina where the unexploded ordnance represents a high risk.

The combined use of laser scanning and aerial photogrammetry proved to be a fast, safe and efficient method to perform landslide surveys in such areas, providing a useful tool to the geophysicist's team involved in the international no profit Project "Assessment of flood damaged infrastructures in Bosnia & Herzegovina and Serbia", led and funded by SEG (Society of Exploration Geophysicists) and AGES (Association of Geophysicists and Environmentalists of Serbia).

References

2014 South East Europe Flood. https://en.wikipedia.org/wiki/2014_Southeast_Europe_floods

Agisoft (2016) Agisoft PhotoScan user manual: professional edition, Version 1.2. http://www.agisoft.com/pdf/photoscan-pro_1_2_en.pdf. Accessed 5 Sept 2016

Baseflight Firmware installation and setup guide. https://github.com/multiwii/baseflight Accessed 5 Sept 2016

CHDK Script. http://chdk.wikia.com/wiki/CHDK. Accessed 5 Sept 2016

Eisenbeiß H (2009) UAV photogrammetry. ETH, Zurich, Switzerland
Golden Software, Surfer v.12 user manual. http://downloads.goldensoftware.com/guides/Surfer12_Users_Guide_Preview.pdf. Accessed 5 Sept 2016
APM Copter installation and setup guide. http://ardupilot.org/copter/. Accessed 5 Sept 2016
Reg A (2010) Unmanned aircraft systems: uav design, development and deployment. Wiley, New York
Riegl, VZ 400 datasheet. http://www.riegl.com/uploads/tx_pxpriegldownloads/10_DataSheet_VZ-400_2014-09-19.pdf. Accessed 5 Sept 2016
Riegl laser measurement system, Riscan PRO manual v1.2. http://www.utdallas.edu/∼aiken/LASERCLASS/riscan_pro.pdf. Accessed 5 Sept 2016
Riegl laser measurement system, 3D Terrestrial Scanner Riegl VZ-400 System Configuration 03/14. http://www.riegl.com/uploads/tx_pxpriegldownloads/30_SystemConfiguration_VZ-400_03-14_03-03-2014.pdf. Accessed 5 Sept 2016
Rinaudo F (2016) UAV (Unmanned Aerial Veicles). Possibili utilizzi per il monitoraggio dei beni architettonici e paesaggistici. In Patrimonio culturale: tecniche innovative per il progetto di conservazione, Rosa Anna Genovese. Giannini Editore, Napoli, pp 365–378. ISBN 978-88-7431-822-3
Snezana K (2016) Assessment of flood damaged infrastructures in Bosnia & Herzegovina and Serbia, progress report
Stretti G (2015) Il pilota di droni. Guida ai Sarp, IBN
Bosnian Military Geographic Institute (1990) Geological map of Brcko District
Caroti G, Zaragoza, IM-E, Piemonte A (2015) Accuracy assessment in structure from motion 3d reconstruction from UAV-born images: the influence of the data processing methods, Remote sensing international archives of the photogrammetry, remote sensing and spatial information sciences

Kinematic Positioning: From Mobile Mapping Systems to Unmanned Aerial Vehicles at Pisa University

Gabriella Caroti and Andrea Piemonte

Abstract Since the 1990s, with the availability of satellite positioning techniques, enabling to determine three-dimensional point coordinates in a global reference system with topographic accuracy, several applications dedicated to mapping of the territory by means of mobile geo-referenced sensors have steadily been developed. This paper discusses the experiences gained in this field at the University of Pisa—Laboratory of Topography over more than twenty years of experimental work. These activities, often conducted in cooperation with the University of Trieste and in particular with Professor Giorgio Manzoni, have always featured a multidisciplinary approach. Different types of sensors have been installed, at first in land-based vehicles and currently on unmanned aerial systems: GPSs, GNSSs and INSs, carbon monoxide and particulate matter measuring systems, single- and multiple-axis laser scanners, industrial and photography cameras. Use of these sensors, besides drafting and testing maps of the territory in several areas (cartography, road cadastre, pollution monitoring, city modelling …), allowed to keep track of the development of instrumentation and methods of kinematic positioning.

Keywords MMS · UAV · Kinematic positioning

1 Introduction

Satellite location systems, able to provide absolute positioning of any point in near-real time, have prompted development of several applications ever upon their availability in the 1990s.

G. Caroti (✉) · A. Piemonte (✉)
Civil and Industrial Engineering Department, University of Pisa, Pisa, Italy
e-mail: gabriella.caroti@unipi.it

A. Piemonte
e-mail: andrea.piemonte@unipi.it

R. Cefalo et al. (eds.), *New Advanced GNSS and 3D Spatial Techniques*,
Lecture Notes in Geoinformation and Cartography,
DOI 10.1007/978-3-319-56218-6_21

This paper, meant as a tribute to the memory of Professor Manzoni, reviews the advances achieved over the past 20 years by the Geomatics research group at the Engineering School, Pisa University.

By cooperating with Professor Manzoni, Pisa Geomatics research group has been among the first academic users of GPSs, also developing, in cooperation with several other research centres, one of the first Mobile Mapping Systems (MMS) for academic use.

The members of the Pisa group have taken advantage of Professor Manzoni's vision of the future in geomatics applications, which provided integration between different sensors, methodologies and disciplines.

2 1990s—From Static to Kinematic Survey

The first paper (Manzoni and Palla 1992) referring to the presence of a GPS instrument at Pisa University dates back to 1992. It is a report of research activity in cooperation between Professors Giorgio Manzoni (Trieste University) and Brunetto Palla (Pisa University), showing the results of comparisons between GPS (Trimble 4000SL—Fig. 1) and classical ground surveys. Those were pioneering days for GPS research in Italy, and surely, Professor Manzoni led the way.

During the 1990s Pisa followed Professor Manzoni in his research work, e.g. beginning to use the GPS/DR (Dead Reckoning) Trimble Placer, an embryonic Mobile Mapping System (MMS) component (Madhukar et al. 1999). Early tests focused on accuracy assessment of stand-alone C/A GPS survey: back then, Selective Availability was still active and the overall number of satellites was lower than that of today. The inertial system drift was also analysed, with several papers investigating drift reduction. Another topic of interest for professor Manzoni was the transmission of GPS correction codes. In Pisa, the first tests of transmission of correction codes used Extended Total Access Communication System (ETACS) mobile phone system; Differential Global Positioning System (DGPS) performance was also tested (Fig. 2), using geostationary services such as those provided by RACAL systems.

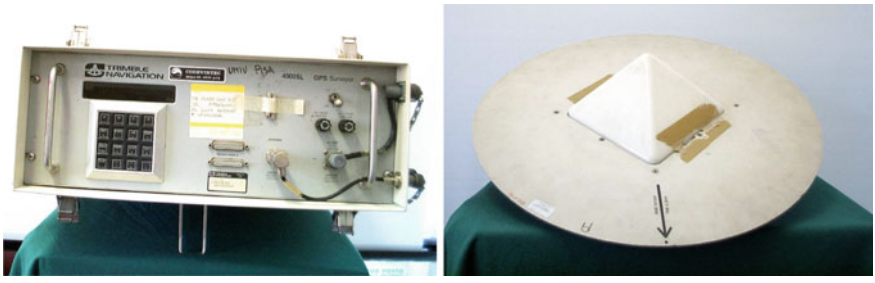

Fig. 1 The 1990s GPS Trimble 4000SL receiver and the geodetic L1 antenna—Pisa University

Fig. 2 Trimble Placer 455DR and Racal system: first Pisa MMS

Fig. 3 Pisa MMS with instrumentation for air pollution monitoring

Improvements in accuracy of GPS surveys brought along the first applications on high-productivity surveys of road geometry, such as the calculation of curvature radii and the subsequent check of the design speed, or the georeferencing, with Stop and Go post-processed double frequency DGPS surveys, of cross sections surveyed by semi-static EDM instrument (El-Sheimy et al. 1995; El-Sheimy 1996; Manzoni et al. 1994; Cefalo et al. 1994).

The throughput of this methodology was about 1 km/h, i.e. two magnitude orders lower than current MMSs.

Another application underlining the multidisciplinary approach of Professor Manzoni referred to air pollution monitoring. A code DGPS integrated with a low cost Inertial System (INS) provided a suitable accuracy for georeferencing static or moving measures of air pollutant concentration (Fernetti et al. 1998).

Trieste and Pisa Geomatics research groups proposed a joint project for a monitoring network based on moving measurements via public urban transportation system. Sensors used in the first experiment included a Babuc CO analyser, georeferenced by integrating data collected by both Placer GPS 455DR and Racal (Fig. 3) sensors.

3 2000s—Mobile Mapping System

At the beginning of the 2000s, a consortium of several universities (including Pisa) led by Professor Manzoni laid out the design for GIGI (GPS Inertial GLONASS Integrated), the first Italian MMS with tactical grade INS, which would later evolve into GIGI One (El-Sheimy and Schwarz 1999; Manzoni et al. 2003a) (Fig. 4).

The navigation system installed on GIGI is the Canadian APPLANIX POS LV, a strapdown system integrating one single- and one double-frequency GPS receiver, a Distance Measuring Indicator (DMI) and a high accuracy Fiber Optic Gyro INS that can work with several different real time differential correction codes (Manzoni et al. 2006).

About at the time GIGI was used at Pisa University in the 2000s, a new MMS, called VINCI'S (Vehicle-borne Integrated Navigation and Cartographic Information prime System), was set up in Pisa. On-board sensors included the Placer, a multi-axis laser scanner, DGPS systems, a camera and the air pollution monitoring instruments (Fig. 5).

Fig. 4 The GIGI MMS (*left*), the Applanix POS-LV system (*middle*) and the MMS last version—GIGI One (*right*)

Fig. 5 VINCI'S, MMS fitted out at Pisa University

This vehicle allowed to improve accuracy and productivity of road geometry surveys, and to adapt air pollution monitoring to the new emergency, i.e. particulate matters (Fig. 6).

This project also prompted a cooperation with the regional agency for environmental protection, as well as fellow researchers studying pollutant dispersion models.

In later years, the GIGI One MMS was used in some specific tests. One of these was dedicated to the survey of cross section of the roads, by means of the mono-axial laser scanner installed by researchers at Trieste. The presence of a high accuracy positioning system on the vehicle allowed direct georeferencing of the point cloud measured by the laser scanner (Fig. 7). Although the raw point cloud had its own local coordinate system, researchers knew the lever arm between the body frame and the local frame, the rotation angles (roll, pitch and heading) of the vehicle part carrying the laser scanner and, eventually, the position vector of the body frame relative to the mapping frame. Based on these premises, GIGI One was able to perform the survey of the cross section of the roads and subsequently to measure the relevant cross slope.

In the 1990s, throughput was 1 km/h; in the 2000s, it increased to 70 km/h.

The availability of GIGI One provided the occasion for developing other studies, like the definition of cross slope just by means of inertial system data, without additional laser scanning instrumentation (Caroti and Piemonte 2010). A simplified vehicle dynamics model provided the basis for a methodology for

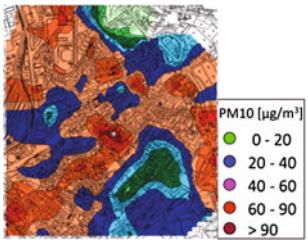

Fig. 6 An example of particulate matters concentration survey

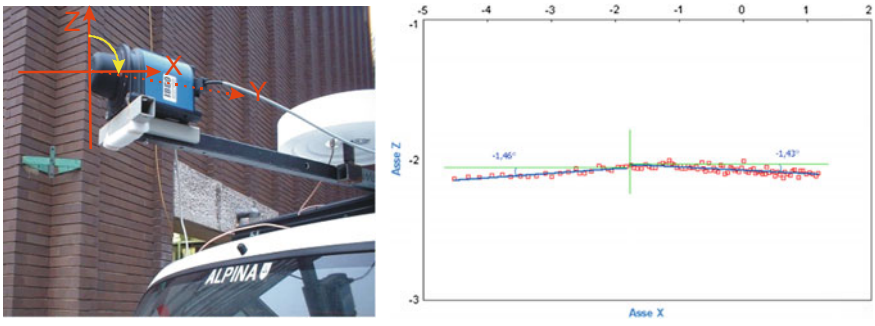

Fig. 7 The IBEO mono-axial Laser Scanner and an example of road cross section survey

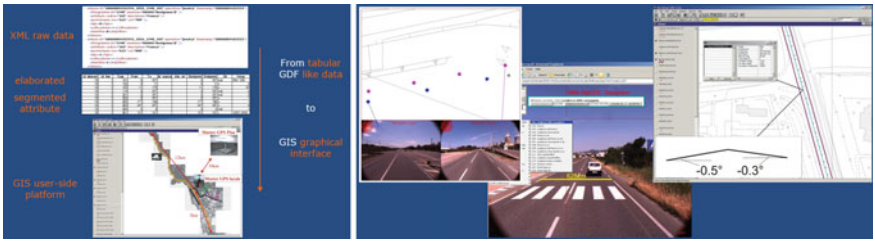

Fig. 8 Data processing flowchart, graphical visualization of digital stereo photos acquired from MMS for road cadastre applications and trajectory overlay on digital maps with the cross-section slope extraction

model calibration and cross slope calculation, by means of high-precision attitude data.

In Italy, the 2000s brought along the Road Cadastre, and in fact the GIGI One project was started precisely to deal with this issue (Manzoni et al. 2003b). The road cadastre is a complex GIS, where the fundamental data are the measures obtained through the MMS, whose position has to be defined with precision of a few centimetres. These data are available in a database that can be queried so to obtain, for example, photo frame position, orientation, path video sequence, road geometry data (width, cross slope, grade, curvature …) and so on (Fig. 8).

4 2010s—UAV

The latest research works carried out at Pisa in the field of kinematic positioning focus on the topic of Photogrammetric Survey from UAV (Unmanned Aerial Vehicles).

The new approach to softcopy photogrammetry realized by Structure from Motion (SfM) and MVS (Multi-View Stereo) algorithms generates very dense 3D colour point clouds, quite similar in size and quality to those produced from laser scanning surveys (Remondino et al. 2014).

Moreover, military achievements of UAVs have provided an effective background for furthering the development of such aircrafts also for civilian destinations.

The UAV (Fig. 9) system available at Pisa research unit and used for surveying activity features an always-on autopilot system, integrating a C/A GPS system and a low cost Micro Electro Mechanical Systems (MEMS) inertial system, which permits autonomous stabilized flight of the UAV on a pre-planned path.

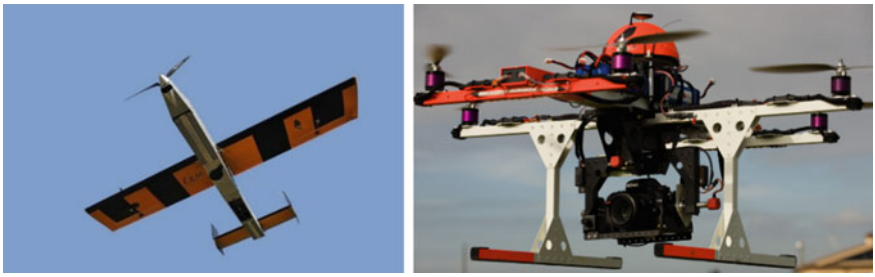

Fig. 9 Fixed and rotary wings UAVs available at Pisa research center

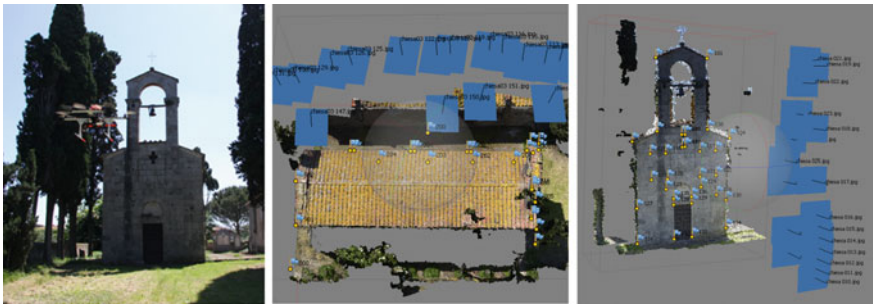

Fig. 10 UAV-borne photogrammetric survey example

The use of multi-rotor systems allows achieving both horizontal and vertical photogrammetric strips in close proximity to the survey objects. Starting from these data is then possible to obtain three-dimensional models that are not only aesthetically pleasing but also carry metric information (Fig. 10). The most common way to provide a coordinate system and a scale to the model is to survey the coordinates of a certain amount of Ground Control Points through GPS or total station surveys (Caroti et al. 2015).

This surveying step increases global costs and time consumption. As an alternative, direct photogrammetry, where the camera external parameters are directly measured, rather than calculated, also provides coordinate system and scale (Colomina and Molina 2014). In this case, it is necessary to directly survey camera roll, pitch and heading angles with a high accuracy. The cost and the weight (for UAVs) of a high-end inertial system could be very high. A middle path is to measure only the position of the camera. To this purpose, a single frequency low cost GPS system with a post-processing differential computation is currently under testing, e.g. an u-blox LEA 6T mounted on a Raspberry card programmed for camera-GPS synchronisation and data querying and storage (Fig. 11).

Fig. 11 UAV and on-board positioning systems used for direct georeferencing

Fig. 12 u-blox and L1-L2 GNSS positioning on checkpoints and on flight strips simulation

Fig. 13 Pisa tribute in memory of Professor Giorgio Manzoni

Current ground tests include comparing the u-blox differential solution with a geodetic double frequency receiver, both on static points and on ground strips simulation (Fig. 12).

The checked accuracy seems more than adequate for cartographic purposes: about 2 cm on planar coordinates and 4 cm on height coordinate. This method

could replace some surveys from manned aircraft such as those for the geometrical characterization of river basins (Caroti et al. 2013).

5 Conclusions

All these applications seem today very accessible and user friendly. The hardware and sensors are very small and the accuracy is quite good even with entry-level systems.

This paper provides a quick overview on how the current surveying methodologies were achieved, always keeping in mind that the levels of miniaturisation and automation available today descend from years of research and development. All the research carried out in the past 20 years allowed to develop the integration between different sensors and the optimisation of data processing, all the while paying a close attention to precision, which is inherent in Geomatics.

Currently, Pisa research centre has installed its geomatics instrumentation on a different kind of vehicle, an UAV, in order to meet new challenges, more related to the applied part of Geomatics, that are facing researchers.

UAVs are the future. Rather than just the Authors' supposition, this is a fact that anyone can check in all market researches in the UAV sector. By now, Professor Manzoni probably would have already crashed several UAVs to the ground, but surely he would have taken on the challenge and kept on experimenting (Fig. 13).

Acknowledgements The Authors wish to thank all the technical staff, students and researchers from the universities of Trieste and Pisa, who have collaborated along all these years, sharing the same passion for surveying and geomatics.

References

Caroti G, Piemonte A (2010) Measurement of cross-slope of roads: evaluations, algorithms and accuracy analysis. Surv Rev 48(350):309–315. doi:10.1179/003962610X12572516251484

Caroti G, Camiciottoli F, Piemonte A, Redini M (2013) The accuracy analysis of Lidar-derived elevation data for the geometric description of cross-sections of a riverbed. In: International archives of the photogrammetry, remote sensing and spatial information sciences—ISPRS archives, 40(5W3):51–57. doi: 10.5194/isprsarchives-XL-5-W3-51-2013

Caroti G, Zaragoza IM-E, Piemonte A (2015) Accuracy assessment in structure from motion 3D reconstruction from UAV-born images: the influence of the data processing methods. Int Arch Photogramm Remote Sens Spatial Inf Sci—ISPRS Arch 40(1W4):103–109. doi:10.5194/isprsarchives-XL-1-W4-103-2015

Cefalo R, Faccioli A, Fonzari S (1994) Applicazioni al rilievo di strade di un sistema DGPS integrato con girobussola ed odometro – Le Strade, Anno XCVI – N°1300 – febbraio 1994, pp 139, 142

Colomina I, Molina P (2014) Unmanned aerial systems for photogrammetry and remote sensing: a review. ISPRS J Photogramm Remote Sens 92:79–97. doi:10.1016/j.isprsjprs.2014.02.013

El-Sheimy N (1996) A mobile multi-sensor system for GIS applications in urban centers. ISPRS 1996, Commission II, Working Group 1, Vienna, Austria, 9–19 July 1996

El-Sheimy N, Schwarz KP (1999) Navigating urban areas by VISAT—a mobile mapping system integrating GPS/INS/digital cameras for GIS application. Navigation 45(4):275–286

El-Sheimy N, Schwarz KP, Wei M (1995) VISAT: a mobile city survey system of high accuracy. In: Proceedings of ION GPS, pp 1307–1315

Fernetti M, Gasparini M, Manzoni G, Purga A (1998) Air pollution mapping by portable sensors and DGPS positioning. In: IV meeting of the environmental and engineering geophysical society (European section), Barcelona (Spain), pp 13–15

Madhukar BR, Nayak RA, Ray JK, Shenoy MR (1999) GPS-DR integration using low cost sensors. In: Proceedings of the 12th international technical meeting of the satellite division of the Institute of Navigation (ION GPS 1999), Nashville, TN, Sept 1999, pp 537–544

Manzoni G, Palla B (1992) Pisan coast (Tuscany, Italy): a comparison of results from GPS and classical ground surveys. Bollettino Oceanografia Teorica ed Applicata X(2-3-4):325–332. ISSN 0006-6729

Manzoni G, Cefalo R, Fonzari S (1994) Urban and suburban road survey by means of real time direct and inverted DGPS – DSNS 94, Londra 18–22 aprile 1994, Poster Session, Proceedings

Manzoni G, Martinolli S, Pagurut R, Palermo C, Purga A, Sluga T (2003a) Road survey by GIGI: status and results. In: Proceedings of the 7th bilateral geodetic meeting ltaly-Poland, Bressanone, South Tirol, ltaly, 22–24 May 2003, Reports on Geodesy n. 2 (65), 2003, Warsaw lnstitute of Technology, lnstitute of Geodesy and Geodetic Astronomy, pp 159–164

Manzoni G, Caroti G, Martinolli S, Pagurut R, Palermo C, Sluga T (2003b) Surveying tools and data processing for road information systems. In: Proceedings of ISPRS-WG VI/3—Geoinformation for practice, Zagreb, 15–18 ottobre 2003, pp 182–186, ISBN/ISSN 1682-1750

Manzoni G, Bolzon G, Cefalo R, Gherdevic D, Martinolli S, Piemonte A, Rizzo R, Sluga T (2006) CER telegeomatics applications and projects in Central Europe. In Reports on Geodesy, vol 6. ISSN: 0867-3179

Remondino F, Spera MG, Nocerino E, Menna F, Nex F (2014) State of the art in high density image matching. Photogram Rec 29(146):144–166. doi:10.1111/phor.12063

Ionosphere TEC Variations Over Bosnia and Herzegovina Using GNSS Data

Medzida Mulic and Randa Natras

Abstract Total Electron Content (TEC) is the key parameter for studying ionosphere and corrections of ionspheric effects on positioning by Global Navigation Satellite Systems (GNSS). TEC variability using GNSS observation data of SRJV station from Sarajevo was analyzed, for the period January 2014–May 2015. Resulting day to day and seasonal variations show expected behavior. Special attention was paid to the analysis of TEC variations during the weeks before and after the earthquakes, that are registered by Federal Hydro-Meteorological Institute in Sarajevo, in February and April 2015, with epicenters located near Sarajevo. Magnitudes of earthquakes were M $\sim$ 4 Richter, lower than the threshold for detection ionospheric earthquake precursors (M $\sim$ 5). For analysis of TEC variations during seismic activities, GNSS observation data of ZADA station for February–April 2015 were used as well. Deviations from 15 day median values of TEC within weeks around these seismic activities were higher than 10 TEC units. A closer examination of the data showed that the anomalies were caused by gap in data and space weather conditions, but the rest of the anomalies are yet to be linked to seismic activities mentioned.

Keywords Ionosphere · Total electron content (TEC) · TEC variability · Space weather · GNSS

1 Introduction

Ionosphere is a region of Earth's upper atmosphere, which is the most dominant source of errors in Global Navigation Satellite Systems (GNSS), such as US Global Positioning System (GPS). Dispersive ionosphere causes delays in transmission of L1 (1575.42 MHz) and L2 (1227.60 MHz) signals. Relative ionospheric delay of

M. Mulic (✉) · R. Natras
Geodesy Department, Faculty of Civil Engineering, University of Sarajevo,
Patriotske lige 30, Sarajevo, Bosnia and Herzegovina
e-mail: medzida_mulic@gf.unsa.ba; medzida_mulic@yahoo.com

R. Cefalo et al. (eds.), *New Advanced GNSS and 3D Spatial Techniques*,
Lecture Notes in Geoinformation and Cartography,
DOI 10.1007/978-3-319-56218-6_22

two signals is proportional to the amount of electrons along the signal path, which represents total electron content (TEC) (Fayose et al. 2012). Total electron content is measured in TEC units (TECU), where 1 TECU = 10^{16} electrons/m^2. Continuous monitoring of the ionosphere allows prediction of its behavior and modeling of its effect on propagation of the GNSS signal.

Studies of TEC variability conducted during the last decades (Pulinets et al. 2006; Liu et al. 2004; Ouzounov et al. 2013; Hazbi et al. 2011) have shown correlation between the state of ionosphere and seismic activities of lithosphere prior to the occurrence of devastating earthquakes. Variations in the ionosphere have been reported several days before strong earthquakes. Research of ionosphere variability in relation to large earthquakes (M > 6) in California, the United States and Mexico indicated increase of TEC values during few days (usually tree to seven) before the seismic shocks, and normalization of TEC values after the earthquake (Pulinets et al. 2006). Investigation of pre-earthquake ionospheric anomalies by the total electron content, from a ground-based GPS receivers, for 20 earthquakes in the Taiwan ($M \geq 6.0$), showed that the pre-earthquake ionospheric anomalies usually appeared during 18:00–22:00 LT (LT = UT + 8 h), within five days prior to 16 of the 20 $M \geq 6.0$ earthquakes (Liu et al. 2004). Few days before major earthquakes in Greece (M > 6) in 2008–2009 anomalous TEC variations were detected and positive deviations were observed from 16 to 4 h local time (Ouzounov et al. 2013). Positive and negative anomalies of TEC values were detected a few hours to 6 days before the large earthquakes, occured in Sumatra during 2004–2007, using ground-based GPS measurements and satellite-based measurements from CHAMP satellite (Hazbi et al. 2011).

To statistically track ionospheric anomalies, as short-term forecast, 15-day median for 15 days preceding the day of consideration was applied (Liu et al. 2006), where the both positive and negative deviations were observed. Identification of possible significant disturbances was made by assumption of normal distribution with mean value μ and standard deviations of TEC. Bounds $\mu \pm 2\sigma$ have been used by Liu et al. (2011), where confidence level is 95%. If the observed TEC falls out of lower or upper bounds, it is declared with confidence of 95% that abnormal signal is detected.

The process which leads to ionospheric anomalies is not yet fully explained and proven. A general concept of mechanisms of lithosphere-atmosphere-ionosphere coupling prior seismic shock has been offered by Molchanov et al. (2004). The ideas for physical mechanism, which would be able to produce electrical fields in the ionosphere that create anomalies registered at the last stage of earthquake preparation cycle, have been proposed by Pulintes (2009).

Territory of Bosnia and Herzegovina (B&H) is one of the relative seismically active zones. This area is tectonically related to the great fault of the earth's crust that extends from northern India (Himalayas) through the territory of Iran, Turkey and Greece (eastern Mediterranean) exceeds the southern part of the B&H territory. According to the data from historical archives of the Center for Seismology at the Federal Hydro-meteorological Institute in Sarajevo, earthquakes of magnitude M > 3.0 were registered on this territory. Epicentral zone of frequent earthquakes

was registered on Mountain Treskavica (Shaking or Quaking mountain in Bosnian language), located southward from Sarajevo.

Aims of this paper were to investigate ionospheric TEC variations over Bosnia and Herzegovina, especially before and after earthquakes with a magnitude M = 4.3 and M = 4.4, registered near Sarajevo. Research was conducted using ground-based TEC measurements from dual frequency receiver at permanent station SRJV and Dobrovolsky formula (Dobrovolsky et al. 1979) for determination of size of the earthquake preparation zone.

2 Methods and Data

GNSS observation data in RINEX (receiver independent exchange) format of the European Permanent Network (EPN) station SRJV in Sarajevo, Bosnia and Herzegovina (latitude +43° 52′ 04.27″N, longitude +18° 24′ 50.06″E) were used for TEC values estimation. EPN Data covered period from beginning of the January 2014 to the end of May, 2015. In addition, data of EPN station ZADA in Zadar (Croatia, +44° 06′ 47.42″N, 15° 13′ 39.31″E) were analyzed for period February to May of 2015, for further analysis of ionospheric variations prior and after the earthquakes, that were investigated in this paper.

Total electron contents were calculated in accordance with Ciraolo methodology (Ciraolo 1993), i.e. using program VShell, from International Center of Theoretical Physics Abdus Salam-ICTP in Trieste. TEC were estimated from dual-frequency measurements using approximations of ionosphere as a thin shell model at height of 400 km above the Earth's surface.

Single-layer model (SLM) assumes that all free electrons are concentrated in an infinitesimally thin layer at a height between 350 and 500 km, which is slightly above the level where is expected the highest electron density (Schaer 1999). For full TEC modeling it was necessary to apply TEC vertical equivalent (VTEC), using mapping function which describes the relationship between STEC and VTEC. Slant TEC (STEC) represents total number of free electrons in the cylinder along the signal path from satellite to receiver. It can be obtained from formula (1), where N represents density of electrons along the line of sight ds:

$$STEC = \int_{receiver}^{satellite} Nds \tag{1}$$

Formula (2) shows the mapping function

$$F(z) = \frac{STEC}{VTEC} \tag{2}$$

Table 1 List of earthquakes with epicenters in the wide area of Sarajevo in 2015

Date	Time LT (UT+1h)	Epicenter	Magnitude (Richter)	Intensity (MCS)	Radius of zone ρ (km)	Distance from SRJV GNSS d (km)
28.02.	09:24	Treskavica	4.3	VI	70.63	30
12.04.	02:05	Pale	4.2	VI	63.97	13
16.04.	04:08	Pale	3.4	V	28.97	13

Special attention in this investigation was paid to connection between the ionosphere and seismic activity in Bosnia and Herzegovina in 2015. The concept is based on the assumption that variations in the ionosphere, as a result of seismic activity, can be observed within the area of earthquake preparation zone. The formula to determine the size of the zone is (Dobrovolsky et al. 1979):

$$\rho = 10^{0.43M}\ \text{km} \tag{3}$$

In formula 3, ρ is radius of the earthquake preparation zone, in km, and M is magnitude of earthquake, on the Richter scale. Calculations (Pulinets et al. 2000) showed that a magnitude threshold for detection ionospheric earthquake precursors is M $\sim$ 5.

Analysis in this paper was done for earthquakes of magnitude greater than 4, but less than 5. Applying the formula Dobrovolsky, preparation zone of those earthquakes covered area of Sarajevo. Table 1 shows an overview of analyzed earthquakes which were registered by Federal Hydro-Meteorological Institute in Sarajevo, as well as radius of earthquake preparation zones and approximate distance to SRJV GNSS station. Distances between epicenters and SRJV GNSS station is more than twice shorter than radius of earthquake preparation zones. Therefore the interest to conduct this research was aroused; despite the magnitude of the earthquakes were less than 5° of Richter.

3 Results and Discussion

3.1 Comparison with TEC Values from TEC Maps, May 2015

TEC vertical equivalent values, calculated by Ciraolo methodology (using program VShell), were compared to TEC vertical equivalent values from the TEC maps for the area of Bosnia and Herzegovina. TEC maps were downloaded from the website of Royal Observatory of Belgium (ROB). These maps are estimated in Near Real-Time for every 15 min, from the GPS data of the EUREF Permanent Network, (Bruyninx 2012). The comparison was done for the period from 1st to 5th May 2015. These periods were chosen because the strong variations of day to day TEC

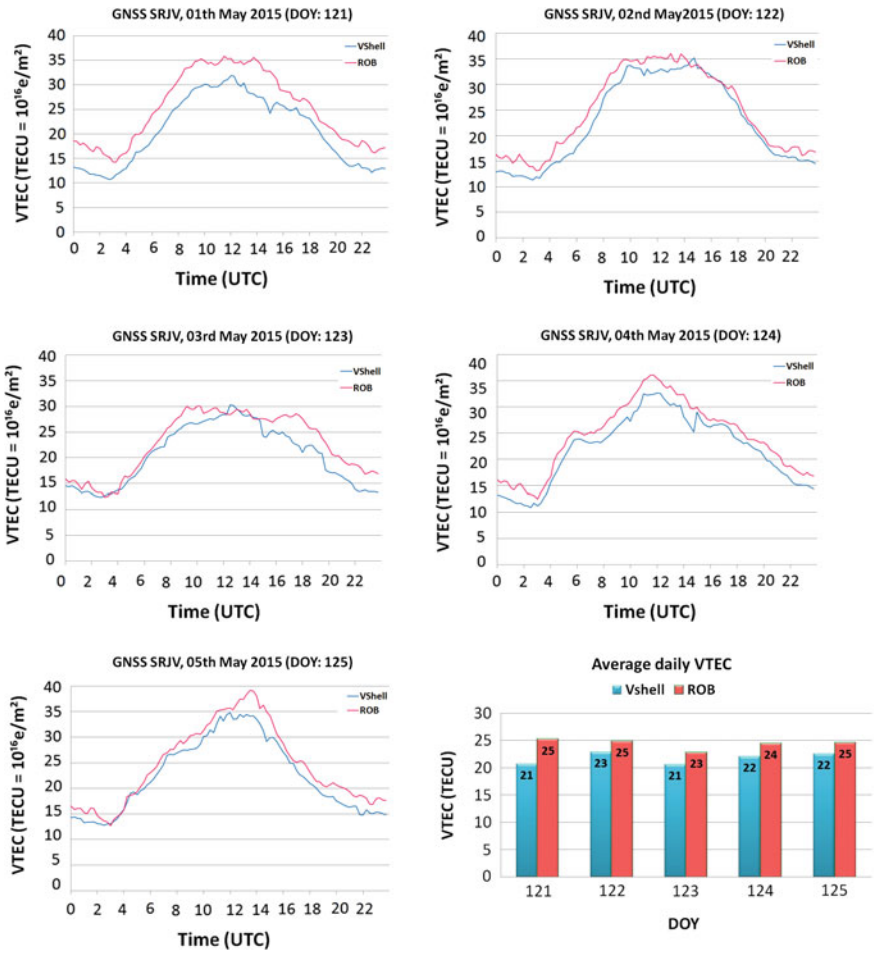

Fig. 1 Comparison of TEC values: VShell and ROB

vertical equivalent estimated from SRJV data in May 2015, recorded at Fig. 1. Results of comparison between estimated VTEC from SRJV data by Ciraolo methodology and ROB data have shown relatively small differences. For observation period with quiet ionosphere (about 4–6 a.m. local time) differences were small. Average differences of daily median TECU vertical equivalents were of 2 TECU for 122, 123 and 124 DOY 2015, but 3 TECU for day 125 and even 4 TECU for day 121. This implies that VShell provides satisfactory results for this research.

Further study should be focused to the calibration of TEC based on GNSS data. Some papers described different approaches and procedures for error investigation, as Ciraolo et al. in 2007, Brunini and Azpilicueta in 2009, Zhang and Teunissen in 2015, Zhang et al. in 2016. This investigation will be continued in this direction with aim to support the first results.

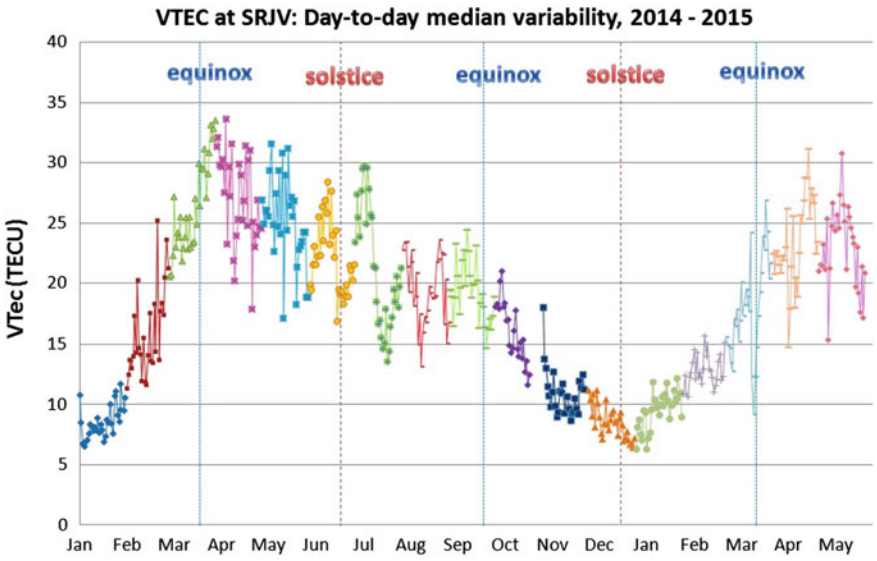

Fig. 2 Day-to-day variability of TEC vertical equivalent, January 2014–May 2015

3.2 *Overview of TEC Variations from January 2014 to May 2015*

Variability of the daily mean TEC for the entire period of this study is shown on the diagrams (Fig. 2). The behavior of the ionosphere from SRJV GNSS data is in line with expectations: values of TEC vertical equivalents are higher in the first five months of 2014 than in 2015, due to the movement away from 24 solar maximum. Standard devotions of daily variations in relation to the monthly medians generally were around 30%, while in the winter months and around solstice even greater.

Figure 3 shows variability of the mean monthly values of VTEC, together with standard deviations of daily median VTEC vertical equivalents. The highest monthly values of VTEC as well as the highest standard deviations were observed during the months of equinoxes, while the lower values of VTEC and lower standard deviations were mostly observed around solstices. These results also indicate expected seasonal variations of TEC vertical equivalents.

3.3 *Analyze of the TEC Variability During Seismic Activities in 2015*

Diagrams (Fig. 4) represent differences between TEC vertical equivalent values and monthly TEC median for all tree listed earthquakes. Dispersions of TEC around

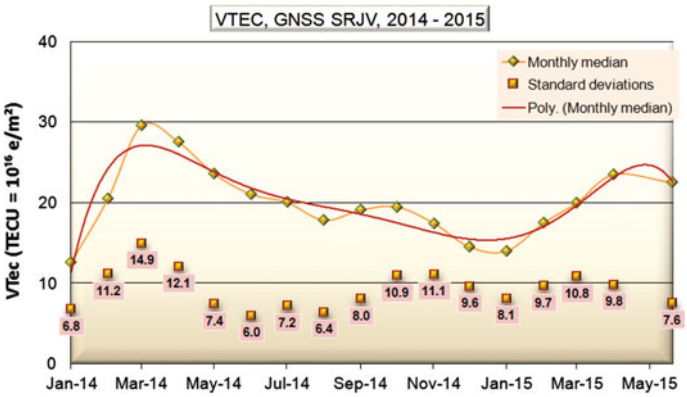

Fig. 3 TEC vertical equivalents for SRJV-monthly median and standard deviations, January 2014–May 2015

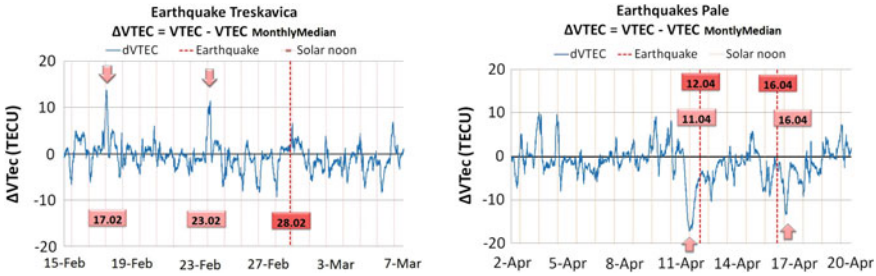

Fig. 4 Difference between TEC vertical equivalent and monthly median for earthquakes: epicenter Treskavica (*left*) and epicenter Pale (*right*)

median, for more than 10 TECU, were observed on fifth and eleventh day before seismic event Treskavica (February 28, 9:24 a.m. LT, M4.3) and on seventh and eighth day before seismic event at Pale (April 12, 02:05 a.m. LT, M4.2), as well as the major variation was observed on the day prior the earthquake Pale. Second earthquake in Pale (April 16, 04:08 a.m. LT, M3.4) happened on fourth day and additional TEC anomalies were observed as well.

For statistical analysis 15-day median were calculated for 15 days preceding the day of earthquakes of M $\sim$ 4 which corresponds to procedure (Liu et al. 2006), as well as additional 15-day median for 15 days after seismic shock (Fig. 5). Lower and upper bounds were determined by $\mu \pm 2\sigma$ at 95% confidence level (Liu et al. 2011). Peak, bigger than upper bound, was notable from 11 a.m. to 1 p.m. (UT) on 17th February. On 23th February TEC value reached the upper bound at 12 p.m. and lasted to 1 p.m. (UT). At the same time TEC values did not exceed lower bound. More detailed view on these anomalies is given on Fig. 6.

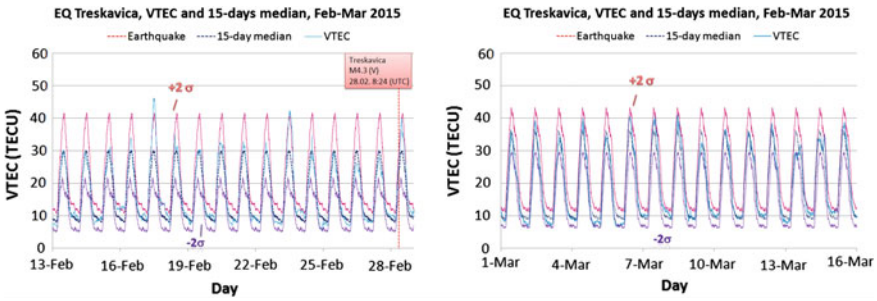

Fig. 5 TEC vertical equivalent values with 15-day medians and ±2σ upper and lower bounds (σ—standard deviation), earthquake Treskavica

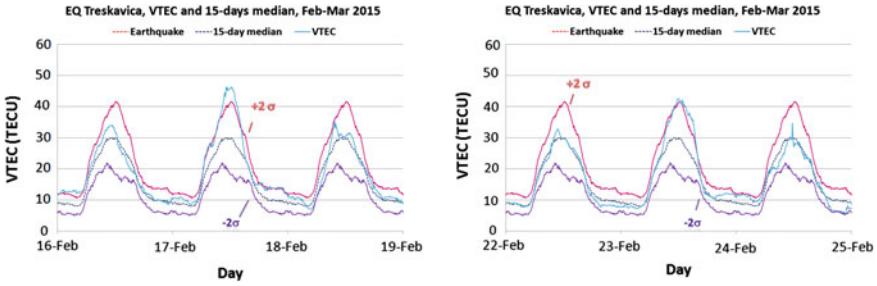

Fig. 6 Anomalous TEC for SRJV detected, correlated with space weather events

Deviations of VTEC for more than 10 TECU from monthly median were registered on 17th and 23rd February (Fig. 4). Disturbances in the Earth's magnetic field were observed on 17th and 18th February, and on 23th and 24th February with moderate geomagnetic storms, so intuitive conclusion is that detected TEC anomalies could be caused by space weather. To investigate causes of anomalies, TEC vertical equivalent data of EPN station ZADA (Croatia) were introduced in this research. Station ZADA is located at similar latitude as station SRJV, but outside of the earthquake preparation zone. Further step in the analysis was calculation of the difference between SRJV and ZADA TEC values, which should remove the effect of space weather. Diagram (Fig. 6) shows their differences in TEC vertical equivalent values for the period of earthquake Treskavica, indicating the remains of the anomalies which are over the bounds ($\mu \pm 2\sigma$ (95%)).

TEC signatures of the both EPN stations were similar. Differences outside the upper or lower bounds ($\mu \pm 2\sigma$) were observed before earthquake on 18th and 24th February and after earthquake on 4th March. Closer examination to TEC data from the both stations shows anomalous TEC signature from data of ZADA on 18th of February, which could be caused by the small gaps of observation data on the ZADA station. Anomalies on 24th February were detected at the both stations, first at TEC from data of SRJV station around local noon and at TEC from ZADA

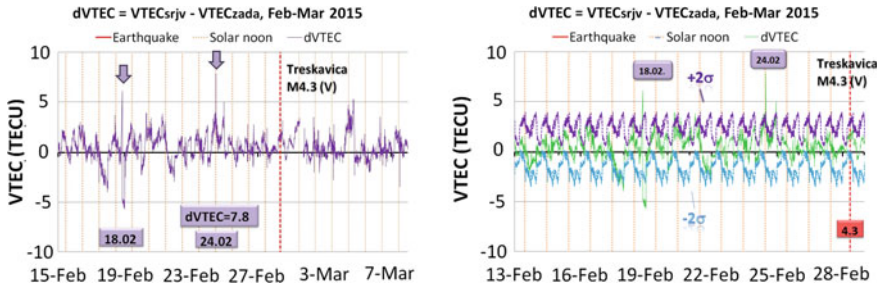

Fig. 7 Difference between TEC vertical equivalent values of SRJV minus ZADA, within weeks around earthquakes, Treskavica (*left*). Upper and lower bounds of ΔVTEC = VTECsrjv-VTECzada, determined with $\mu \pm 2\sigma$, Treskavica (*right*)

station after sunset on 24th February. Anomalies were also detected on 4th March, but closer and more detail examination shows very similar signature of TEC values at the both station, with the difference that TEC values were slightly higher at SRJV station. This investigation with deviations of VTEC observed on 17th and 23rd February (station SRJV, Fig. 4) were similar to observed deviations of TEC values from ZADA station. Differences of TEC values from the both stations for that period did not exceed lower or upper bound (Fig. 7), except for the days when ionosphere was disturbed by space weather events. However, these anomalies in SRJV TEC data requires further investigation using other GNSS stations out of earthquake influence, because data of ZADA had short gaps in the observation.

Statistical analysis of 15-day median for 15 days before the earthquake at Pale $M \sim 4$ is shown at Fig. 8, together with statistical analysis of 15-day median for days after the earthquake. Lower and upper bounds were calculated by $\mu \pm 2\sigma$. TEC values for first 14 days, which preceded a day before earthquake with epicenter at Pale, did not exceed bounds $\pm 2\sigma$. On the day before the earthquake occurrence, as well as during the day of seismic shock, anomalies of TEC were observed. This time they exceeded the lower bound. Also TEC values reached the lower bound during the occurrence of second earthquake, with the same epicenter but lower magnitude $M \sim 3.4$ (Fig. 9).

Figure 8 shows anomalies for TEC vertical equivalent values SRJV station in relation to earthquake Pale ($\sim$13 km far from SRJV station). First seismic shock occured around midnight (UT) on 12th April. On the day prior first earthquake TEC vertical equivalent values fell out the lower bound TEC values. Lower values continued during the night, after the seismic shock. Second earthquake occurred four days later on 16th April around 2 a.m. (UT). During the day prior earthquake low TEC values, as well as anomalies were observed. After earthquake, on 16th April, TEC values fell out the lower bound from 11:30 a.m. to 15:10 a.m. (UT), which is around local noon. Low values of TEC continued during the rest of the day and also the next day, except the period from 11:50 a.m. to 17:30 p.m. (17th April).

Figure 10 (left) shows that values of ΔVTEC exceeded upper bound on 5th, 7th, 8th and 9th April. During those days TEC vertical equivalent values of SRJV

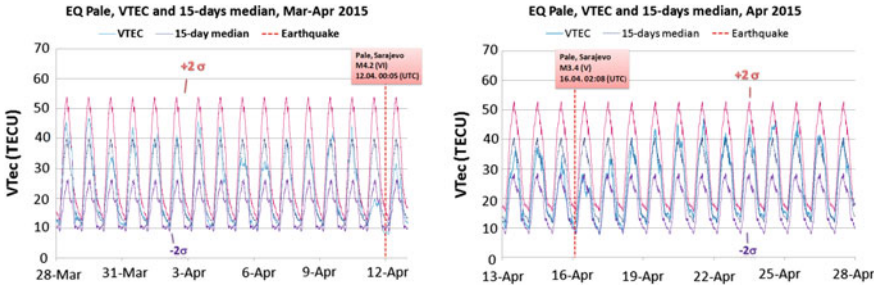

Fig. 8 TEC vertical equivalent values with 15-day medians and ±2σ upper and lower bounds (σ—standard deviation), earthquake Pale

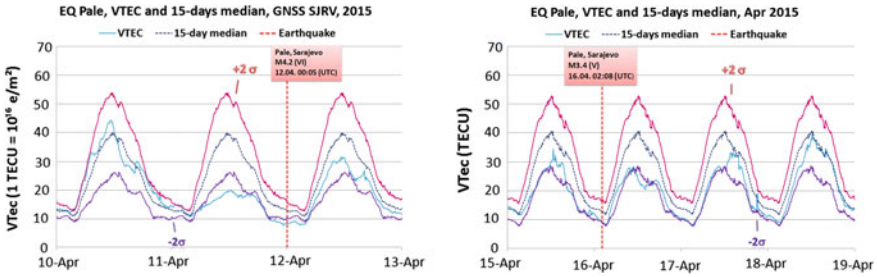

Fig. 9 Detected anomalies, earthquakes in Pale, April 2015, 12th and 16th

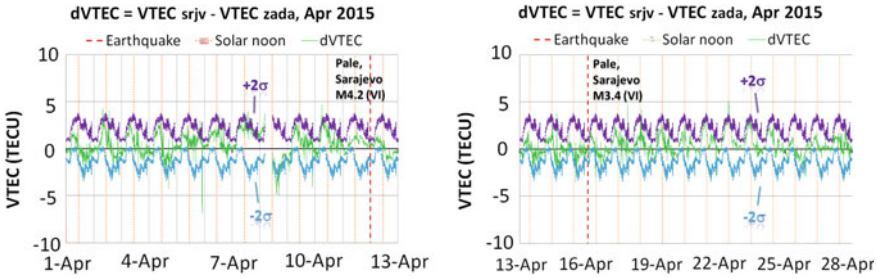

Fig. 10 Upper and lower bounds of ΔVTEC = VTECsrjv-VTECzada, determined with μ ± 2σ, in Pale, prior the first (*left*) and after second (*right*) seismic event

station did not exceed ±2σ bounds (Fig. 8). Closer examination indicated that anomalies were observed on data of ZADA station. Diagram on the right shows variation of TEC vertical equivalent differences values, after the second event, with negative anomalies on about 8 h after the earthquake and then positive anomalies on 17th and 22th April. Planetary K-index showed that disturbances in magnetic field with minor and moderate geomagnetic storms were observed on 10th and 11th April, as well during 15th–17th April.

It is important to conclude that further investigation of estimated TEC data accuracy would help this study. In this moment, based on these investigation results, it may be concluded that anomalies of TEC vertical equivalent values related to earthquakes in Pale indicate ionosphere-seismicity connection, even the magnitudes of the earthquake were as small as 4.2M or 3.4M.

4 Conclusion

This paper briefly shows research on the variations of total electron content in the ionosphere above the territory of Bosnia and Herzegovina for the period January 2014–May 2015, with special focus on the state of ionosphere for the periods of seismic activities registered near Sarajevo M $\sim$ 4 in 2015.

Results indicate that TEC is a complex parameter, which varies during the different seasons, months, within 24 h, but also that anomalies can be sudden and large in short intervals. There are noticeable changes in behavior of TEC within different seasons, and also similarity of TEC variations during one season. Results showed that variations of TEC sometimes differ from expected, due to external influences. Standard devotions of daily variations in relation to the monthly medians generally were around 30%, while around solstice even greater.

Research on the ionospheric anomalies in relation to seismic activity was conducted applying 15-day median for 15 days preceding the day of earthquake. Also, 15-day median for 15 days after earthquake was calculated for analyzing TEC values after the earthquake. Statistical analysis were conducted using $\mu \pm 2\sigma$ to determine the lower and upper bound of analyzed TEC values. TEC values which have fallen out these boundaries were further examined. Confidence level of detection of an abnormal signal in this procedure is 95%. TEC vertical equivalent values from EPN station ZADA at similar latitude, but outside the radius of earthquake preparation zone were used for further analysis. Signature of TEC vertical equivalent values from both stations had mostly similar signature. K_p index during those periods showed disturbances in Earth's magnetic field, correlated with minor and moderate geomagnetic storm occurrences, which possibly caused anomalous of TEC vertical equivalent at the both stations.

Differences outside the upper or lower bounds ($\mu \pm 2\sigma$) were observed before earthquake Treskavica on 18th and 24th February and after earthquake on 4th March. Closer examination of TEC data from the both stations shows anomalous TEC signature from data of ZADA on 18th of February, which could be caused by the small gaps of observation data on the ZADA station. Anomalies on 24th February were detected at the both stations, first at TEC from data of SRJV station around local noon and at TEC from ZADA station after sunset on 24th February. The appearance of the magnetic storms blurred the opportunity to explore the impact of earthquakes as well.

Some anomalous deviations were observed at the both stations SRJV and ZADA, but some differences occurred as well, which may be explained as the ionosphere-lithosphere coupling. However, these anomalies in SRJV TEC data requires further investigation using other GNSS stations out of the earthquake influence zone, because data of ZADA had short gaps in the observation.

Results indicate that it's hard to determine a presence of anomalies in ionospheric TEC signature related to seismic activity, prior and after the examined earthquakes $M < 5$, with epicenters in the near of the permanent GNSS station. Disturbances in the ionosphere during the period of earthquake occurrences, due to external influences such as space weather and disturbances in Earth's geomagnetic field were presented as well. Big variations of TEC values were registered in a wider region. Based on these results related to earthquakes in Pale, it may be concluded that some anomalies of TEC vertical equivalent values show ionosphere-seismicity connection, and cannot be neglected, even if the magnitude of the earthquake is less than 5 M. But this conclusion is based on TEC behavior when GNSS station is close to the epicenter, in our case 13 km.

References

Brunini C, Azpilicueta F (2009) Accuracy assessment of the GPS-based slant total electron content. J Geodesy 83(8):773–785

Bruyninx C et al (2012) Enhancement of the EUREF permanent network services and products. Geodesy Planet Earth IAG Symp Ser 136:27–35. doi:10.1007/978-3-642-20338-1_4

Ciraolo L (1993) Evaluation of GPS L2-L1 biases and related daily TEC profiles. In: Proceedings of the GPS/ionosphere workshop, Neustrelitz, Germany, pp 90–97

Ciraolo L, Azpilicueta F, Brunini C, Meza A, Radicela SM (2007) Calibration errors on experimental slant total electron content (TEC) determined with GPS. J Geodesy 81(2): 111–120. doi:10.1007/s00190-006-0093-1

Dobrovolsky IR, Zubkov SI, Myachkin VI (1979) Estimation of the size of earthquake preparation zones. Pure Appl Geophys 117:1025–1044

Fayose RS, Babatunde R, Oladosu O, Groves K (2012) Variation of total electron content (TEC) and their effect on GNSS over Akure, Nigeria. Appl Phys Res 4(2)

Hasbi AM, Ali MAM, Misran N (2011) Ionospheric variations before some large earthquakes over Sumatra. Nat Hazards Earth Syst Sci 11:597–611

Liu JY, Chuo YJ, Shan SJ, Tsai YB, Chen YI, Pulinets SA, Yu SB (2004) Pre-earthquake ionospheric anomalies registered by continuous GPS TEC measurements. Ann Geophys 22:1585–1593

Liu JY, Chen YI, Chuo YJ, Chen CS (2006) A statistical investigation of preearthquake ionospheric anomaly. J Geophys Res 111:A05304. doi:10.1029/2005JA011333

Liu Z, Luo W, Ding X, Chen W (2011) The new characteristics of ionospheric total electron content (TEC) disturbances prior to four large earthquakes. Department of Land surveying and Geo-informatics, The Hong Kong Polytechnic University

Molchanov O, Fedorov E, Schekotov A, Gordeev E, Chebrov V, Surkov V, Rozhnoi A, Andreevsky S, Iudin D, Yunga S, Lutikov A, Hayakawa M, Biagi PF (2004) Lithosphere-atmosphere-ionosphere coupling as governing mechanism for preseismic short-term events in atmosphere and ionosphere. Nat Hazards Earth Syst Sci 4:757–767

Ouzounov DP, Pulinets SA, Davidenko DV, Kafatos M, Taylor PG (2013) Space-borne observations of atmospheric pre-earthquake signals in seismically active areas. Case study for Greece 2008–2009

Pulinets SA (2009) Physical mechanism of the vertical electric field generation over active tectonic faults. Adv Space Res 44:767–773

Pulinets SA, Boyarchuk KA, Khegai VV, Kim VP, Lomonosov AM (2000) Quasielectrostatic model of atmosphere-thermosphere-ionosphere coupling. Adv Space Res 26:1209–1121

Pulinets S, Kotsarenko AN, Perez-Enfiquez R, Ciraolo L, Pulinets IA (2006) New ionosphere variability index and its anomaly variation related to major earthquakes occurred in California, USA and Mexico

Schaer S (1999) Mapping and predicting the earth's ionosphere using the global positioning system. PhD thesis, Bern University, Switzerland

Zhang B, Teunissen PJG (2015) Characterization of multi-GNSS between-receiver differential code biases using zero and short baselines. Sci Bull 60(21):1840–1849. doi:10.1007/s11434-015-0911-z

Zhang B, Teunissen PJG, Yuan Y (2016) On the short-term temporal variations of GNSS receiver differential phase biases. J Geodesy, Dec 2016. doi:10.1007/s00190-016-0983-9